LONDON METROPOLITAN UNIVERSITY

Plastic Optical Fibre Couplers with Wavelength Division Multiplexing Capability for Short-Range Peer-to-Peer Communication in Networking and Industrial Applications

Tinopera Matata BEng (Hons), MSc

A thesis submitted in partial fulfilment
of the requirements for the London Metropolitan University
for the degree of Doctor of Philosophy

October 2024

Abstract

This thesis presents a study on the design and simulation of adjustable, multi-output plastic optical fibre (POF) array couplers for wavelength-division multiplexed (WDM) transmission in the visible spectrum. The research focuses on three configurations—1×2, 1×4, and 1×8—and introduces a novel architecture that allows precise control of optical power splitting ratios, offering greater flexibility than conventional couplers with fixed branching ratios.

The innovation lies in two integrated design mechanisms that enable both coarse and fine adjustment of optical power distribution. The first is the coupling POF immersion-depth adjustment, which provides coarse tuning by varying the insertion depth of the coupling fibre into the backbone fibre to control the power received at each output port. The second is the reflector-length adjustment, which allows fine control by modifying the reflector length between the polished surfaces of the backbone and coupling fibres. Together, these mechanisms permit accurate tailoring of the optical power split at the design stage, eliminating the need for post-fabrication calibration and enhancing design flexibility.

This controllability improves optical network performance by enabling power optimisation across all ports, thereby reducing the need for repeaters, simplifying system design, and lowering overall cost. The proposed designs were evaluated using theoretical ray-optics modelling and LightTools ray-tracing simulations, which confirmed that the couplers exhibit high coupling efficiency and low insertion loss.

Simulation results show that the 1×2 coupler delivers an average of 46.5% of the input power to each output port (93% efficiency, 3.3 dB insertion loss per port). The 1×4 coupler provides approximately 22% per port (86% efficiency, 6.7 dB insertion loss), while the 1×8 coupler distributes 8% per port (62% efficiency, 11 dB insertion loss). All designs comply with the GR-1209-CORE specification for insertion loss per port. Although primarily optimised for signal reception, modifications were simulated to evaluate their suitability as transmitting couplers, indicating promising potential for future development.

This work advances the field of short-reach optical communications by proposing design-time adjustable POF array coupler architecture that combines mechanical simplicity, presettable power ratios, and high optical efficiency. The study demonstrates a cost-effective, scalable path toward reliable connectivity for industrial and in-home networks, based entirely on simulations.

Acknowledgements

I am deeply indebted to many individuals who have supported me throughout this research project. First and foremost, I dedicate all my achievements to my late father, whose unwavering strength and spirit inspired me to pursue and complete this work. Though he is no longer with us to witness its conclusion, I hope his soul rests in peace.

I extend my heartfelt gratitude to Professor Bal Virdee of London Metropolitan University, whose motivation and encouragement guided me through some of the most challenging moments of this journey. His boundless enthusiasm for my work, coupled with his invaluable guidance and advice, kept me focused. I greatly admire his patience and constant encouragement to persevere when times were tough; without his support, completing this research would have been far more difficult.

I would also like to offer special thanks to Dr Kevin Munisami of Kingston University for providing the LightTools modelling software used in this research. His insightful discussions on various optical simulations and his encouragement to pursue journal publications were incredibly helpful. I am profoundly grateful for his contributions to my work.

Additionally, I wish to express my sincere appreciation to Dr. Nick Ioannides for allowing me to be one of the PhD research students at London Metropolitan University. His guidance, advice, patience, and unwavering enthusiasm were invaluable throughout this project. I also want to acknowledge the tremendous support provided by the library staff during my research.

Finally, my deepest thanks go to my wife and family for their unwavering and endless support throughout my studies. Their encouragement made this accomplishment possible.

Author's Declaration

I, Tinopera Matata, declare that all the material in this thesis is my work. This thesis contains no material submitted previously, in whole or in part, for the award of any other academic degree or diploma.

Table of Contents

List of Figures

List of Tables

List of Abbreviations

AI	Artificial Intelligence
AR	Augmented Reality
COC	Cyclo-Olefin Copolymers
CYTOP	Cyclic Transparent Optical Polymer
dB	Decibel
DFT	Dielectric Thin Film
DSI POF	Double Step-Index Plastic Optical Fibre
DSLM	Digital Spatial Light Modulator
EMC	Electromagnetic Compatibility
EMD	Equilibrium Modal Distribution
EMI	Electromagnetic Interference
ETL	Electrically Tuneable Lens
FBTC	Fused Biconical Taper Coupler
Gb	Gigabits
GHz	Giga Hertz
GI-POF	Graded Index Plastic Optical Fibre
IL	Insertion Loss
kHz	Kilo Hertz
LAN	Local Area Network
LED	Light Emitting Diode
Mb	Megabits
MC-DSI-POF	Multi-Core Double Step-Index Plastic Optical Fibre
MC-SI-POF	Multi-Core Step-Index Plastic Optical Fibre
MHz	Mega Hertz
MMF	Multi-Mode Fibre
M-PAM	Multi-level Pulse Amplitude Modulation
mPOF	Microstructure Plastic Optical Fibre
MSI POF	Multi-Step-Index Plastic Optical Fibre
NA	Numerical Aperture
NIST	National Institute of Standards and Technology
OFDM	Orthogonal Frequency Division Multiplexing
OSI	Open System Interconnection
PA	Polyamide
PC	Poly Carbonate
PCS	Plastic Clad Silica

PE	Polyethene
PFA	Poly Fluoroalkyl Acrylates
PMMA	Polymethylmethacrylate
PMMA d-8	Deuterated PMMA
POF	Plastic Optical Fibre
PS	Polystyrene
PVC	Polyvinylchloride
RF	Radio Frequency
RFI	Radio Frequency Interference
RI	Refractive Index
SERCOS	Serial Real-time Communication Systems
SI-POF	Step-Index Plastic Optical Fibre
SMF	Single Mode Fibre
SR	Splitting Ratio
Tg	Glass Transition Temperature
TIR	Total Internal Reflection
WDM	Wavelength Division Multiplexing

Chapter 1

Plastic Optical Fibre (POF) Couplers, Overview and Thesis Outline

1.0 Background to Optical Fibre and POF Couplers

The rapid expansion in data centres, 5G wireless communication, augmented reality (AR), autonomous vehicles, and artificial intelligence (AI) has dramatically increased the demand for higher data rates and greater processing throughput. While electronics are reaching their limits in meeting these demands, photonics integration has become crucial for sustaining this progress (Soref, 2018). Integrated photonics enables denser, more complex network designs, overcoming issues such as waveguide crossings and crosstalk (Sun, 2019).

This growing demand is further fuelled by bandwidth-intensive applications such as streaming services, online commerce, and real-time communication platforms like FaceTime, Zoom, and WhatsApp (Cisco, 2020). Recent advancements in plastic optical fibre (POF) technology have significantly impacted communication networks, enabling data transmission rates exceeding 10 Gbps. These advancements help meet the growing need for fewer repeaters, thereby reducing costs and energy consumption (Ziemann et al., 2014).

Moreover, the global shift towards renewable energy sources, driven by the imperative to reduce CO_2 emissions, has accelerated the adoption of solar and wind power systems. POF and POF-based couplers are increasingly relevant in these systems, particularly for automation, environmental monitoring, and equipment condition monitoring (Langer et al., 2020). POF systems offer high flexibility and robustness, essential for reliable data transmission in energy infrastructure.

1.1 Deficiencies of Existing Optical Couplers

Optical signals provide substantial advantages, including high bandwidth, low latency, reduced energy dissipation, and immunity to electromagnetic interference (Kazovsky et al., 2012). Silica glass optical fibres surpass electrical cables in long-haul communication due to their low signal loss over extended distances. In contrast, electrical cables experience

significant signal loss at high frequencies, leading to reduced energy efficiency for high-throughput transmission (Agrawal, 2012).

Optical couplers, essential components of integrated photonic systems and optical fibre networks, split optical energy according to specific ratios based on their design. However, most commercially available multimode POF power splitters and couplers have fixed branching ratios, which often deviate from intended values due to design limitations, fabrication tolerances, and manufacturing process variations (Mohamed-Kassim, 2017).

This presents a challenge: mass-producing couplers with various branching ratios is time-consuming and cost-inefficient. The rapid development of integrated optical devices requires more precise power-splitting ratios for specific applications. Fixed-ratio couplers are inadequate for modern demands, particularly in terms of scalability and adaptability. Additionally, current POF couplers lack the necessary bandwidth and port configurations to keep pace with advancements in POF technology (Ziemann et al., 2014).

1.2 Research Motivation and Innovation

This research addresses the gap between advancements in POF technology and the development of suitable POF-based couplers. The focus is on designing and simulating novel 1x2, 1x4, and 1x8 POF-based array couplers that provide multiple output ports and broadband transmission for short-range applications, including domestic networking and industrial systems (Ziemann et al., 2014).

The innovation lies in developing adjustable optical couplers that allow precise control over splitting ratios and other optical parameters for each output port. This flexibility is achieved through two design mechanisms:

1. **Immersion Depth Adjustment:** Varying the immersion depth of the coupling POF into the backbone POF provides coarse control over the output power distribution.
2. **Reflector Length Adjustment:** Adjusting the reflector length between the polished faces of the backbone and coupling POFs fine-tunes the output power.

These innovations enable the proposed POF-based array couplers to adapt to specific application requirements, reducing the need for repeaters, lowering system costs, and improving energy efficiency. By precisely adjusting optical parameters during the design phase, these couplers offer high performance and flexibility, surpassing conventional fixed-ratio couplers.

1.3 Applications and Performance

The POF-based array couplers developed in this research operate in the visible spectrum, transmitting wavelengths of 650 nm (red), 570 nm (yellow), 520 nm (green), and 470 nm (blue). These couplers are designed to meet the requirements of the physical layer (Layer 1) of the Open Systems Interconnection (OSI) model (Ziemann et al., 2014).

This research introduces novel adjustable POF-based couplers that address the limitations of existing fixed-ratio couplers. These innovations enable greater flexibility in optical power distribution, high-efficiency signal transmission, and reduced energy consumption, making them ideal for short-range applications such as domestic and industrial networking. The research bridges the gap between POF technology advancements and the development of practical, high-performance couplers suitable for modern communication systems.

1.4 Research Aims and Objectives

This research aims to design and simulate novel POF-based 1x2, 1x4, and 1x8 array couplers for short-range domestic networking and industrial applications using ray tracing software. The research also investigates the impact of the coupling POF's immersion depth on the optical power at the output ports, as well as the effect of inserting a 100% reflector between the polished faces of the coupling POF and the backbone POF on the coupler's performance parameters.

The specific objectives of this doctoral research are as follows:

1. Review the latest advancements in POF technology and evaluate the capabilities and limitations of currently available POFs used in POF-based couplers.
2. Identify and analyse existing POF-based coupler types, including their architectures, operating principles, performance parameters, capabilities, limitations, and applications.
3. Propose the design of innovative POF-based array couplers to address the limitations of current models.
4. Calculate the performance potential of the proposed POF-based couplers, including their ability to meet data rate requirements and other performance metrics.

5. Investigate the effect of immersion depth of the coupling POF into the backbone POF on the coupler's performance parameters.
6. Research the impact of inserting a reflector between the polished faces of the coupling POF and the backbone POF on the optical coupler's performance.
7. Examine the effect of inserting an optical reflector at the rear end of the backbone POF on the output optical power distribution.
8. Apply ray optics theory to determine the design specifications of a single POF-based coupler, focusing on performance parameters.
9. Perform a theoretical analysis using ray optics theory to assess the performance capabilities and limitations of the proposed POF-based array couplers.
10. Extend the design specifications from the single coupler to assess the performance parameters of various POF-based array couplers, including 1x1, 1x2, 1x4, and 1x8 configurations.
11. Model and verify the performance of the proposed 1x2, 1x4, and 1x8 POF-based array couplers using ray tracing optical modelling software, LightTools.

These objectives aim to advance POF-based coupler design, enhancing their adaptability and efficiency for various short-range applications.

1.5 Original Contribution to Knowledge

This PhD research makes several original contributions to the field of POF technology, particularly in the design and simulation of novel POF-based multiple-port 1x2, 1x4, and 1x8 array couplers for industrial and domestic applications. These couplers are designed to handle bandwidths and transmission rates up to 1 Gb/s. Additionally, the research investigates how varying the immersion depth of the coupling POF into the backbone POF affects coupler performance, as well as the impact of inserting a 100% reflector between the polished faces of the coupling and backbone POFs. Key findings include the identification of coarse adjustment through immersion depth and fine adjustment via the optimising reflector in controlling the array coupler parameters.

The original contributions are summarised as follows:

- **First Contribution (Objectives 1 and 2):** Analyses the feasibility of using POF in optical couplers, reviews the capabilities and limitations of available POFs and

multimode optical components, and evaluates existing POF-based couplers in terms of performance parameters, architecture, operational principles, capabilities, limitations, and applications.

- **Second Contribution (Objectives 3 and 4):** Proposes the design of innovative POF-based array couplers and calculates their capability to meet performance requirements, including potential data rates.
- **Third Contribution (Objectives 5, 6, and 7):** Investigates the effect of immersion depth and reflector insertion on the performance of the coupler, demonstrating how these factors influence optical parameters.
- **Fourth Contribution (Objectives 8 and 9):** Focuses on the theoretical design of POF-based array couplers, applying ray optics theory to determine design specifications and performing a theoretical analysis to assess performance capabilities and limitations.
- **Final Contribution (Objectives 10 and 11):** Applies the design specifications for single couplers to model the performance parameters of various POF-based array couplers (1x1, 1x2, 1x4, and 1x8) using LightTools software, ensuring consistency between theoretical designs and simulated performance.

These contributions enhance the understanding of POF-based coupler design, offering innovative solutions to meet the increasing demands for high-speed, efficient optical networks in short-range applications.

1.6 Thesis Scope

This thesis is divided into two main parts: the first focuses on the theoretical design and mathematical analysis of POF-based optical couplers. In contrast, the second part involves creating realistic models of these couplers using the optical ray-tracing software, LightTools. The simulations conducted in LightTools validate the theoretical designs and analyses, with model dimensions aligning with theoretical calculations. The thesis compares performance parameters from theoretical analysis with those from simulations. While the fabrication of optical coupler prototypes was not included due to time constraints and equipment limitations, the realistic models produced by LightTools were sufficient to achieve the research objectives.

1.7 Thesis Structure

This thesis comprises eight chapters that detail the conceptualisation, theoretical designs, simulations, and analysis of novel POF-based array couplers. Each chapter is summarised below:

1.7.1 Chapter 1: Introduction

This chapter introduces the research scope, aims, objectives, and methodology. It also outlines the research contributions to the field of plastic optical fibre (POF) technology.

1.7.2 Chapter 2: Literature Review: Plastic Optical Fibre

This chapter provides an in-depth review of recent advancements in POF technology, including its material structure and performance characteristics. It discusses ray optics theory relevant to optical transmission in POFs, along with the capabilities and limitations of POF as a transmission medium. A key focus is on the technological aspects of POF, including recent developments in bandwidth and polymerisation, as well as the advantages of POF over traditional glass optical fibres. The chapter also covers the core, cladding, and jacket materials of POF, as well as the intrinsic and extrinsic loss factors affecting its reliability and performance. Two key research questions are addressed:

1. What are the latest advancements in POF technology, specifically in material science and properties?
2. How does POF compare to other transmission media in telecommunications applications, such as POF-based array couplers?

1.7.3 Chapter 3: Plastic Optical Fibre Couplers and Their Performance Parameters

This chapter reviews recent studies on POF-based optical couplers, discussing the available types, architecture, performance parameters, and applications. Key research questions addressed in this chapter include:

- How can theoretical models predict the performance of POF-based optical couplers?
- What are the challenges and limitations of current couplers, and how can they be improved?

- How do design and structural parameters influence POF coupler performance?
- What factors impact the efficiency of POF-based couplers?

1.7.4 Chapter 4: Investigating the Effect of Immersion Depth and Backbone Reflector on Optical Splitter Coupler Parameters

This chapter begins by using the LightTools optical modelling software to verify the appropriate bending radius for this research, ultimately selecting 25mm. The chapter then covers the theoretical design and characterisation of a 1x2 beam-splitting coupler, exploring the effect of immersion depth on the coupler's performance parameters and the impact of inserting a 100% reflector between the polished surfaces of the coupling and backbone POF. Finally, LightTools simulations are used to model the 1x2 optical beam splitter, with performance metrics such as insertion loss, excess loss, coupling ratios, uniformity, and efficiency compared and analysed.

1.7.5 Chapter 5: Theoretical Analysis of Plastic Optical Fibre Coupler Arrays

This chapter focuses on the theoretical design and analysis of POF-based 1x2, 1x4, and 1x8 array couplers. It builds on the techniques developed in Chapter 4 to optimize the optical power output by adjusting the immersion depth and incorporating reflectors. Additionally, the chapter investigates the performance parameters of these array couplers, including insertion loss, excess loss, coupling ratios, uniformity, and efficiency.

1.7.6 Chapter 6: LightTools Coupler Design Modelling and Simulations

This chapter validates the theoretical designs of the POF-based 1x2, 1x4, and 1x8 optical couplers using LightTools, an industry-standard optical ray-tracing software from Dassault Systèmes. The simulations verify the calculated performance parameters—excess loss, insertion loss, coupling ratios, and efficiency —using the same optimisation techniques as in the theoretical analysis.

1.7.7 Chapter 7: Comparison of Theoretical and Simulated Results

This chapter presents a comparison between the theoretical and simulated results of the coupler performance parameters. It highlights the similarities and differences between the two approaches and discusses possible reasons for any discrepancies.

1.7.8 Chapter 8: Conclusion, Recommendations, and Further Work

This final chapter discusses the outcomes and limitations of the proposed POF coupler designs. It summarises the contributions to knowledge and offers recommendations for further research to enhance the performance of POF-based couplers.

1.8 Technical Papers

Two papers based on this research will be disseminated at scientific venues.

1. *Characterisation of POF-based 1x2 splitting optical coupler with different immersion depths and a backbone reflector*.
2. *Output Power Optimisation of Plastic Optical Fibre (POF) based 1x2 and 1x4 Array Couplers Using Optical Reflectors*.

1.9 References

- Agrawal, G. P. (2012). *Fiber-Optic Communication Systems*. John Wiley & Sons.
- Cisco (2020). *Annual Internet Report (2018–2023)*. Cisco Systems.
- Kazovsky, L. G., Wong, S. W., & Yen, S. L. (2012). *Broadband Optical Access Networks*. John Wiley & Sons.
- Langer, H., Krug, J., & Petermann, M. (2020). *Plastic Optical Fibers in the New Age of Photonics: Developments and Applications*. IEEE Photonics Journal, 12(4).
- Mohamed-Kassim, N. S. (2017). *Analysis of POF Splitters and Couplers with Fixed Branching Ratios*. Optoelectronics Letters, 13(3).
- Soref, R. (2018). *Silicon Photonics: A Review of Recent Advances*. IEEE Journal of Selected Topics in Quantum Electronics, 23(2).
- Sun, C. (2019). *Integrated Photonics for Dense and Complex Networks*. Nature Photonics, 13, 165–173.
- Ziemann, O., Krauser, J., Zamzow, P. E., & Daum, W. (2014). *POF Handbook: Optical Short Range Transmission Systems*. Springer Science & Business Media.

Chapter 2

Plastic Optical Fibre (POF) Characterisation

2.1 Introduction

This chapter provides a comprehensive review and characterisation of plastic optical fibre (POF) and assesses its feasibility for fabricating POF couplers. It begins with an overview of POF's history, the materials science involved in its production, and the various materials used to manufacture it.

Subsequent sections detail the fabrication methods for POF, its mechanical properties, and its refractive index distribution. Ray-optics theory relevant to optical transmission in plastic optical fibre is discussed, along with the capabilities and limitations of POF as a transmission medium, including attenuation and modal dispersion. This section also covers PMMA POF transmission characteristics, loss mechanisms, techniques for mitigating modal dispersion, frequency response, and bandwidth.

The chapter then compares the main advantages of POF with those of other transmission media, such as glass fibre, coaxial cables, copper wire, and wireless technologies, focusing on parameters such as bandwidth and attenuation. The limitations of POF are also examined.

Finally, recent developments in POF material structures are reviewed, emphasising technological advancements such as improvements in bandwidth and polymerisation, as well as the various application areas of POFs.

2.2 Historical Background

The history of Plastic Optical Fibre (POF) is closely linked with the evolution of optical communication and polymer science. In the 1960s, the concept of optical fibre emerged following significant advancements in light-based communication, particularly with the development of the laser. Initially, optical fibres were made from glass, but researchers began exploring polymers for their flexibility, ease of handling, and lower cost.

In the 1970s, researchers focused on creating optical fibres from plastic materials. The primary challenge was developing polymers with the necessary optical clarity and low

attenuation to be suitable for communication. Polymethyl methacrylate (PMMA) was identified as a promising material due to its transparency and ease of fabrication.

By the early 1980s, advancements in polymer chemistry and fibre drawing techniques made the commercial production of POF feasible. Companies in Japan and Europe started manufacturing POF for specific applications, mainly in automotive and short-distance data communication.

The 1990s saw significant improvements in POF technology, including reductions in signal attenuation and increased bandwidth. These advancements expanded POF applications into home networking, industrial automation, and consumer electronics. The development of graded-index POF (GI-POF) marked a significant milestone by offering improved data transmission characteristics.

In the 2000s, research and development efforts focused on enhancing POF data transmission capabilities for high-speed networks. The use of perfluorinated polymers enabled the creation of POFs with even lower attenuation, making them more competitive with glass fibres for specific applications.

Today, POFs are used in various domains, including automotive networks, medical devices, industrial control, consumer electronics, telecommunications, and local area networks (LANs). Ongoing research aims to reduce signal attenuation further, increase bandwidth, and improve the mechanical properties of POFs.

2.3 POF Material Science and Mechanical Structure

A polymer is a substance composed of chemically uniform macromolecules, which may differ in polymerisation or molecular weight (D. Zaremba, 2017). Polymers consist of one or more monomers, which are low-molecular-weight compounds with functional groups that can react to form high-molecular-weight compounds through step or chain-growth reactions. Polymers made from only one type of monomer are called homopolymers, while those made from two or more different monomers are known as copolymers.

Since the inception of POF in the 1960s, research in polymer science has introduced a wide range of materials (D. Zaremba, 2017). Currently, the primary materials used for optical fibres are silica (glass) and organic polymers. Both glass optical fibres (GOFs) and polymer optical fibres (POFs) have distinct characteristics, making them suitable for a range of optical applications.

POF is structurally similar to glass optical fibre and operates as a classical dielectric waveguide with a round cross-section in the optical wavelength range. POF consists of three layers: the core, cladding, and protective jacket, as illustrated in Figure 2.1. An optical fibre includes a core with a refractive index n_{core} and a surrounding cladding layer with a refractive index n_{cladding}. According to Jamshid Heidarialamdarloo (2018), if the core's index is higher than the cladding's index, optical energy is guided within the core due to total internal reflection at the core-cladding interface.

In a typical PMMA step-index POF, the fibre core diameter is about 980 µm and the refractive index is 1.492. This core is surrounded by a thin fluorinated polymer cladding, 10 µm thick, with a refractive index of 1.417. The core and cladding are nearly transparent dielectric materials. The core diameter of POFs varies from 200 to 920 µm, while the cladding's outer diameter is typically 20-50 µm larger than the core diameter (Panchuk et al., 2022).

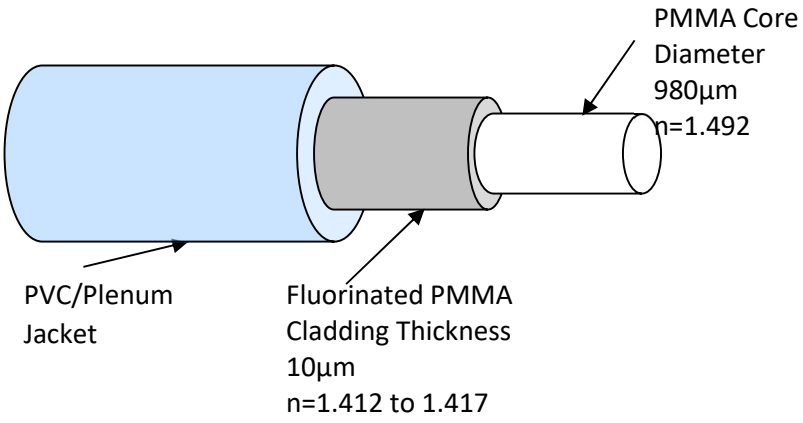

Figure 2-1: Step Index (SI) plastic optical fibre profile (Panchuk et al., 2022)

The core and cladding are enclosed in polyvinylchloride (PVC) or chlorinated polyethene to provide mechanical protection. The optical phenomenon called total internal reflection (TIR) guides the optical energy inside the core at the core-cladding boundary.

2.3.1 Core Material

A key requirement for both core and cladding materials in POF is high transparency. Thermoplastics have been the preferred choice for core fibre fabrication until recently. According to D. Zaremba (2017), polymers such as PMMA, polystyrene (PS), and

polycarbonate (PC) are well-established materials used in the POF industry for core fabrication. Over the past four decades, perfluoro polymers have also been developed to achieve higher optical performance.

2.3.1.1 Poly Methyl Methacrylate

PMMA, as described by D. Zaremba (2017), is an amorphous homopolymer derived from the monomer methyl-2-methylpropenoate. It belongs to the acrylate polymer family, which is known for its high transparency. Commercially, PMMA is referred to by various trade names, including Plexiglass, Lucite, Oroglas, and Acrylite, and is used in a wide range of applications, from building materials to data communication. The chemical structure of PMMA is illustrated in Figure 2.2.

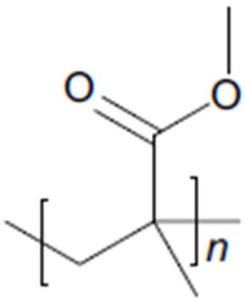

Figure 2-2: Chemical structure of the PMMA (D. Zaremba (2017))

The glass transition temperature (Tg) of PMMA, as noted by D. Zaremba (2017), varies with its composition, typically ranging from 110°C to 120°C. Key material properties of PMMA include its density (1.17–1.20 g/cm^3), refractive index (RI) at 589 nm (1.49), and tensile strength (48–76 MPa). However, PMMA has low toughness, making it sensitive to impact loading, which can lead to stress cracks.

PMMA fibres have limited transmission distances due to intrinsic losses. The theoretical minimum attenuation for PMMA-based POFs is 106 dB/km at 650 nm. This attenuation arises from factors such as vibrational overtones, electronic transition absorption, and Rayleigh scattering, with overtones being most significant in the visible and near-infrared regions.

Extrinsic losses, as explained by D. Zaremba (2017), include contaminants such as dust and material impurities, scattering from micro-voids, and fibre-processing issues, such

as fluctuations in core diameter, cladding delamination, and misalignment errors. Successive improvements in fibre production have reduced these extrinsic losses to minimal levels. Currently, PMMA step-index POFs (SI-POFs) typically have a 1 mm diameter, a numerical aperture (NA) of 0.5, and an attenuation of less than 130 dB/km at 650 nm. The operating temperature of PMMA fibres depends on the type but generally ranges from 55°C to 105°C, as specified by manufacturers.

2.3.1.2 Deuterated Polymers

In deuterated polymers, deuterium atoms replace some or all the hydrogen atoms in the polymer. While the chemical properties of these molecules remain almost unchanged, their physical properties can vary. According to D. Zaremba (2017), deuterated polymers are less reactive with oxygen at elevated temperatures and when exposed to UV light compared to non-deuterated polymers. Additionally, deuterated polymers exhibit increased light transmission between 500 and 900 nm, weaker inter-chain forces, and higher heat capacity and density.

Conventional POFs made from polymers such as PMMA, PS, and PC exhibit relatively high optical losses of around 100 dB/km. In contrast, deuterated PMMA (PMMA-d8) shows significantly reduced optical loss of approximately 20 dB/km at 680 nm (D. Zaremba, 2017). Schleinitz (DuPont) developed the first step-index PMMA-d8 (SI-PMMA-d8) POFs in 1977, which initially had an attenuation of 180 dB/km at 690 nm. Over time, Kaino improved these fibres by using PMMA-d5 and PMMA-d8 as core materials. The SI-PMMA-d5 fibre exhibited a minimal loss of 41 dB/km at 565 nm, while the SI-PMMA-d8 fibre showed a loss of 20 dB/km at 680 nm. The chemical structures of the deuterated monomers are shown in Figure 2.3.

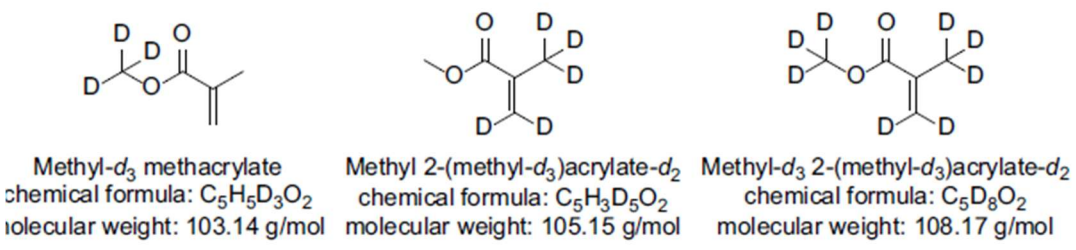

MMA-d3 MMA-d5 MMA-d8

Figure 2-3 Chemical structure of Deuterated monomers MMA-d3, MMA-d5 and MMA-d8 (D. Zaremba, 2017).

This fibre exhibits two additional loss windows: 25 dB/km at 780 nm and 50 dB/km at 850 nm. Although these POFs have reduced optical losses, their commercial use has been limited by significant water absorption and the high production cost.

Figure 2.4 illustrates the transmission loss spectra of PMMA and deuterated PMMA-d5/d8 step-index core fibres. Despite the advantages of deuterated SI-POFs made from PMMA-d5 or PMMA-d8, they were ultimately unsuccessful due to several drawbacks. First, the production of deuterated monomers requires expensive deuterated precursors, making them unsuitable for large-scale applications in the communication market. Second, deuterated fibres exhibit increased water absorption, which significantly raises attenuation.

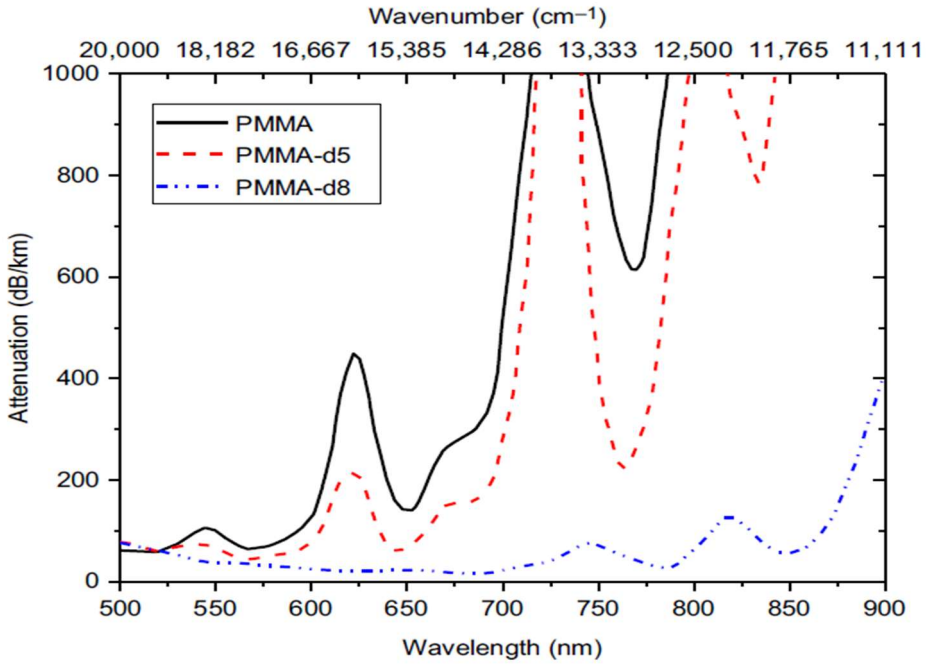

Figure 2-4: Transmission loss spectra of poly-methyl-methacrylate (PMMA) and deuterated PMMA-d5/d8 core fibres (D. Zaremba, 2017).

2.3.1.3 Polystyrene POF

Polystyrene (PS) POF is used in applications similar to those of PMMA POF. PS-based fibres are mechanically stronger than those made from PMMA, but they have higher attenuation. Typically, the core material is polystyrene, while the cladding is often PMMA. Both PMMA and PS core POFs are commonly used as step-index (SI) POFs for standard applications.

2.3.1.4 Polycarbonate POF

Polycarbonate (PC) is an engineering plastic known for its excellent mechanical properties and impact resistance. The main advantage of using PC for fibre cores lies in its balanced optical and mechanical properties. Its glass transition temperature (Tg ≈ 145°C) is higher than that of PMMA and PS, making it particularly suitable for high-temperature applications. However, PCs are fragile under significant deformation, and high humidity can accelerate their ageing process. PC core POF is primarily developed for industrial applications where high temperatures are a factor. A key drawback of PC-based POFs is their high optical attenuation.

2.3.1.5 Cyclic Transparent Optical Polymer (CYTOP)

CYTOP POF is a type of plastic optical fibre designed to suppress water vapour absorption. In CYTOP POF, fluorine replaces hydrogen in the core polymer, resulting in low attenuation—about 16 dB/km. Unlike deuterated or fluorinated POF, CYTOP POF effectively prevents moisture absorption, enhancing its performance. The chemical structure of CYTOP POF is shown in Figure 2.5.

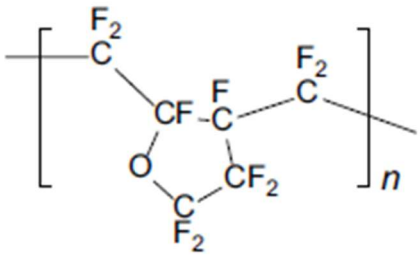

Figure 2-5: The chemical structure of the CYTOP POF (D. Zaremba, 2017).

CYTOP is a highly amorphous and transparent polymer with excellent thermal and chemical properties. Most commercially available graded-index plastic optical fibres (GI-POFs) made from CYTOP have a core diameter of 120 µm and a numerical aperture (NA) of 0.185. CYTOP-based GI-POFs exhibit an attenuation of 10 dB/km at 1000 nm, with a theoretical minimum of 0.7 dB/km.

2.3.1.6 Perfluorinated (Lucina) POF

Another type of POF is the Lucina POF (Panchuk et al., 2022). In Lucina POFs, both the core (n = 1.354, diameter = 120 µm) and the cladding (n = 1.342) are made from perfluorinated polymers, ensuring excellent adhesion between the layers. With a core diameter of 500 µm, Lucina POFs exhibit lower modal dispersion across the spectral range compared to PMMA-based POFs. In wavelengths below 1000 nm, the dispersion is even less pronounced compared to glass fibres. These perfluorinated POFs are suitable for transmission in the near-infrared range (850 to 1330 nm), achieving a transmission rate of approximately 1.2 Gb/s/km and an attenuation of 30 dB/km.

2.3.1.7 Other Polymer Types

Other materials used for POFs include chlorinated polymers, polystyrene (PS), and synthetic polymers such as cyclo-olefin copolymers (COC) and silicones (D. Zaremba, 2017). POFs come in various refractive-index profiles, including step-index (SI-POF), low-NA SI-POF, Double Step Index POF (DSI-POF), Multistep Index POF (MSI-POF), Graded Index POF (GI-POF), and semi-graded index profiles (semi-GI-POF). Multi-core plastic optical fibre cables, such as MC-SI-POF and MC-DSI-POF, are used in applications that require high data transmission and image-guiding. Table 2-1 summarises the key characteristics of these POF types.

2.3.2 Cladding Materials

The primary requirements for cladding materials include a low refractive index close to that of the core material and good film-forming ability (D. Zaremba, 2017). Cladding provides the core with enhanced mechanical and thermal resistance. Since the development of glass and polymer optical fibres, various cladding polymers have been introduced. Perfluoro and partially fluorinated polymers are commonly used for cladding but are unsuitable for the fibre core.

2.3.2.1 Fluoropolymers

Partly or fully fluorinated (perfluorinated) molecules reduce attenuation in POFs and are ideal for fibre cladding due to their low refractive indices (D. Zaremba, 2017). However, fully halogenated copolymers and perfluoropolymers are highly crystalline, leading to high optical losses caused by Rayleigh scattering. These polymers are also unsuitable for bulk polymerisation and exhibit high melt viscosity, which complicates fibre drawing. Thus, perfluoropolymers are not ideal core materials for POFs. The low refractive index of half-halogenated polymers makes it challenging to find compatible cladding materials, though they remain suitable for Step Index POFs.

In general, perfluorinated polymers are valued for their chemical resistance and improved electrical properties, which result from the shielding provided by the polymer chain. Though some perfluorinated and partially fluorinated polymers have been blended with other polymers for core material applications, most are used in claddings. Recent research has focused on amorphous cyclic perfluorinated polymers, with early examples including Teflon and CYTOP.

2.3.3 Jacket Material

The application and selection of a jacket or sheath play a key role in determining the final properties of polymer optical fibres (POFs). These properties, such as thermal and mechanical characteristics, are crucial for the long-term reliability of POFs. Materials like polyethene (PE), chlorinated PE, polyamide (PA), and polyvinyl chloride (PVC) are suitable for use as the jacket. This jacket improves the mechanical strength of the fibre during micro-bends and facilitates easier handling and transportation (Panchuk et al., 2022).

2.4 Fabrication Methods of POF

Plastic Optical Fibre (POF) is an optical fibre made from polymer materials, commonly used for short-distance communication, especially where flexibility and ease of handling are essential. The most common material for POF is PMMA (polymethyl methacrylate), though perfluorinated polymers are also used.

Table 2-1: Types of Plastic Optical Fibre (POF)

Material	Core Diameter (µm)	Wavelength (nm)	Attenuation (dB/Km)	Core / Cladding Refractive Indices	Numerical Aperture	Bandwidth (GHz/km)	Applications
PMMA (Polymethyl methacrylate)	200 - 1000	538	55	1.492 /1.417	0.47	0.003	LANs, Industrial Communication and Sensing
PS (Polystyrene)	500 - 1000	570	330	1.592 /1.416	0.73	0.0015	Industrial Short Haul Communication and Sensing
PC (Polycarbonate)	500 - 1000	670	600	1.582 /1.305	0.78	0.0015	Communication and Sensing
CYTOP (Cyclic Transparent Optical Polymer)	125 - 500	1310	16	1.353 /1.34	0.19	0.59 (GIPOF)	LANs
PCS (Plastic Clad Silica)	110 - 1000	820	5.6	1.46 / 1.41	0.4	0.005	Communication, Medical, Industrial and Sensing

2.4.1 Materials Preparation

The first step in POF fabrication is the selection of monomers. The core of the POF is typically made of PMMA, while the cladding is formed from a lower-refractive-index polymer, such as a fluorinated polymer. These monomers are polymerised through methods such as bulk, solution, or suspension polymerisation.

2.4.2 Preform Fabrication

There are three primary methods for pre-form fabrication. The most common is the Rod-in-Tube method, where a rod of core material is inserted into a tube of cladding material (Silvio Abrate, 2013). The second method is the Casting Method, where the core material is cast into a mould, followed by casting the cladding material around it. The final method is co-extrusion, in which both core and cladding materials are extruded simultaneously to form the preform.

2.4.3 POF Manufacturing Process

POF can be manufactured using either the preform-drawing or extrusion process.

2.4.3.1 Drawing Process

In the drawing process, shown in Figure 2.6, the preform is heated to a carefully controlled drawing temperature to prevent polymer degradation. Once heated, the preform is drawn into a fibre by pulling it through a furnace at a speed of about 0.5 m/s (Silvio Abrate, 2013). The drawing speed and temperature control the fibre's diameter. After drawing, the POF is cooled to retain its shape and structural integrity.

2.4.3.2 Manufacturing by Extrusion

The extrusion process for producing POF begins with the monomer, which is first distilled and then placed into a reactor along with an initiator and a polymerisation controller (Silvio Abrate, 2013). After polymerisation at around 150°C, the polymer is pushed through a nozzle using pressurised nitrogen, which helps control the core diameter. The cladding is then extruded over the core at approximately 200°C. Extrusion is a simple and cost-effective method for manufacturing PMMA-SI-POF.

2.4.3.3 Surface Coating and Curing

After the fibre drawing process, a protective coating is applied to the POF surface to improve its mechanical strength and protect it from environmental factors (Silvio Abrate, 2013). The coating is then cured (hardened) using either UV or thermal curing methods.

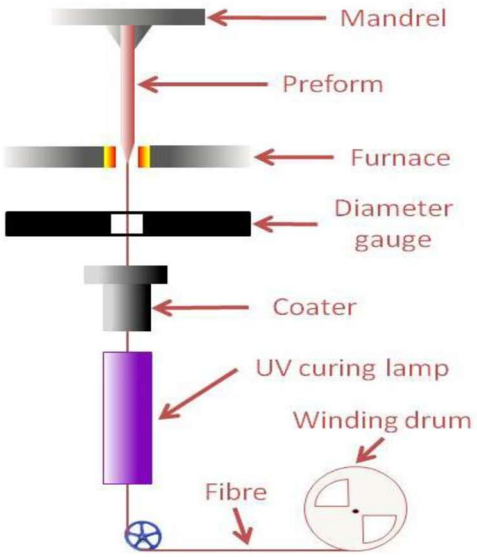

Figure 2-6: POF manufacturing by fibre drawing (Silvio Abrate, 2013)

2.4.3.4 Quality Control and Testing

The final stage of the manufacturing process involves dimensional control, during which the fibre diameter and uniformity are continuously monitored (Silvio Abrate, 2013). Optical testing follows, during which the optical properties, such as attenuation and bandwidth, are measured. Finally, mechanical testing evaluates the fibre's strength, flexibility, and durability. These steps ensure that the final POF meets the required optical and mechanical properties for various applications.

2.5 POF Mechanical Characteristics and Properties

2.5.1 Temperature coefficient, Young's Modulus and water absorption

Unlike silica glass fibres (Jamshid Heidarialamdarloo, 2018), PMMA has a significantly larger negative thermo-optic coefficient, a lower Young's modulus of elasticity, high water absorption, and biological compatibility. The Young's modulus of plastic optical fibre is nearly half that of silica fibre. Due to its flexibility, the minimum bend radius of POFs is smaller than that of silica glass fibres, allowing PMMA POF to be installed in places where silica glass fibres cannot. On the other hand, plastic is more ductile and less rigid than silica, making it more resistant to mechanical shock (Jamshid Heidarialamdarloo, 2018). Polycarbonate POFs exhibit mechanical properties similar to PMMA fibres, and these mechanical properties directly influence the transmission rate through POF.

2.5.2 POF Ageing and Non-Mechanical Load

Organic polymers (D. Zaremba, 2017) are susceptible to ageing effects, which can reduce the optical and mechanical performance of POF. These processes damage the polymer's backbone chain and side groups. Factors such as thermal load, humidity, and radiation can accelerate degradation. Degradation can lead to polymer chain scissoring, plasticization of the matrix, differential swelling, and embrittlement of the macromolecules. In addition, osmotic cracks and hydrothermal shocks may occur, further degrading the material in rapidly changing environmental conditions.

2.5.3 Effect of Temperature and Humidity

Ageing due to temperature and humidity can lead to long-term degradation of polymers. Studies (D. Zaremba, 2017) show that humid environments accelerate degradation. Water reduces the glass transition temperature, accelerating degradation at that temperature.

A key limitation of POFs is their temperature sensitivity, as they can only operate up to 80-100°C. Beyond 100°C, POFs begin to lose transparency and rigidity. However, with special cross-linked polyethene or polyolefin elastomer jackets, POFs can withstand temperatures up to 135°C.

Moisture levels also affect POF performance, although fluorinated plastic fibres show minimal changes in attenuation due to moisture, as they do not absorb water. Nonetheless, POFs have a limited lifespan in optical transmission links and are highly dependent on temperature and humidity. Careful selection of cladding and coating materials is crucial, as oxygen and water can diffuse into the polymer core, accelerating material degradation.

2.6 POF Refractive Index Distribution

Plastic optical fibres are classified into two types based on their refractive index distribution: step-index (SI) fibres and graded-index (GI) fibres. A step-index POF has a core with a uniform refractive index surrounded by a cladding of a lower refractive index. The core diameter typically ranges from 250 to 980 µm, with 980 µm being the most common. In a graded-index POF, the refractive index of the core decreases from the centre, while the cladding refractive index remains constant. Both step-index and graded-index POFs serve as the foundation for other index profiles.

2.6.1 Step Index POF

A step-index POF consists of a core with a uniform refractive index, surrounded by a thin cladding with a slightly lower refractive index. Unlike graded-index fibres (Jamshid Heidarialamdarloo, 2018), the change in refractive index at the core-cladding boundary is abrupt. As an optical waveguide, the fibre supports one or more confined transverse modes for light propagation. Light rays travel along different paths, or modes, within the fibre. While some rays move in straight lines through the core, most follow a zigzag path due to total internal reflections at the core-cladding interface, as shown in Fig. 2.7. As a result, the distance each light ray travels and the corresponding transit times vary. These differences in transit time cause dispersion, resulting in broadened light pulses, as illustrated in Fig. 2.8.

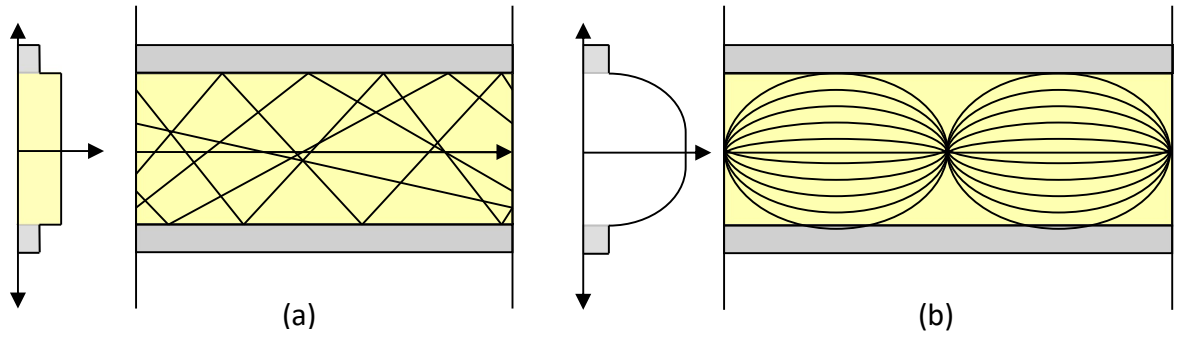

Figure 2-7: Transmission through the (a) step-index (SI) POF and (b) graded Index (GI) POF. (Jamshid Heidarialamdarloo, 2018)

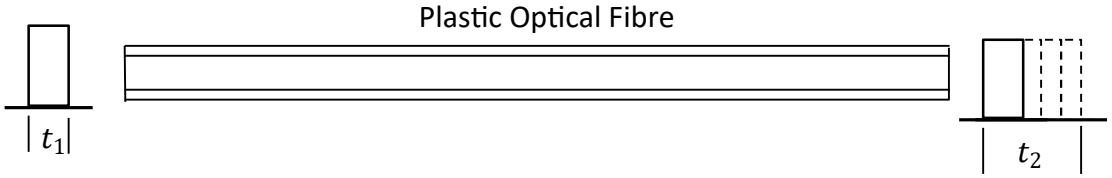

Figure 2-8: Dispersion in step-index POF

2.6.2 Graded Index POF

The profile of a graded-index (GI) fibre differs from that of a step-index fibre. While the cladding has a constant refractive index, the core's refractive index varies with distance from its centre, forming a parabolic index profile. The refractive index is highest at the centre and gradually decreases towards the core-cladding interface (Panchuk et al., 2022).

Optical rays travelling through the core's centre, where the refractive index is higher, cover shorter distances but move at lower velocities. In contrast, light rays near the core-cladding interface, where the refractive index is lower, travel longer distances at higher velocities. Rays that do not travel through the core's centre follow a sinusoidal path due to refraction within the graded-index profile.

A well-chosen profile exponent can help compensate for these transit-time differences, with an exponent of 2 ideal for minimising chromatic dispersion.

Research in GI POF is progressing rapidly. For example, Azusa Inque (2019) developed GI POF with strong mode coupling and low scattering loss, a feature closely tied to specific microscopic heterogeneities in the core material. This mode coupling significantly reduces reflection noise, enhancing transmission quality compared to silica-based GI multi-mode fibres (MMF) for lengths under 30 m. Such fibres are particularly suitable for domestic applications. However, since GI POF is beyond the scope of this research, it will not be discussed further.

2.7 Principle of Optical Propagation in POF

There are two ways of describing light propagation (Wave/ Particle duality). Firstly, light can be defined as a stream of particles called photons. Each photon carries energy given by the formula (M. Beckers, 2017):

$$E = h \times f \quad \text{Joules (J)} \tag{2.1}$$

Where: E is the photon energy in Joules.

h is the Plank's constant (6.62×10^{-34}Js).

f is the frequency of the light.

Solving Maxwell's equations would fully describe the characteristics of an optical fibre, but this is beyond the scope of this thesis. Nevertheless, the approximations from geometrical optics are sufficient to provide an overview of how an optical fibre functions.

2.7.1 Snell's Law, Critical Angle and Total Internal Reflection (TIR)

Light can also be defined as an electromagnetic wave with a particular frequency, whose speed is reduced when it propagates through a medium such as plastic. The term refractive index (n) of a medium expresses the ratio of the velocity of light in vacuum (c_v) to the velocity of light in that medium (c_m) and is calculated as (Appajaiah, 2005):

$$n = \frac{c_v}{c_m} \qquad 2.2$$

The relationship between the wavelength, velocity of light and the frequency is given by the formula given below (Appajaiah, 2005):

$$c = f \times \lambda \qquad 2.3$$

From Eqn. 2.1 and 2.3, it is evident that in the propagation of an electromagnetic wave, the frequency (*f*) and energy (E) remain unaltered, but the speed and the wavelength of light passing through the medium will change.

Snell's Law of Refraction states that when light propagates from a medium with a lower refractive index (n_1) to a medium with a higher refractive index (n_2) (an optically denser material) at an angle θ_1, most of the optical energy will be refracted towards the normal (the axis of incidence) at an angle θ_2. As shown in Fig. 2.9, the remaining optical energy will be reflected at the interface of the two materials within the high-refractive-index medium. When light rays travel from a medium of high refractive index to a medium of low refractive index, they are refracted away from the normal.

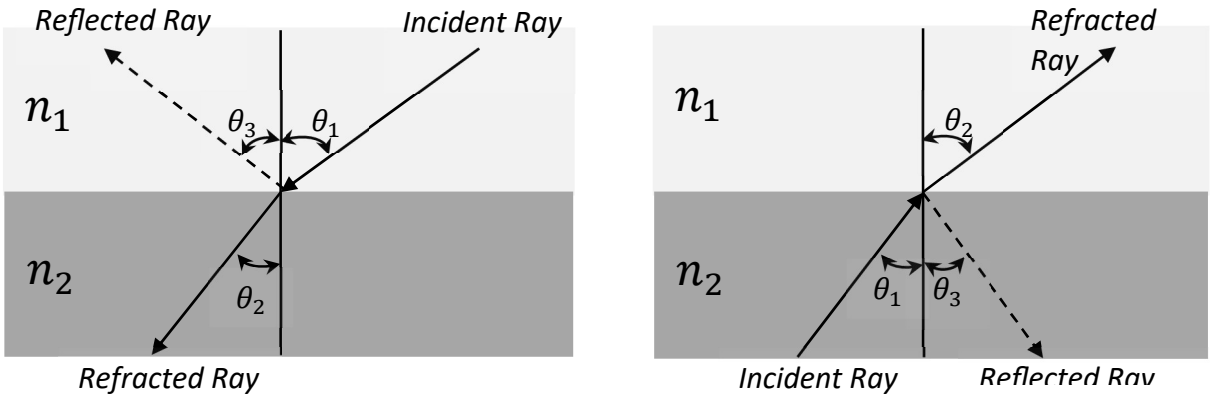

Figure 2-9: Refracted and reflected light rays. (M. Beckers, 2017)

Refraction is expressed as (M. Beckers, 2017):

$$\frac{\text{Sin } \theta_1}{\text{Sin } \theta_2} = \frac{n_2}{n_1} \qquad 2.4$$

Where: n_1 is the refractive index of an optically dense medium.

n_2 is the refractive index of an optically less dense medium.

If the angle of incidence (θ_I) is continuously increased, a point will be reached where the light rays will no longer be refracted into the other material but instead will be refracted at an angle of 90°, causing them to propagate along the interface of the two materials, as illustrated in Fig.2.10(a). At this point, the angle of incidence is known as the critical angle.

If the angle of incidence is increased beyond 90°, all the light is reflected, a phenomenon known as total internal reflection (TIR), as shown in Fig. 2.10(b).

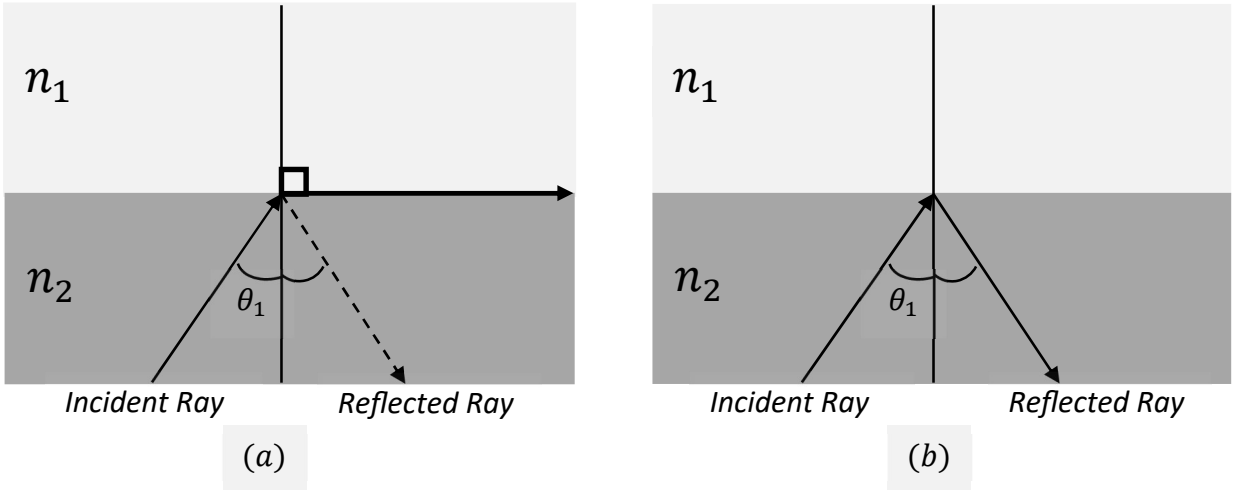

Figure 2-10: Critical angle and total internal reflection (M. Beckers, 2017).

For the boundary case of total reflection, the angle of refraction θ_2 will be equal to 90^0; the following applies:

$$\frac{\text{Sin } \theta_1}{\text{Sin } 90^0} = \frac{n_2}{n_1} \qquad 2.5$$

$$\text{Sin } \theta_{critical} = \frac{n_2}{n_1} \qquad 2.6$$

$$\theta_{critical} = \text{Arcsin } \frac{n_2}{n_1} \qquad 2.7$$

2.7.2 Numerical Aperture

The critical parameter (Jamshid Heidarialamdarloo, 2018) of optical fibre is its acceptance angle, or numerical aperture (NA), which is determined by two indices. The sine of the critical angle $\theta_{critical}$ is called the numerical aperture (NA) (Jamshid Heidarialamdarloo, 2018):

$$NA = Sin\theta_{critical} = \sqrt{n_2^2 - n_1^2} \quad 2.8$$

The manufacturer's datasheet always stipulates the optical fibre's numerical aperture (NA). The launching angle at the air fibre core interface is known as the acceptance angle and double the acceptance angle is called the aperture angle.

The numerical aperture can also be calculated using the relative refractive index difference $n_2 - n_1$, as follows (Jamshid Heidarialamdarloo, 2018):

$$NA = Sin\theta_{critical} = n_2\sqrt{2(n_2 - n_1)} \quad 2.9$$

In a step-index plastic optical fibre (POF), the numerical aperture (NA) depends solely on the difference in refractive indices between the core and cladding materials and remains constant along the entire length of the fibre. The NA is a crucial parameter for POFs (Jamshid Heidarialamdarloo, 2018) as it determines the fibre's ability to accept and guide optical energy. A higher NA means the fibre can accept more optical energy.

Typical POFs exhibit a much higher NA (approximately 0.5) compared to silica glass fibres. While a higher NA allows more optical energy, lowering the NA can improve transmission speeds and bandwidth. This is because reducing the NA reduces the number of modes propagating through the fibre, thereby reducing modal dispersion. Less modal dispersion leads to higher bandwidth.

Optical sources and detectors also have numerical apertures, which depend on their emission and reception angles. For efficient power coupling into the optical fibre, it's essential to match the POF's NA to that of the light source. The same principle applies when coupling optical energy from the fibre to a detector: the NA of the POF should match the NA of the detector.

One key advantage of POFs over silica glass fibres is their larger core diameter and NA. This makes coupling light into POFs easier and more cost-effective.

2.8 Modes in a Step Index POF

Light propagating through a POF can follow various paths, as illustrated in Fig. 2.11. Radiation modes are those that radiate from the core into the cladding when the angle of total internal reflection (TIR) is exceeded. These modes do not participate in signal transmission and are challenging to quantify. Cladding modes, on the other hand, occur when optical rays are reflected at the cladding interface and its surrounding medium (e.g., air), provided the surrounding medium has a lower refractive index than the cladding. In practical POFs, the cladding is typically enclosed in an absorbing jacket made of polyethene, polyvinyl chloride (PVC), or chlorinated polyethene, which reduces the likelihood of cladding modes.

In a multi-mode fibre (Naji Ali, 2017), higher-order modes propagate at steep angles close to the critical angle, while lower-order modes propagate at shallow, grazing angles. Both higher-order and lower-order modes are measurable.

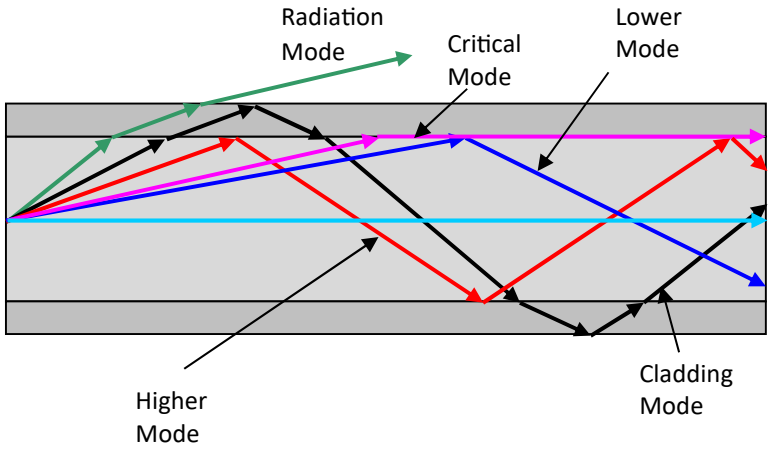

Figure 2-11: The propagation modes in a step-index plastic optical fibre (A. Bunge, 2017).

The wavelength of light determines the number of modes propagating through a plastic optical fibre. Each wavelength from a broad-spectrum source, such as an LED, generates these modes. Within the POF, the modes can be classified as meridional and skew modes. Guided meridional modes propagate through the fibre, crossing its axis, while skew modes do not cross the axis and instead follow screw-like paths, losing energy to the cladding.

2.8.1 Meridional Modes

In meridional modes (Fig. 2.10a), the incident light rays lie within the same plane and pass through the axis of the plastic optical fibre. The numerical aperture specification accounts for these meridional modes. The path length travelled by the meridional rays is given by (Keiser G. , 2003):

$$\text{Propagation Length} = \frac{\text{Fibre Length}}{\text{Cos } \beta} \qquad 2.10$$

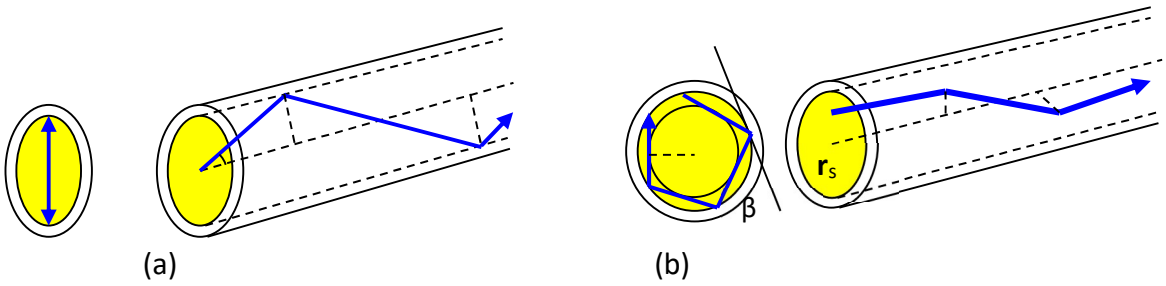

Figure 2-12: (a) Meridional ray transmission, and (b) Skew ray transmissions (A. Bunge, 2017).

2.8.2 Skew Modes

In certain conditions, some rays propagate through the plastic optical fibre in a screw-like path without ever crossing the fibre's axis. These skew modes are considered leaky waves because they transfer energy to the cladding. Despite this energy loss, skew modes can still be measured over considerable distances (several tens of meters) in plastic optical fibre. They influence both measurement techniques and the transmission process. As illustrated in Fig. 2.10(b), skew modes propagate in screw-like paths and form an angle greater than 90° with the tangential plane at the core/cladding interface. Their projection onto the cross-sectional area resembles a polygonal line, indicating that these rays do not cross a circular region of radius $\mathbf{r_s}$ around the axis.

2.8.3 The V-Parameter and Number of Modes in POF

David R. Gozzard (2022) noted that the number of propagation modes supported by a step-index fibre is related to the dimensionless V-parameter. The V-parameter determines the number of modes transmitted in a plastic optical fibre and is calculated from the numerical aperture (NA), the wavelength λ, and the plastic optical fibre core radius α (A. Bunge, 2017)

.

$$V = \frac{2\pi\alpha}{\lambda} \text{ x NA} \tag{2.11}$$

$$V = \frac{2\pi\alpha}{\lambda} \sqrt{n_{core}^2 - n_{cladding}^2} \tag{2.12}$$

Where: V is the V-parameter

α is the core radius.

λ is the wavelength.

NA is the numerical aperture.

n_{core} is the refractive index of the core material.

$n_{cladding}$ is the refractive index of the cladding material.

Only one mode propagates in an optical fibre if the V-parameter is less than 2.405; otherwise, multi-mode propagation will occur. The number of guided modes that will propagate along the fibre can be approximated to be (A. Bunge, 2017):

$$N = \frac{V^2}{2}\left[\frac{g}{g+2}\right] \tag{2.13}$$

Where g is the profile exponent

For step-index profiles $g \to \infty$

Therefore $N = {}^{V^2}/_{2}$ (Step index optical fibre) 2.14

For graded-index profile $g \to 2$:

Therefore $N = {}^{V^2}/_{4}$ (Graded Index optical fibre) 2.15

2.8.4 Calculation of the Wavelength V- Parameter

In this research project, the EskaTM CK-40 plastic optical fibre was used to illustrate the calculation of the number of modes a particular POF can carry. EskaTM CK-40 plastic optical fibre has a core diameter of 0.98mm, a core refractive index (η) of 1.49, and a numerical aperture of 0.5. The colour wavelengths of interest in this research are as follows:

- Red wavelength (λ_R) = 650 nm
- Yellow wavelength (λ_Y) = 560 nm
- Green wavelength (λ_G) = 520 nm
- Blue wavelength (λ_B) = 475 nm

Using Eqn. 2.11, the V-parameter and the number of modes per wavelength can be calculated as follows:

$$V_R = \left[\frac{2x\pi x0.49x10^{-3}}{650x10^{-9}}\right]x0.5$$

$$= \underline{\underline{2368.277539}}$$

$$V_Y = \left[\frac{2x\pi x0.49x10^{-3}}{560x10^{-9}}\right]x0.5$$

$$= \underline{\underline{2748.893572}}$$

$$V_G = \left[\frac{2x\pi x0.49x10^{-3}}{520x10^{-9}}\right]x0.5$$

$$= \underline{\underline{2960.346924}}$$

$$V_B = \left[\frac{2x\pi x0.49x10^{-3}}{475x10^{-9}}\right]x0.5$$

$$= \underline{\underline{3240.800843}}$$

2.8.5 Calculation of the Number of Modes in the Plastic Optical Fibre

Calculating the number of modes per wavelength can employ equation 2-143 above and the V-parameter figure calculated in this chapter's subsection 2.8.4 above. As given in equation 2-14, the number of guided modes that will propagate along the fibre is approximately:

$$N \approx V^2/2 \qquad \text{(Step index optical fibre)}$$

Therefore, the number of modes for the red colour (650 nm) wavelength:

$$N_R \approx {2369.277539^2}/{2}$$

$$N_R \approx 2806738$$

The number of modes for the yellow colour (560 nm) wavelength:

$$N_Y \approx {2748.893572^2}/{2}$$

$$N_Y \approx 377827$$

The number of modes for the green colour (520 nm) wavelength:

$$N_G \approx {2960.346924^2}/{2}$$

$$N_G \approx 4381827$$

The number of modes for the blue colour (470 nm) wavelength:

$$N_B \approx {3240.800843^2}/{2}$$

$$N_B \approx 5251395$$

Table 2-2: The V-parameter and the number of modes in the plastic optical fibre

Wavelength (nm)	V-Parameter	Number of Modes
650 Red (λ_R)	2368	2806738
560 Yellow (λ_Y)	2749	3778271
520 Green (λ_G)	2960	4381827
470 Blue (λ_B)	3240	5251395

Table 2-1 demonstrates that the V-parameter and the number of modes propagating through the POF increase as the wavelength decreases. Specifically, the red wavelength (650 nm) corresponds to the lowest V-parameter and the fewest number of modes, while the blue wavelength (470 nm) corresponds to the highest V-parameter and the greatest number of transmitted modes.

2.8.6 Single Mode and Multi-Mode Plastic Optical Fibre

Plastic optical fibres can be classified into two categories based on propagation: single-mode optical fibres and multi-mode optical fibres. The optical fibres discussed so far are multi-mode, where light rays travel along multiple paths within the POF.

According to Jamshid Heidarialamdarloo (2018), a single-mode fibre (SMF) supports only one propagation mode per polarisation direction for a given wavelength. In an SMF, light travels along the core axis, eliminating intermodal dispersion. This absence of intermodal dispersion increases bandwidth by preventing pulse broadening caused by different optical paths, making SMFs ideal for data communication.

The standard single-mode fibre used in telecommunications is the SMF-28E. It has a narrow core diameter of about 9 µm, a cladding diameter of 125 µm, and operates over a wavelength range of 1310 nm to 1625 nm. Typical optical attenuation for SMFs is about 0.2 dB/km at 1550 nm and 0.35 dB/km at 1310 nm. The low attenuation, combined with optical amplifiers, enables long-haul transmission, making SMFs suitable for high-bandwidth applications such as intercontinental data transmission. However, SMF-POF lacks some key advantages of POFs, such as ease of installation and low cost of connecting elements, such as connectors.

2.9 Plastic Optical Fibre Transmission (Attenuation) Windows

In a step-index plastic optical fibre, minimum attenuation occurs in certain regions of the visible and near-infrared spectrum, known as the transmission (attenuation) windows, as shown in Fig. 2.13. These windows correspond to wavelengths of 470 nm (Blue), 520 nm (Green), 570 nm (Yellow), and 650 nm (Red). Outside these attenuation windows, POFs exhibit high attenuation due to modal dispersion.

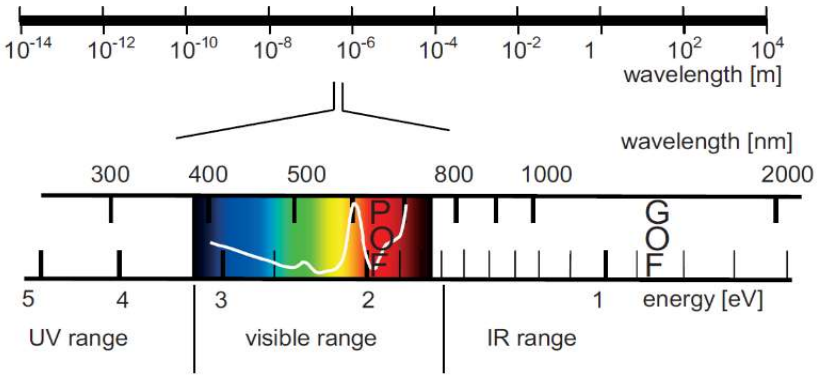

(a)

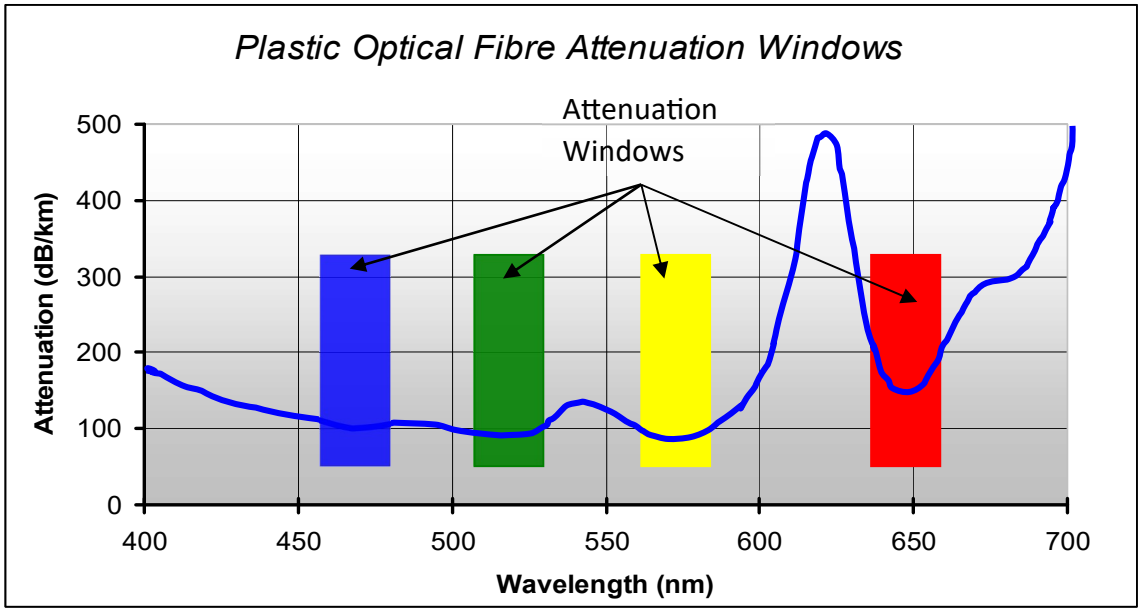

(b)

Figure 2-13: (a) Electromagnetic spectrum showing the visible range in which the plastic optical fibre operates, and (b) the plastic optical fibre attenuation windows (Ziemann, 2014).

2.10 Step Index PMMA POF Transmission Characteristics and Loss Mechanisms

This section explores the properties of step-index POF and their impact on light propagation. These properties include attenuation, dispersion, bending radius, coupling loss, mode coupling, and mode conversion.

2.10.1 Attenuation

In any optical fibre cable, light travelling along the fibre experiences attenuation, or power loss. This power loss increases with the distance the light travels through the fibre. The core diameter also influences attenuation; a smaller core diameter results in higher attenuation. This is due to geometrical and structural imperfections that become more pronounced with smaller diameters. Manufacturing smaller POFs is more challenging due to greater thermal gradients, leading to more imperfections.

Additionally, light rays strike the core-cladding interface more frequently in smaller diameters, where imperfections are more common. Attenuation also depends on the spectral width and the numerical aperture (NA) of the light source; increases in either lead to higher attenuation. Plastic optical fibres act as low-pass filters, with attenuation being more significant at higher light frequencies.

2.10.1.1 Goos-Hänchen shift effect

The Goos-Hänchen shift occurs at the core/cladding interface due to total internal reflection. Some of the electromagnetic field escapes into the cladding at a distance determined by the wavelength. This shift causes the reflected ray to slightly penetrate the core-cladding interface, increasing cladding attenuation. As illustrated in Fig. 2.14, the Goos-Hänchen shift effect contributes to higher attenuation and power loss in plastic optical fibres. Attenuation mechanisms in POFs involve a combination of intrinsic and extrinsic factors.

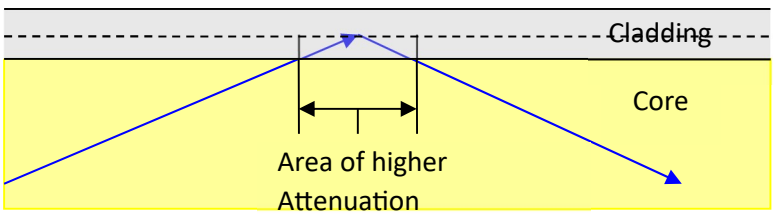

Figure 2-14: Goos-Hänchen shift (Ziemann, 2014).

2.10.1.2 Intrinsic Factors

Intrinsic factors affecting attenuation include Rayleigh scattering and absorption by the constituent materials.

- *Rayleigh Scattering:* This scattering occurs due to fluctuations in composition, orientation, and density within the core and cladding of the plastic optical fibre. These microscopic non-uniformities cause optical energy to scatter as it propagates, leading to a loss of some of it. Geometrical and structural imperfections, such as changes in diameter, core index profile, bubbles, cracks, dust, and defects at the core-cladding interface influence Rayleigh scattering. This type of scattering loss is roughly independent of wavelength.
- *Absorption:* Absorption is caused by electronic transitions within molecular bonds and impurities in the PMMA material (molecular vibrational absorption). These impurities absorb light energy and convert it into a small amount of heat. Because Rayleigh scattering and absorption depend on the fibre's composition, they cannot be eliminated through the manufacturing process.

2.10.1.3 Extrinsic Factors

Extrinsic factors are losses that do not occur in an ideal plastic optical fibre and include:

- *Absorption by Contaminants:* Organic and metallic pollutants (e.g., nickel, cobalt, chromium, manganese, and iron) can increase absorption. Contaminants are often introduced during the manufacturing process, making their presence unavoidable.
- *Environmental Effects:* Losses can also arise from environmental factors, such as dust particles, microfractures, bubbles, and other structural imperfections that occur during manufacturing.
- *Radiation Losses:* These losses are due to physical micro-bends, macro-bends, and other structural imperfections in the fibre.

As light travels through an optical fibre of length L, its power decreases exponentially due to attenuation. Attenuation is a non-dimensional variable (Jamshid Heidarialamdarloo, 2018), and the following equation applies to optical power (Jamshid Heidarialamdarloo, 2018):

$$P_L = P_o \times e^{-\alpha' L} \quad 2.16$$

In logarithmic terms, the optical power at a distance L can be calculated as follows:

$$P_L = P_{in} \times 10^{-\frac{\alpha' L}{10}} \quad 2.17$$

Where: P_L is the power of light at length L

P_{in} is the power of light at the front of the optical fibre.

α' is the attenuation coefficient in km^{-1}

The attenuation coefficient of the optical fibre expresses the attenuation value as a function of the fibre length. Attenuation can be logarithmically expressed as follows (Yau et al. (2022)):

$$A = \frac{10}{L} \text{Log} \frac{P_o}{P_L} = 4.343\alpha' \quad 2.18$$

As stated by Isaac N. Osahon (2018), attenuation in plastic optical fibres is both wavelength- and mode-dependent. For step-index POF (SI-POF), the attenuation at a wavelength of 650 nm can be as high as 0.15 dB/m. The path difference between rays travelling parallel to the axis and those travelling at angles close to the critical angle for total internal reflection can become significant. Consequently, attenuation will be greater for rays that experience multiple reflections within the fibre.

In plastic optical fibres, the wavelength range of interest is in the visible spectrum, between 450 nm and 650 nm, due to relatively low attenuation in this range, as shown in Fig. 2.13. The lowest attenuation occurs at wavelengths of 470 nm (Blue), 520 nm (Green), 560 nm (Yellow), and 650 nm (Red). Fluorinated polymers used as cladding for PMMA fibres contribute significantly to mode-dependent attenuation, with attenuation values reaching 10,000 dB/km.

2.10.1.4 Dispersion and Bandwidth

Dispersion refers to the broadening of light pulses caused by differences in transit times among various core modes as light travels through the fibre. In step-index POF

transmission, dispersion limits both the transmission bandwidth and data rate. In a multi-mode fibre (Naji Ali, 2017), higher-order modes propagate at angles close to the critical angle, while lower-order modes travel at more shallow angles. The differential path lengths cause lower-order modes to exit the fibre before higher-order modes, resulting in pulse broadening. The time delay spread, or modal dispersion, can be determined using Equation 2.19.

For step-index POF, the data rate is limited to 100 Mb/s over 100 meters. The standard numerical aperture (NA) for PMMA SI-POF is 0.5, and the maximum operating temperature ranges from +70°C to 85°C. Modifying the refractive index profile can enhance bandwidth and data rates.

Three types of dispersion affect optical fibres:

- Mode Dispersion: Caused by different paths taken by light modes within the fibre.
- Chromatic Dispersion: Wavelength-dependent dispersion.
- Polarisation Mode Dispersion: Dispersion caused by polarisation effects.

When an optical ray propagates parallel to the fibre axis, the distance L_0 covered is minimal. In contrast, if the ray makes the complementary critical angle θ_c with the axis, the distance is maximised. The difference in time at which the two rays reach the end of the fibre is given by (Agrawal, 2021):

$$\Delta t = t_2 - t_1 = \frac{n_{co}}{c} L_0 \left[\frac{1}{\text{Sin } \theta_c} - 1\right] \qquad 2.19$$

Where: Δt is the time difference.

c is the speed of light

θ_c is the critical angle.

n_{co} is the refractive index of the core material.

L_0 length of the POF

Chromatic dispersion includes material dispersion and waveguide dispersion.

- *Material Dispersion:* This occurs due to the light source's spectral width. For example, an LED has a broader spectral width than a laser diode, leading to greater material dispersion. This type of dispersion happens because the refractive index of a material varies with wavelength. Consequently, different components of the light spectrum travel at different speeds, leading to pulse broadening.
- *Waveguide Dispersion:* This type of dispersion is generally less significant in fibres that support many modes, such as plastic optical fibres (POFs). It arises from the interaction between the wavelength and the core radius, affecting the propagation speed of each mode.

2.10.1.5 Bending Radius and Loss

The manufacturer-specified bending radius is crucial for determining attenuation at different radii and identifying the point at which attenuation increases irreversibly. Macro bends occur during POF installation. With slight curvature, losses are minimal. However, as the bending radius decreases, radiation losses increase. For the same diameter, these losses are typically higher in glass optical fibres compared to step-index POFs.

Optical power decays exponentially with decreasing bending radius. Key parameters affecting bending sensitivity include fibre diameter, bending radius, light wavelength, and numerical aperture (NA). A larger NA means that the permissible bending radius is narrower relative to the fibre diameter. The NA is the sine of the acceptance angle, which defines the maximum angle at which light can be guided through the fibre.

A higher NA facilitates easier light launching into the fibre, reduces additional losses at fibre bends, and increases mode dispersion. Since bandwidth is proportional to the fibre's NA, reducing the NA can increase transmission capacity. However, a lower NA also increases bending sensitivity.

2.10.1.6 Mode Coupling and Mode Conversion

Mode coupling refers to the transfer of optical energy from one propagation mode to others at scattering centres, leading to attenuation. This phenomenon primarily occurs at the core/cladding interface. It is challenging to create an ideal surface at the sub-

nanometre scale, especially with larger polymer molecules involved. Irregularities and non-homogeneities in the fibre contribute to mode coupling, leading to significant energy transfer between adjacent modes.

This energy interchange results in considerable power loss and increased bandwidth. The distance over which mode interchange is complete is known as the equilibrium or coupling length. The modal distribution at this distance is called the equilibrium modal distribution (EMD).

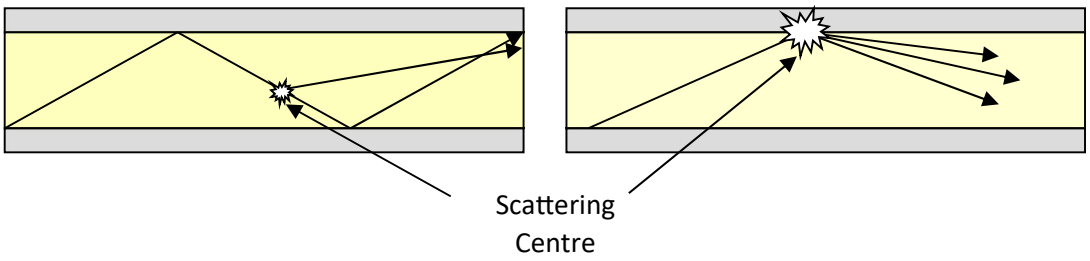

Figure 2-15: Mode coupling (Ziemann, 2014)

Mode coupling, as illustrated in Fig. 2.16, depends on the propagation angle and affects the bandwidth of a fibre. When collimated light is launched into the fibre, energy is gradually transferred to modes with larger angles. As a result, higher-angle modes contribute to mode dispersion, thereby reducing the fibre's overall bandwidth.

Mode conversion is a specific type of mode coupling that occurs at the core/cladding interface. It is influenced by microbends, which arise from fluctuations in the refractive-index difference within the fibre.

2.11 Techniques to mitigate against modal dispersion

Modal dispersion is a significant limitation of step-index POF (SI-POF), restricting the link bandwidth to approximately 40 MHz over 100 meters. To enhance the bandwidth-length product, recent research has focused on reducing modal dispersion by experimenting with different polymer materials.

In their work, Naji Ali (2017) proposed a method to mitigate modal dispersion in standard 1 mm SI-POF by reducing the fibre's effective numerical aperture. This technique involves using a spatial mode filter made from a polycarbonate capillary tube. Naji Ali

(2017) experimentally demonstrated error-free 1 Gb/s non-return-to-zero (NRZ) transmission over 30 meters of SI-POF.

Yau et al. (2022) showed, through link modelling, that improving the bandwidth-length product involves minimising modal dispersion per unit length. They identified optimal core and cladding materials with refractive indices of 1.4865 and 1.4756, respectively, yielding a minimum dispersion of 36.169 ps/m. With these materials, the bandwidth was improved to 121.65 MHz over 100 meters of SI-POF. This represents an approximately 80 MHz increase in bandwidth compared to the standard SI-POF, which is limited to about 40 MHz over the same length due to modal dispersion.

The total dispersion is estimated for an SI-POF with the length L, as shown in equation 2-20 (Yau et al. (2022)).

$$\Delta\tau_{max} = \frac{L(NA)^2}{2c_0 n_{core}} \tag{2.20}$$

The bandwidth, *BW,* is estimated as follows:

$$BW = \frac{0.44}{\Delta\tau_{max}} \tag{2.21}$$

Substituting equation 2-20 into equation 2-21 yields:

$$BW = \frac{0.88c_0 n_{core}}{L(NA)^2} \tag{2.22}$$

In Equation 2.22, Yau, et al (2022) illustrated that the bandwidth is inversely proportional to the length of the fibre; hence, the quality of the fibre can be characterised by the bandwidth-length product and presented as follows:

$$BW \times L = \frac{0.88c_0 n_{core}}{(NA)^2} \tag{2.23}$$

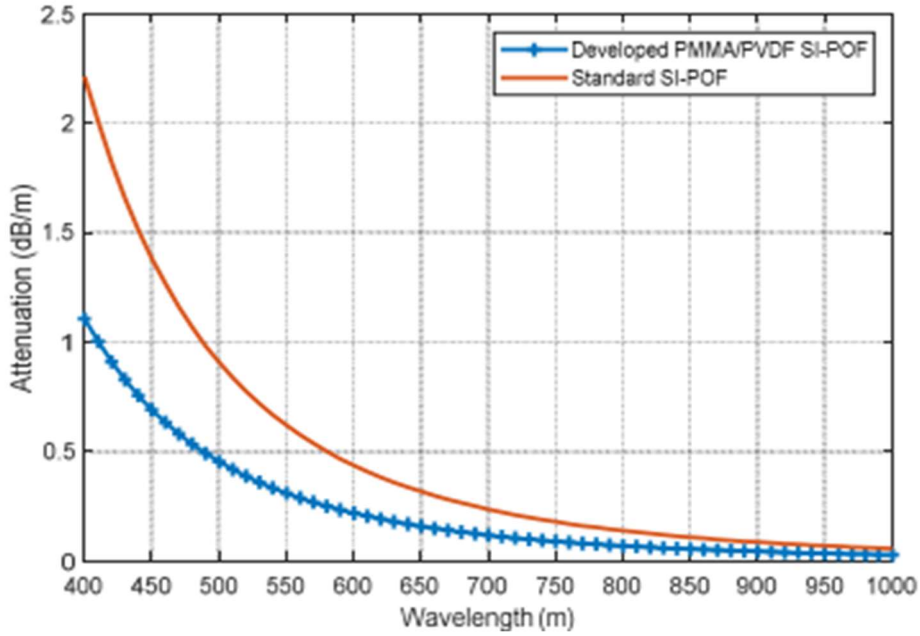

Figure 2-16: Attenuation graphs showing the improved performance of the developed SI-POF compared to the standard SI-POF (Yau, et al. 2022).

Equations 2.20 and 2.21 illustrate that reducing the numerical aperture (NA) by a factor of two decreases dispersion by a factor of four and improves the bandwidth-length product by the same factor. Additionally, a reduction in NA occurs if the refractive index difference between the core and cladding materials is minimised. According to Yau et al. (2022), a lower NA leads to a higher bandwidth-length product, but this benefit comes with drawbacks, such as a smaller acceptance angle, stricter coupling and adjustment requirements, and potentially increased sensitivity to bending losses.

Naji Ali (2017) discussed several techniques to increase data rates in both the electrical and optical domains. Electrical domain techniques include modulation and equalisation methods such as multilevel pulse amplitude modulation (M-PAM), multi-carrier orthogonal frequency-division multiplexing (OFDM), and both fixed and adaptive equalisation. In the optical domain, wavelength-division multiplexing (WDM) and spatial filtering techniques, such as restricted mode launching and high-sensitivity photodetectors with small active areas, have proven effective. Electrical solutions often involve complex signal processing and high fabrication costs.

2.12 POF Frequency Response and Bandwidth

The bandwidth of plastic optical fibre (POF) communication is related to distance, as shown in Eqn. 2.22. As the length of the POF cable increases, factors affecting bandwidth also increase. Increased modal dispersion broadens the pulse width, leading to greater inter-symbol interference and a reduction in the maximum data transmission rate.

Higher-order modes experience more attenuation and mode mixing, primarily due to imperfections at the core-cladding interface. This results in the evolution of equilibrium modal distribution (EMD) after a certain fibre length. Equilibrium is typically reached around 15 meters for a numerical aperture (NA) of approximately 0.5. For smaller NAs, equilibrium is reached at longer lengths.

For PMMA step-index POF, the bandwidth is nearly 40 MHz over 100 meters, limiting the data rate to under 100 Mb/s with binary modulation. Increasing the POF length decreases bandwidth, as shown in Table 2-3. To optimise optical power consumption, binary signalling is preferred for POF lengths under 40 meters, while 4-PAM signalling is recommended for lengths over 40 meters.

According to the Nyquist Theorem, the maximum data rate in digital systems is given by (Fund, 2017):

$$R_{max} = 2B\text{Log}_2\ M \qquad 2.24$$

Where:

R_{max} = Maximum Bit Rate (bit/s)

B is the channel bandwidth in Hz

M is the number of discrete signal levels (e.g. M = 2 for binary digits)

Therefore, if $M = 2$, then $\log M_2 = 1$, so:

$$R_{max}\ (\text{bit/s}) = 2 \times \text{Bandwidth (Hz)} \qquad 2.25$$

Table 2-3: Step index plastic optical fibre bandwidth characteristics

Bandwidth (MHz)	20m	40m	115m	200m
Electrical	256	108	43	31
Optical	200	156	64	45

Isaac N. Osahon (2018) demonstrated that one effective solution to the bandwidth limitations of step-index plastic optical fibre (SI-POF) is the use of a multilevel pulse amplitude modulation (M-PAM) scheme combined with equalisation techniques.

Additionally, Panchuk et al. (2022) noted that increasing the bandwidth of SI-POF can be achieved by employing a multistep refractive index profile. For instance, a step-index fibre with a double-step refractive index profile operating at a wavelength of 520 nm can support optical signal transmission rates of up to 125 Mbps.

2.13 Why Plastic Optical Fibre?

Isaac N. Osahon (2018), Naji Ali (2017), and N. S. Mohamed-Kassim (2017) agree that plastic optical fibre (POF) is gaining prominence as an affordable medium for short-range and indoor networks. Its advantages include immunity to electromagnetic interference (EMI), lightweight, small size, and ease of termination and connection. This section compares POF to other transmission media over short distances.

2.13.1 POF versus Glass Optical Fibre

Step-index plastic optical fibre (SI-POF) with a PMMA core is a leading choice for "last mile" communication due to its lower cost and easier installation compared to glass fibre. Seiji Sasho (2017) highlighted the growth of POF communication, which led to the creation of the international product specification IEC 60793-2-40 A4a. This specification categorises SI-POF by its large fibre diameter (1 mm) and high numerical aperture (NA 0.5).

Despite its benefits, SI-POF suffers from higher losses per unit length due to modal dispersion, limiting its use to short-haul "last mile" links of up to 100 meters. Additionally, as an organic material, POF is sensitive to environmental factors, such as moisture.
PMMA, used in POF, has a higher thermo-optic coefficient, a lower Young's modulus, higher water absorption, and better biological compatibility than silica (Jamshid Heidarialamdarloo, 2018).

Microstructured polymer optical fibres (mPOFs) are also gaining attention for their ability to maintain single-mode operation over a broad wavelength range and to control modal properties such as confinement loss and dispersion.

POF's plastic nature offers durability and flexibility, with a bending radius half that of glass. Its high NA facilitates easier light coupling from an optical source. Additionally, POF is more resilient to impacts and vibrations, making it suitable for installation in tight spaces.
POF's larger diameter allows the use of low-precision tools and plastic connectors, which are less expensive and less prone to damage compared to glass fibre. POF is easier to install and align, reducing overall system costs. Most POFs are made from inexpensive PMMA, providing advantages in material cost, processing, and connection. POF is less affected by dust and water compared to glass fibre.

POF uses visible-range optical sources (Jamshid Heidarialamdarloo, 2018), and non-collimated optical launch is inherently eye-safe. It achieves equilibrium modal distribution (EMD) within 15 to 20 meters, whereas glass optical fibre takes several kilometres. POF's ease of handling and lower manufacturing and installation costs give it an edge over single-mode silica fibre.

2.13.2 POF versus Twisted Copper Cables

The primary advantage of plastic optical fibre (POF) over twisted copper cables is its immunity to electromagnetic interference (EMI), radio frequency interference (RFI), and switching transients that produce electromagnetic pulses (EMP). Twisted copper wires have limited capacity for digital transmission, whereas POF offers better signal quality because it is immune to EMI.

- *Immunity to EMI:* POF is made from dielectric (non-conducting) materials, so it neither generates nor receives EMI. This makes POF suitable for use in environments with intense magnetic fields, such as power electronics, radar systems, antennas, and nuclear facilities.
- *Lightning Resistance:* POF cables are not susceptible to lightning strikes when used overhead and do not exhibit earth loops or require EMI shielding. As an electrical insulator, POF ensures networking devices remain electrically isolated.
- *Safety in Hazardous Environments:* POF does not produce sparks or arcing at abrasions, breaks, or short circuits. This property makes it ideal for use in electrically hazardous environments, such as areas with explosives or flammable fuels.
- *Vibration Resistance:* POF can withstand higher levels of vibration than copper cables and requires only simple tools for termination.

- *Signal Security:* POF offers high signal security since it does not radiate energy, making it difficult to tap into without detection.
- *Cost and Availability:* Copper is a critical commodity with fluctuating prices, whereas the primary material used to produce POF is a polymer, which is readily available and cost-effective.
- *Skin Effect:* Unlike POF, copper wire experiences the "skin effect" at higher frequencies, where current is restricted to the outer layer of the wire. This effect increases with frequency, causing the wire to radiate energy and potentially inducing crosstalk from nearby cables. POF does not exhibit the skin effect and does not radiate electromagnetic energy.

  Frequency Response: At low frequencies, copper wires can transmit signals over long distances.

  However, at high frequencies, the skin effect reduces the effective cross-sectional area of the wire, increasing resistivity, as illustrated by equation 2.25 (Lina Sanchez-Botero, 2022).

$$R = \rho \frac{L}{A} \qquad 2.26$$

Where R is the resistance of the wire

ρ is the wire's resistivity

L is the length of the wire

A is the cross-sectional area of the copper wire.

Equation 2.18 shows that reducing the cross-sectional area of a wire increases its resistance, thereby increasing attenuation. The same effect occurs when the wire's length is increased. Additionally, the "skin effect" also limits the bandwidth of copper wires.

- *No Licensing Requirement:* Implementing a POF transmission link does not require a government emission license, as optical fibre is a non-radiating means of transmitting information. Instead, the primary concern is negotiating the right-of-way for the fibre cable route, which is generally more straightforward than the lengthy licensing process.

- *Duct Congestion Relief:* POF helps alleviate duct congestion in cities thanks to its smaller size (50% smaller than twisted-pair cables) and lighter weight (4 times lighter than Cat5e). Given these advantages, POF cables are typically superior to copper cables for storage, transportation, and installation. They offer comparable strength and durability while being easier to handle. POF is beneficial for new building connections where existing infrastructure constraints make twisted-pair cables impractical.
- *Power Efficiency:* POF transceivers consume less power than copper transceivers. POF effectively supports high-demand services, such as triple-play (video, data, and voice streaming), and ensures quality of service (QoS).

2.13.3 Plastic Optical Fibre versus Coaxial Cable

One significant advantage of POF over coaxial cable is its non-conducting nature. Most POF cables are dielectric, containing no conductive materials. This provides complete immunity to electromagnetic interference (EMI) and radio frequency interference (RFI) and reduces the impact of lightning strikes. Another benefit of POF is that its attenuation rate remains consistent across its operating frequency range, unlike coaxial cables, which experience higher attenuation at higher frequencies. This characteristic enables POF to achieve high data rates and long distances. The attenuation characteristics of coaxial cable are illustrated in Fig. 2.17.

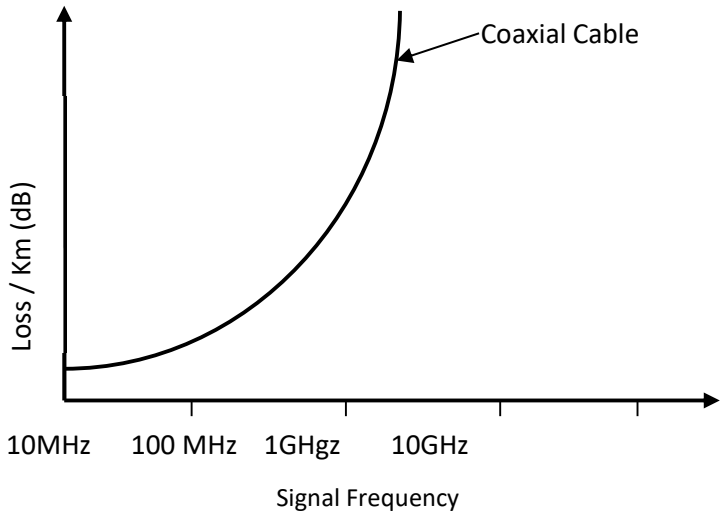

Figure 2-17: Coaxial cable attenuation characteristics.

2.13.4 POF versus Wireless Media

Wireless media have two significant disadvantages as a transmission medium. Firstly, their network capabilities and behaviour can be unpredictable under certain weather conditions. Issues such as fading, delay spread, distance, the Doppler effect, interference, obstacles, and blind spots can all lead to variations in bandwidth, data delivery latency, jitter, and error rates. Secondly, wireless communication technologies lack safeguards against unwanted eavesdropping, making them less secure for sensitive transmissions. In contrast, POF technology generally performs better because it is a cable solution not affected by external electromagnetic radiation and operates in a spectrum free of other transmissions.

2.13.5 Challenges / Disadvantages of Plastic Optical Fibre

As noted by Isaac N. Osahon (2018) and Naji Ali (2017), the primary drawback of step-index plastic optical fibre (SI-POF) is modal dispersion, which limits the link bandwidth to about 40 MHz. For a 50 m link, the dispersion-limited bandwidth is only 80 MHz, corresponding to a data rate of about 160 Mbps using non-return-to-zero (NRZ) signalling over 100 m.

Plastic optical fibre also exhibits significant attenuation, with a minimum of 150 dB/km at 650 nm compared to 0.25 dB/km at 1550 nm for single-mode fibre. This high attenuation limits the reach of POF links to short distances and low data rate transmissions. Additionally, POF is restricted to use at temperatures below 80°C.

2.14 Applications/Uses of POF

Plastic optical fibre has been developed and commercialised for various applications:

2.14.1 Automotive Networks

In the automotive industry, POF is used due to its lightweight, small cross-section, and insensitivity to electromagnetic interference. It helps reduce vehicle weight and fuel consumption, improve traffic safety, and enhance overall vehicle quality. The POF's bandwidth, combined with its resistance to bending, vibrations, and external disturbances, makes it ideal for automotive-embedded multimedia systems. Its unique properties ensure reliable communication in harsh automotive conditions.

2.14.2 Sensors in the Medical industry

In medicine, POF opens new possibilities and addresses barriers in the healthcare system. POF-based devices and sensors offer advantages such as immunity to electromagnetic fields, high flexibility, lower Young's modulus (providing high sensitivity to mechanical parameters), impact resistance, and compatibility with biomedical materials. A critical feature of POF is its biodegradability, which enhances its application scope and opens new avenues in biomedicine. Additionally, porous polymer fibres can be utilised for local drug delivery in cancer treatment.

2.14.3 Industrial Control

POF is also significant in industrial control applications. Its primary advantage is its resistance to electromagnetic interference (EMI). Standards used in industrial automation, such as SERCOS (SErial Real-time COmmunication System), Profibus, and INTERBUS, benefit from POF's lightweight, small cross-section, and EMI insensitivity.

2.15 Recent Advancements in POF Technology

POF technology has seen exciting advancements in recent years, redefining data transmission and connectivity. New polymer formulations and advanced manufacturing techniques have improved POF durability, flexibility, and signal integrity. These innovations are making plastic optical fibres a more feasible alternative to glass fibres across various applications, offering cost-effective and adaptable solutions while maintaining robust performance and reliability (Ghosh, 2024).

2.15.1 **Advanced Fabrication Techniques**

In 2021, TE Connectivity and Saint-Gobain made significant strides in POF technology. TE Connectivity enhanced the extrusion process by developing advanced dies and polymer blends, improving the uniformity of core and cladding layers in POFs (Ghosh, 2024). This advancement resulted in fibres with superior optical performance and structural integrity, addressing issues of signal attenuation and durability. Saint-Gobain applied its expertise in moulding techniques to create POFs with intricate geometries, allowing precise control over optical properties. The combined efforts of these companies improved POF

performance and reduced production costs, making advanced POFs more accessible for various applications.

2.15.2 Enhanced fibre Coatings and Integrated Photonics

Fibre coatings made from fluoropolymers or silicon-based compounds reduce signal attenuation and increase fibre longevity. Corning's advanced coatings, introduced in 2020, enhance resistance to moisture and abrasion, extending fibre life to over 25 years. A partnership between Corning and the National Institute of Standards and Technology (NIST) in 2021 led to the development of new coating technologies that further improve fibre durability and performance, supporting more reliable, long-lasting fibre-optic networks.

Integrated photonics in POFs enhances data transmission by embedding photonic devices directly within the fibre, improving functionality and performance. This integration enables miniaturised, high-efficiency components such as modulators and detectors, which are essential for high-speed communication. For instance, integrating modulators can support data rates of up to 10 Gbps, while embedded detectors can improve signal-to-noise ratios by 15-20 dB compared to traditional setups. Research by Fraunhofer HHI and the University of Erlangen-Nuremberg in 2023 demonstrated that integrating silicon photonic devices with POFs achieves data rates up to 10 Gbps with minimal signal loss.

Another promising development is the use of fibre Bragg gratings (FBGs) in POFs (Panchuk et al., 2022). Optical fibres with built-in Bragg gratings offer smooth refractive index distributions and enable the design of filters and other devices with unique functionalities. Long-period gratings (LPGs) can be recorded with periodicities from 100 µm to 1 mm, allowing for resonant wavelengths in the 500-750 nm range.

2.15.3 Low-loss and high-bandwidth plastic optical fibres

Low-loss optical fibres minimise signal degradation by using materials and manufacturing techniques that reduce scattering and absorption. Silica-based fibres doped with germanium can achieve an attenuation as low as 0.2 dB/km at 1550 nm. As of August 2024, Corning’s advanced fibres, developed in collaboration with global telecom providers, have

significantly improved signal clarity and data transmission efficiency, enhancing network performance and supporting the expansion of high-speed communications.

High-bandwidth plastic optical fibres enable rapid data transmission over short distances due to their large core size and high numerical aperture. Made from polymers such as polymethyl methacrylate, these fibres offer bandwidths of up to 1.5 GHz·km and data rates of up to 1 Gbps. Mitsubishi and Broadcom collaborated in 2022 to optimise POF materials and integrate these advanced fibres into data communication systems, driving innovation in the field and enhancing modern communication networks.

2.15.4 Micro-structured POF

Research into micro-structured optical fibres (MPOFs) has gained renewed interest (Panchuk et al., 2022). MPOFs feature a cladding with hollow channels filled with air that extends along the entire length of the fibre. This microstructure influences light propagation through the fibre. Two types of MPOFs are distinguished: solid-core and hollow-core. The microstructure of the air channels defines the fibre's refractive index profile, which can be step, graded, or more complex (Panchuk et al., 2022). MPOFs made from a single polymer material address issues related to rheological properties and dopant concentration fluctuations, resulting in lower optical losses and a broader range of usable polymers.

2.16 Future Use and Development of POF

Global warming and climate change, driven by CO2 emissions from fossil fuels, have created a need for alternative and renewable energy systems. This has led to increased use of solar panels and wind generators for residential, office, and industrial power needs. POFs hold significant potential in this context, with applications in automation systems, station information networks, environmental monitoring, and equipment condition monitoring. Ongoing research into polymer-optic technologies should focus on improving performance metrics to meet these evolving needs.

2.17 Summary

This chapter reviewed the development and characterisation of plastic optical fibre (POF) and its feasibility for the fabrication of POF couplers. It covered the historical background, material science, and different types of materials used in POF manufacturing. The discussion then shifted to fabrication methods, mechanical characteristics, properties, and refractive index distribution. The chapter also explored ray-optics theory relevant to optical transmission in POF and addressed its capabilities and limitations, including attenuation and modal dispersion. The transmission characteristics, loss mechanisms, and techniques to mitigate modal dispersion were discussed, alongside the frequency response and bandwidth.

The review compared POF with other transmission media, such as glass fibre, coaxial cable, copper wire, and wireless technology, focusing on bandwidth, attenuation, and other parameters. Recent developments in POF technology were highlighted, including advancements in material structure, bandwidth achievement, and application areas. The chapter identified knowledge gaps, particularly regarding improvements in bandwidth and dispersion.

2.18 References

- A. Bunge, M. B. (2017). *Polymer Optical Fibres.* Aachen, German: Woodhead Publishing
- Appajaiah, A. (2005). Climatic Stability of Polymer Optical Fibers (POF). *Potsdam University*. Berlin, German.
- Azusa Inque, Y. K. (2019, April*). Unconventional plastic optical fibre design for very short multimode fibre link.* Optics Express, Vol 27(9), 1-9.
- M. Beckers, B. W.-A. (2017). *Polymer Optical Fibres.* Aachen, German: Woodhead Publishing.
- (A. Bunge, 2017)D. Zaremba, R. E. (2017). *Materials, chemical properties and analysis. (pp. 153-186).* ScienceDirect.
- David R. Gozzard, R. C. (2022). *Optical couplers and step-index fibres fabricated using FDM 3D printers.* Optics Letters, Vol 47(19/1),

- Fund, F. (2017, February 13). Retrieved from Run my testbed experiment: https://witestlab.poly.edu/blog/nyquist-formula-relating-data-rate-and-bandwidth/?utm_source=chatgpt.com
- Ghosh, K. (2024, August 22). *Novel Breakthroughs in Plastic Optical Fiber Technology Are Restructuring the Industry: An Overview.* Allied Market Research, p. 1.
- Isaac N. Osahon, M. S. (2018). *10-Gb/s Transmission Over 10-m SI-POF With M-PAM and Multilayer Perceptron Equalizer.* 2018 IEEE Photonics Conference (IPC).
- Jamshid Heidarialamdarloo. (2018). *Advanced communications with plastic optical fibres.* Miami: ProQuest.
- Lina Sanchez-Botero, D. S.-B. (2022). Are Liquid Metals Bulk Conductors? *Advanced Materials*, 1-12. doi:DOI: 10.1002/adma.202109427
- N. S Mohamed-Kassim, (2017). *High-resolution tunable POF multimode power splitter.* Optics Communications, 136-143.
- Naji Ali, A. L. (2017). *Achieving 1 Gbps Over Step-Index Plastic Optical Fiber Using Spatial Mode Air-Gap Filter.* IEEE Photonics Technology Letters, Vol. 29, No. 8, April 15, 2017, Vol. 29(No. 8).
- Panchuk, et al (2022). *Polymer Optic Fibers: Potential of Development and Application in Networks.* IEEE. doi:10.1109/3ICT56508.2022.9990760
- Seiji Sasho (2017). *Optical Coupler with Multicore Plastic. IEEE Photonics Technology Letters, 659-662.* Retrieved July 10, 2021
- Silvio Abrate, R. G. (2013). *Step Index PMMA Fiber and their Applications*. IntechOpen.
- Yau I, (2021). *Mitigating the Effect of Modal Dispersion of Plastic Optical Fibre. Journal Of Science, Technology And Education, 1-7*.

Chapter 3

Plastic Optical Fibre-Based Couplers and Their Performance Parameters

3.1 Introduction

This chapter reviews POF-based optical couplers, focusing on their performance parameters and applications across various industries. Optical power splitters (OPS) or couplers are critical, nearly indispensable passive components in all-optical fibre systems (Jing Yang, 2021). These bidirectional passive components can split or combine optical power. Typically, they distribute light from a primary fibre into one or more fibre branches. The splitting property of multimode couplers arises from the numerous modes propagating within multimode fibres. Each mode transfers a portion of its power to a corresponding mode in a second fibre within the coupler.

According to N. S. Mohamed-Kassim (2017), most multimode POF power splitters available on the market have fixed branching ratios. However, these ratios often deviate slightly from their intended values due to design flaws and fabrication tolerances. Dimensional variations inherent to the manufacturing process make it time-consuming and cost-ineffective to mass-produce optical couplers with numerous branching ratios. Jing Yang (2021) supports the views of N. S. Mohamed-Kassim (2017) and Syed Azer Reza (2019), stating that optical power splitters or couplers are not only used to distribute optical power or signals into multiple channels, but also in specialised applications such as power equalisers, optical switches, and ring lasers, where fixed branching ratios are insufficient. Yang (2021) further emphasises that variable couplers can significantly enhance the flexibility of optical fibre systems, enabling adjustment of branch ratios without altering the system's structure.

3.2 Properties of an Optical Power Splitter/Coupler

Ideally, POF-based optical couplers should distribute optical energy evenly across the branch fibres without introducing any scattering loss or noise. They should also be

insensitive to the polarisation of the optical energy modes (J.M. Senior, 2009). The following properties are desirable for any optical coupler: ease of handling, consistent coupling behaviour, low manufacturing costs, compact size, good thermal and mechanical stability, low mode dependence, and effective isolation between input channels.

In practice, however, optical couplers introduce some scattering losses and generate noise, along with other modal effects in optical fibre networks (J.M. Senior, 2009). These scattering losses limit the number of terminals that can be connected and restrict the network's overall span. Additionally, noise and modal effects can degrade the signal-to-noise ratio, thereby impacting network performance. Dispersion may also lead to inter-channel interference, as discussed in the previous chapter.

N. S. Mohamed-Kassim (2017) emphasised the importance of precise splitting ratios for specific applications, especially with the rapid advancements in integrated optical devices and photonics. As a result, there is a high demand for optical power splitters that can be tuned to achieve the desired splitting ratio.

In their work, N. S. Mohamed-Kassim (2017) explored the use of plastic optical fibres to create Y-shaped power splitters. The splitting ratio was adjusted by altering the angle between the input fibre and the two fixed output fibres, as shown in Figure 3-3 of this chapter. Jing Yang (2021) proposed a variable fibre optical coupler based on triangular prisms, where the power ratio could be continuously tuned by adjusting the prism’s beam width. By varying the prism's axial displacement, the splitting ratio could be varied from 50:50 to 90:10. Similarly, Syed Azer Reza (2019) introduced a hybrid optical fibre design that combined a conventional Digital Spatial Light Modulator (DSLM) with a tuneable focus Electrically Tuneable Lens (ETL).

3.3 Performance Parameters of POF Couplers

The performance of optical couplers, including POF couplers, depends on the wavelength. Couplers are typically specified over a wavelength range, known as the bandpass, within which their performance is guaranteed. The performance is evaluated using key characteristic parameters, as outlined by Sariki et al. (2021). This section explores the parameters that affect the performance of most POF couplers, which are critical in designing the array couplers proposed in this research.

3.3.1 Excess Loss

According to Sariki, et al., (2021) the excess loss is the ratio of the optical power launched at the input port to the total output power measured across all output ports, expressed in decibels (dB). It represents the input power that is lost and not available at the output ports, primarily due to scattering or absorption within the coupler. Imperfections also influence the excess loss in the manufacturing process. For a 1x2 coupler, excess loss can be calculated using the following expression (Sariki, et al., (2021):

$$\text{Excess Loss } (\eta_e) = 10 \text{ Log } \left[\frac{P_{0(1)+} P_{0(2)}}{P_{in}}\right] \text{ dB} \quad 3.1$$

The excess loss is a figure of merit that represents a coupler's overall efficiency, typically less than 0.1 dB for an excellent optical coupler.

3.3.2 Splitting (Coupling) Ratio

As noted by Sariki et al. (2021), the splitting (or coupling) ratio is the percentage of the input optical power directed to a specific output port. This is a crucial parameter because it indicates how power is distributed among the coupler's output ports at a given operational wavelength. The coupling ratio can be calculated using the following formula (Sariki et al. (2021):

$$\text{Coupling Ratio} = \left[\frac{P_{oc}}{P_{01} \pm \text{---} + P_{oN}}\right] X\ 100\% \quad 3.2$$

Where: P_{oc} = coupled output port

P_{o1} = coupled output port

P_{oN} = coupled output port N

The splitting ratio describes how the input light in a coupler is divided between the output ports. It can range from 0% to 100% and is always specified for a particular wavelength. Since the coupling coefficient depends on wavelength, the splitting ratio will vary with wavelength.

3.3.3 Insertion Loss

Insertion loss, as described by Sariki, et al., (2021), is the ratio of the optical power launched at the input port of the coupler to the optical power measured at any single output port, expressed in decibels (dB). The bidirectional coupler loss represents the total loss encountered as light travels from a specific input port through the coupler to the output port. This loss is the sum of the excess loss and the coupling ratio (both expressed in dB) along a given light path. The insertion loss of fibres can be calculated using the following formula:

$$\text{Insertion Loss } (\eta_i) = 10 \text{ Log} \left[\frac{P_{out}}{P_{input}}\right] \text{ dB} \quad 3.3$$

If it is assumed that in an ideal optical coupler, the light distribution between the N output routes is homogeneous (equal) among the number of outputs (N), so each output receives $\frac{1}{N}$ of the input power. In decibels, that equal division is a loss of $10\text{Log}_{10}\left[\frac{1}{N}\right]$, so the Insertion loss (η_i) is then related to the excess loss (ηe) as follows (Keiser, 2011)
:

$$\eta_i = \eta_e + 10\text{Log}_{10}\left[\frac{1}{N}\right] \quad 3.4$$

$$\eta_i = \eta_e - 10\text{Log}_{10}N \quad 3.5$$

Where:

η_i is the insertion loss of the optical coupler

η_e is the excess loss of the optical coupler

N is the number of the optical output ports

3.3.4 Coupling (Splitting) Tolerance

Coupling tolerance is the acceptable margin of error in the coupling ratio, typically 1% to 5%, due to manufacturing variations. As a result, it is unlikely that the input optical power will be distributed exactly equally between the output ports.

3.3.5 Uniformity

Uniformity (U), measured in decibels (dB), represents the difference between the insertion losses of the best and worst-performing ports in a multi-port coupler. It is a crucial parameter for ensuring consistent performance in multi-port couplers. Uniformity measures the consistency of the coupling ratio when different ports are used as inputs in an N x N coupler, reflecting how evenly power is distributed across all ports. It can be expressed either as a percentage or as a loss term in dB, and is calculated using the following formula (Lee, 2021)

:

$$U = IL_{max} - IL_{min} \tag{3.6}$$

Where:

U is the Uniformity

IL_{max} = Maximum Insertion Loss in the coupler

IL_{min} = Minimum Insertion Loss in the coupler

3.3.6 Coupler Losses

These are the losses due to a coupler. Generally, the loss is calculated as:

$$\text{Coupler Loss} = 10 \text{ Log } \left[\frac{P_{in} - P_{out}}{P_{in}}\right] \text{ dB} \tag{3.7}$$

3.3.7 Return Loss

Return loss is the ratio of optical power from the reflected port to the transmitter port of the coupler (Sariki, et al., 2021):

$$\text{Return Loss} = -10\text{Log}\left[\frac{\text{Reflected Optical Power}}{\text{Transmitted Optical Power}}\right] \tag{3.8}$$

3.3.8 Directionality Loss / Crosstalk

According to G. P. Agrawal, the directionality loss is the ratio of power coupled in the desired direction to that in the opposite direction, expressed in decibels. Directionality loss,

also known as crosstalk, is a slight loss caused by backscatter within the coupler, in which a portion of the optical energy is reflected back into the input port. This loss is typically around -40 dB. The directionality loss can be calculated using the following expression (Agrawal, 2021):

$$\text{Directionality Loss} = 10 \text{ Log} \left[\frac{P_{\text{forward}}}{P_{backward}}\right] \text{ dB} \quad 3.9$$

Where:

$P_{forward}$ is the port optical power

$P_{backward}$ is the port reflected power

3.3.9 Return Loss / Directivity

Return loss, also referred to as directivity, is the ratio of the optical power reflected from the coupler's port to the optical power incident on the transmitter input port, expressed in decibels (dB) (Sariki et al., 2021).

Return loss measures how efficiently the coupler transmits light to the output ports and indicates the amount of light reflected within the coupler. Directivity, which is the opposite of directionality loss, represents the ratio of the reflected power to the input power and is also expressed in dB. It can be calculated using the following formula (Sariki et al., (2021):

$$\text{Directivity} = 10 \text{ Log} \left[\frac{P_{\text{reflected}}}{P_{\text{in}}}\right] \text{ dB} \quad 3.10$$

Where:

$P_{reflected}$ is the port reflected power reaching the input port

P_{in} is the input optical power

In practice, all output ports are immersed in an index-matching liquid during directivity measurements. This ensures that Fresnel reflections, arising from the index mismatch between the fibre terminals and air, do not affect the measurement of back-reflected optical power. Directivity is also known as near-end isolation.

3.3.10 Throughput Loss

Throughput loss is the ratio of the optical power at the throughput port to that at the input port. The throughput port is the one with greater power when the splitting ratio between the output ports is unequal. Ideally, throughput loss should equal the insertion loss.

3.3.11 Wavelength Isolation

Wavelength isolation, also known as far-end crosstalk, measures how well a wavelength-division demultiplexer separates different wavelengths at its output. It is defined as the ratio of the optical powers at the demultiplexer's two output ports at a given wavelength, expressed in decibels (dB).

3.4 POF-Based Couplers

Optical couplers split optical power among three or more fibres or combine optical power from different sources. While optical couplers passively split optical power, they can also use optical amplifiers to boost power before or after the split, in which case they are known as active optical couplers. The configuration of optical couplers depends on several factors, with the most common being the number of ports and direction (unidirectional or bidirectional). A coupler with one fibre at one end and two fibres at the other is called a 1x2 coupler. Alicia López (2018) noted that one challenge with optical couplers is that when they split optical energy, spatial disturbances can alter the modal power distribution in POFs, resulting in localised power transfers between modes and changes in transmission properties.

3.4.1 POF Butt Coupler

In a POF butt coupler, the polished end faces of optical fibres are placed together, as shown in Fig. 3-1, and joined with index-matching resin. This type of coupler relies on the lateral offset of overlapping fibre end faces to couple light. The degree of overlap between the input optical fibre (P_1) and the output optical fibres (P_2 and P_3) determines how the input optical energy is split, and thus the coupling ratio (J.M. Senior, 2009).

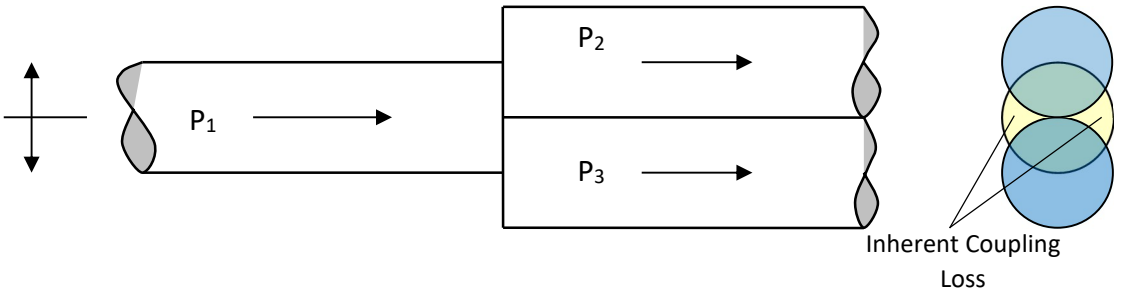

Figure 3-1: Components of a butt coupler (J.M. Senior, 2009).

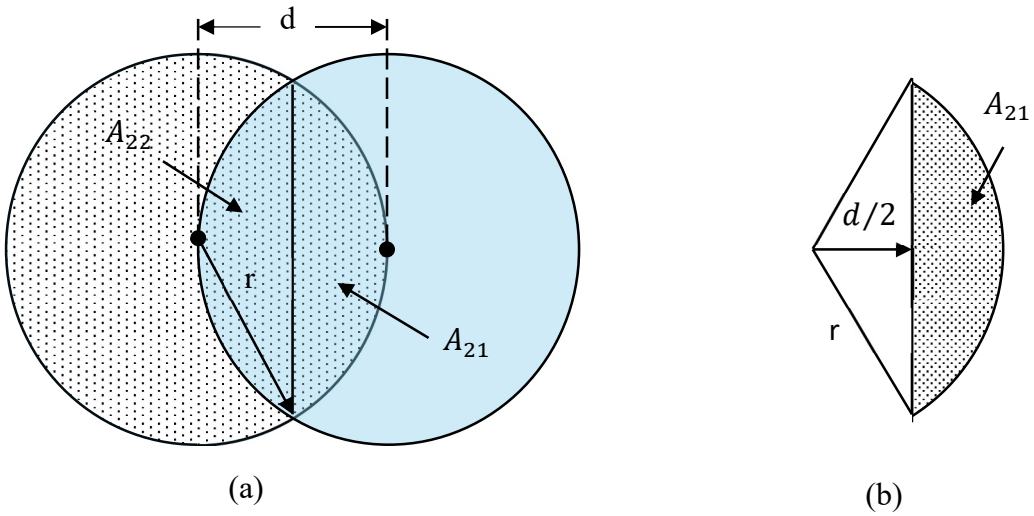

*Figure 3-2: (a) Overlap area between two identical fibres can be obtained from the sector calculation, (b) showing one of the overlap sectors 21 (*N. S. Mohamed-Kassim, 2017).

N. S. Mohamed-Kassim (2017) achieved asymmetric splitting ratios by applying the concept of power transmission through angular misalignment. The power transmitted from Fibre-1 to Fibre-2 and Fibre-3 is determined based on the overlapping cross-sectional areas of the fibre end faces. The total power in Fibre-2 (P_{22}) can be estimated by calculating the overlap area between Fibre-1 (A_{21}) and Fibre-2 (A_{22}), as illustrated in Fig. 3(a).

The area of a segment (A_{21}) can be determined by deducting the area of the triangle from the sector, as shown in Fig. 3-2(b), and can be expressed as (N. S. Mohamed-Kassim, 2017):

$$A_{21} = 2r^2 \cos^{-1}\frac{d}{2r} - \frac{d}{2}\sqrt{4r^2-d^2} \qquad 3.11$$

Where: d is the length of the overlapped area between the two centres of the POFs,

d/2 is defined as the half of the overlapped area between the two centres of the POFs.

r is the radius of the POF.

The disadvantage of the butt coupler is that some of the input optical power is launched off-axis, resulting in high excess loss.

The power transmitted within fibre 2 and fibre 3 is calculated using:

$$P_2 = (A_{21}+A_{22})I \quad 3.12$$

$$P_3 = (A_{31}+A_{32})I \quad 3.13$$

Where *I* is the radiance of the light source, the optical parameters of the coupler, such as insertion loss, excess loss, and splitting ratios, are estimated using the equations in section 3.3.

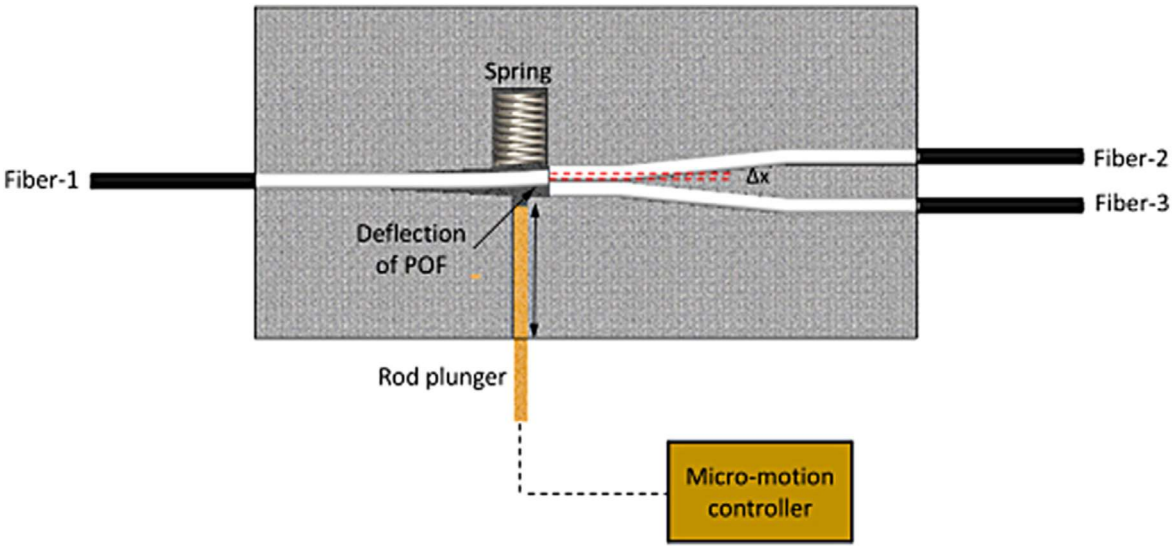

Figure 3-3: Schematic design of a tuneable polymer optical power splitter (N. S Mohamed-Kassim, 2017)

Using the same concept of power transmission through angular misalignment, N. S. Mohamed-Kassim (2017) developed a tunable coupler, illustrated in Figure 3-3. The design consists of a deflectable input fibre (Fibre-1), two fixed output fibres (Fibre-2 and Fibre-3),

a spring, and a rod plunger. The rod plunger, controlled by a micro-motion controller, deflects the input fibre while the spring provides resistance. By adjusting the rod plunger in 5-micron steps across a range of Δx = ±0.5 mm, the splitting ratio (SR) can be varied from 1.0% to 98.0% for $P2$ and from 99.0% to 2.0% for $P3$. Unlike fixed optical power splitters, this tunable splitter allows precise adjustment to meet specific requirements (Bazakutsa et al., 2022).

3.4.2 Y-Splitter / Coupler

According to M.S.M. Ghazali (2021), Y-branch splitters are typically made by polishing two fibres and attaching them. Other methods for constructing Y-branch splitters include hot embossing and microinjection, but these methods require advanced production equipment and precise assembly tools.

To simplify the process, M.S.M. Ghazali (2021) proposed an alternative technique to manufacture a 1×2 symmetric and asymmetric Y-branch waveguide coupler using soft lithography mould replication and Epoxy OG142 as the optical core. This proposed coupler demonstrated an insertion loss of 1 dB.

Unlike the butt coupler, the POF Y-splitter shown in Fig. 3-4 has polished output fibres whose end faces fully overlap. Both output plastic optical fibres are connected to the input fibre, and the input fibre end face is carefully prepared with an index-matching medium to minimise losses at the junction.

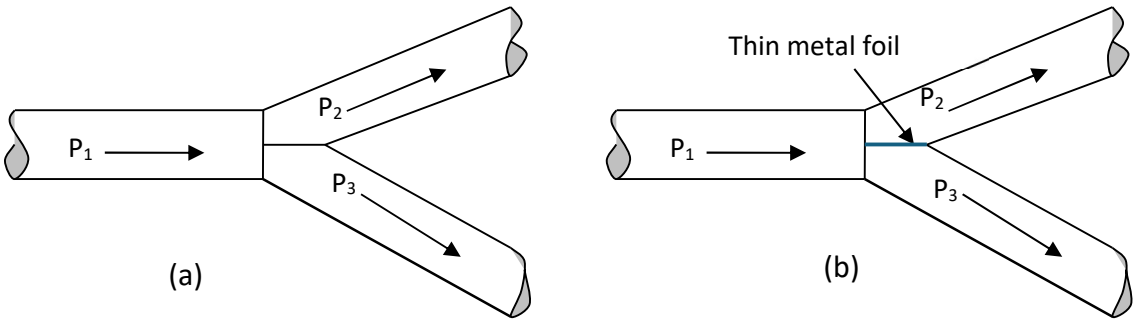

Figure 3-4: Fork Type Coupler (M.S.M. Ghazali, 2021)

A thin metal foil (or evaporated metal film) can be placed between the output optical fibres, as shown in Figure 3-4 (b), to reduce crosstalk between them. This foil can improve crosstalk attenuation by approximately 5 dB. The coupler can be configured as either a fixed

symmetrical (50:50) or asymmetrical (e.g., 20:80) coupler, depending on the desired coupling ratio of the output fibres. The typical excess loss with precision cutting ranges from 1 to 2.5 dB. However, a significant drawback of the fork-type coupler is the high cost of polishing and the difficulty of achieving precise alignment.

The beam splitter coupler (Paschotta, 2024) features a partially reflecting thin film applied directly to the end face of the fibre, which is cut at a 45-degree angle, as illustrated in Fig. 3-5. This thin film acts as a semi-transparent mirror that reflects a portion of the incident light. The properties of the thin film determine the degree of splitting of the incoming optical energy. This type of coupler can achieve an excess loss of 1 to 2 dB and is commonly used in wavelength-division multiplexing (WDM) couplers.

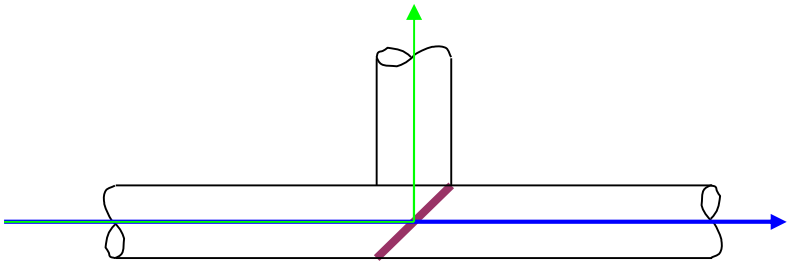

Figure 3-5: Optical beam splitter. (Paschotta, 2024)

Alicia López (2018) designed and characterised an optical Y-coupler, evaluating its spectral, spatial, and temporal performance characteristics. This included measuring insertion loss as a function of wavelength, angular power distribution, and frequency response. The results revealed that optical Y-couplers tend to equalise the spatial power distribution, which can reduce the fibre bandwidth. These findings highlight the significance of considering the impact of such devices on the transmission properties of any POF system.

3.4.3 Bend Couplers

In bend couplers, the input optical fibre is curved around a specific radius r, as shown in Fig. 3-6. Higher-order modes exit the fibre at the bend and are guided through a transparent resin to a connected fibre with a smooth end face. As the bending radius decreases, both the coupling ratio and insertion loss increase.

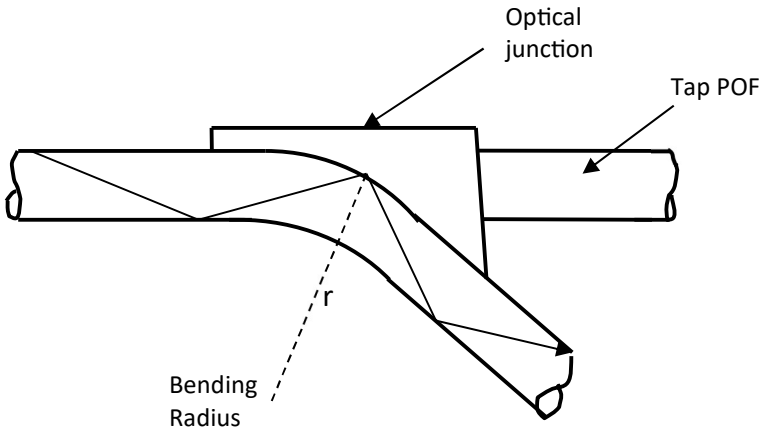

Figure 3-6: The bend coupler

Bending the POF causes the guided modes within the core to be converted into cladding and radiated modes (N. S. Mohamed-Kassim, 2017). At the high refractive junction, these modes are transferred to the adjacent plastic optical fibre.

3.4.4 Tee-Couplers

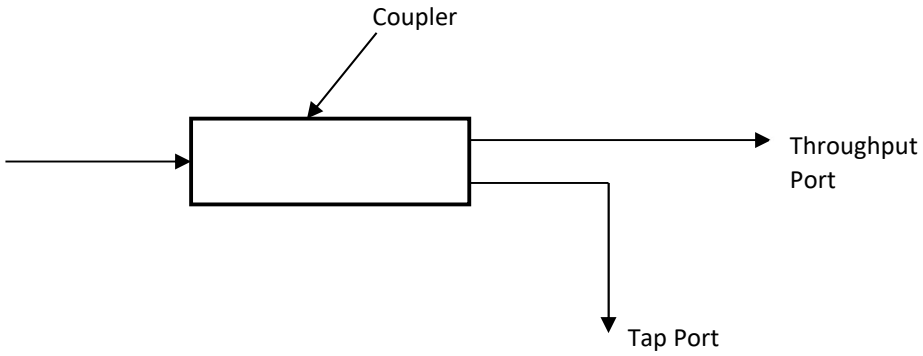

Figure 3-7: Tee coupler

Tee-couplers are 1x2 couplers designed to split the input optical power into two output fibres, as shown in Fig. 3-7. They are straightforward to manufacture and widely available, often with connectors. However, as additional devices are connected to the outputs, the power at each output can decrease rapidly, potentially making the output unreliable. Increasing the input optical power may also overload the first device connected to it.

3.4.5 Fused Biconical Taper (FBT) Couplers

The manufacturing process for fused optical couplers, as described by Bazakutsa et al. (2022), involves several stages. First, the protective acrylic shell is removed from the optical fibres. Next, the exposed fibre sections are cleaned with isopropyl alcohol to remove any residual acrylic. The cleaned fibres are then interwoven, placed in special holders, and stretched while being heated. During stretching, optical power is continuously supplied to the coupler input, and the power at each output is monitored. The process is stopped once the desired power division between the outputs is achieved.

In a fused biconical taper coupler, two or more plastic optical fibres are tensioned and twisted together, as depicted in Fig. 3-8. The twisted fibres are then fused at the tapered section using hot air or ultrasonic welding, often with heat applied indirectly through a metal tube. This simple fabrication method effectively spreads incoming light energy across the fused section, distributing optical power to each output fibre. When more than two fibres are fused, a star coupler is formed.

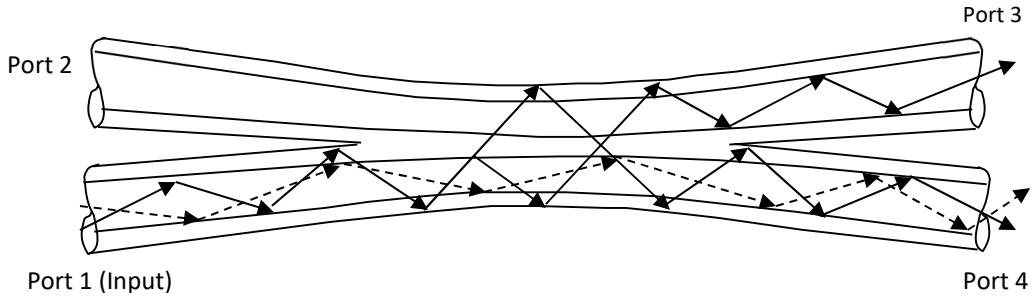

*Figure 3-8: Fused Biconical Taper (FBT) coupler (*Bazakutsa et al. (2022)

The Fused Biconical Taper (FBT) coupler typically exhibits low excess loss of around 0.5 dB and low crosstalk, typically better than -50 dB. The cross-sections of the two fibres determine the splitting ratio of an FBT coupler. This type of coupler can be made using either multimode or single-mode optical fibres.

Bazakutsa et al. (2022) noted that fused biconical couplers offer a notable advantage over planar optical splitters, which require complex processes such as photolithography, material sputtering, or ion-exchange techniques. They emphasised that

the properties of fused optical couplers, produced by stretching under a hydrogen burner flame, depend significantly on both the heating and stretching conditions and the type of optical fibres used. Optical fibres with higher bending resistance require greater stretching to transfer power efficiently between fibres.

However, fused biconical couplers have notable disadvantages, including the generation of modal noise and unequal losses between outputs. The splitting ratio can vary due to differences in optical modes, leading to multiple loss values through the coupler. Additionally, the FBT coupler's performance is wavelength-dependent. Other limitations include irregular heating during the fusing process, which can cause defects or damage in the taper region and affect light transmission. According to Syed Azer Reza (2019), FBT couplers can also experience high losses and significant attenuation variations with different input wavelengths and optical power levels.

3.4.6 Polished Asymmetrical Coupler

Polishing can be an alternative method for fabricating asymmetric multimode couplers. In this approach, the core and cladding of two optical fibres are polished flat and then brought together to form a coupler, as shown in Fig. 3-7. K. Sunil Kumar (2016) designed and fabricated simple, low-cost 2x2 and 1x2 couplers using acrylic cement. The fibres were finely polished to specific lengths and depths by removing sections of the cladding and 500 microns of the plastic fibre's core. The fibres were then joined with acrylic cement. Characterisation of these couplers revealed that at a wavelength of 650 nm, the coupler achieved a 52:48 coupling ratio with an insertion loss of 2.83 dB.

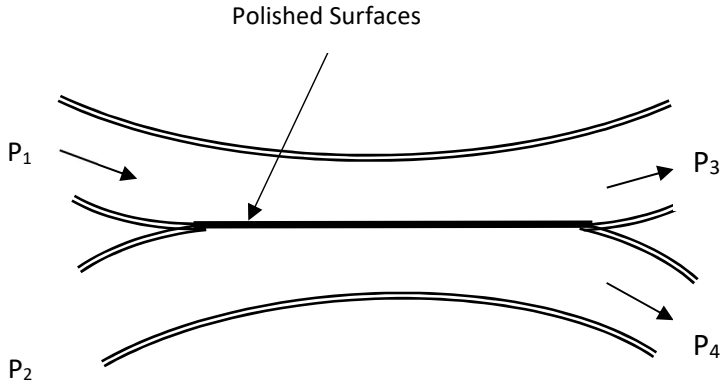

Figure 3-9: Polished asymmetric coupler (J.M. Senior, 2009).

In a polished coupler, the highest-order modes are initially confined within the cores of a multimode fibre. However, when these modes reach the polished section, they eventually spill into the cladding modes due to the significant refractive-index difference between the cladding and the surrounding air. Excess loss can be minimised by carefully calculating and controlling the dimensions of the polished section.

3.4.7 Micro Bend-Type Coupler

A micro-bend-type coupler creates periodic deformations in the optical fibre, facilitating mode coupling between radiation and guided optical light, as shown in Fig. 3-8. This mode coupling is achieved mechanically by pressing the optical fibre against a transparent grating.

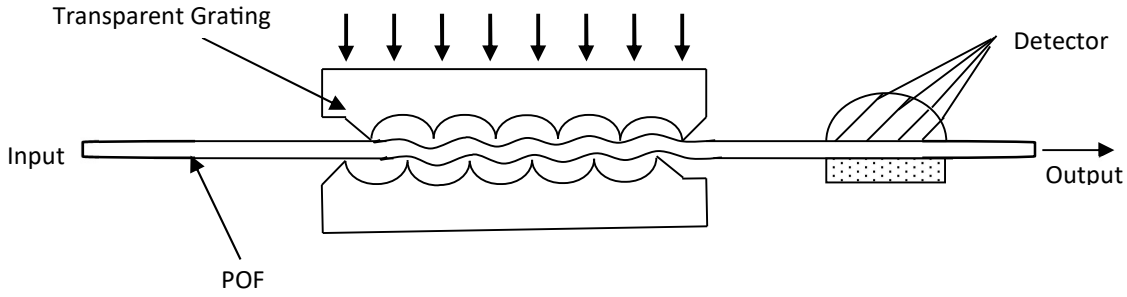

Figure 3-10: Micro-bend optical coupler (J.M. Senior, 2009).

In micro-bend-type couplers, mode coupling results in radiated optical power that is collected by lenses. The coupling ratios are determined by the amount of pressure applied to the fibre. These couplers are advantageous for their low excess loss, typically around 0.05 dB.

3.4.8 Mixing Rod Couplers

A mixing rod coupler uses a glass rod with a length and diameter of a few millimetres, as shown in Fig. 3-9. The rod's length must be sufficient to allow light from all input fibres to spread uniformly across its diameter and illuminate the rod's other end (J.M. Senior, 2009). This ensures that all optical fibres receive an equal amount of optical energy. In this type of coupler, a thin glass platelet can be used to mix the optical energy from one fibre and

distribute it among the output fibres. The mixing rod coupler has an insertion loss of 12.5 dB for an 8x8 transmissive star coupler and a port-to-port uniformity of ±0.7 dB.

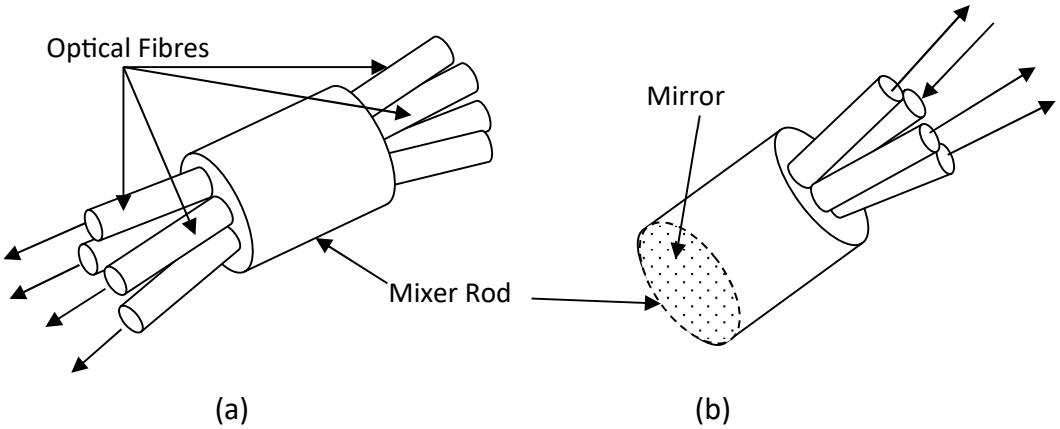

Figure 3-11: Mixing-rod coupler (J.M. Senior, 2009).

3.4.9 Wavelength Division Multiplexing Couplers

Wavelength Division Multiplexing (WDM) couplers are specialised components designed to simultaneously transmit optical power from multiple wavelength sources through a single optical fibre. These couplers can function as either wavelength multiplexers or demultiplexers. Key parameters for WDM couplers include channel spacing (the wavelength range over which wavelength-dependent attenuation occurs)nd inter-band isolation (J.M. Senior, 2009). High inter-channel isolation is crucial at the receiver end to minimise crosstalk between channels.

WDM couplers fall into three main categories: optical filters, dispersive (diffractive grating), and surface-interaction types. Many WDM couplers are hybrid devices combining dispersive and optical filter elements (J.M. Senior, 2009).

In diffraction grating-based WDM couplers, optical power is directed according to the grating constant, the wavelength of the light, and the angle of incidence, as shown in Fig. 3-12. There are two primary types of diffraction gratings:

- *Littrow Grating*: This type uses a single lens and a separate plane grating.
- *Concave Grating*: This type combines both diffraction and focusing functions, eliminating the need for a separate lens.

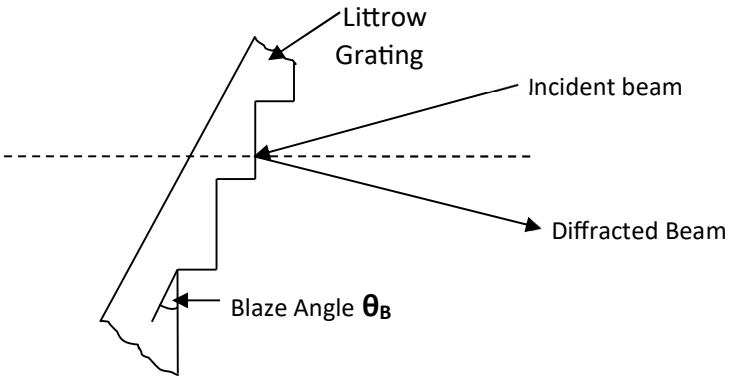

Figure 3-12: Littrow grating (J.M. Senior, 2009).

For a given wavelength λ, the blaze angle is given by (J.M. Senior, 2009) :

$$\Theta_B = \mathrm{Sin}^{-1}\left[\frac{\lambda}{2\Lambda}\right] \qquad 3.14$$

Where Λ is the grating period.

Other WDM couplers use optical spectral filters, which are primarily categorised into two types: absorption filters and interference filters. According to Syed Azer Reza (2019), thin-film interference filters are a cost-effective alternative to fused fibre couplers for broadband wavelength-selective applications. These filters are made from glass substrates and are relatively inexpensive to produce.

Dielectric thin-film (DFT) filters are among the most widely used WDM couplers. They consist of alternating layers of materials with low (e.g., magnesium fluoride) and high (e.g., zinc sulphide) refractive indices. Each layer has a thickness equal to one-quarter of the wavelength, as depicted in Fig. 3-13.

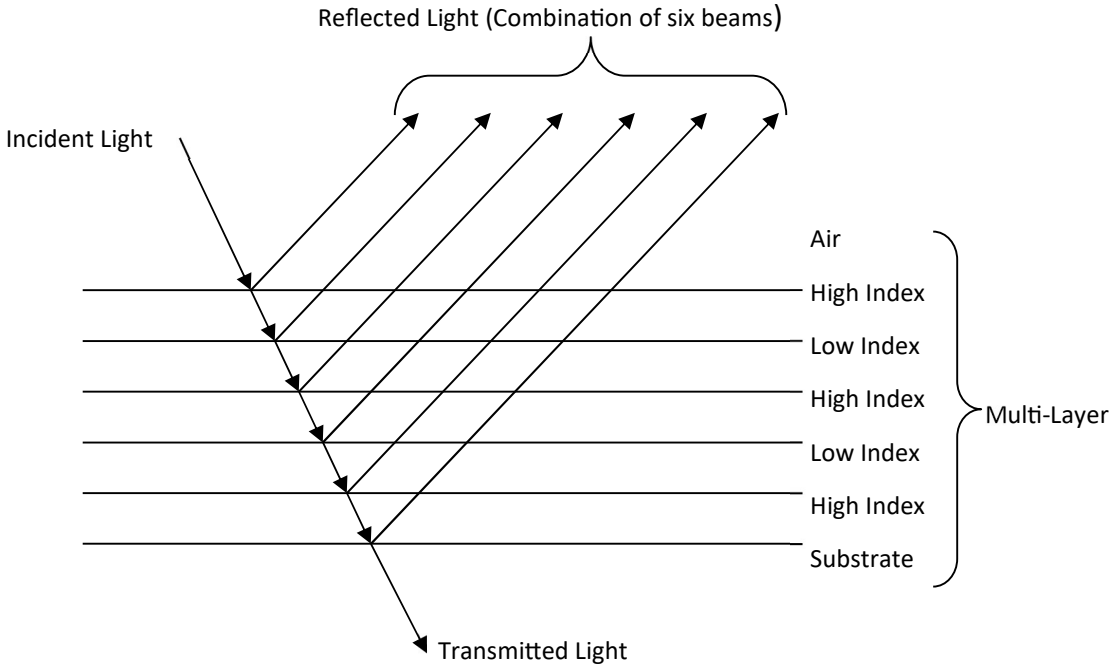

Figure 3.15: Multilayer interference filter structure. (J.M. Senior, 2009)

In a Dielectric-Thin-Film (DFT) WDM coupler, optical light reflected from the low-index layers experiences a 180° phase shift, while light reflected from the high-index layers does not. This results in constructive interference at the filter's front face (J.M. Senior, 2009). The wavelength range with high reflectance is determined by the ratio of the low to high refractive indices, with reflectance dropping sharply outside this range. DFT filters can be used to construct high-pass, low-pass, or high-reflectance coatings.

3.5 Application of Optical Fibre-Based Couplers

Optical fibre-based power splitters are utilised in various applications, including laser transmitters and receivers, narrowband and broadband optical amplifiers, monitoring fibre-optic communication channels, optical gain controllers, and Wavelength Division Multiplexed (WDM) add-drop modules. Additionally, optical fibre tap couplers are essential in fibre optic networks, as they periodically extract a portion of the incoming optical signal to test signal quality, network noise performance, and losses.

3.6 Summary

The chapter detailed several performance parameters critical for evaluating couplers. Excess loss measured the difference between the input power and the total output power, highlighting the optical energy lost within the coupler. The coupling ratio defined how input light was distributed among the output ports and varied with wavelength. Insertion loss refers to the loss of optical power as light travels through the coupler from the input port to a single output port. Uniformity assessed the consistency of coupling ratios across different output ports. Directionality loss (crosstalk) was measured as the power reflected at the input port, with lower values indicating better performance. Return loss, or directivity, quantifies the amount of reflected power relative to the input power, indicating how well the coupler transmits light. Throughput loss measured the power loss from the input port to the throughput port, where light power was typically highest. Wavelength isolation assessed how well the coupler separated different wavelengths at its output, which was crucial for minimising crosstalk in WDM systems.

Various types of optical couplers were discussed, including butt couplers, which rely on the overlap of fibre end faces and are used to split light based on the degree of overlap. Y-splitters or couplers split light into two branches and can be fabricated using methods such as polishing and soft lithography, which are known for their simplicity and cost-effectiveness. Fused biconical taper (FBT) couplers, created by fusing and tapering optical fibres, were noted for their low excess loss and crosstalk but could suffer from issues related to modal noise and wavelength-dependent losses. Polished asymmetrical couplers involve polishing fibres to achieve desired coupling ratios and might experience losses due to mode conversion at the polished sections. Micro-bend-type couplers apply periodic bending to the fibre to achieve mode coupling with minimal excess loss, making them advantageous for their low loss. Mixing rod couplers used a glass rod to mix optical power from multiple fibres, ensuring uniform distribution. Wavelength Division Multiplexing (WDM) couplers managed multiple wavelengths simultaneously and were essential in WDM systems. Optical filters, dispersive gratings, and surface interaction filters each served specific roles in wavelength separation and multiplexing.

3.7 References

- Alicia López, M. Á. (2018). *Characterization of a Y-Coupler and Its Impact on the Performance of Optical Fiber Links.* MDPI, 1-8.
- Bazakutsa, P. V., Boev, M. A., & Nikitin, A. I. (2022). *Fused optical couplers: power transfer between optical fibres*. 2012 IEEE 4th International Conference on Adaptive Science & Technology (ICAST) (pp. 1-5). Moscow: IEEE.
- Jing Yang, Y. L. (2021). *Variable-fiber optical power splitter design based on a triangular prism.* Applied Optics, 1-6.
- J.M. Senior. (2009). *Optical Fibre Communications, Principles and Practise, 3rd ed, Harlow, UK, l, 2009, p269.* In J. Senior, Optical Fibre Communications, Principles and Practise, 3rd Edition (pp. p256 - p275).
- Keiser, G. (2011). *Optical Fiber Communications* (4th ed.). New York: McGraw-Hill.
- K. Sunil Kumar1, D. (2016). *Fabrication and characterization of Low-cost Plastic optical fibre couplers*. International Research Journal of Engineering and Technology (IRJET)(Volume: 03 Issue: 06 | June-2016), 1972 - 1975.
- M.S.M. Ghazali, F. R. (2021). *Manufacturing of Polymer-based 1×2 Y-branch Symmetric and Asymmetric Waveguide Coupler through Moulding Technique.* International Journal Of Automotive And Mechanical Engineering, 8998 – 9005.
- N. S Mohamed-Kassim, et. al. (2017). *High-resolution tunable POF multimode power splitter. Optics Communications, 136-143.*
- Paschotta, D. R. (2024). *https://www.rp-photonics.com/beam_splitters.html*.
- Sariki, et al., (2021). *Design and fabrication of POF Couplers/Splitters for Networking and Displacement Sensing.* 2021 International Symposium of Asian Control Association on Intelligent Robotics and Industrial Automation (IRIA) (pp. 183 -186). Goa, India: IEEE.
- Syed Azer Reza, T. S. (2019*). A dual-mode variable optical power splitter using a Digital Spatial Light Modulator and a variable focus lens.* Optical Fiber Technology, 118-125.

Chapter 4

The Immersion Depth and Backbone Reflector Effect an Optical Splitter Coupler's Parameters

4.1 Introduction

In this chapter, a 1x2 optical coupler is used to explore two techniques for adjusting the coupler's output power to achieve accurate splitting ratios for specific applications. The methods investigated are: (1) varying the immersion depth (as shown in Figure 4-5) of a polished and bent plastic optical fibre (POF) into a backbone POF, and (2) inserting a 100% reflective film or coating of variable length between the contact surfaces of the polished bent POF and the backbone POF.

Section 4.4 details the theoretical design and characterisation of a 1x2 beam-splitting coupler. The theoretical analysis in this section examines how changing the immersion depth of the bent POF affects the coupler's performance parameters. Additionally, it investigates the impact of inserting a 100% reflector between the polished surfaces of the backbone POF and the immersed POF.

In Section 4.5, the 1x2 optical beam-splitting coupler is modelled and characterised in LightTools software. The results are then compared to the theoretical findings from Section 4.4. The performance parameters evaluated include insertion loss, excess loss, coupling (splitting) ratios, uniformity, coupler efficiency, and their relationships to immersion depth.

4.2 Plastic Optical Fibre Characteristics

The optical couplers simulated in this research use cylindrical plastic optical fibres with a 1 mm diameter. The POF selected for this research is the step-index Polymethyl-Methacrylate (PMMA) fibre, known as Eska™ CK-40, supplied by Mitsubishi Rayon Co. Ltd. This fibre was chosen for its availability at London Metropolitan University (LondonMet) and its step-index profile. The Eska™ CK-40 POF has a core diameter of 0.98 mm and a numerical aperture of 0.5. The core's refractive index is 1.49, while the cladding has a refractive index of 1.402. The POF, made from PMMA, features a core diameter of 980 µm

and a thin 10 µm polymer cladding layer. Table 4-1 shows an extract of the Eska™ CK-40 POF datasheet. Throughout the research, a predefined LED optical field profile was used as the input light source, radiating 100 mW at four wavelengths: 470 nm (blue), 520 nm (green), 570 nm (yellow), and 650 nm (red). The 100mW input power was selected to simplify calculations and measurements.

Table 4-1: Datasheet extract of EskaTM CK-40 PMMA Plastic Optical Fibre Characteristics

	Units	**Min**	**Typical**	**Max**
Core Material	Polymethyl-Methacrylate Resin (PMMA)			
Cladding Material	Fluorinated Polymer			
Refractive Index Profile	Step-index			
Core Refractive Index	1.49			
Numerical Aperture	0.5			
Number of Fibres	1			
Core Diameter	µm	920	980	1040
Cladding Diameter	µm	940	1000	1060
Approximate Weight	g/m	1		

4.3 Ray Tracing Simulation to Verify the Effect of Bending Radius on Plastic Optical Fibre (POF) Attenuation and Optical Output

The bending radius specification determines how optical fibre attenuation varies with different bending radii, beyond which attenuation increases irreversibly. For the Eska™ CK-40 PMMA plastic optical fibre, the datasheet specifies a minimum bending radius of 20 mm.

To investigate this, LightTools, an optical modelling software, ran a ray-tracing simulation of the Eska™ CK-40 PMMA plastic optical fibre. The goal was to determine the bending radius at which attenuation from the bending of the POF does not affect the propagation of optical energy.

4.3.1 The Effect of Bending Radius on Optical Power Transmission

This subsection describes a simulation aimed at verifying how the bending radius affects the propagation of optical energy in a step-index plastic optical fibre (SI-POF). Figure 4.1 illustrates the ten-bend POF model used for the simulations. At one end of the SI-POF, a multi-mode LED source emits optical energy that travels through ten microbends in the fibre. At the other end, an optical receiver (a photodiode) measures the transmitted optical energy and converts it to electrical power (milliwatts). The simulation examined four wavelengths: green (520 nm), blue (470 nm), yellow (570 nm), and red (650 nm). The simulation used an input power of 100 mW and 100,000 modes to obtain a clear irradiance pattern through the design models.

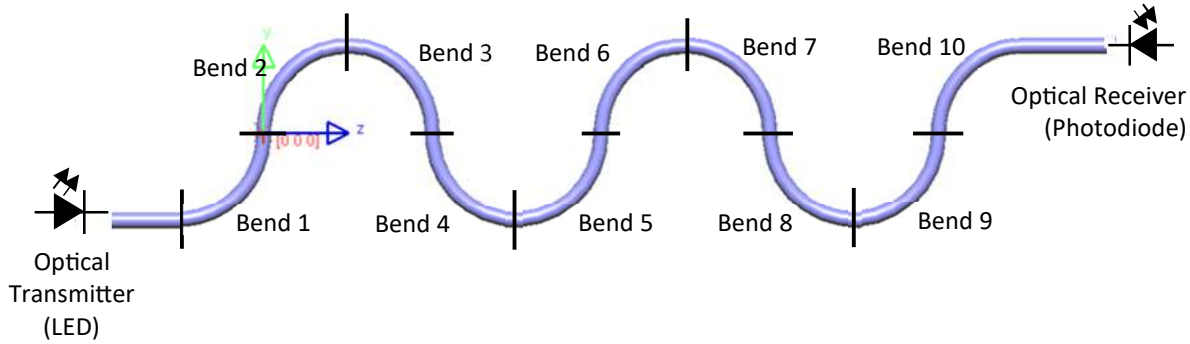

Figure 4-1: Bending radius simulations showing the optical power going through 10 micro-bends.

The methodology involved initiating the simulation with a single 90° bend of a specified radius, then progressively increasing the number of bends to 10 while measuring the receiver's output optical power at each step. This process was repeated with bending radii of 3.5 mm, 5 mm, 10 mm, 20 mm, 25 mm, and 30 mm. Figures 4.2 and 4.3 present the simulation results.

Key findings from the results in Figure 4.2 include:

1. *Bending Radii Below 10 mm*: At bending radii below 10 mm, the simulation showed that the plastic fibre behaves as a lossy transmission medium. The tight bends cause many optical modes to approach the bends at angles significantly greater than the critical angle. Consequently, a large portion of the optical modes is refracted into the cladding rather than being reflected into the core by total internal reflection

(TIR). For instance, with a 3.5 mm bending radius, the optical power drops by 35% after 10 bends, corresponding to an attenuation of nearly 2 dB.

2. *Bending Radii of 10 mm and Above:* When the bending radius is 10 mm or greater, the optical output power through the POF experiences only minimal attenuation. On average, 95% of the input optical power across all wavelengths reaches the output, resulting in an attenuation of 0.02 dB. At these bending radii, all-optical modes travel around the bends at angles less than the critical angle, ensuring they reflect into the POF core via TIR.
3. *Effect of Micro-Bends*: The simulation, particularly with the 3.5 mm bending radius, reveals fascinating insights into the orientation and impact of micro-bends in plastic optical fibre. Specifically, light modes experience greater attenuation when transitioning from an odd-numbered bend to an even-numbered bend. In other words, significant attenuation occurs when light modes pass through two 90° bends in opposite directions. However, no such attenuation is observed when the light modes traverse two 90° bends (i.e., a 180° angle) in the same direction. These findings were consistent across different wavelengths.

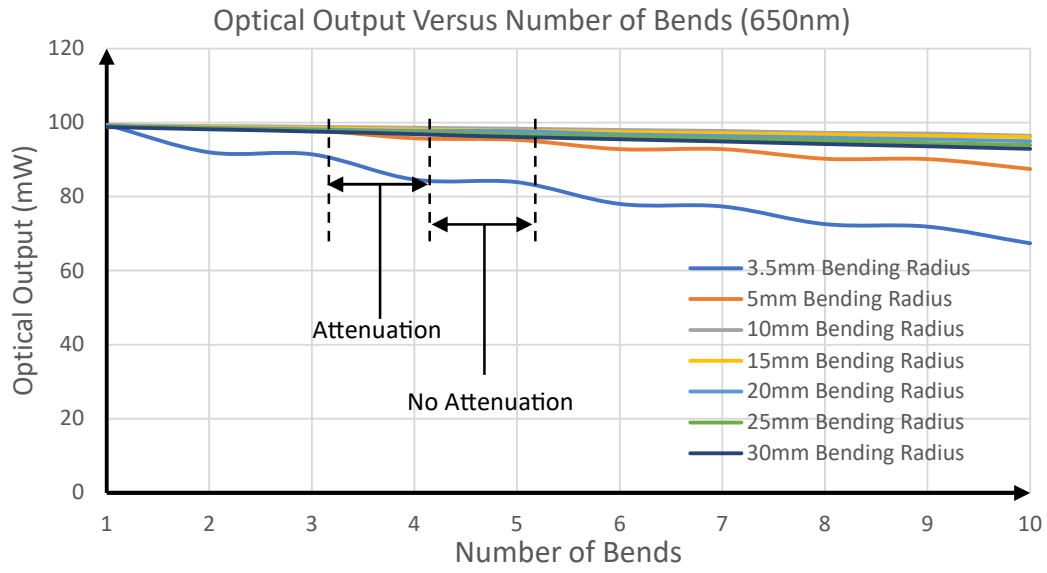

Figure 4-2: The relationship between the bending radius and the output optical power.

4.3.2 Effect of Bending Radius on Wavelength

The simulation results showed that for bending radii greater than 10 mm, the transmitted optical power through the plastic optical fibre is only marginally affected. Almost all optical modes travel at angles less than the critical angle, ensuring propagation through the POF via total internal reflection (TIR). Figure 4.3 supports the findings discussed in subsection 4.3.1 and illustrates the attenuation characteristics of the simulated POF.

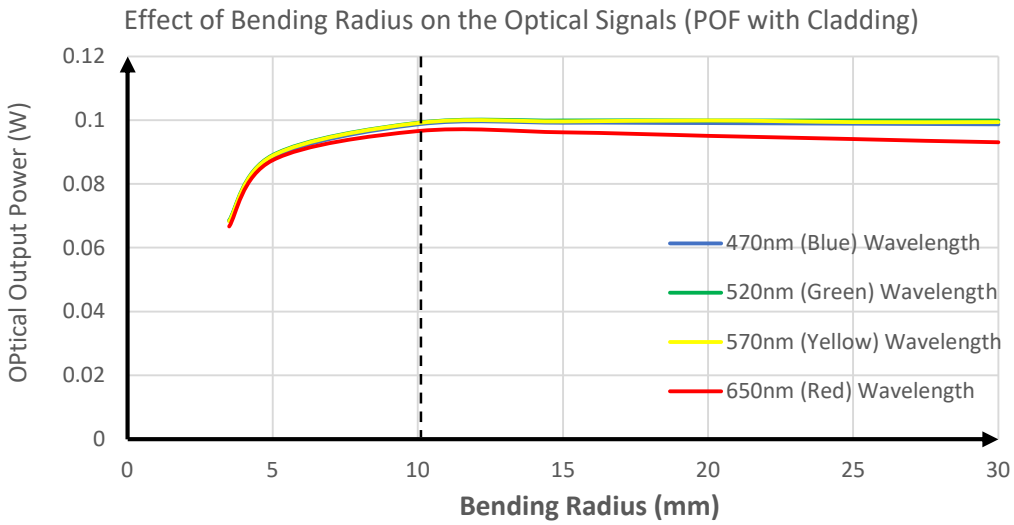

Figure 4-3: Bending radius characteristics for SI-POF at different optical wavelengths.

The simulation results also revealed that the attenuation of optical power by the POF varies with wavelength. For a bending radius of 30 mm, where the output power remains unaffected by the number of bends, the 470 nm (blue) wavelength experiences the lowest attenuation of 0.01 dB. This is followed by the 520 nm (green) wavelength with an attenuation of 0.02 dB, the 570 nm (yellow) wavelength with an attenuation of 0.03 dB, and the 650 nm (red) wavelength with an attenuation of 0.31 dB. Higher wavelengths correspond to greater attenuation. On average, 99% of the input optical power reaches the output at 470 nm (blue), 520 nm (green), and 570 nm (yellow), compared to 93% at 650 nm (red). These results confirm that, as specified in the datasheet, the attenuation characteristics of the plastic optical fibre depend on the wavelength of the optical power due to the wavelength-dependent refractive index of the POF core material.

4.4 Theoretical Analysis of 1x2 POF Coupler

This section presents two theoretical investigations into methods for adjusting the output power of the 1x2 coupler shown in Figure 4.4. The first investigation examines the effect of embedding or immersing the curved POF of the coupler into the backbone POF at various depths corresponding to different splitting ratios. For each splitting ratio, the output power is measured at the output ports, i.e., ports P_{out} and P_B. Five splitting ratios were tested, covering immersion depths from 10% to 50%. In this context, immersion depth refers to the extent to which the bent POF extends into the backbone POF, which, in turn, affects the splitting ratio.

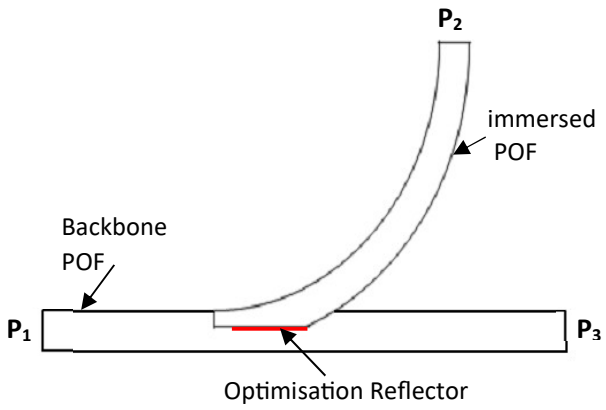

Figure 4-4: Components of the proposed beam splitting coupler, including the optimisation reflector.

In the second investigation, a 100% reflector, which could be a film or coating, is inserted between the polished surfaces of the immersed POF and the backbone POF. This reflector is positioned at the bevelled edge of the polished backbone POF and is referred to as an "optimisation reflector." In this thesis, "optimisation" refers to the fine adjustments made to the optical power propagating through the coupler to achieve optimal performance.

4.4.1 1x2 Coupler Construction

The primary 1x2 coupler, depicted in Figure 4.4, serves as the fundamental component for the array couplers discussed in the subsequent chapters of this research. This coupler consists of one arm bent at a 25 mm radius and polished on one side, and a backbone POF

that remains straight and polished on the side that interfaces with the bent or curved POF. Although the datasheet for the Eska™ CK-40 specifies a minimum bending radius of 20 mm, this thesis uses a bending radius of 25 mm, exceeding the minimum requirement. The bent POF is then immersed in the backbone POF at various depths, as illustrated in Figure 4.5. The coupler also includes a 100% reflector, whose operation is described in Section 4.4.2.

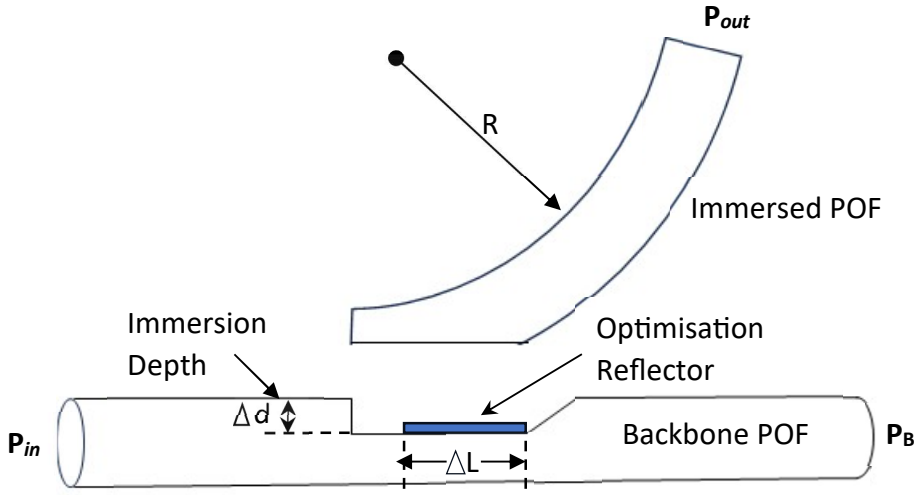

Figure 4-5: Illustration of the components of a 1x2 beam splitting coupler and the concepts of immersion depth and optimisation reflector.

4.4.2 Principle of Operation

The meridional modes applied at port P_{in} by a multi-mode transmitting source (LED) propagate through the backbone POF. For simplicity, skew modes are not considered in this theoretical analysis. When the propagating modes reach the junction where the immersed POF intersects with the backbone POF, some modes are coupled into the immersed POF, resulting in an output at port P_{out}. The magnitude of this output optical power depends on the immersion depth (splitting ratio). The remaining optical energy is received at the backbone port P_B.

The immersed POF is side-polished to achieve an immersion depth of 10% to 50%, meaning that only an arc of up to half the core and cladding will interact with the backbone POF, as shown in Figure 4.6. The immersion depth determines the interaction arc between the polished immersed POF and the transmitted propagation modes, thereby affecting the optical power at the output ports, i.e., P_{out} and P_B. A greater immersion depth (splitting

ratio) corresponds to a wider interaction arc and captures more optical modes in the immersed POF.

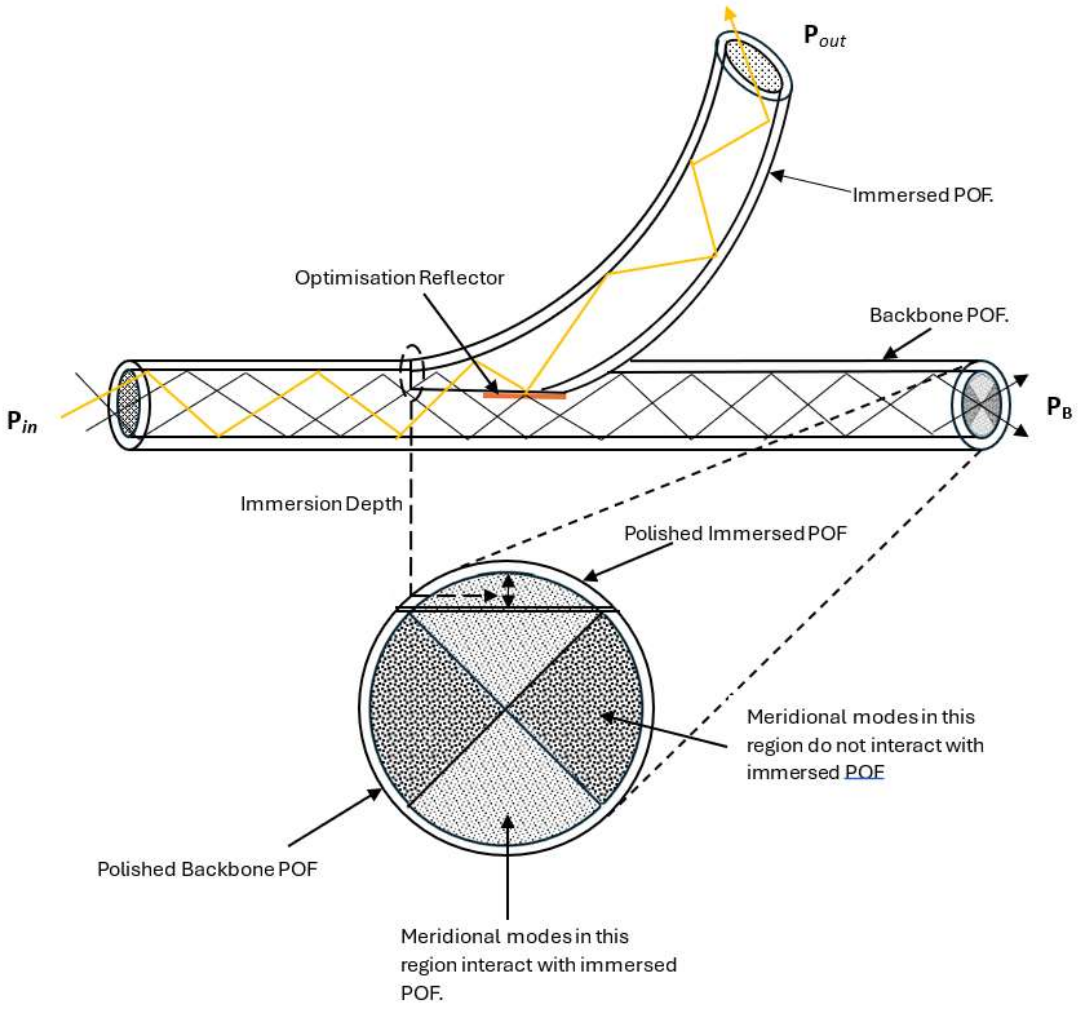

Figure 4-6: This diagram illustrates the propagation of meridional modes within the 1x2 optical coupler. It shows the cross-sectional areas of both the immersed and backbone POFs, highlighting the regions in the backbone POF where optical modes either interact or do not interact with the immersed POF.

As shown in Figure 4.6, depending on the polarisation of the meridional modes, some optical modes at the backbone output port P_B may never interact with the immersed POF, regardless of the immersion depth. The optical power received at port P_B includes both non-interacting modes and modes that interacted with the immersed POF but were not captured by it. This theoretical understanding will be validated through optical simulations using LightTools ray tracing software.

A 100% reflector (either a film or coating) placed between the polished surfaces of the immersed and backbone POFs is used to adjust the optical energy coupled into the

immersed POF. Along with the immersion depth, the length of this optimisation reflector affects the output power at port P_{out}. Changing the length of the optimisation reflector will result in corresponding variations in the optical energy received at port P_{out}.

4.4.3 The Effect of Immersion Depth on Coupler Output and Parameters

This subsection theoretically investigates how splitting ratios, ranging from 10% to 50% immersion depth, impact the optical power received at the output ports, namely, port P_{out} and the backbone port P_B. Figure 4.7 shows the cross-sectional areas of the immersed and backbone POFs, as well as the immersion depth of the coupler. Port P_{in} is the input port, with a theoretical input optical power of 100 mW. Figures 4.7(a) and (b) illustrate these cross-sectional areas and the immersion depth of the coupler. This Figure is used to theoretically analyse the immersion depth characteristics of the 1x2 optical coupler. The theoretical calculations assume that fibre Fresnel loss is negligible.

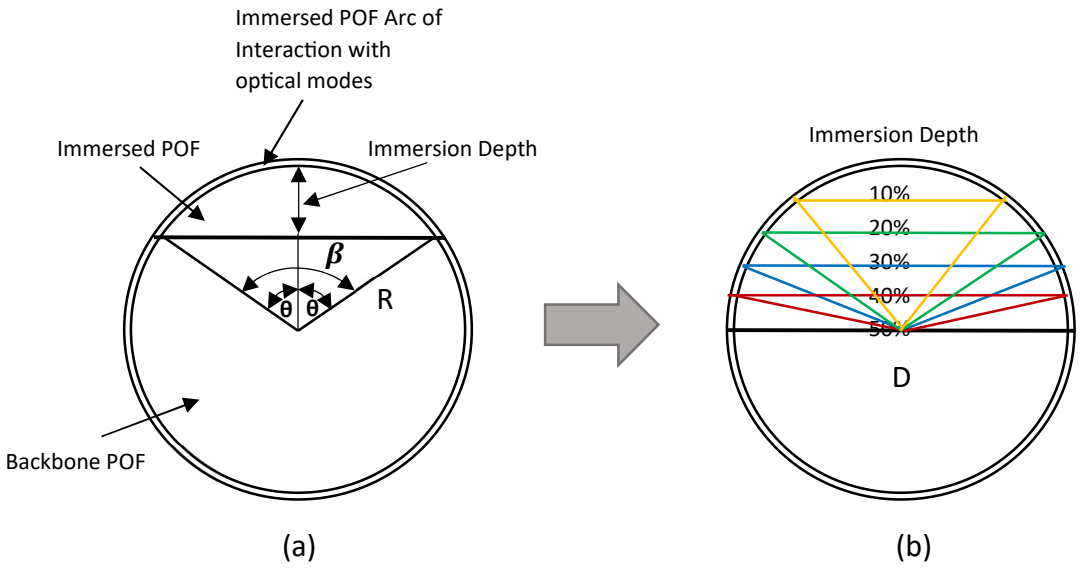

Figure 4-7: Cross-sectional diagram of the backbone POF and the immersed POF, used to determine the length of the arc on the polished immersed POF that interacts with the optical modes from the backbone POF.

Circumference of the Plastic Optical Fibre core (*C*):

$$C = \pi D \qquad 4\text{-}1$$

Where *D* is the diameter of the POF

$$C = \pi \times 0.98$$

$$\underline{C = 3.079 \text{ mm}}$$

The angle subtended at the centre of POF by the arc due to the immersed plastic optical fibre is derived from Figure 4-7:

$$\beta = 2\theta \qquad 4\text{-}2$$

Where

$$\theta = \cos^{-1}\left[\frac{\text{Core Radius of POF - Immersion Depth}}{\text{Core Radius of POF}}\right] \qquad 4\text{-}3$$

It is to be noted that the radius of POF includes the cladding as well. The arc length of the polished POF immersed in the backbone optical fibre was calculated as follows:

$$L_{arc} = {}^{\beta}/_{360} \times C \qquad 4\text{-}4$$

Immersed POF Port Output (P_{out})

$$P_{out} = P_{in}\left[\frac{L_{arc}}{C}\right] \qquad 4\text{-}5$$

Backbone Port Output (P_B)

$$P_B = P_{in}\left[\frac{C - L_{arc}}{C}\right] \qquad 4\text{-}6$$

Where: P_{in} = Transmitter optical power into the POF

L_{arc} = length of the immersed POF arc of mode interaction

C = Circumference of the backbone POF

P_B = Optical output power at the other end of the backbone POF

Equations 4.5 and 4.6 were used to calculate the optical power received at the output ports P_{out} and P_B for immersion depth ratios ranging from 10:90 to 50:50. The primary focus is on the output power at port P_{out}. The results, shown in Table 4-2 and the corresponding line graph in Figure 4-8, indicate that the coupled optical power is proportional to the immersion depth; however, the levels of proportionality are not direct.

Table 4-2: The immersion depth, the angle subtended at the centre by the immersed POF and the arc length of the immersed POF.

Splitting Ratio (Immersion Depth)	Arc length L_{arc} (mm)	P_{out} (mW)	P_B (mW)
10:90 (10%)	0.604	19.6	80.4
20:80 (20%)	0.894	29.0	71.0
30:70 (30%)	1.127	37.0	63.0
40:60 (40%)	1.338	43.0	57.0
50:50 (50%)	1.5395	50.0	50.0

At lower immersion depths, the relationship between immersion depth and coupled optical power is not directly proportional. For example, an immersion depth of 10% (10:90) does not result in 10% of the optical power being coupled to the output port. However, this proportionality improves as the immersion depth increases, becoming more accurate at 50:50. The results indicate that there is no relationship between immersion depth and the length of the mode arc of interaction (L_{arc}).

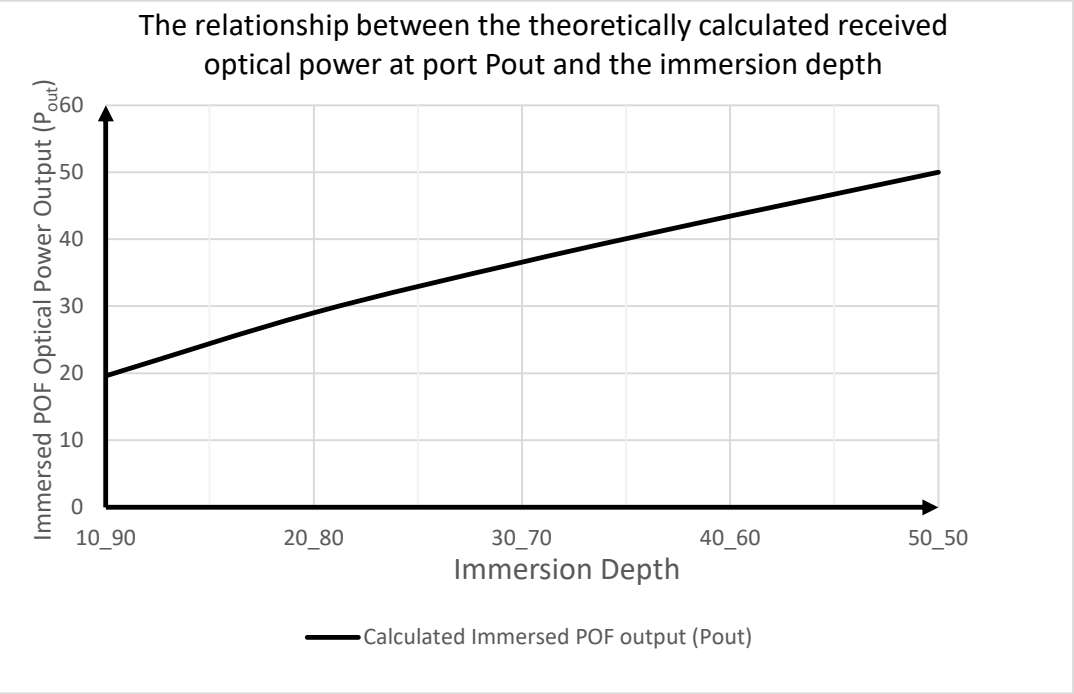

Figure 4-8: The relationship between the theoretically calculated received optical power at port Pout and the immersion depth.

When the immersion depth changes by 10%, the variation in received optical power ranges from 6 mW to 10 mW. The results for the optical power received at the output port P_{out} confirm the assertion made in Section 4.4.2 that immersion depth determines the optical power at the output ports. The calculated output power results are plotted in Figure 4.8.

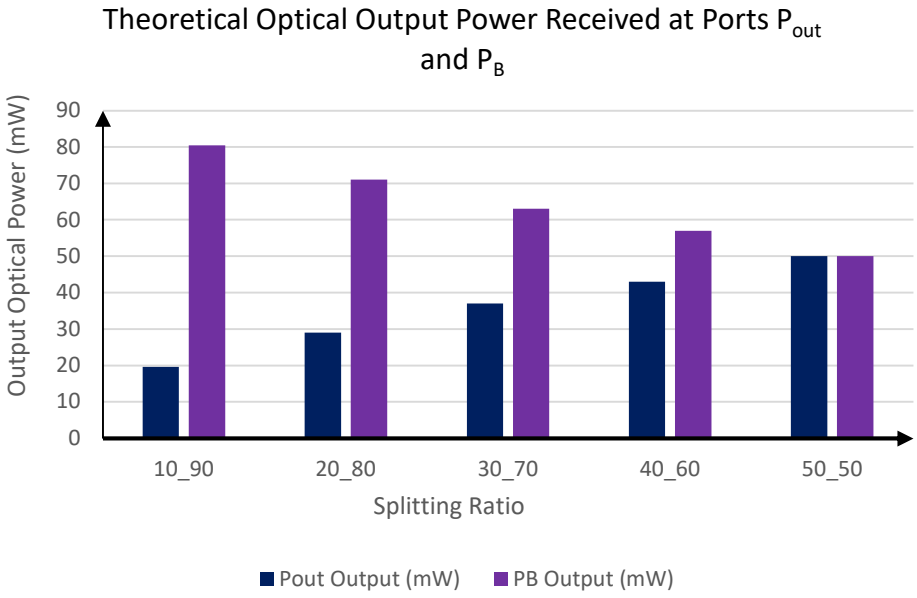

Figure 4-9: The graphs show the theoretical optical output power received at the immersed POF (P_{out}) and the backbone port (P_B) at different immersion depths.

It can be observed that the more profound (deeper) the immersion depth, the broader the arc of interaction and the more optical modes coupled into the immersed POF. Figure 4.6 shows that the mode from two opposite arcs will interact with the immersed POF. Mathematically, the percentage modes that interact with the immersed POF can be calculated as follows:

$$M_{interaction} = \frac{2L_{arc}}{C} x100\ \% \qquad 4\text{-}7$$

But from equation 4-4

$$L_{arc} = {}^{\beta}/_{360}\, x\ C$$

Substituting equation 4-4 into equation 4-7:

$$M_{interaction} = {}^{2\beta}/_{360} \ \% \qquad 4\text{-}8$$

Where $M_{interaction}$ = the percentage modes that interact with the immersed POF.

Equation 4.7 was used to calculate the percentage modes of the optical power that will interact with the immersed POF. The calculation results are tabulated in Table 4.3.

Table 4-3: The percentage modes of optical power interacting with the immersed POF.

Splitting Ratio (Immersion Depth)	Arc length L_{arc} (mm)	Percentage modes that interact with immersed POF (%)
10:90 (10%)	0.604	39
20:80 (20%)	0.894	58
30:70 (30%)	1.127	74
40:60 (40%)	1.338	86
50:50 (50%)	1.5395	100

When comparing the calculations in Tables 4.2 and 4.3, it was observed that, for all splitting ratios, half of the optical modes that interact with the immersed POF are coupled to it and reach the output port P_{out}. The other half of the modes is received at the backbone output P_B.

Figure 4.8 also shows that the optical power received at the backbone port (P_B) is directly opposite in value to the optical power at the coupling output, P_{out}. The received output power at port P_B is inversely proportional to the immersion depth. As the immersion depth increases, the received output power reduces.

4.4.4 Coupler Parameters

The relevant performance parameters of the coupler—namely, insertion loss, excess loss, uniformity, coupling (splitting) ratio, and coupler efficiency—were calculated from the results. These parameters are presented in Table 4.4.

Table 4-4: Results showing the theoretical performance parameters of the analysed 1x2 optical beam splitter.

Splitting Ratio / Immersion Depth	Excess Loss (dB)	Insertion Loss (dB)	Uniformity (dB)	Coupling Ratio (%)	Coupler Efficiency (%)
10:90 (10%)	0.0	- 7.0	- 0.3	20	100
20:80 (20%)	0.0	- 5.4	- 0.2	29	100
30:70 (30%)	0.0	- 4.3	- 0.1	37	100
40:60 (40%)	0.0	- 3.6	- 0.1	43	100
50:50 (50%)	0.0	- 3.0	0.0	50	100

The coupler is assumed to use ideal POFs with no absorption or scattering losses. Consequently, the excess loss is 0 dB, and the coupler efficiency is 100%. Insertion loss decreases with increasing immersion depth, while uniformity improves.

Table 4.4 shows that the coupling (splitting) ratio is proportional to the immersion depth. However, the rate of proportionality decreases progressively as the immersion depth increases.

4.4.5 Effect of the Optimisation Reflector on the Coupler Parameters

This section examines the impact of inserting a 100% reflective film or coating between the immersed POF and the backbone POF on the optical power received at output ports P_{out} and P_B. The purpose of the reflector is to optimise the optical power, as detailed in Section 4.4. For this analysis, the optimisation reflector is assumed to be perfectly reflective on all sides and to introduce no additional losses. Figure 4.10 shows the propagation of meridional modes across the interface between the immersed POF and the backbone POF, with the reflector included. Power scattering occurs as the modes interact at the junction of the immersed POF and the backbone POF. The splitting ratio and the reflector's properties determine the extent of mode scattering.

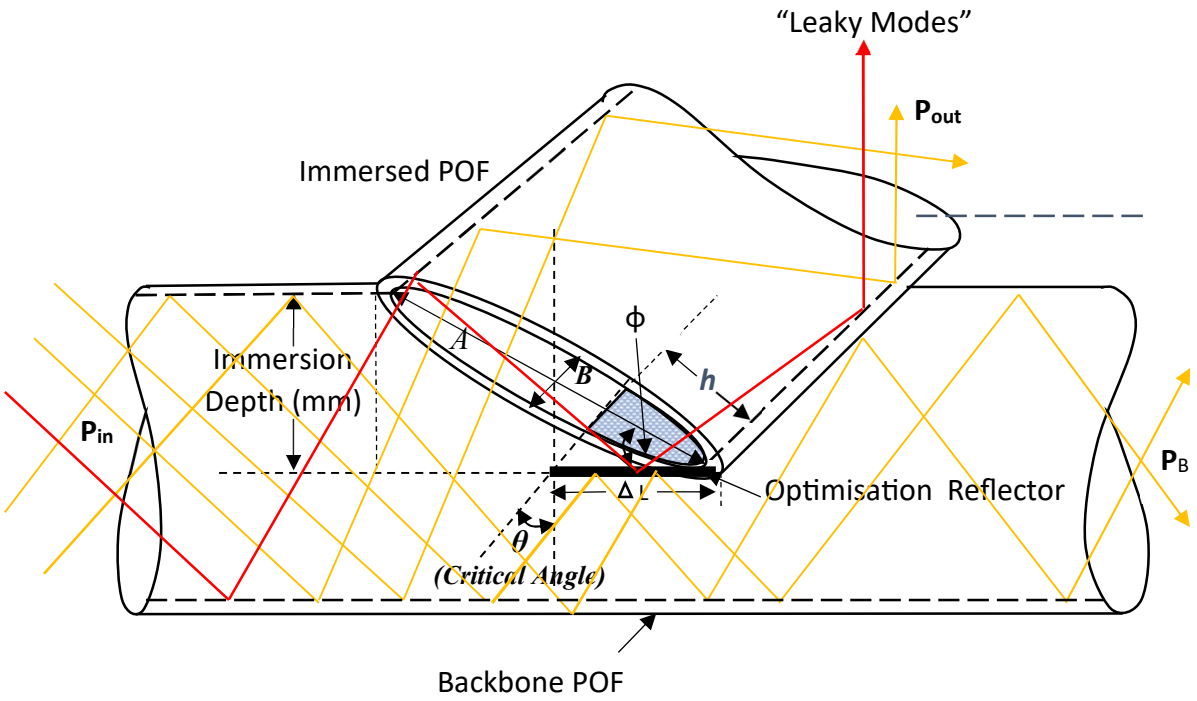

Figure 4-10: Illustration diagram for the theoretical 1x2 optical beam splitting coupler analysis.

In Figure 4.10, the angle ϕ causes the value of h to approximate the length of the optimisation reflector. As the length of the optimisation reflector is adjusted, h and the shaded segment area of the POF core ellipse also change. The shaded segment area represents the portion of the immersed POF core that the optimisation reflector prevents from capturing optical modes. Although some modes (indicated as red modes in Figure 4.10) may pass through the shaded segment of the immersed POF, they do not affect the operation of the optimisation reflector. These modes, termed "leaky modes," are not included in the calculation results but will be measured during the simulation phase of the section.

The reflector alters the optical power received at port P_{out} by reflecting some modes that would otherwise be captured by the immersed POF and redirecting them to the backbone port P_B. As the reflector length increases, more modes are reflected and redirected to port P_B, resulting in less optical power at port P_{out}.

The primary output of interest is P_{out}, which is the optical power received from the immersed POF when input power is applied at port P_{in}. The length of the optimisation

reflector was incrementally increased by 1 mm up to a maximum length of 7 mm, with splitting ratios ranging from 10:90 to 50:50.

The optical power received at the output port P_{out} for various lengths of the optimisation reflector was calculated as follows:

$$P_{out} = \text{Immersion Depth Output} \left[\frac{\text{Area of Ellipse-Area of Shaded Segment}}{\text{Area of the Ellipse}}\right] \quad 4\text{-}9$$

$$\text{Immersion Depth Output} = P_{in}\left[\frac{L_{Arc}}{C}\right] \quad 4\text{-}10$$

This thesis utilises the standard geometric formula (Equation 4-11) for the area enclosed by an ellipse with major axis length = A and minor axis length = B.

$$\text{Area of Ellipse} = \pi \times \frac{A}{2} \times \frac{B}{2} \quad 4\text{-}11$$

Another mathematical formula employed in this thesis is the area of an elliptical segment formula given in equation 4-12 (Korn, 2000):

$$\text{Area of Shaded Segment} = \frac{AB}{4}\left[\text{ArcCos}\left(1-\frac{2h}{A}\right) - \left(1-\frac{2h}{A}\right)\sqrt{\frac{4h}{A}-\frac{4h^2}{A^2}}\right] \quad 4\text{-}12$$

When equations 4-11 and 4-12 are applied to the diagram in Figure 4-10 to derive the formula for the resultant port immersion depth optical power output (P_{out}). Equations 4-13 and 4-14 give the resultant formula. The port immersion depth optical power output (P_{out}) refers to the optical power received at the output of the immersed POF when no reflector is inserted. The expression to determine optical power output was derived to be:

$$P_{out} = \left[\frac{4P_{in}L_{Arc}}{\pi ABC}\right]\left[\frac{\pi AB}{4} - \frac{AB}{4}\left[\text{ArcCos}\left(1-\frac{2h}{A}\right) - \left(1-\frac{2h}{A}\right)\sqrt{\frac{4h}{A}-\frac{4h^2}{A^2}}\right]\right] \quad 4\text{-}13$$

$$P_{out} = \left[\frac{P_{in} L_{Arc}}{C}\right]\left[1 - \frac{1}{\pi}\left[\text{ArcCos}\left(1-\frac{2h}{A}\right) - \left(1-\frac{2h}{A}\right)\sqrt{\frac{4h}{A} - \frac{4h^2}{A^2}}\right]\right] \quad 4\text{-}14$$

Where:

P_{in} = Transmitter optical power into the POF

L_{arc} = length of the arc provided by the immersed POF at that port output

C = Circumference of the backbone POF

A = Main axis of the immersed POF core ellipse

B = Secondary axis of the immersed POF core ellipse

h = height of the immersed POF core shaded segment (assumed to be equal to the length of the optimisation reflector)

4.4.6 The Results

An input optical power of 100 mW was applied at port P_{in}, and the output optical power was measured at port P_{out}. The results were calculated using Equation 4-14 and are presented in Table 4-5.

Table 4-5: The results show the effect of the optimisation reflector on the output power received at the output port of the coupler (P_{out}).

Immersion Depth or the splitting ratio	Length of the Optimisation Reflector (mm)						
	0	1	2	3	4	5	6
10:90	20	18	15	11	8	4	1
20:80	29	26	21	16	10	5	1
30:70	37	33	26	19	11	4	0
40:60	44	39	31	22	13	5	0
50:50	50	45	35	25	15	5.4	0

The results showed that for a given immersion depth, the optical energy received at the output port (P_{out}) was inversely proportional to the length of the optimisation reflector. In

other words, as the length of the optimisation reflector increased, the optical energy received at port P_{out} decreased. This relationship is illustrated in Figure 4-11.

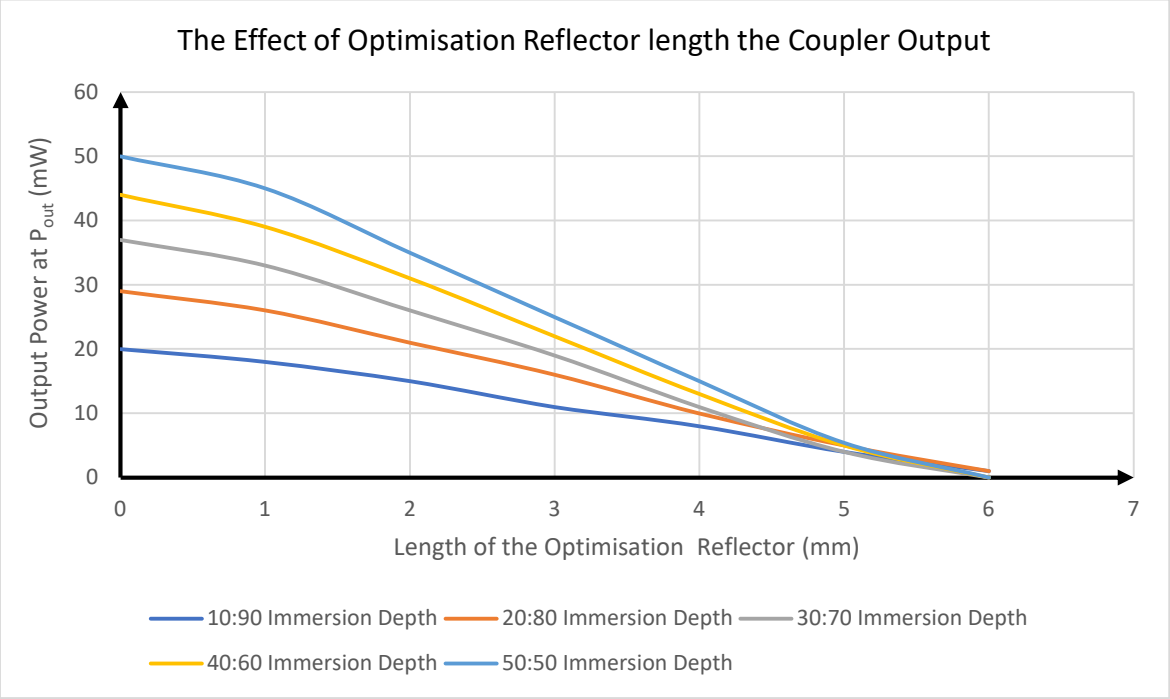

Figure 4-11: The effect of inserting a reflector between the coupling POF and the backbone POF.

The value of angle ϕ is less than 5^0 for all immersion depths, leading to the following conclusions:

1. The value of A was approximately equal to the maximum length of the optimisation reflector.
2. The value of h is equal to the length of the optimisation reflector at a given time.

Based on these assumptions, the maximum length of the reflector, L_R(max), is 6 mm, at which point the optical output power received at port P_{out} becomes zero, as shown in Figure 4.11.

The immersion depth allows for coarse adjustment of the power received at the coupling output port P_{out}. In other words, the output power (P_{out}) is fixed for each specific immersion depth. Conversely, the optimisation reflector enables fine adjustment, as changing its length modifies the output optical power (P_{out}) from zero up to the maximum value set by the immersion depth. Figure 4-11 demonstrates that a 50:50 immersion depth

yields the highest rate of change in output power per millimetre for the optimisation reflector, while a 10:90 immersion depth yields the smallest change.

4.4.7 Coupler Performance Parameters

The primary coupler performance parameter calculated in Table 4.6 is the insertion loss. Using the assumption that the coupler experiences no losses, resulting in an excess loss of 0 dB and a coupling efficiency of 100%. The coupling ratio ranges from 0% or 1% to the maximum value determined by the immersion depth, in Table 4.4. The insertion loss was calculated using Equation 3.3.

Table 4-6: The effect of the optimisation reflector on the insertion loss

Length of Reflector (mm)	Coupler Insertion Loss (dB)				
	10_90	20_80	30_70	40_60	50_50
0	7.0	5.4	4.3	3.6	3.0
1	7.4	5.9	4.7	4.0	3.4
2	8.2	6.6	5.5	4.7	4.2
3	9.4	7.7	6.6	5.9	5.2
4	11	9.2	8.2	7.4	7
5	13	11.6	10.5	10	9.6
6	17	16	14.9	14.1	13.6

Table 4.6 illustrates that for every 1 mm change in the length of the optimisation reflector, there was a corresponding increase in the insertion loss. The relationship between the insertion loss and the change in the length of the optimisation reflector is shown in Figure 4.11.

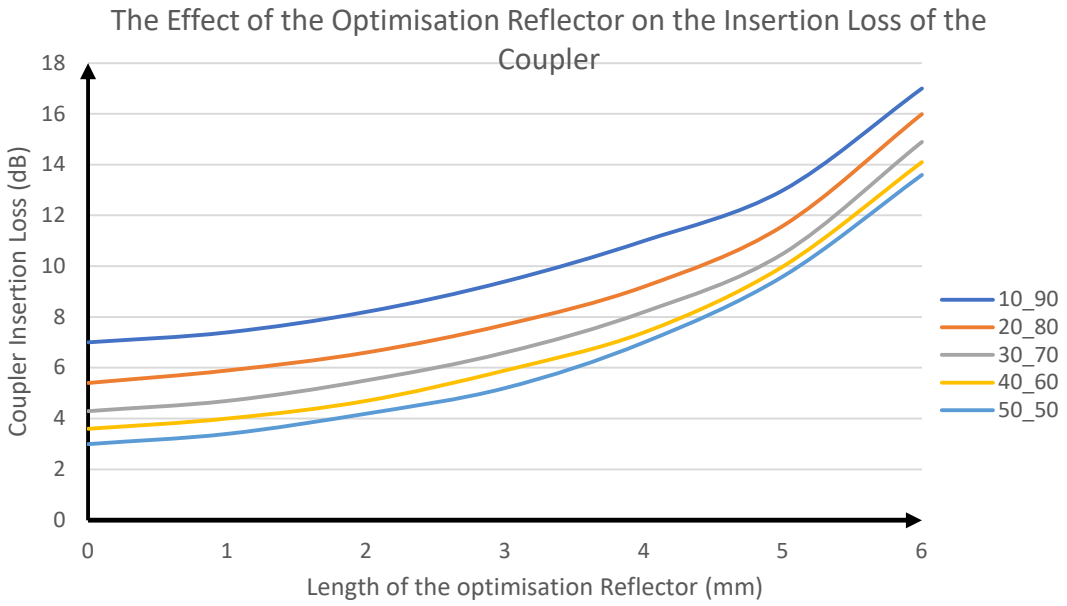

Figure 4-12: The graph showing the theoretical analysis of insertion loss due to the increase in length of the optimisation reflector for different immersion depths.

This analysis shows that the change in insertion loss across all immersion depths follows a similar semi-parabolic trend, with a peak at a reflector length of 6mm. For all immersion depths, the coupler uniformity was 0.7 dB.

The splitting ratio of 10:90 had the highest insertion loss, followed by 20:80, 30:70, and 40:60. Overall, the 50:50 splitting ratio had the least insertion loss. The results also showed that the difference in insertion loss decreases with increasing immersion depth. The explanation for this phenomenon is that as the immersion depth increases, more optical power is coupled to the port P_{out}.

4.5 Simulation and Characterisation of a 1x2 POF Coupler

This simulation aims to validate the theoretical analysis presented in Section 4.4. Two ray-tracing simulations were conducted using LightTools optical modelling software. The first simulation investigated the effect of immersion depth on the optical parameters of the simulated coupler. The second simulation, as discussed in Section 4.4.5, analysed the impact of inserting an optimisation reflector between the polished surfaces of the immersed POF and the backbone POF. Figures 4.12a and 4.12b illustrate the LightTools simulation models used in these two simulations.

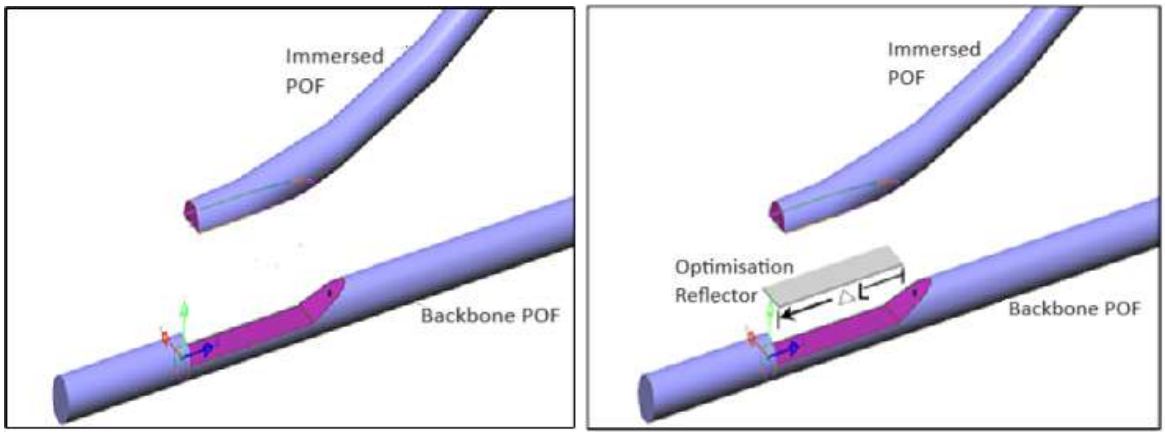

(a) (b)

Figure 4-13: Illustrations of the simulated components of the 1x2 beam-splitting coupler and the optimising reflector.

4.5.1 Simulation to verify the effect of the Immersion Depth on the Coupler Output

In this simulation, Light-Emitting Diodes (LEDs) served as the light source, while a photodiode served as the optical receiver. The simulated Plastic Optical Fibre (POF) is a step-index polymethyl methacrylate (PMMA) fibre, specifically Eska™ CK-40. This fibre has a core diameter of 980 µm, a thin 10 µm polymer cladding layer, and a numerical aperture of 0.5. The refractive indices of the core and cladding are 1.49 and 1.402, respectively. The coupler model used for the simulation is shown in Figure 4.14.

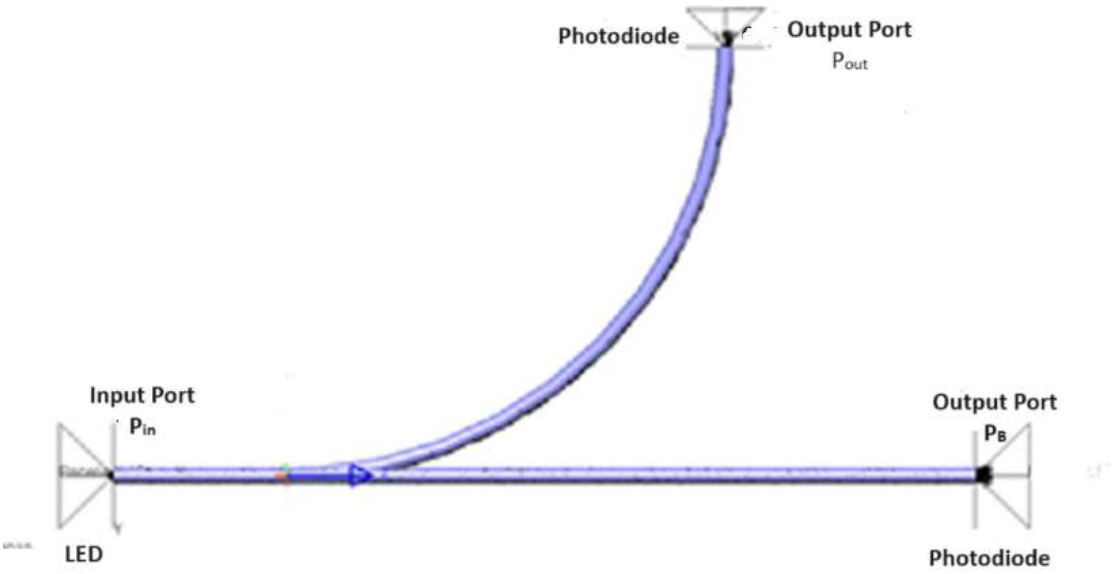

Figure 4-14: Model for simulating a 1x2 optical coupler.

A simulated input power of 100 mW was applied at the input port (P_{in}). The resulting output power was measured at both the immersed POF output port (P_{out}) and the reverse backbone port (P_B).

4.5.2 Results and Discussion

4.5.2.1 Received Optical Output Power at Port P_{out}

This simulation covered splitting ratios from 10:90 to 50:50. Table 4-7 shows the results, and Figure 4-15 shows the plots of the four wavelengths simulated.

Table 4-7: The effect of the simulated immersion depth on the received output optical power P_{out}

Splitting Ratio (Immersion Depth)	P_{out} (mW)	P_B (mW)
10:90 (10%)	19.6	79.4
20:80 (20%)	29.0	70.0
30:70 (30%)	34.6	65.4
40:60 (40%)	43.0	56.0
50:50 (50%)	56.6	42.4

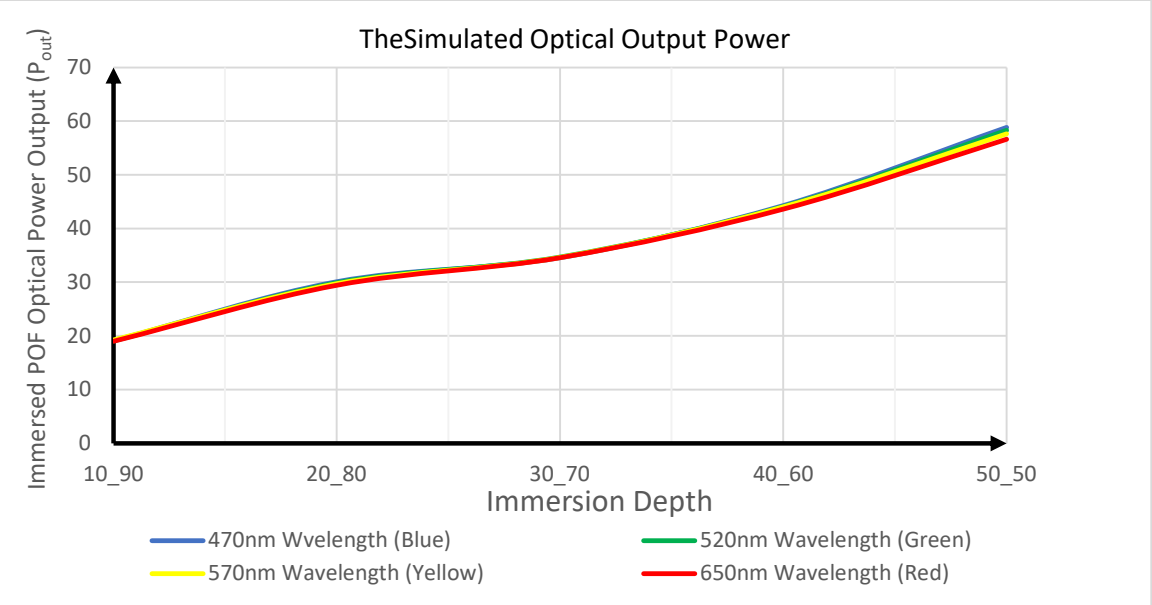

Figure 4-15: The plot graph of the results obtained from the simulation of a 1x2 beam splitter.

The simulations used four wavelengths—470, 520, 570, and 650 nm—and all exhibited the same trend: greater immersion depth yields higher received optical power. Consistent with theory, these results indicate that backbone-based couplers with an immersion depth of 40% (targeting a 40:60 split) can be fabricated reliably. The Section 4.4.3 formula can then be used to predict the output power at each port.

4.5.2.2 Irradiance and Scatter Plot Diagrams at Output Port P_{out}

The simulation results include the received optical power and irradiance, as well as scatter plots of the output port powers P_{out} and P_B. Irradiance, a radiometric term, measures the power per unit area of electromagnetic radiation incident on a surface, with SI units of watts per square meter (W/m^2) or milliwatts per square millimetre (mW/mm^2). Scatter plots, or x-y graphs, are used to visualise correlations between two variables and identify patterns.

In this simulation, both irradiance and scatter plots are vital as they provide a visual representation of the concentration and distribution of optical power received at the ports P_{out} and P_B. Figure 4.16 displays the irradiance and scatter plots for the various immersion depths used in the simulation. All wavelengths exhibited similar irradiance and scatter plots, as illustrated in Figure 4.16.

Splitting Ratio	Irradiance (mW/mm^2)			Scatter Plot (mW/mm^2)	
	Input Port (P_{in})	Output Port (P_{out})	Output Port (P_B)	Output Port (P_{out})	Output Port (P_B)
10:90	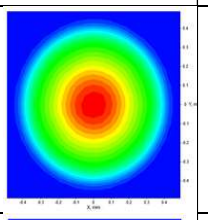	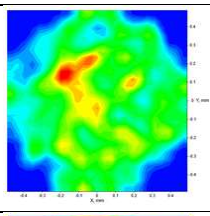	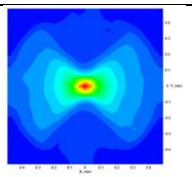	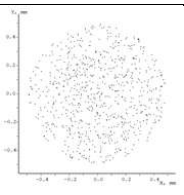	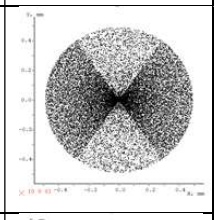
20:80	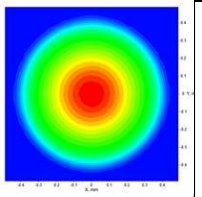	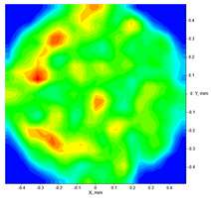	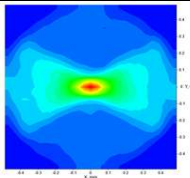	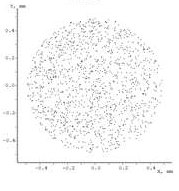	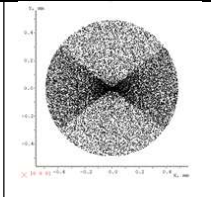
30:70	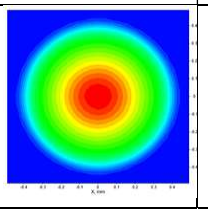	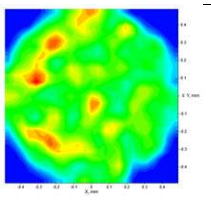	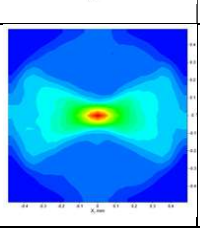	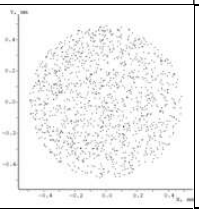	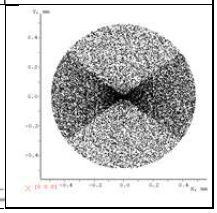

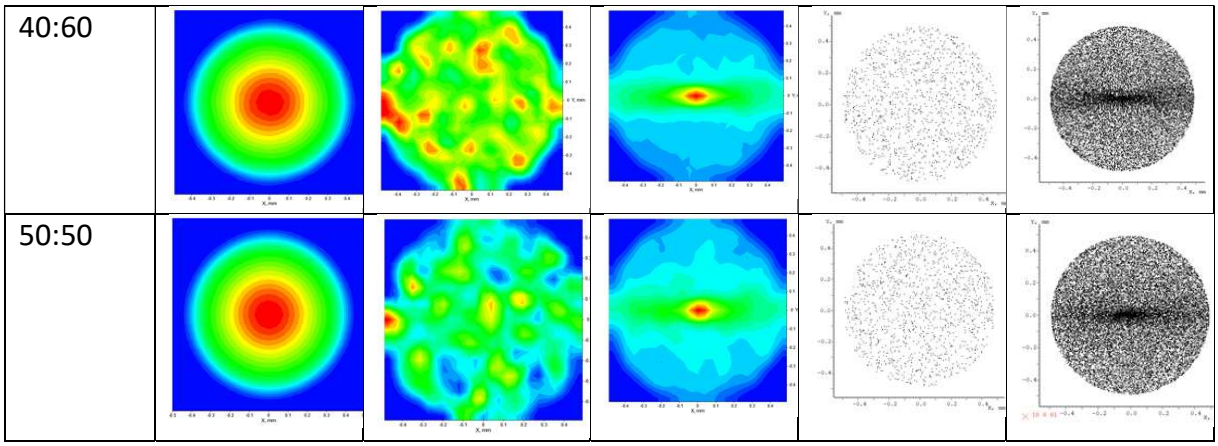

Figure 4-16: The irradiance and scatter plots resulting from different immersion depths used in the simulation.

4.5.2.3 Coupler Performance Parameters

Table 4-8 shows the optical performance parameters derived from simulation results for a 1x2 optical beam splitter. These coupler performance parameters included insertion loss, excess loss, uniformity, and coupler efficiency. The simulation results are very similar to those of the theoretical analysis.

Table 4-8: Results showing the simulated performance parameters of the analysed 1x2 optical beam splitter.

Splitting Ratio / Immersion Depth	Excess Loss (dB)	Insertion Loss (dB)	Uniformity (dB)	Coupling Ratio (%)	Coupler Efficiency (%)
10:90 (10%)	- 0.04	-7.2	-0.3	20	99
20:80 (20%)	- 0.04	-5.2	-0.2	29	99
30:70 (30%)	- 0.04	-4.6	-0.1	35	99
40:60 (40%)	- 0.04	-3.5	-0.03	48	99
50:50 (50%)	- 0.04	-2.3	-0.1	58	99

From Table 4-8, it is evident that Excess Loss is 0.04 for all immersion depths, while Insertion Loss and Uniformity decrease as the immersion depth increases. The coupling radio increases in unison with the immersion depth. The coupler achieved 99% efficiency at all the immersion depths.

4.6 Comparison between Theoretical Analysis and Simulation Analysis Results

The irradiation pattern at the output port (P_{out}) shows that the received coupled optical power is scattered for all immersion depths. This scattering occurs as the meridional modes are transferred from the polished backbone optical fibre to the side-polished immersed POF. The scattering process was discussed in Section 4.4.5 and is illustrated in Figure 4.16. A detailed example of this power-scattering effect is shown in Figure 4.17, which depicts the irradiance diagram for a splitting ratio of 40:60.

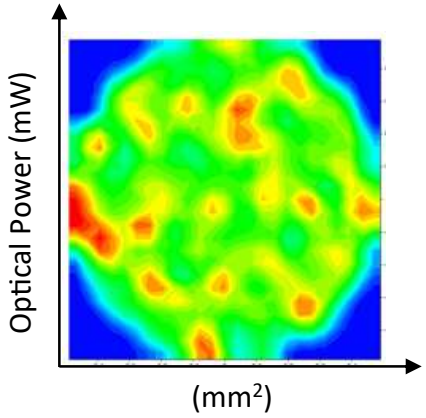

Figure 4-17: Scattered irradiance on the output port P_{out}.

The irradiance and scatter plots for the backbone output P_B, shown in Figure 4.14, are consistent with those in Figure 4.6 of Subsection 4.4.2. The simulation results confirm the theoretical analysis from Section 4.4.3, which states that some optical modes at the backbone output port do not interact with the immersed POF. Only modes that interact with the immersed POF are present at the output port. The immersion depth determines the optical power at the output ports by defining the interaction arc between the immersed polished POF and the transmitted propagation modes. Greater immersion depths result in a broader interaction angle and more optical modes being coupled into the immersed POF. Figures 4.17 illustrate typical scatter plots obtained at the backbone output P_B, similar to the theoretical scatter diagram in Figure 4.6.

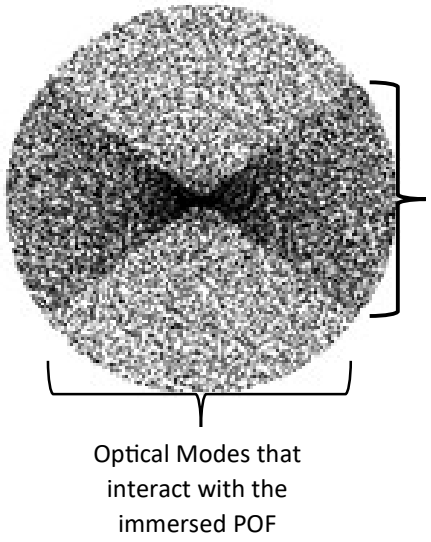

Figure 4-18: The scatter plot at the backbone output. The value of all the modes determined the splitting ratio.

4.6.1 Simulated Output P_{out} and Comparison with Calculated Results

Figure 4.18 presents both the theoretically calculated and simulated results. The simulation results show that all wavelengths exhibit similar characteristics. The theoretical calculations did not account for wavelength variations. Simulations in Section 4.5.1 demonstrated that all wavelengths propagate similarly through the POF. Additionally, the calculations did not consider skew modes, mode scattering, or mode coupling, as these factors were deemed to have minimal impact on the expected results.

Table 4-9: The comparison table between the theoretically calculated received output power and the simulated received output power. The table also shows the percentage differences

Splitting Ratio (Immersion Depth)	Theoretical P_{out} (mm)	Simulated P_{out} (mW)	Result Difference (mW)	Percentage Difference (%)
10:90 (10%)	19.6	19.0	- 0.6	- 3.1
20:80 (20%)	29.0	29.5	+ 0.5	+1.7
30:70 (30%)	36.6	34.4	- 2.2	-6.0
40:60 (40%)	43.0	43.6	+ 0.6	+1.4
50:50 (50%)	50.0	56.6	+ 6.6	+13.2

Table 4-9 and the graph in Figure 4-16 illustrate that, for all wavelengths, the optical power coupled to the immersed POF reaches its maximum at an immersion depth of 50% (50:50). This is because the curvature of the immersed POF, which is responsible for coupling the optical power, is optimised at this immersion depth.

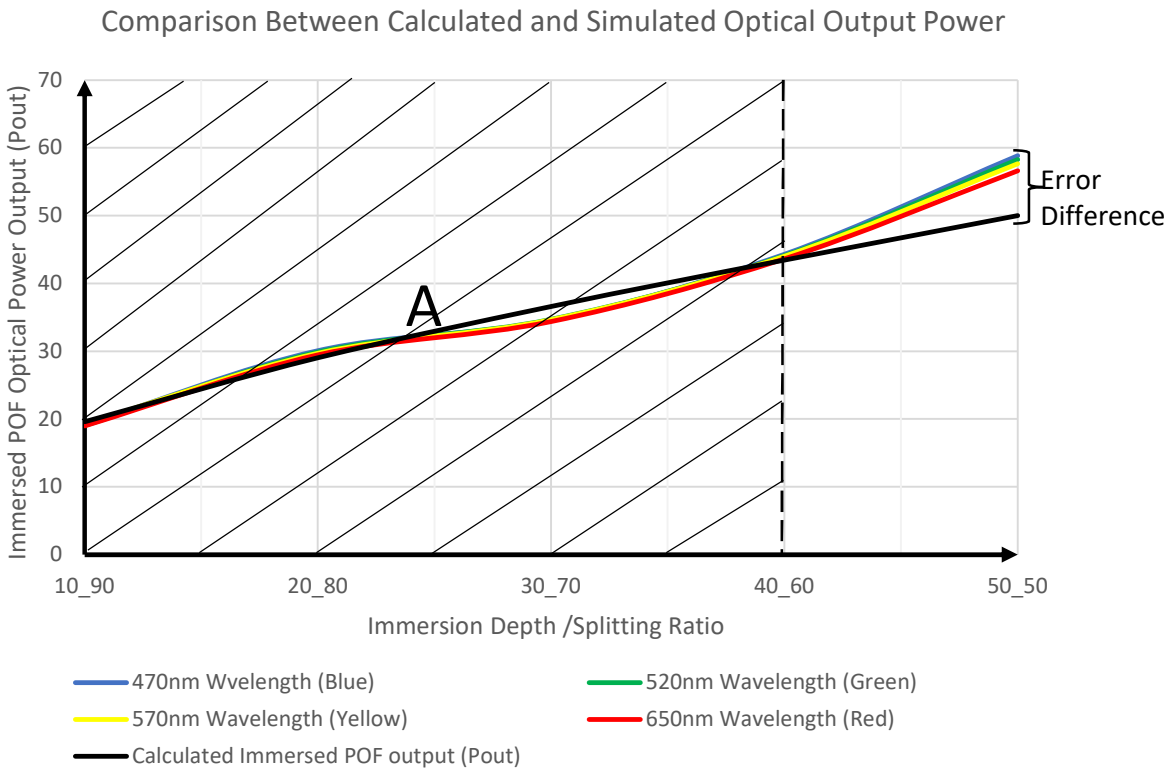

Figure 4-19: The simulated optical output power (P_{out}) at different immersion depths and comparison with the calculated results.

The simulations agree with the theoretical calculations for immersion depths from 10% (10:90) to 40% (40:60)—the range marked as Region A in Figure 4-18—confirming the validity of the Section 4.4.3 formulas up to a 40:60 split. The mean calculation–simulation discrepancies are: 3.1% (10:90), 1.7% (20:80), 6.0% (30:70), 1.4% (40:60), and 13.2% (50:50). The larger error at 50:50 arises from the stronger curvature where the POF is immersed, which limits modes needed at Pout, while the theoretical model assumes an ideal POF. In contrast, the simulations include parasitics—skew rays, mode coupling, and mode scattering—whose contributions raise the received output power. We also observe that insertion loss tends to be higher at the odd immersion depths (10:90, 30:70, 50:50). Notably, the discrepancy roughly doubles from 10:90 → 30:70 (3.1% → 6.0%) and from 30:70 → 50:50 (6.0% → 13.2%). Further investigation is warranted.

4.6.2 Optical Performance Parameters of a Simulated Coupler and the Comparison with Theoretical Results

The optical performance parameters of the coupler, as calculated from the simulation results, matched those obtained from the theoretical analysis in Subsection 4.4.7. A comparison of these results is presented in Table 4-10.

Table 4-10: The table shows the simulated coupler's optical performance parameters for different immersion depths, compared with theoretical calculations.

Splitting Ratio	Excess Loss (dB)		Insertion Loss (dB)		Uniformity (dB)		Coupling Ratio (%)		Coupler Efficiency (%)	
	Cal	Sim	Cal	Sim	Cal	Sim	Cal	Sim	Cal	Sim
10:90	0.0	- 0.04	- 7.0	-7.2	- 0.3	-0.3	20	20	100	99
20:80	0.0	- 0.04	- 5.4	-5.2	- 0.2	-0.2	29	29	100	99
30:70	0.0	- 0.04	- 4.3	-4.6	- 0.1	-0.1	37	38	100	99
40:60	0.0	- 0.04	- 3.6	-3.5	- 0.1	-0.03	43	48	100	99
50:50	0.0	- 0.04	- 3.0	-2.3	0.0	-0.1	50	58	100	99

As in the theoretical analysis, the simulated coupler assumed an ideal, impurity-free POF. However, the LightTools model also included parasitic effects at the fibre joint—notably skewed modes, mode coupling, and scattering (Figure 4-17). Under these conditions, the excess loss was 0.04 dB and the coupler efficiency was 99%. Results show that insertion loss decreases and uniformity improves as immersion depth increases. Consistently, Table 4-10 indicates that the coupling (splitting) ratio also increases with immersion depth. Table 4-11, derived from Table 4-10, reports the dB and percentage differences between the theoretical predictions and the simulated performance parameters.

Table 4-11: The level (dB)/percentage difference between the theoretical analysis and simulation coupler performance parameters.

Splitting Ratio	Excess Loss Difference (dB)	Insertion Loss Difference (dB)	Uniformity Difference (dB)	Coupling Ratio Difference (%)	Coupler Efficiency Difference (%)
10:90	0.04	0.2	0	0	1
20:80	0.04	0.2	0	0	1
30:70	0.04	0.2	0	1	1
40:60	0.04	0.1	0.1	1	1
50:50	0.04	0.7	0.1	7	1

Table 4-11 indicates that the theoretical predictions and LightTools simulations agree closely across most immersion depths. Specifically, the excess loss differs by only 0.04 dB, and the coupler efficiency by 1%. Uniformity matches within 0 dB for 10:90–30:70 and within 0.1 dB at 40:60 and 50:50. For the range 10:90–40:60, the maximum insertion-loss deviation is 0.2 dB, and the largest coupling-ratio deviation is 1%—differences that are practically negligible for design and verification.

These small discrepancies primarily arise from two sources: (i) the idealised assumptions in the theoretical model (loss-free, impurity-free POF), and (ii) numerical effects such as rounding and truncation in intermediate calculations. In contrast, the simulations explicitly capture parasitic phenomena at the fibre joint including skewed modes, mode coupling, and scattering (Figure 4-17), which contribute marginally to the received power and thus to the observed deltas.

A notable exception occurs at the 50:50 immersion depth, where parasitics become more pronounced: the insertion-loss difference increases to 0.7 dB (compared with ≤0.2 dB elsewhere), and the coupling-ratio difference rises to 7% (vs. ~1% in other cases). This degradation is consistent with the stronger curvature and modal constraints near equal splitting, which enhance sensitivity to non-idealities.

The results validate the Section 4.4.3 formulas up to at least 40:60, and they delineate a practical operating window (10:90–40:60) where theory and simulation align within tight tolerances. For designs pregeometry or, applying calibration factors, refining polish/reflector geometry, or incorporating parasitic-aware corrections in the design equations is recommended, and further targeted investigation is warranted.

4.7 Simulation of the Effect of an Optimisation Reflector on the Coupler Performance Parameters

In this simulation, we examine the 1x2 POF coupler, which serves as the basis for the optimised array couplers discussed in Chapter 5. As described in Section 4.4, "optimisation" involves inserting a hypothetical 100% reflector (film or coating) with no losses between the polished surfaces of the backbone POF and the immersed POF. Figure 4.12(b) illustrates a typical setup of the simulated coupler.

The reflector's role is to reflect optical energy from all sides. By placing this reflector between the polished surfaces of the backbone POF and the immersed POF, the incoming optical power is split between the two components. As a result, some optical energy is directed to the output port P_{out}, while the rest is transmitted to the backbone POF output P_B.

Figure 4.12(b) shows that varying the length of the optimisation reflector impacts the output optical energy until it reaches a plateau. Additionally, the immersion depth of the splitting POF into the backbone POF also affects the optical energy received at the output port. The length of the backbone reflector is measured from the bevelled side of the backbone POF. The results of this simulation are shown in Figure 4.18.

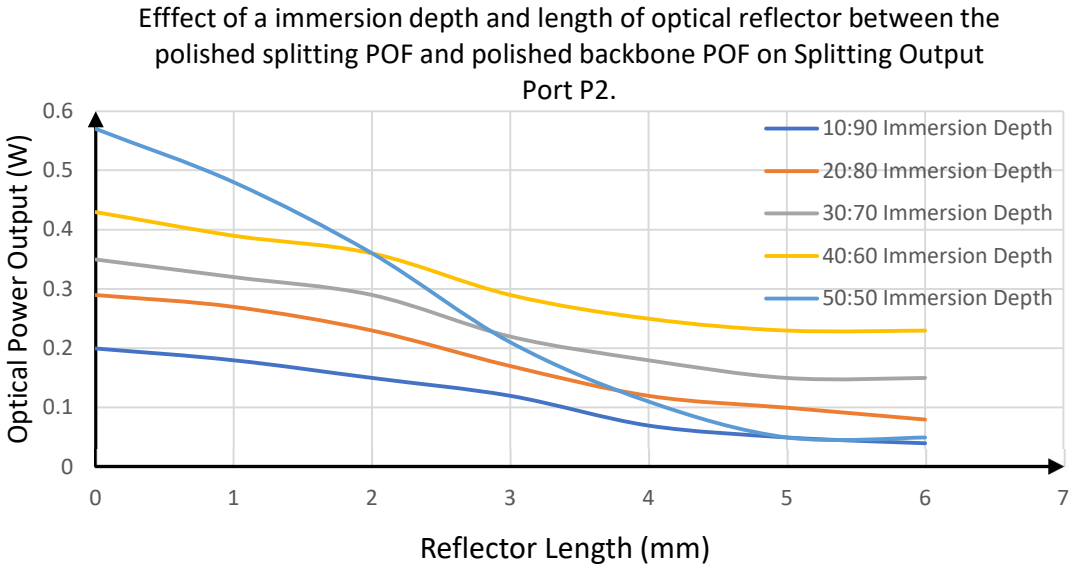

Figure 4-20: The Effect of the optimisation reflector on the port output power.

The simulation results reveal that the optical energy received at the output port P_{out} decreases as the length of the optimisation reflector increases. Additionally, the immersion depth of the splitting coupler determines the maximum optical power received at P_{out} for each splitting ratio.

Figure 4.18 illustrates that varying the length of the optimisation reflector affects the output for splitting ratios from 10:90 up to 40:60 in a similar manner. The graphs for these splitting ratios—10:90, 20:80, 30:70, and 40:60—exhibit similar gradients until the reflector length reaches 5mm. At the 50:50 immersion depth, the trendline becomes steeper. This is expected because, at a 50:50 splitting ratio, the immersed POF interacts with all optical modes propagating through the backbone fibre from the input port. Consequently, any change in the reflector length causes a more pronounced change in the received optical power (P_{out}) compared to other immersion depths.

Figures 4.18 show that, for reflector lengths between 5mm and 6mm, the output optical power levels off at a value determined by the splitting ratio. Beyond a length of 5mm, the reflector blocks all modes from coupling into the immersed POF, except for the leaky modes described in Section 4.4.5.

For all immersion depths except 50:50, the insertion loss levels off at specific reflector lengths. For immersion depths of 30:70, 40:60, and 50:50, the insertion loss plateaus at a reflector length of 5mm. For immersion depths of 10:90 and 20:80, the insertion loss plateaus at a length of 6mm. Beyond these plateau points, increasing the reflector length has no further impact on the optical power received at the output port.

4.8 Summary

This research focused on the 1x2 optical beam-splitting coupler, which served as the foundational element for designing future array couplers. The chapter included both theoretical analysis and LightTools simulations of the 1x2 POF coupler and compared the results obtained from these methods to ensure accuracy and reliability.

Initially, the research aimed to determine the feasible bending radius for the coupler designs. The datasheet for the POF specified a minimum bending radius of 20mm. To verify this, section 4.4 employed LightTools optical modelling software. The simulations demonstrated that the optical energy remained unaffected at a bending radius of 10mm or

greater. Despite the datasheet's recommendation of a minimum radius of 20mm—twice the radius used in simulations—a bending radius of 25mm was selected for the research. This choice was crucial for validating the configuration and operation of the ray tracing software used in the subsequent analyses throughout the thesis.

The chapter also explored two techniques for adjusting the coupler output to achieve accurate splitting ratios tailored to specific applications. The first technique involved varying the immersion depth of a polished and bent POF immersed in a backbone POF. The second technique focused on inserting a 100% reflector (film or coating) of variable length between the contact surfaces of the polished bent POF and the backbone POF. Both techniques were analysed theoretically and through simulations, with the results being consistent and highly encouraging.

The results revealed that the coupled optical power to the output port was proportional to the immersion depth. However, this proportional relationship was not perfectly linear. For instance, an immersion depth of 10% (10:90) did not correspond directly to 10% of the optical power being coupled to the output port. Additionally, the coupler's insertion loss decreased with increasing immersion depth, suggesting improved performance with deeper immersion.

When a reflector is inserted between the backbone POF and the immersed POF, increasing the length of the optimisation reflector reduces optical output power and increases insertion loss. This effect was due to the reflector's ability to redirect some of the optical power away from the output port.

Overall, the research confirmed that immersion depth could be effectively used for coarse adjustment of port output power, while the optimisation reflector provided a means for fine-tuning the output power. These findings demonstrated promising results for future coupler designs, affirming that the theoretical models and simulations used in this research are reliable for predicting and optimising coupler performance.

4.9 References

Korn, G. A. (2000). *Mathematical Handbook for Scientists and Engineers.* New York: Dover Publications.

Thomas, G. B. (2018). *Thomas' Calculus* (14th Ed ed.). London: Pearson Education.

Chapter 5

Theoretical Analysis of Plastic Optical Fibre (POF) Based Couplers

5.1 Introduction

This chapter presents a theoretical analysis of novel array couplers designed for networking and other industrial applications. Section 5.2 introduces the proposed POF-based array couplers, detailing their configurations and expected operating principles. The optical fibre used in this research is a step-index PMMA POF, specifically Eska™ CK-40, which features a core diameter of 0.98 mm and a numerical aperture of 0.5.

In Section 5.3, the mathematical and theoretical design of a 1x1 POF-based array coupler is outlined. This 1x1 coupler serves as the foundation for developing 1x2, 1x4, and 1x8 array couplers. Various mathematical formulas were applied to calculate the theoretical dimensions of these couplers.

Section 5.4 focuses on the architecture of the primary 1x1 coupler and provides derivations for formulas used to calculate the output power of the proposed array couplers. Methods for optimising output power are also introduced in this section.

Sections 5.5 through 5.8 present the detailed designs and configurations of the 1x2, 1x4, and 1x8 POF-based couplers. The performance characteristics of the couplers are evaluated, with a focus on techniques to optimise or equalise the received optical power. These techniques include adjusting the immersion depth of the immersed POF, inserting a reflector between the polished surfaces of the backbone and immersed POF, and placing a reflector at the opposite end of the backbone POF to enhance optical power reflection into the coupler. The sections also investigate coupler performance parameters in relation to the type of POF used, calculating insertion loss, excess loss, coupling (splitting) ratios, uniformity, and coupler efficiency, and examining their correlation with immersion depth.

Finally, Section 5.9 examines the transmission and reception data rate capabilities of the designed array coupler. These calculations are critical for determining the feasible number of primary splitting couplers connected to the backbone POF to form the array — specifically the 1x2, 1x4, and 1x8 configurations — and for precisely analysing the coupler's power budget.

5.2 Proposed Plastic Optical Fibre (POF) Based Array Couplers

This section introduces the design and characterisation of three types of step-index POF-based optical couplers: 1x2, 1x4, and 1x8, as illustrated in Figure 5-1. These array couplers are constructed by immersing multiple 1x2 couplers into a backbone POF. For example, a 1x2 coupler consists of two couplers immersed in the backbone POF.

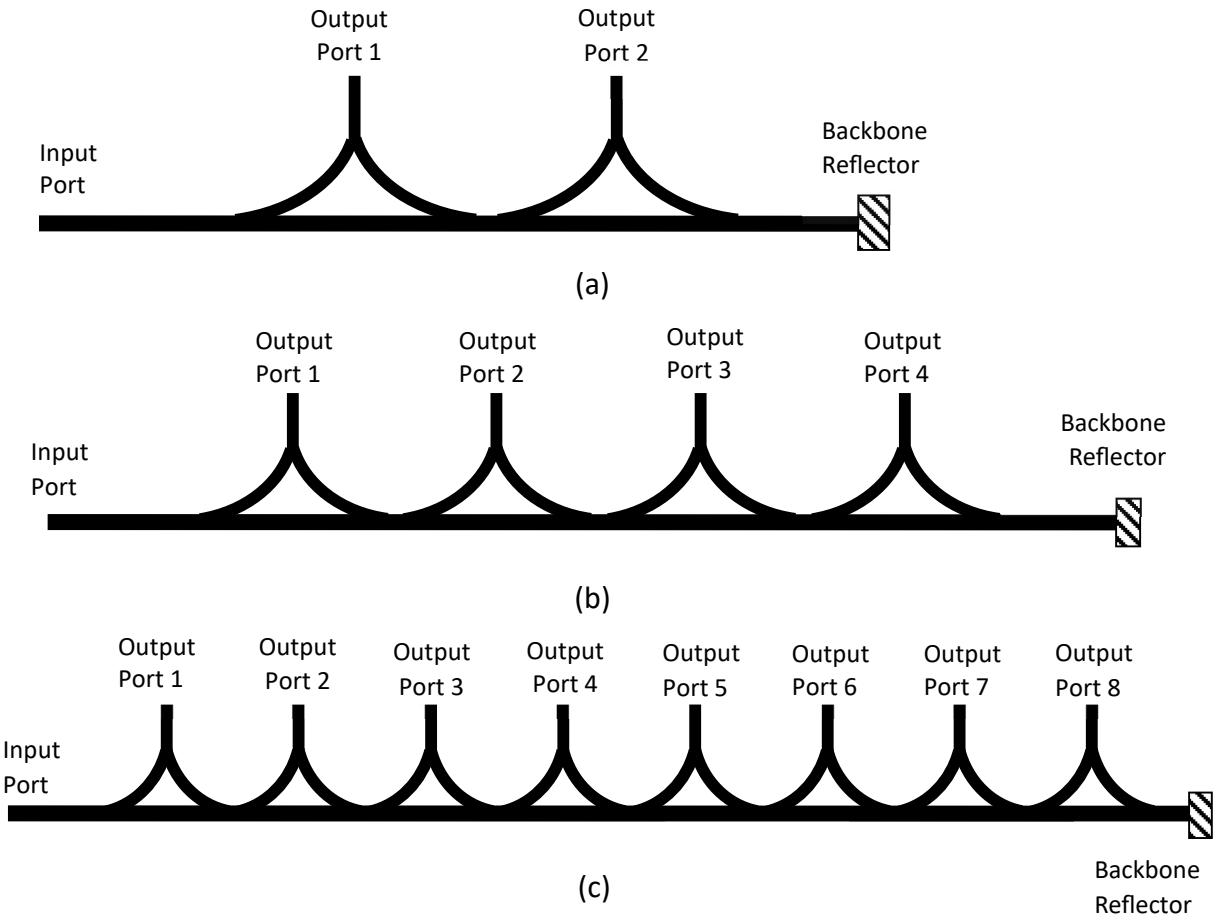

Figure 5-1: Shows the proposed theoretical POF-based array coupler designs for 1x2, 1x4 and 1x8 optical couplers. The diagram also shows the backbone reflector, which is expected to reflect the optical power from the backbone POF into the coupler.

Initially, the POF-based array couplers were designed as passive optical power receivers, with one of the backbone ports serving as the input port. Optimising the received power was expected to be achieved through two methods discussed in Chapter 4: adjusting the immersion depth for each output port and inserting a reflector between the polished surfaces of the backbone POF and the immersed POF. The length of this reflector determined the amount of power received at each output port. Additionally, a reflector

was inserted at the end of the backbone POF to reflect optical energy back into the backbone, thereby increasing the optical power received at the output ports.

A single array coupler cannot be used for both transmitting and receiving optical power simultaneously because the configuration, including immersion depth and reflector optimisation, would need to differ for each function. To use the coupler for transmission, the output ports would need to function as input ports.

5.2.1 Principle of Coupler Operation

As shown in Figure 5-1, optical power is applied to the input port of the backbone POF, and the output power is derived from each of the output ports. The power received at these output ports depends primarily on the immersion depth and the length of the optimisation reflector, as detailed in subsection 4.4.2.

Optical energy that is not coupled to the output ports remains in the backbone POF and continues to propagate. Without intervention, this energy would be lost. However, the reflector placed at the end of the backbone POF redirects this optical power back into the backbone, allowing it to couple to the output ports and increase the received power.

The key performance parameters for each array coupler include insertion loss, excess loss, coupling (splitting ratios), uniformity, and coupler efficiency. These parameters are influenced by both the immersion depth and the length of the optimisation reflector.

5.2.2 Coupler Design and Dimensions

This section covers all the calculations and measurements necessary for designing the array coupler. The array coupler is constructed by connecting two 1x2 couplers back-to-back and immersing them in a backbone POF, as shown in Figure 5-2. The bending radius of the immersed POF is 25 mm.

The design of the array coupler begins with calculating the intersection angle (ϕ) between the two arms of the 50:50 beam-splitting coupler and the immersion angle (θ) at which the curved POFs of the coupler enter the backbone POF. Both curved POFs have a bending radius of 25 mm. Additionally, the lengths of the polished surfaces on both the backbone POF and the immersed POFs were calculated using Figures 5-3 and 5-4, which illustrate and support these calculations.

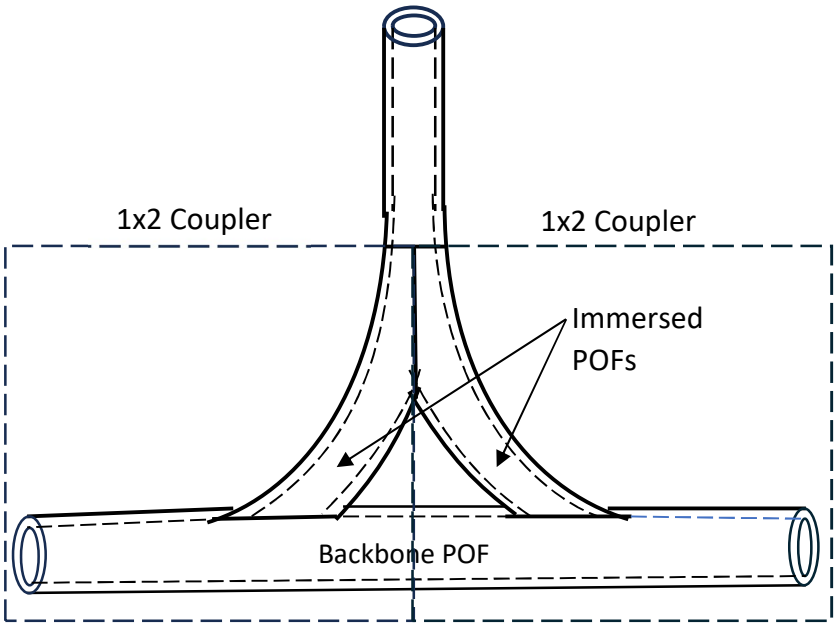

Figure 5-2: An array coupler comprising two 1x2 couplers connected back-to-back. This coupler forms the basic building block of the couplers discussed in this chapter.

5.2.2.1 Calculations for the Intersection Angle (θ) and the Immersion Angle (θ)

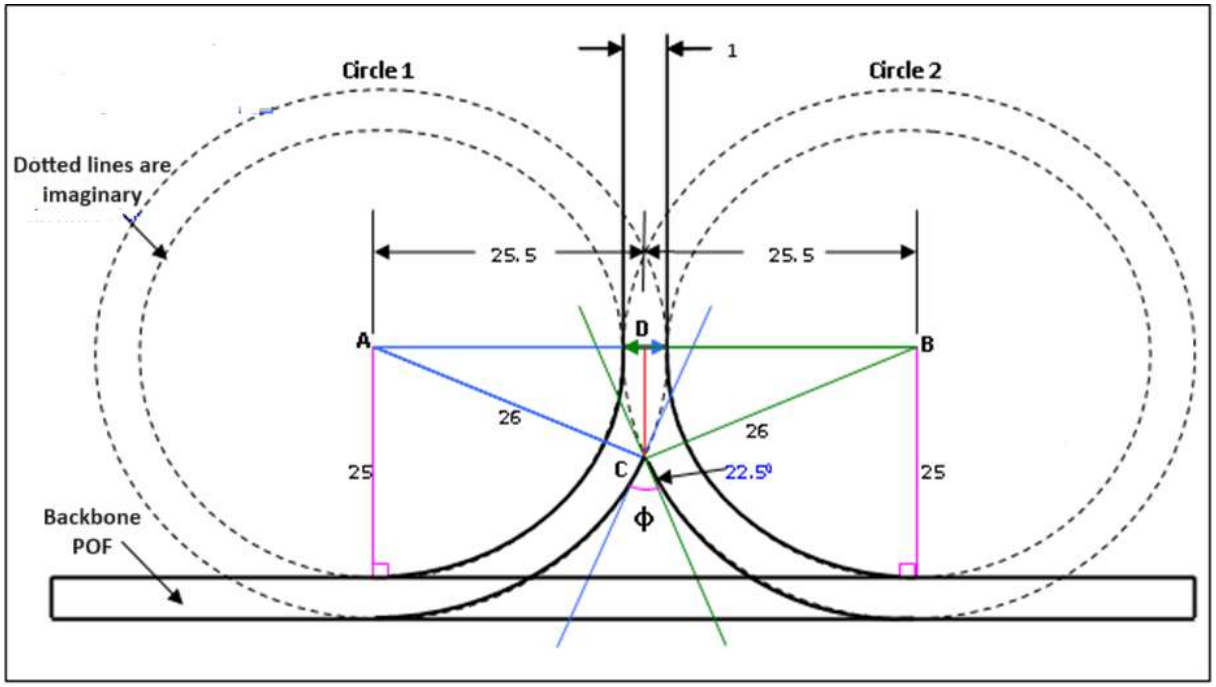

Figure 5-3: Diagram for the calculation of the Intersection angle. All the measurements are in millimetres (mm).

(i) Intersection Angle

Let: P = Radius of Circle 1

Q = Radius of Circle 2

D = distance between the centres

Using the Intersection Angle Formula (Korn, 2000):

$$\phi = \text{Sin}^{-1}\left[\sqrt{2P^2Q^2+2P^2D^2+2Q^2D^2-P^4-Q^4-D^4}\Big/2PQ\right] \quad 5.1$$

$$\phi = \text{Sin}^{-1}\left[\sqrt{2x26^2x26^2+2x26^2x51^2+2x26^2x51^2-26^4-26^4-51^4}\Big/2x26x26\right]$$

$$\underline{\phi = 22.5^0}$$

(ii) Polished side length ($\overline{CD}$)

$$\overline{CD} = \sqrt{\overline{BC}^2-\overline{BD}^2}$$

$$= \sqrt{26^2-25.5^2}$$

$$\underline{\overline{CD} = 5.07\text{mm}}$$

iii) Immersion angle:

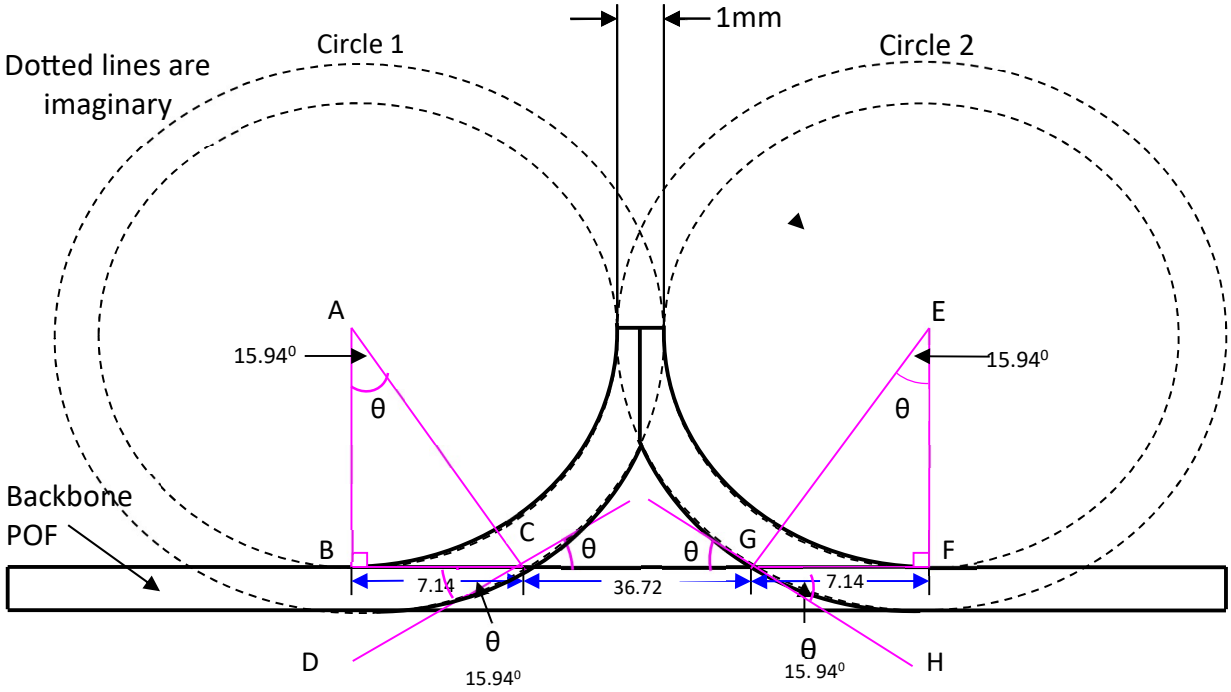

Figure 5-4: Diagram for the calculation of the Immersion angle.

Let angle $B\hat{A}C = B\hat{C}D = \theta$

$$\theta = \cos^{-1}\frac{25}{26}$$

$$\underline{\theta = 15.94^0}$$

(iii) Length of line BC:

By Pythagoras' Theorem:

$$\overrightarrow{BC} = \sqrt{26^2 - 25^2} \qquad 5.2$$

$$\underline{\overrightarrow{BC} = 7.14\text{mm}}$$

(iv) Arc length of the inner circle:

$$Arc_{inner} = {}^{\theta}/_{360} \times 2\pi r \quad 5.3$$

$$Arc_{inner} = {}^{90}/_{360} \times 2\pi \times 25$$

$$\underline{Arc_{inner} = 39.27mm}$$

(v) Arc length of the outer circle:

$$Arc_{outer} = {}^{\theta}/_{360} \times 2\pi r \quad 5.4$$

$$Arc_{outer} = {}^{90}/_{360} \times 2\pi \times 26$$

$$\underline{Arc_{outer} = 40.8\ mm}$$

5.3 Array Coupler Structure

As described in Chapter 4, the plastic optical fibre (POF) used in this research is a step-index Polymethyl Methacrylate (PMMA) type with the specifications of Eska™ CK-40. This POF has a core diameter of 0.98 mm, a numerical aperture of 0.5, and an overall diameter (core and cladding) of 1 mm.

As shown in Figure 5-5, the coupler consists of two POF arms bent at a radius of 25 mm. These two curved POFs converge at one end to form a beam-splitting coupler, while the other ends are immersed into the backbone POF at a launching angle of 160°. The design aims to achieve low excess and insertion loss when connected to the polished backbone (bus) POF.

The polished arms of the beam splitter intersect at an angle of 22.5°, ensuring a 50/50 coupling ratio while minimising excess loss. The research simulates the polished backbone fibre at the points where the beam splitter arms are immersed, with the immersion depth determining the output power and coupling efficiency.

This coupler can support four wavelengths—470 nm (Blue), 520 nm (Green), 570 nm (Yellow), and 650 nm (Red)—in a Wavelength Division Multiplexing (WDM) optical

transmission. These wavelengths experience low attenuation in the visible range, where the proposed array couplers are designed to operate.

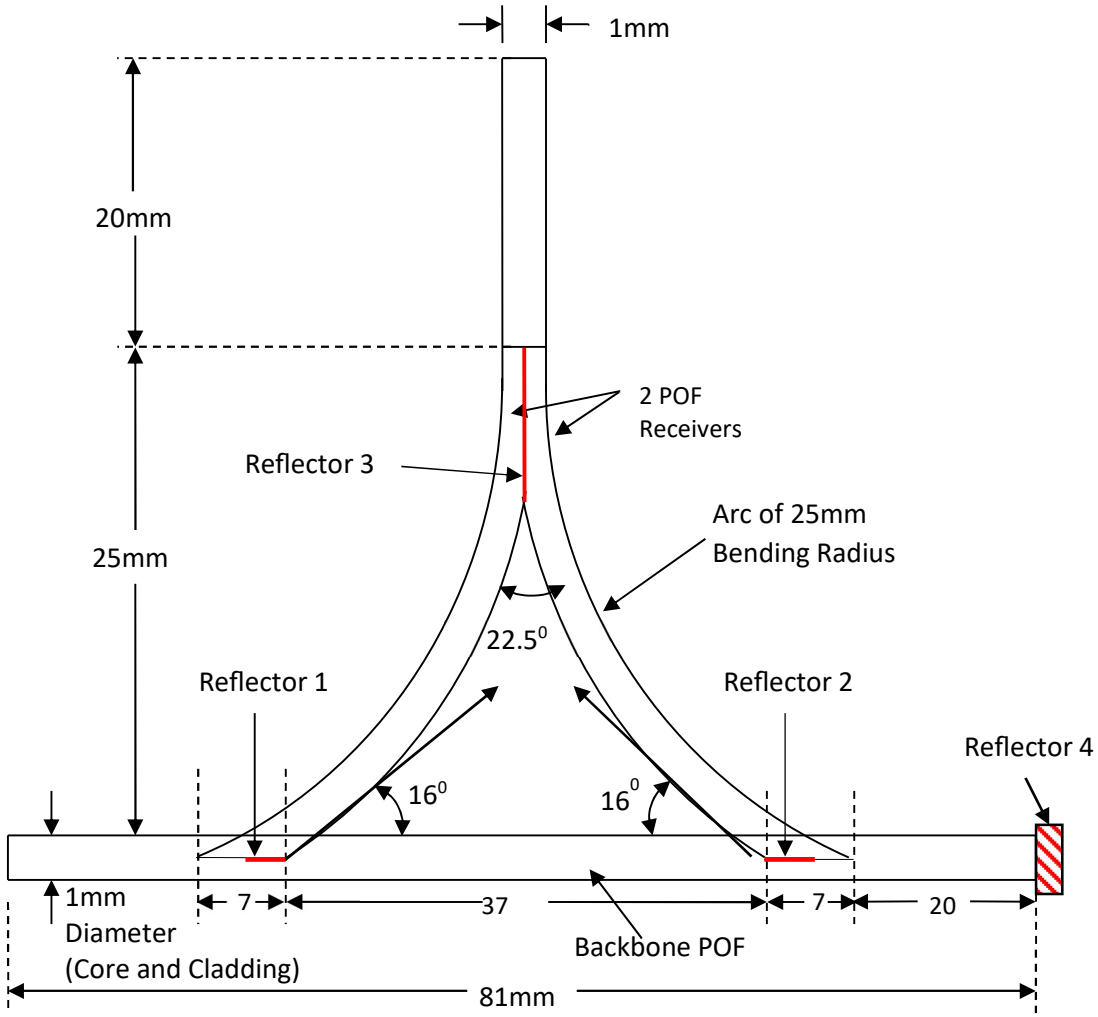

Figure 5-5: Basic POF coupler dimensions.

The array coupler utilises four types of reflectors:

- *Reflectors 1 and 2* are optimisation reflectors placed at the junction between the immersed POF and the backbone POF to enhance the output at the ports, as discussed in Chapter 4, Section 4.4.2.
- *Reflector 3* is positioned at the junction between the two arms of the beam splitter to prevent optical power from leaking between the arms.
- *Reflector 4* is placed at the end of the backbone POF to reflect optical power back into the coupler, thereby increasing the power received at the output ports.

A 1x2 array coupler is created by combining two of the couplers shown in Figure 5-5. Similarly, 1x4 and 1x8 array couplers are formed by combining 4 and 8 single array couplers, respectively.

5.3.1 Port Outputs Calculations Formulae

This section covers the derivations required to calculate the optical energy received at each output port. The calculations are based on the methods described in Section 4.5.1 of Chapter 4, and the formulae presented here are used to determine the output power of the proposed array couplers.

Coupling Port Output

$$P_1=P_{in}\left[\frac{L_{arc}}{C}\right] \tag{5.5}$$

Backbone Output:

$$P_B= P_{in}\left[\frac{C-L_{arc}}{C}\right] \tag{5.6}$$

Where: P_{in} = Transmitter optical power into the POF

P_1 = Received optical power at output port 1

P_B = Optical output power at the other end of the backbone POF

L_{arc} = length of the arc provided by the immersed POF at that port output

C = Circumference of the backbone POF

Note: L_{arc} Refers to the deepest immersion depth in the array coupler. Additionally, Equation 5-5 does not account for the effect of inserting the optimisation reflector between the polished surfaces of the backbone POF and the immersed POF. If the optimisation reflector is included, equation 5.7 (Formerly equation 4.14) applies.

$$P_{out} = \left[\frac{P_{in}L_{Arc}}{C}\right]\left[1 - \frac{1}{\pi}\left[\text{ArcCos}\left(1-\frac{2h}{A}\right) - \left(1-\frac{2h}{A}\right)\sqrt{\frac{4h}{A}-\frac{4h^2}{A^2}}\right]\right] \tag{5.7}$$

5.3.2 Calculation of Array Coupler Port Output Power

Figures 5-6 will illustrate a 1x8 array coupler without any optimisation optical reflectors, serving as an example to calculate the optical output power.

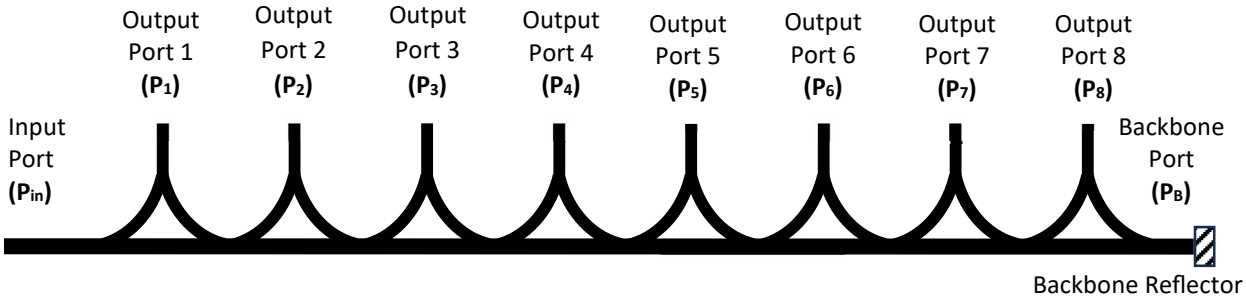

Figure 5-6: 1x8 array coupler used for calculating the optical port output power. This coupler does not have a backbone reflector at the end of the backbone POF.

In Figure 5-6, for the first calculations, the backbone reflector and the reflected power were ignored. Consequently, if the input power is applied at port P_{in} the optical power at each output port can be calculated as follows:

$$P_1 = P_{in}\left[\frac{L_{arc(1)}}{C}\right] \quad 5.8$$

$$P_2 = \frac{L_{arc(2)}}{C}\left[P_{in}-[P_1+P_B]\right] \quad 5.9$$

$$P_3 = \frac{L_{arc(3)}}{C}\left[P_{in}-[P_1+P_2+P_B]\right] \quad 5.10$$

$$P_4 = \frac{L_{arc(4)}}{C}\left[P_{in}-\left[P_1+P_2+P_3+P_B\right]\right] \quad 5.11$$

$$P_5 = \frac{L_{arc(5)}}{C}\left[P_{in}-\left[P_1+P_2+P_3+P_4+P_B\right]\right] \quad 5.12$$

$$P_6 = \frac{L_{arc(6)}}{C}\left[P_{in}-\left[P_1+P_2+P_3+P_4+P_5+P_B\right]\right] \quad 5.13$$

$$P_7 = \frac{L_{arc(7)}}{C}\left[P_{in}-\left[P_1+P_2+P_3+P_4+P_5+P_6+P_B\right]\right] \quad 5.14$$

$$P_8 = \frac{L_{arc(8)}}{C}\left[P_{in}-\left[P_1+P_2+P_3+P_4+P_5+P_6+P_7+P_B\right]\right] \quad 5.15$$

Therefore, using equations 5.8 through to 5.15, equation 5.16 became the resultant formula for subsequent optical power received at each output port, which was given as:

$$P_n = \frac{L_{arc(n)}}{C}\left[P_{in}-\left[\sum P_{T-n}+P_B\right]\right] \quad 5.16$$

Where: P_{in} = Transmitter optical power into the POF

P_n = Optical output power at the n^{th} port

P_{T-n} = Total Optical output power at all the preceding ports before the n^{th} port.

P_B = Optical output power at the other end of the backbone POF

$L_{arc(n)}$ = length of the arc provided by the immersed POF at that port output

C = Circumference of the backbone POF

5.3.3 The formula for the Reflected Power at Output Ports

In Figure 5-6, if the backbone reflector is taken into consideration, the reflected optical power received at the output port is calculated as follows:

$$P'_n = \frac{L'_{arc(n)}}{C}\left[P'_r-\left[\sum P'_{T-n}+P'_{in}\right]\right] \quad 5.17$$

Where: P'_r = The reflected optical power into the POF

P'_n = Optical output power at the n^{th} port from the reflector

P'_{T-n} = Total reflected optical output power received at all the preceding ports before port P'_n

P'_{in} = reflected optical output power received at the other end of the backbone POF, i.e. P_{in}

$L'_{arc(n)}$ = length of the arc provided by the immersed POF in the reflector direction

C = Circumference of the backbone POF

5.3.4 Total Port Output Power

The total optical power received at any output port is the sum of the power from the incident input port, $P_{in,}$ and the power from the reflected optical energy. Therefore, the formula for the total optical power at each output port is calculated as shown in equations 5.18 and 5.19.

$$P_{n(T)} = P_n + P'_n \tag{5.18}$$

$$P_{n(T)} = \frac{L_{arc(n)}}{C}\left[P_{in} - \left[\sum P_{T-n} + P_B\right]\right] + \frac{L'_{arc(n)}}{C}\left[P'_r - \left[\sum P'_{T-n} + P'_{in}\right]\right] \tag{5.19}$$

5.4 Array Coupler Design

This section explores the theoretical designs of the 1x2, 1x4, and 1x8 array couplers. Different splitting ratios are used to calculate the output optical power at each port before proceeding to modelling and simulation. For each splitting ratio, the optical power at the output ports was plotted, with the backbone fibre serving as the input. These calculations helped identify the splitting ratios that would optimise performance for each 1x2, 1x4, and 1x8 array coupler. The port output power was expressed as a proportion of the input optical power.

5.4.1 Effect of Splitting Ratios on Received Optical Power

To evaluate the received port output power for different splitting ratios in 1x8 POF-based couplers, the backbone POF port was used as the input. The optical output power was calculated using Equation 4.5 from Chapter 4. The 1x8 array coupler depicted in Figure 5-7 does not include optical reflectors.

In this calculation, the input power was applied at the backbone POF input port $P_{in,}$ and the incident output power received at each output port is calculated using Equation 5.16. The immersion depths used in the calculation are 10:90 (10%), 20:80 (20%), 30:70 (30%), 40:60 (40%) and 50:50 (50%).

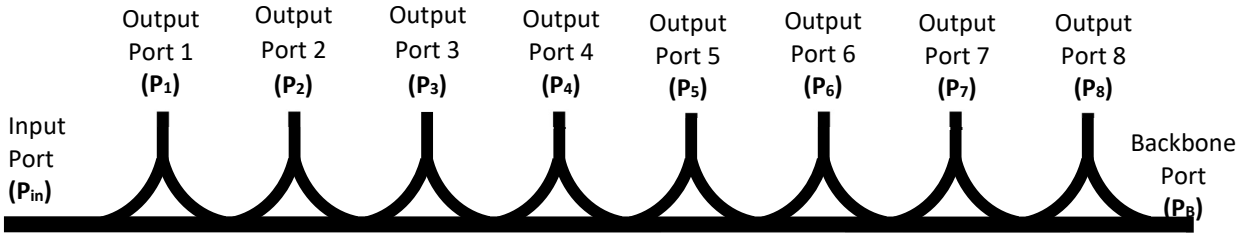

Figure 5-7: 1x8 array coupler for calculating the optical port output power. This coupler does not have a backbone reflector at the end of the backbone POF.

Table 5-1 shows the optical output power received at each port for various immersion depths. For all calculations, an assumed input power of 100 mW was used. Assuming that inherent POF losses are negligible, Table 5-1 shows that approximately 4.3% of the optical energy from the 10:90 couplers reaches port 8 from the backbone POF. In contrast, with a 50:50 splitting ratio, only 0.4% of the input optical power reaches port 8. Additionally, Table 5-1 indicates that the 10:90 immersion depth achieves a coupling efficiency of 82.6%, whereas the 50:50 immersion depth achieves nearly 100%. The optical output results are illustrated in Figure 5-8.

Table 5-1: Port Outputs of The POF for Different Splitting Ratios

Port Number	Splitting Ratio				
	10.90	20:80	30:70	40:60	50:50
1	19.6	29.0	36.6	43.5	50.0
2	15.8	20.6	23.2	24.6	25.0
3	12.7	14.6	14.7	13.9	12.5
4	10.2	10.4	9.3	7.9	6.3
5	8.2	7.4	5.9	4.4	3.1
6	6.6	5.2	3.7	2.5	1.6
7	5.3	3.7	2.4	1.4	0.8
8	4.3	2.6	1.5	0.8	0.4
% Total Port Output	82.6	93.6	97.4	99.0	99.6
%Power Left in POF	17.4	6.4	2.6	1.0	0.4

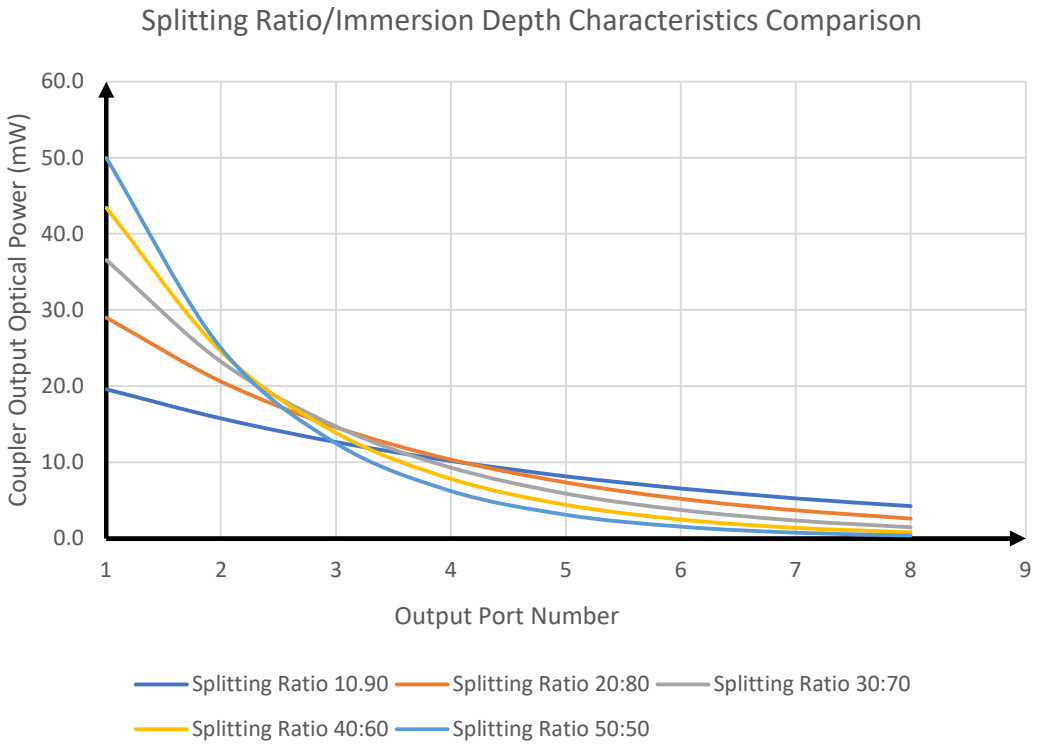

Figure 5-8: Port out of the POF for different splitting ratios.

In Figure 5-8, a graph shows the port output power for various splitting ratios, illustrating how the optical energy at each port changes with immersion depth. The chart reveals that the received optical power decreases exponentially with increasing immersion depth, with the highest rate of decay at 50:50. The 10:90 immersion depth shows a near-linear graph, with the highest amount reaching the output port 8.

5.5 1x2 Array Coupler Design

In this section, the received optical power for each output port of the 1x2 coupler at various immersion depths was calculated and plotted as bar graphs. The 1x2 POF-based coupler is created by combining two single-array couplers in series. The theoretical calculations of optical power were used to determine the optimal immersion depth for each immersed POF. The 1x2 coupler design did not include a reflector at the end of the backbone POF. Table 5-2 shows the iterations of immersion depths used to determine the depth of each immersed POF.

Table 5-2: 1x2 POF Coupler: Output Ports for Various Splitting Ratios

Port Number	Splitting Ratio				
	10.90	20:80	30:70	40:60	50:50
1	19.6	29.0	36.6	43.5	50.0
2	15.8	20.6	23.2	24.6	25.0
Total Port Output (mW)	35.4	49.6	59.8	68.0	75.0
Power Left in POF (mW)	64.6	50.4	40.2	32.0	25.0
Excess loss (dB)	- 4.5	-3.1	-2.2	-1.7	-1.2

The calculation in Table 5-2 indicates that the 10:90 splitting ratio performs the worst, with an excess loss of -4.5 dB and a coupling efficiency of only 35.4%. In contrast, the 50:50 immersion depth provides the best performance, with an excess loss of -1.2 dB and a coupling efficiency of 75%.

The theoretical design of the POF-based 1x2 coupler includes immersing two 50:50 beam-splitting couplers into a backbone POF, as depicted in Figure 5-9. Despite a coupling efficiency of 75%, the 1x2 POF-based coupler still loses 25% of the input power at the end of the backbone coupler. Fresnel reflections at the backbone POF/air interface are considered negligible. This coupler exhibits an excess loss of -2.4 dB, with port insertion losses of -3 dB on port 1 and -6 dB on port 2. The results are illustrated in the bar graph shown in Figure 5-10.

In the 1x2 coupler, output port 1 receives twice as much optical power as output port 2. Sub-section 5.6.3 will explore methods to optimise the optical power distribution so that both ports receive nearly equal optical power.

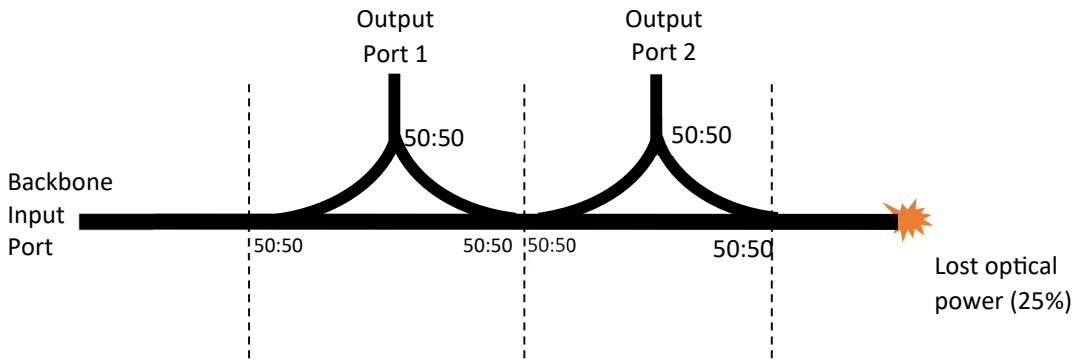

Figure 5-9: A 1x2 POF-based optical coupler design without a backbone POF end reflector.

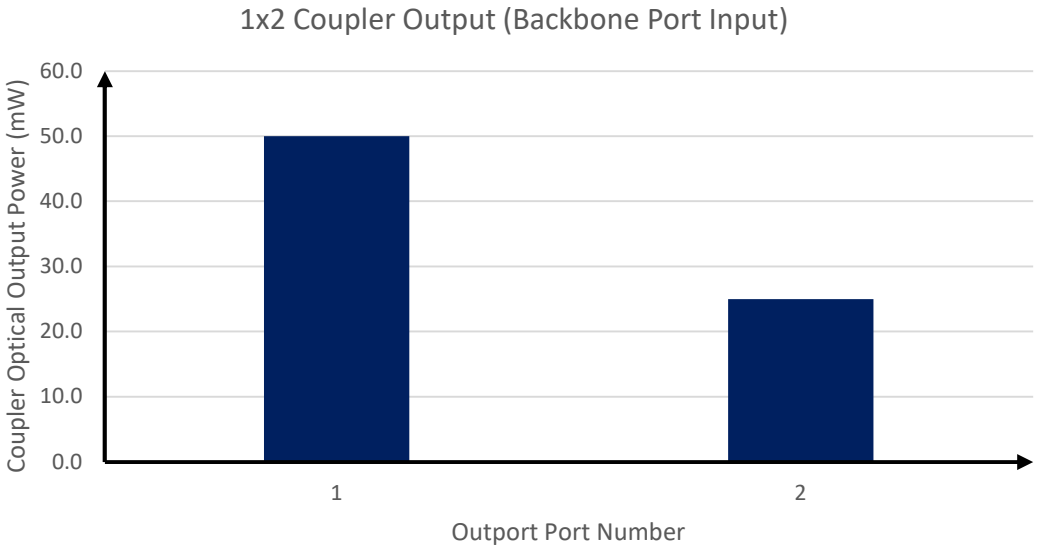

Figure 5-10: Non-optimised port output power of the 1x2 POF-based optical array coupler.

5.5.1 Receiving 1x2 Array Coupler with Backbone End Reflector

In the configuration shown in Figure 5-10, 25% of the input optical power remains in the backbone POF after passing through the last output port, resulting in significant optical power loss. To optimise the coupler's performance, the splitting ratio for the first immersed POF was adjusted to 30:70. The immersion depths for the reflected power were set to 40:60 for output port 1 and 50:50 for output port 2. These optimisation parameters are detailed in Table 5-3.

The backbone port remained as the input port. A reflector was added at the end of the backbone POF to reflect any optical power that travels through the backbone and might

otherwise be lost. This reflected power is redirected back into the coupler to be received at the output ports, as illustrated in Figure 5-11.

Table 5-3: 1x2 POF Coupler Splitting Ratios

Port Number	Port Output		
	Incident (30:70)	Reflected (60:40/50:50)	Incident +Reflected
P_B	0	7.9	7.9
1	37	7.9	44.9
2	31.5	15.8	47.3
Total	59.8	40.2	100

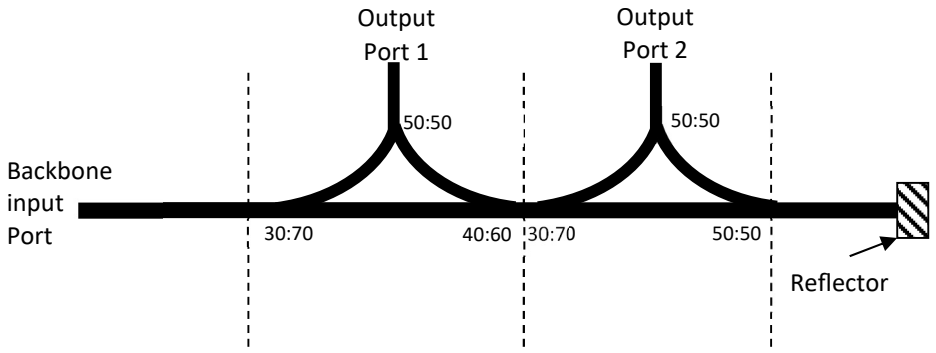

Figure 5-11: 1x2 POF coupler configuration with a backbone reflector inserted at the end of the backbone POF.

The reflected optical modes will then be coupled to the output ports and augment the optical energy received at the output port via the incident modes. The coupler managed to achieve near optimisation with the insertion of a backbone reflector. There is no need to find alternative ways to achieve optimisation, such as inserting the backbone reflector, as described in Chapter 4.

Regarding performance parameters, the theoretically optimised 1x2 POF-based array coupler achieves a coupling efficiency of 92.2%, an improvement from the previous 75%, and an excess loss of 0.4 dB. For output port 1, the insertion loss is 2.2 dB and the coupling ratio is 51%. For output port 2, the insertion loss is 4 dB and the coupling ratio is 49%. The coupler's uniformity is measured at 0.8 dB.

5.5.2 Transmitting 1x2 Array Coupler Design without an Optimisation Reflector

The coupler shown in Figure 5-11 can also function as a transmitting coupler, with ports 1 and 2 serving as input ports. However, as illustrated in Figure 5-13, using port 1 as the input port complicates the optimisation of output power because 50% of the input optical power is directly transmitted to the backbone port instead of entering the coupler

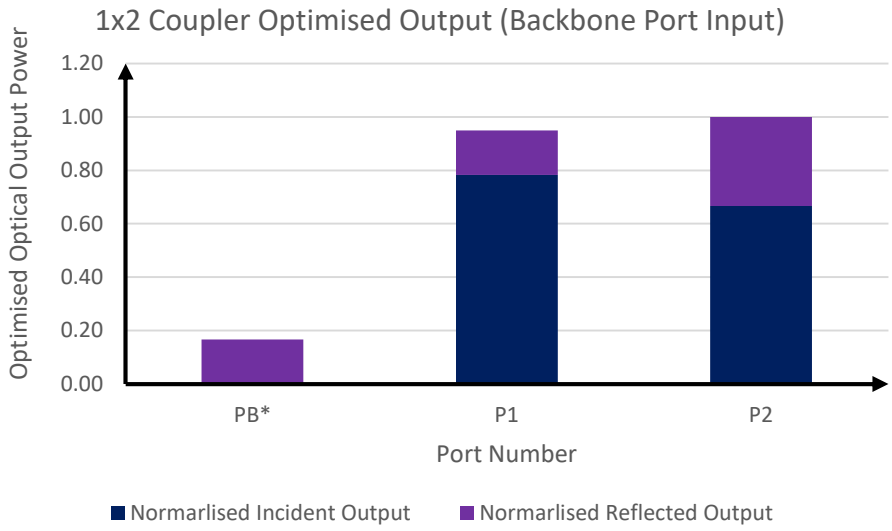

Figure 5-12: 1x2 Coupler output with the input at the backbone POF

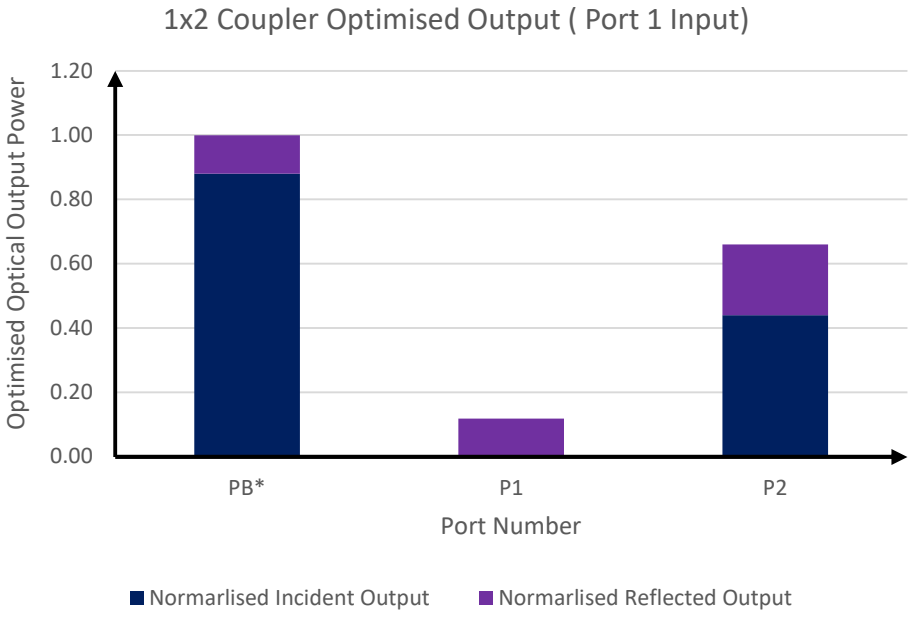

Figure 5-13: 1x2 coupler output with the input at port 1

In this configuration, the 1x2 POF-based coupler achieves a coupling efficiency of 94.3% and an excess loss of 0.3 dB. The insertion loss is 2.5 dB at the backbone port and 4.3 dB at output port 2. The coupling ratio at the backbone port is 60%, while the output port 2 has a coupling ratio of 40%, resulting in a compromise. The coupler uniformity is measured at 0.08 dB.

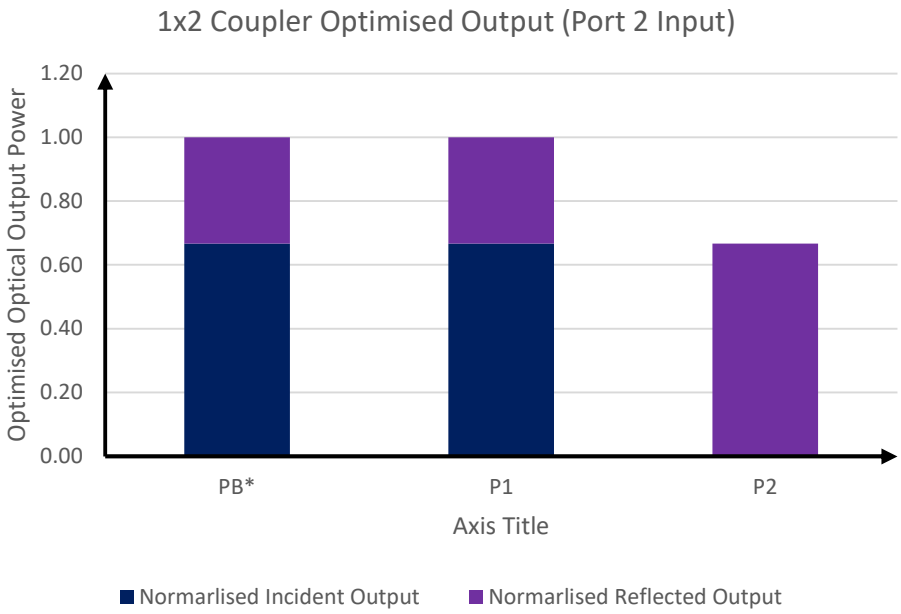

Figure 5-14: 1x2 coupler output with the input at port 2.

In Figure 5-11, using port 2 as the input port enabled effective optimisation of the port output power, as shown in Figure 5-14. In this setup, the 1x2 POF-based coupler achieves a coupling efficiency of 75% and an excess loss of 1.2 dB. The insertion loss is -3 dB at both the backbone port and output port 1. Both the backbone port and output port 1 have a coupling ratio of 50%. The coupler's uniformity is 0 dB. While this configuration optimises output power, it reduces overall coupler efficiency, with 25% of the input power being reflected at port 2.

5.6 1x4 POF-based Array Coupler Design

The same methods and procedures used in Section 5.6 were applied to calculate and plot the results for the 1x4 POF-based array coupler. Table 5-4 shows the characterisation of immersion depth iterations. The theoretical design involves immersing four 50:50 beam-splitting couplers into a backbone POF, as illustrated in Figure 5-15.

Table 5-4 shows that a 1x4 array coupler with a 10:90 immersion depth achieves a coupling efficiency of only 58.2%, whereas a 50:50 immersion depth achieves nearly 94% efficiency. Although immersion depths of 30:70, 40:60, and 50:50 result in coupling efficiencies above 80%, they suffer from poor uniformity. To balance these factors, the 1x4 array coupler was designed with 20:80 splitting ratios for all immersed POFs, improving uniformity and providing a coupling efficiency of 75%.

Table 5-4: 1x4 POF Coupler; Port Outputs for Different Splitting Ratios

Output Port Number	Splitting Ratio				
	10:90	20:80	30:70	40:60	50:50
1	19.6	29	36.6	43.5	50
2	15.8	20.6	23.2	24.6	25
3	12.6	14.6	14.7	13.9	12.5
4	10.2	10.4	9.3	7.9	6.2
% Port Total Used	58.2	74.6	83.8	89.9	93.8
%Power Left in POF	41.8	25.4	16.2	10.1	6.2

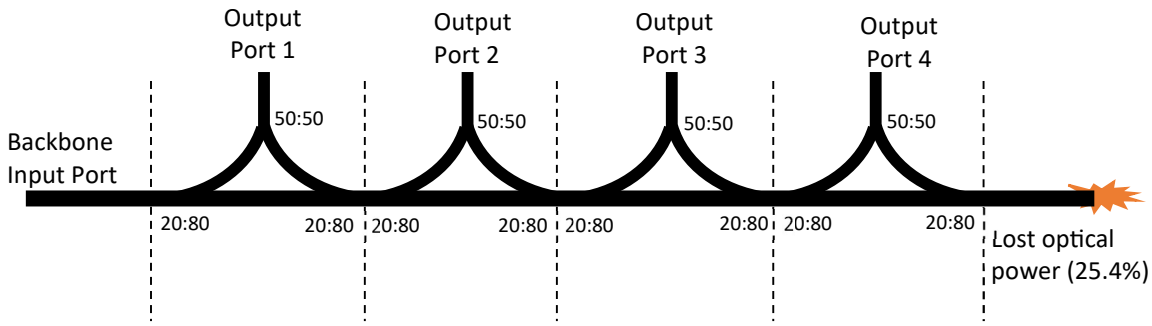

Figure 5-15: 1x4 Array coupler with no reflector connected at the far end of the backbone POF.

At the 20:80 immersion depth, Table 5-4 indicates that the coupler loses 25.4% of the input power at the end of the backbone POF, with minimal optical energy being reflected into the backbone POF due to Fresnel reflections at the POF/air interface. Consequently, with a quarter of the input power lost in the backbone POF, the 1x4 array coupler shown in Figure 5-15 exhibits suboptimal coupling performance. Figure 5-16 shows that the optical power at the output ports decreases progressively from output port 1 to output port 4.

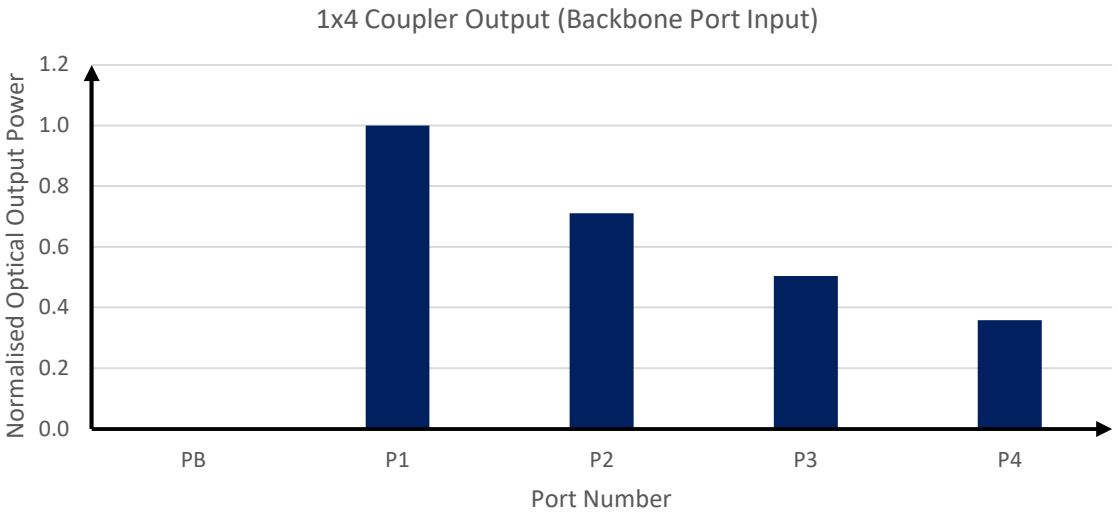

Figure 5-16: 1x4 POF coupler; port output comparison graph for different splitting ratios.

Regarding the performance parameters, the coupler has an excess loss of 1.3 dB and a uniformity of 0.2 dB. The insertion losses for output ports 1, 2, 3, and 4 are 5.4 dB, 6.9 dB, 8.4 dB, and 9.8 dB, respectively. These values indicate that the insertion loss increases progressively from output port 1 to output port 4, with port 4 showing the worst performance.

5.6.1 1x4 Array Coupler with Backbone End Reflector

To improve coupler performance, an optical reflector was added at the far end of the 1x4 array coupler. This reflector redirects optical power that would otherwise be lost back into the coupler, allowing it to be received at the output ports. For this configuration, the splitting ratios are set to 20:80 for the incident optical modes and 30:70 for the reflected optical modes. The backbone port continues to serve as the input port, as illustrated in Figure 5-17.

Table 5.5 shows the percentage of output power measured at the output ports. The addition of a reflector at the far end of the backbone POF significantly improved the performance of the 1x4 array coupler, increasing the coupling efficiency from 74.6% to 95.9%. However, the coupler still did not optimise the distribution of optical power across the output ports. As illustrated in Figure 5-18, output port 1 continues to receive the highest power, while output port 4 receives the least. The excess loss improved from 1.3

dB to 0.2 dB, and the insertion loss at the output ports was measured at 5 dB, 6.1 dB, 6.9 dB, and 7.1 dB for ports 1, 2, 3, and 4, respectively. Additionally, uniformity improved from 0.2 dB to 0.09 dB.

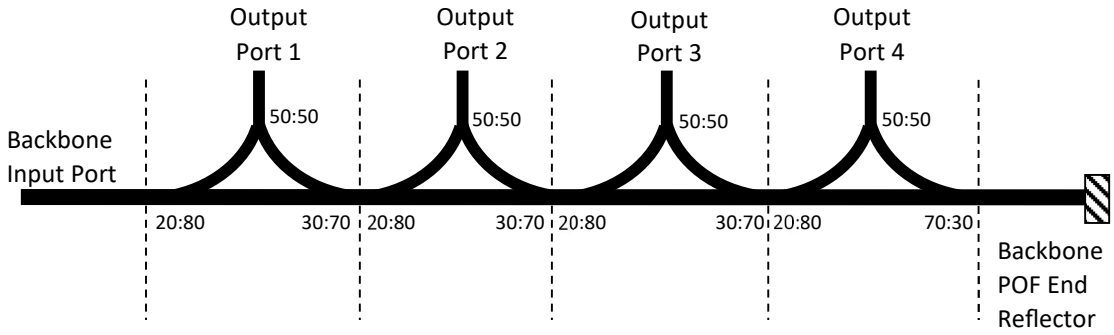

Figure 5-17: 1x4 POF array coupler configuration.

Table 5-5: Splitting Ratios for The Incident and the Reflected Pulses

Port Number	Output Port		
	Incident Signal (20:80)	Reflected Signal (30:70)	Sum of Incident + Reflected Signals
P_B	0	4.1	4.1
P1	29	2.4	31.4
P2	20.6	3.7	24.3
P3	14.6	5.9	20.5
P4	10.4	9.3	19.7
Total	74.6	21.3	100

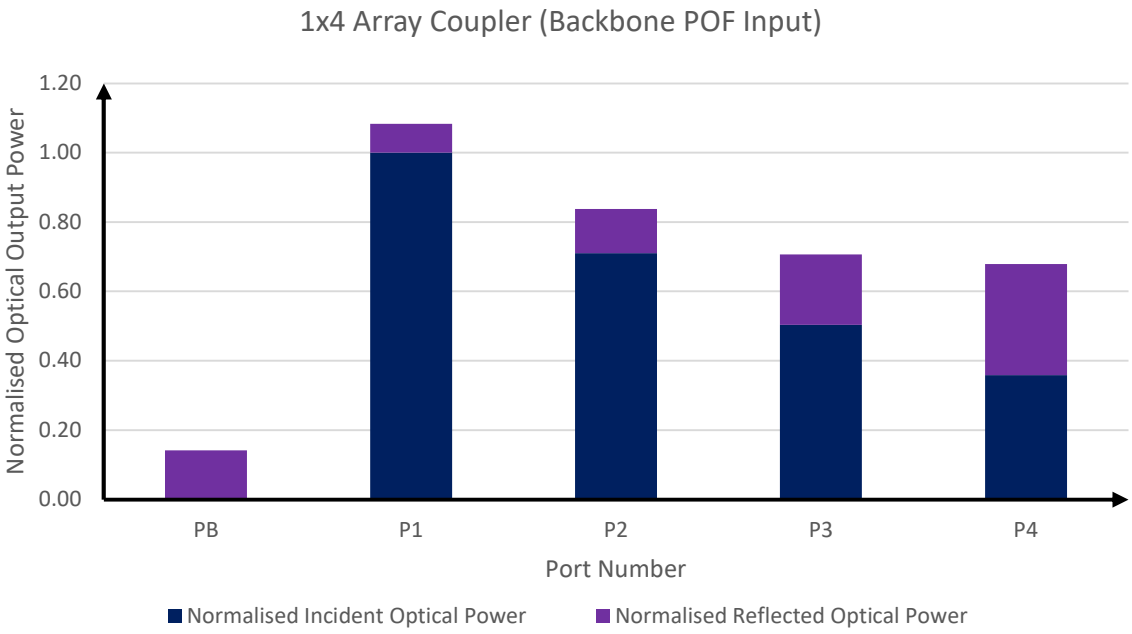

Figure 5-18: 1x4 Coupler output with the input at the backbone POF.

5.6.2 Optimisation of the 1x4 Array Coupler with an Optimisation Reflector and Backbone POF End Reflector

This section discusses the optimisation process for the 1x4 array coupler using a combination of techniques. Optimisation was achieved through the following methods:

1. *Immersion Depths:* Adjusting the immersion depth provided a coarse adjustment of the optical power at each output port. This method helped determine the maximum optical power at each port.

2. *Optimisation Reflector:* Positioned between the backbone POF and the immersed POF, this reflector allowed for fine-tuning of the received optical power at each port.

3. *Backbone POF End Reflector:* This reflector, placed at the far end of the backbone POF, reflected optical energy into the array coupler, enhancing overall performance.

These combined techniques enabled precise control over the distribution and optimisation of optical power across the array coupler's output ports.

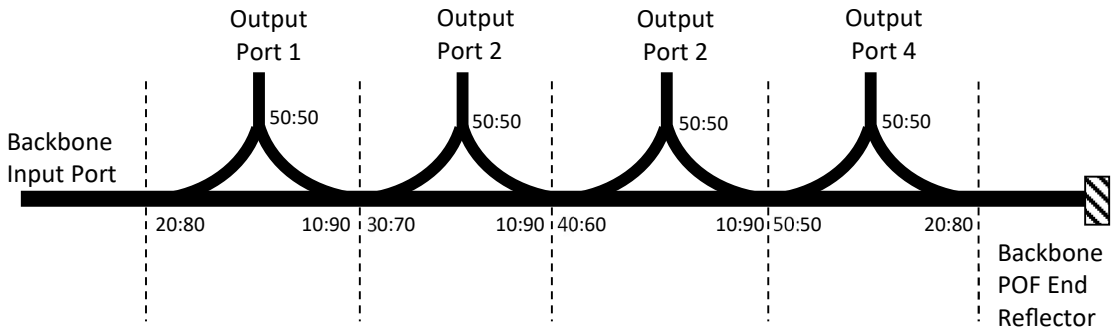

Figure 5-19: Fully optimised POF-based 1x4 array coupler.

To fully optimise the output power at each port, the coupler configuration was modified by adjusting the immersion depths and adding optimisation reflectors between the immersed POF and the backbone POF. The resulting optimised array coupler is illustrated in Figure 5-19. Details of this new configuration are provided in Table 5-6. Note that this version of the coupler does not include an optimisation reflector for reflected optical energy.

Table 5-6: Complete Optimisation Parameters and Output Measurements of the 1x4 Array Coupler

Output Port	Splitting ratio	Reflector Length	Incident Output	Reflected Output	Total Output
P_B*	0	0	0	6.4	6.4
P1	20:80 / 10:90	2.0 / No Reflector	21.9	1.6	23.5
P2	30:70 / 10:90	2.0 / No Reflector	21	2	23
P3	40:60 / 10:90	1.0 / No Reflector	22	2.4	24.4
P4	50:50 / 20:80	No reflector	17.6	5.1	22.7

Table 5-6 and Figure 5-20 demonstrate that total optimisation was achieved when the backbone port was used as the input port. The optimised coupler attained a coupling efficiency of 93.6%, uniformity of 0.02 dB, and an excess loss of 0.29 dB. The insertion losses for the output ports were 6.3 dB for port 1, 6.4 dB for port 2, 6.1 dB for port 3, and 6.4 dB for port 4. Additionally, the port coupling ratios were 25%, 25%, 26%, and 24% for ports 1, 2, 3, and 4, respectively. These insertion loss and excess loss values meet the optical performance criteria specified in the GR-1209 CORE specification.

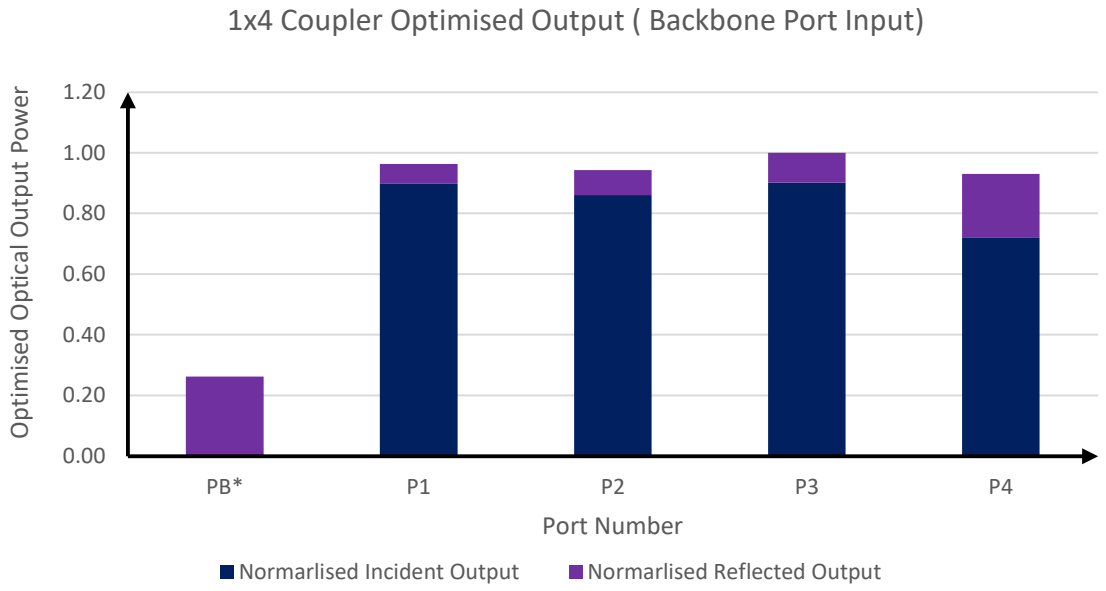

Figure 5-20: Complete optimisation of the received output optical power of the 1x4 array coupler with the backbone port used as the input port.

5.6.3 Transmitting 1x4 Array Coupler with an Optimisation Reflector and Backbone POF End Reflector

The coupler design shown in Figure 5-19 is effective as a receiving coupler but does not perform well as a transmitting coupler when ports 1 to 4 are used as input ports. The immersion depths and lengths of the optimisation reflectors, as illustrated in Figure 5-17, do not yield optimal performance when these ports are used as inputs for transmission.

To address this, a new design for a transmitting 1x4 coupler was developed, as shown in Figure 5-21. This design includes optimisation reflectors specifically for managing the reflected optical power. Ports 1 to 4 were used as input ports, and the performance results are detailed in Figures 5-22 to 5-25.

Table 5-7 provides information on the immersion depths and lengths of the optimisation reflectors used in this transmitting coupler. These dimensions and configurations are determined by the input at port 1 and are fixed for the other input ports (ports 2-4).

Table 5-7: Transmitting 1x4 Array Coupler Immersion Depth and Lengths of the Optimisation Reflectors

Output Port	Immersion Depth	Reflector Length
P_B*	0	0
P1	50:50 / 50:50	No reflector
P2	20:80 / 30:70	3 mm/3 mm
P3	30:70 / 20:80	3 mm/3 mm
P4	50:50 / 50:50	3 mm/3 mm

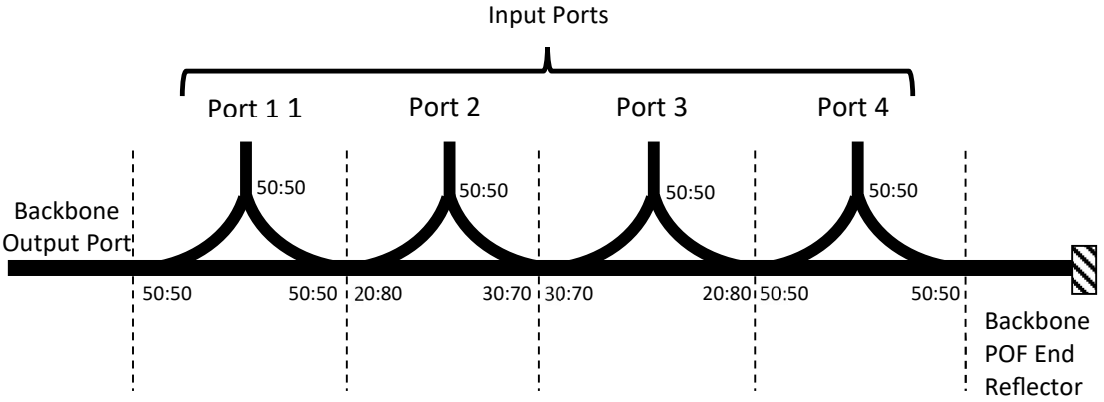

Figure 5-21: 1x4 Array coupler with ports 1 to 4 used as input ports.

When port 1 was used as the input port, the backbone port received more than 50% of the optical power, as shown in Figure 5-22. This occurs because the coupler at port 1 splits the input power equally, directing half to the backbone POF. The remaining half is distributed among the other three ports. Therefore, optimisation efforts for output power focused on ports 2 to 4, as illustrated in Figure 5-22.

When Port 2 was used as the input port, output power optimisation was achieved for Ports 1 (the backbone port), 3, and 4, as shown in Figure 5-23. However, the level of optimisation differed between these sets of ports. The coupler optimised Ports 1 and the backbone port to a significantly greater extent than Ports 3 and 4.

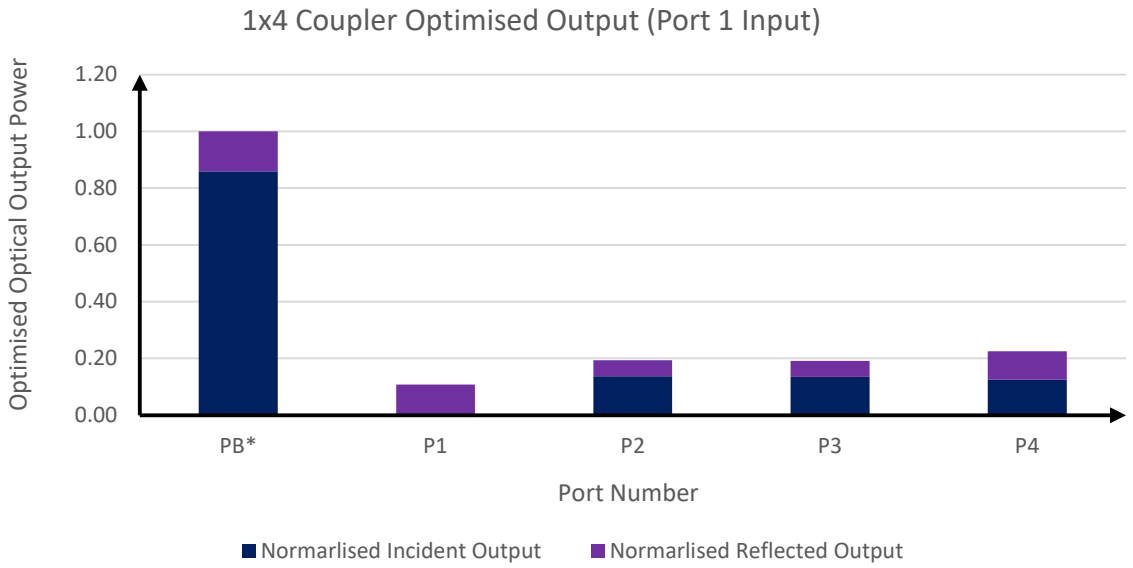

Figure 5-22: 1x4 Coupler outputs when the input optical power was applied at port 1.

When Port 3 was used as the input port, the coupler optimised power for Ports 1 and the backbone port, but not for Ports 2 and 4, as shown in Figure 5-24. While it is possible to optimise the coupler's performance with Port 3 as the input by adjusting the immersion depths and lengths of the optimisation reflectors, such changes would negatively impact the optimisation of the other input ports. Therefore, no modifications were made to the coupler configuration to maintain overall performance.

When Port 4 was used as the input port, the coupler optimised power for Ports 1 and the backbone port, but did not optimise it for Ports 2 and 4. Nevertheless, the output power levels at Ports 2 and 4 were increased, as shown in Figure 5-25.

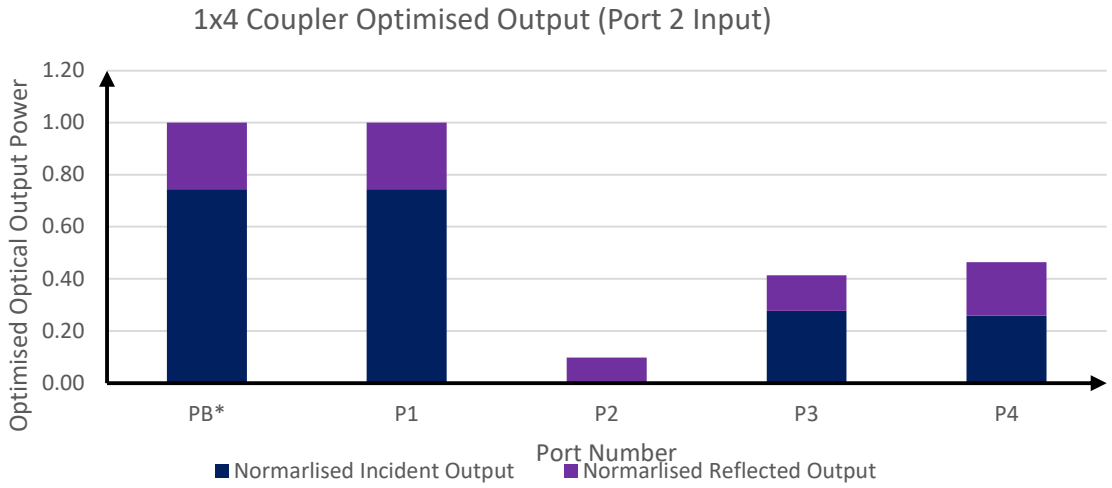

Figure 5-23: 1x4 Coupler output with the input at port 2.

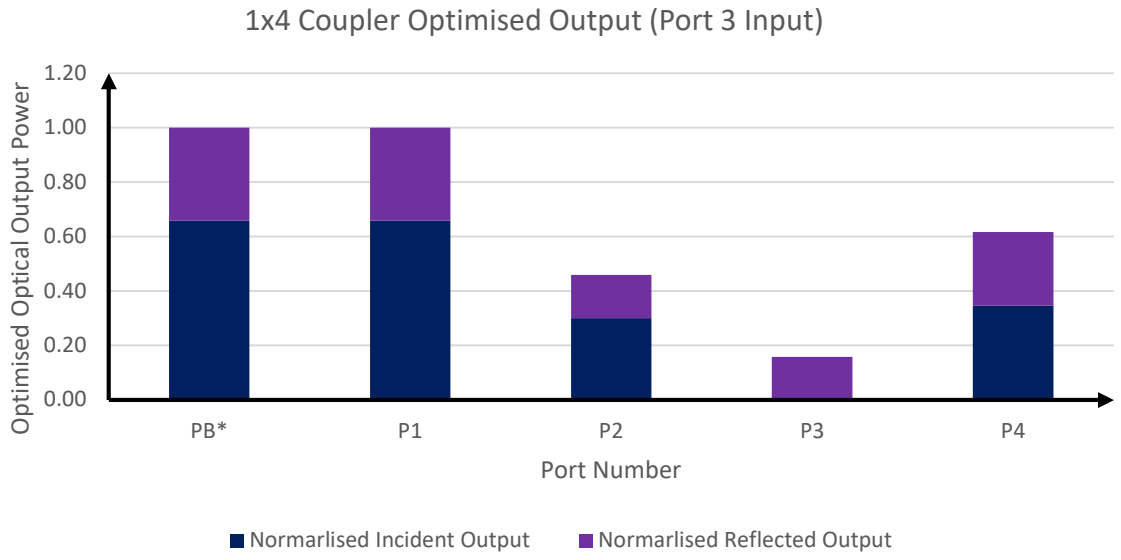

Figure 5-24: 1x4 Coupler output with the input at port 3.

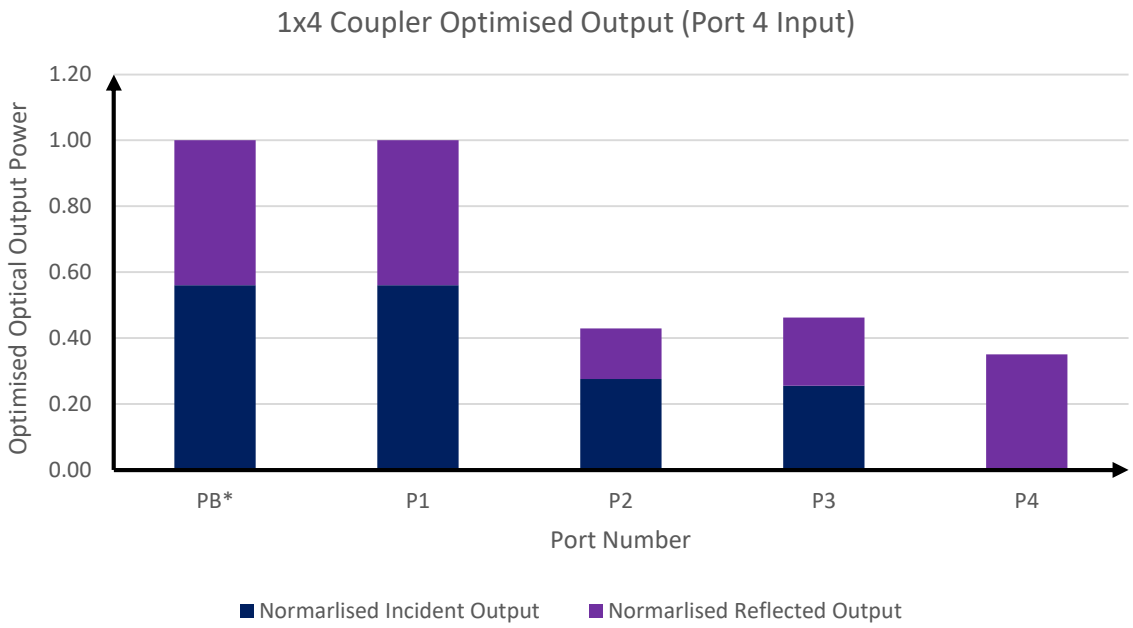

Figure 5-25: 1x4 Coupler output with the input at port 4.

5.6.4 1x4 POF Coupler Performance Parameters

This section examines the performance parameters of the 1x4 array coupler, specifically focusing on insertion loss, excess loss, uniformity, coupling (splitting) ratio, and coupler efficiency. Directivity and directionality are not covered in this research. Details on excess loss, uniformity, and coupler efficiency for each input port are presented in Table 5-8.

Table 5-8: Performance Parameters of the 1x4 Array Coupler for Different Input Ports

Input Port	Excess Loss (dB)	Uniformity (dB)	Coupler Efficiency (%)
P_B	0.3	0.0	94
1	0.3	0.3	94
2	0.1	0.2	97
3	0.2	0.2	95
4	0.6	0.2	88

The coupler demonstrates an excess loss and uniformity of less than 1 dB. When the backbone port is used as the input, the coupler achieves a perfect uniformity of 0 dB. The coupler efficiency exceeds 94% for all input ports except Port 4, which has an efficiency of 88%. Insertion loss values are calculated and provided in Table 5-9.

Table 5-9: Insertion Loss for the 1x4 Array Coupler for Different Input Ports

Output Port	Insertion Loss(dB)				
	P_B	P1	P2	P3	P4
P_B	0	2.4	4.7	5.1	5.1
1	6.3	0	4.7	5.1	5.1
2	6.4	9.6	0	8.5	8.9
3	6.1	9.6	8.5	0	8.5
4	6.4	8.9	8	7.2	0

The Insertion loss varies depending on the input port used, ranging from 2.4 dB to 9.6 dB. When Port 1 was used as the input, the coupler showed a consistent average insertion loss of 6.3 dB. Among the input ports, Port 1 performs the worst, with a maximum insertion loss of 9.6 dB. The coupling ratio for each input port is detailed in Table 5-10.

Table 5-10: Coupling Ratio for Each Input of the 1x4 Array Coupler

Input Port	Coupling Ratio (%)				
	P_B	P1	P2	P3	P4
P_B	0	62	35	33	35
1	25	0	35	33	35
2	25	12	0	15	15
3	26	12	14	0	13
4	24	14	16	20	0

The coupling ratio, like insertion loss, varies depending on the input port, ranging from 12% to 62%. When Port 1 was used as the input, the coupler consistently exhibited an average coupling ratio of 25%. Among the ports, Port 1 performs worst in coupling ratio, with a maximum of 62% (at the backbone port) and a minimum of 12% (at Ports 3 and 4).

5.7 1x8 POF-Based Array Coupler Design

This section examines the theoretical design of the POF-based 1x8 array coupler, which consists of eight POF-based 50:50 beam-splitting couplers immersed in a backbone POF. The immersion depth for each coupler was determined by calculations detailed in Table 5-11. Initially, all couplers were immersed at the same depth. The constructed POF-based 1x8 array coupler is illustrated in Figure 5-26.

Different immersion depths for the 1x8 POF-based optical coupler were tested, with results shown in Table 5-11 and plotted in Figure 5-27. Table 5-11 provides details on the characterisation of these immersion depth iterations.

Table 5-11 shows that a 1x8 array coupler with a 10:90 immersion depth achieves a coupling efficiency of only 82.6%, compared to 99.6% with a 50:50 immersion depth. Although immersion depths of 30:70, 40:60, and 50:50 result in coupling efficiencies of 93% or higher, they suffer from poor uniformity. Therefore, the 1x8 array coupler was designed with a 10:90 immersion depth, which, while offering a lower coupling efficiency of approximately 82.6%, provides superior uniformity compared to other immersion depths.

Table 5-11: 1x8 POF Coupler; Port Output for Different Splitting Ratios

Port Number	Splitting Ratio				
	90:10	80:20	70:30	60:40	50:50
1	19.6	29	36.6	43.5	50
2	15.8	20.6	23.2	24.6	25
3	12.6	14.6	14.7	13.9	12.5
4	10.2	10.4	9.3	7.9	6.2
5	8.2	7.4	5.9	4.4	3.1
6	6.6	5.2	3.7	2.5	1.6
7	5.3	3.7	2.4	1.4	0.8
8	4.3	2.6	1.5	0.8	0.4
% Port Total Used	82.6	93.5	97.3	99	99.6
%Power Left in POF	17.4	6.5	2.7	1	0.4

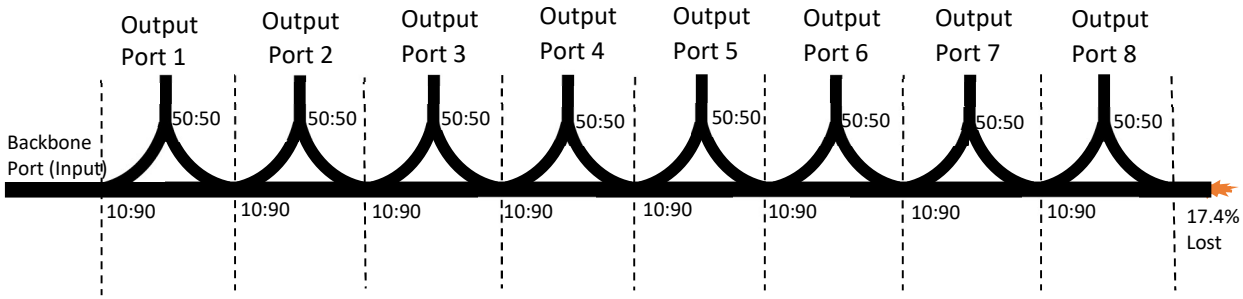

Figure 5-26: 1x8 array coupler with an immersion depth of 10:90 and no reflector at the end of the backbone port.

As shown in Figure 5-26, with an immersion depth of 10:90, the coupler loses 17.4% of the input power at the far end of the backbone POF. Additionally, only a negligible amount of optical energy is reflected into the backbone POF due to Fresnel reflections at the backbone POF/air interface. The significant loss of 17.4% of the input optical power results in poor coupling performance for the 1x8 array coupler depicted in Figure 5-26, indicating that improvements are needed.

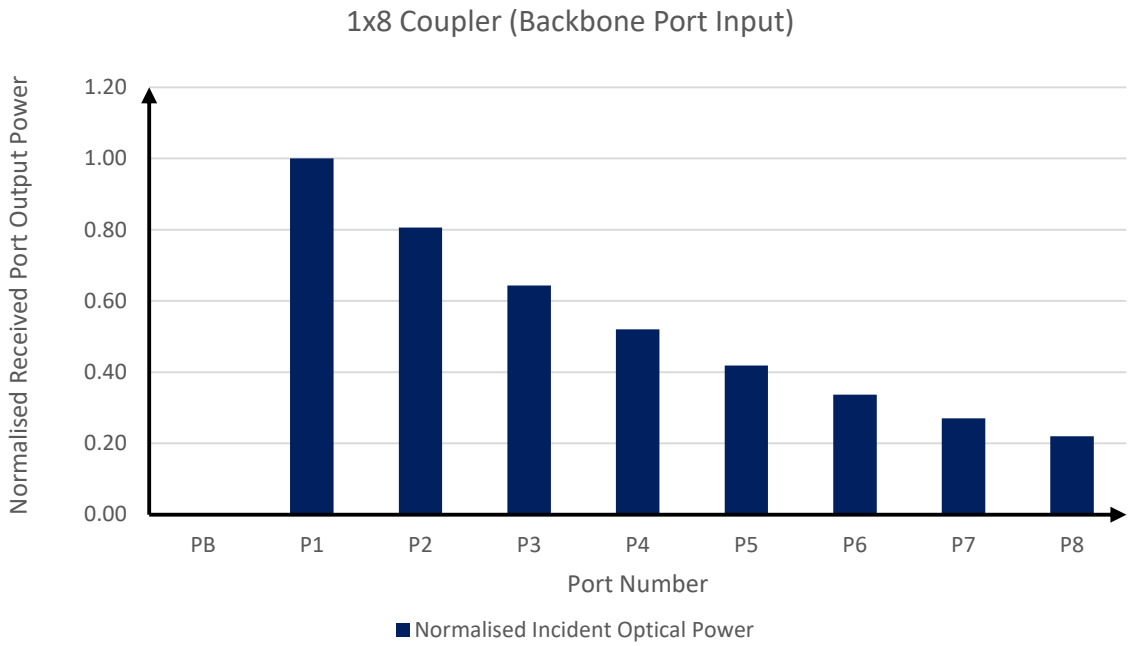

Figure 5-27: Normalised output graph of a 1x8 POF-based array coupler with an immersion depth of 10:90 and no reflector at the end of the backbone POF.

5.7.1 Optimisation of the 1x8 Array Coupler with a Backbone POF End Reflector

To enhance coupler efficiency, an optical reflector was added at the far end of the backbone POF. This reflector reflects optical power that would otherwise be lost, directing it back into the coupler. The reflected optical power is then coupled to the output ports, increasing the optical energy received at the output ports and improving the coupler's overall performance.

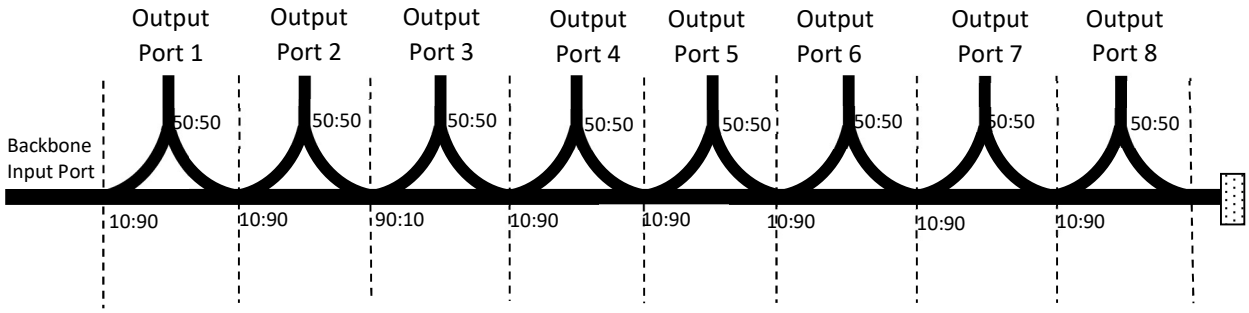

Figure 5-28: 1x8 POF coupler configuration with a backbone reflector connected at the far end of the backbone POF.

Inserting a reflector at the far end of the backbone POF significantly enhanced the coupling efficiency and other performance metrics of the 1x8 array coupler, increasing it from 82.6% to 100%. Despite this improvement, the coupler did not optimise the distribution of optical power at the output ports. As shown in Table 5-12, output port 1 continues to receive the highest amount of optical power, while output port 8 receives the least.

Table 5-12: 1x8 POF Coupler; Splitting Ratios and Port Outputs

Port Number	Port Output			
	Incident Pulse (90:10)	Reflected pulse (80:20)	Sum of the Incident + Reflected Pulses	Percentage (%) Output
P_B	0	1.1	1.1	1.1
1	19.6	0.5	20.1	20.1
2	15.8	0.6	16.4	16.4
3	12.6	0.9	13.5	13.5
4	10.2	1.3	11.5	11.5
5	8.2	1.8	10	10
6	6.6	2.5	9.1	9.1
7	5.3	3.6	8.9	8.9
8	4.3	5.1	9.4	9.4
Total	82.6	17.4	100	100

Figure 5-29 shows that the reflector at the far end of the backbone POF would effectively reflect optical power into the backbone POF and improve the performance parameters. The coupler configuration in Figure 5-28 falls short of achieving port output optimisation. To optimise port output, the research combined different immersion depths, backbone POF far-end reflectors, and reflectors inserted between the backbone port and the immersed POF. The following section provides the details.

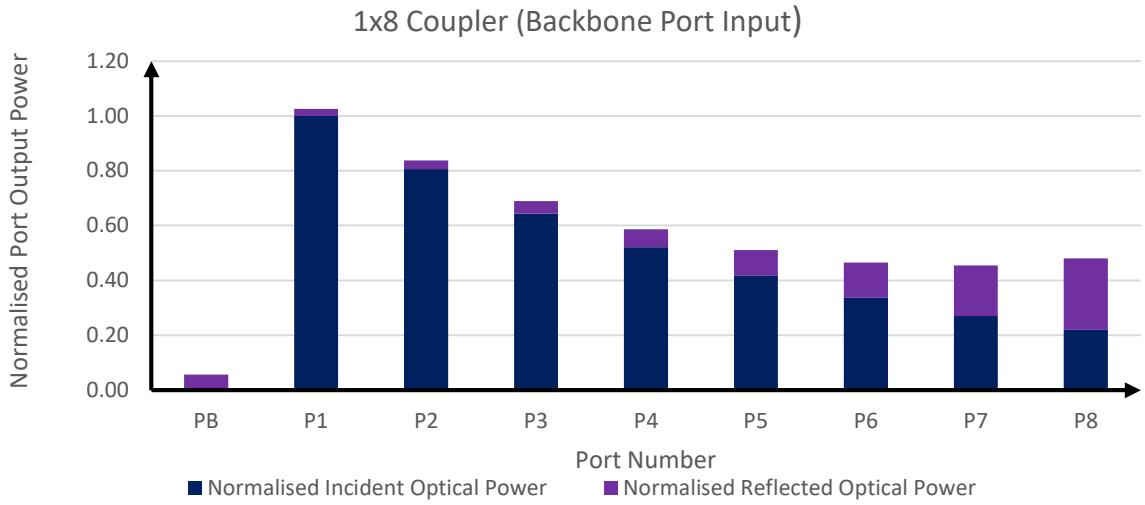

Figure 5-29: 1x8 coupler port output with the input at the backbone POF and a reflector connected at the far end of the backbone POF.

5.7.2 Optimisation of the 1x8 Array Coupler with Optimisation and Backbone POF End Reflector

This section achieved coupler optimisation by combining various immersion depths, a reflector at the far end of the backbone port, and optimisation reflectors positioned between the backbone POF and the immersed POFs. The immersion depth was used for coarse adjustment of the optical power received at each output port, while the optimisation reflector allowed for fine adjustment. The reflector at the end of the backbone POF reflected optical energy back into the array coupler, enhancing the optical power received at the output ports. Figure 5-30 illustrates the coupler configuration with the different immersion depths. The calculated optical power received at each output port is detailed in Table 5-13.

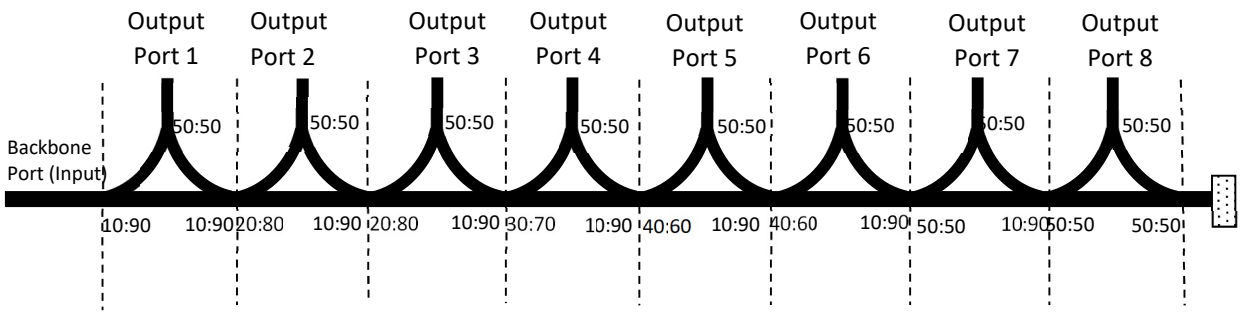

Figure 5-30: A 1x8 POF-based array coupler configuration showing the immersion depth and backbone POF far-end reflector.

Table 5-13: Receiving 1x8 Array Coupler Immersion Depth and Lengths of the Optimisation Reflectors

Port Number	Immersion Depth	Reflector Length	Incident Output	Reflected Output	Total Output
P_B	0	0	0	0.9	0.9
P1	10:90 / 10:90	4.0 / No Reflector	11.3	0.2	11.5
P2	20:80 / 10:90	3.5 / No Reflector	11.6	0.3	11.9
P3	20:80 / 10:90	3.0 / No Reflector	12.3	0.4	12.7
P4	30:70 / 10:90	3.0/ No Reflector	12.1	0.4	12.5
P5	40:60 / 10:90	2.5 / No Reflector	12.2	0.6	12.8
P6	40:60 / 10:90	2.0 / No Reflector	12.2	0.7	12.9
P7	50:50 / 10:90	1.0 / No Reflector	12.3	0.5	12.8
P8	50:50 / 50:50	No Reflector	8	4	12
Total	----------	----------	92	8	100

Table 5-13 and Figure 5-31 show that the research achieved almost total optimisation when the backbone port was used as the input port. The coupler achieved a coupling efficiency of 99.1%, uniformity of 0 dB, and an excess loss of 0.0 dB. The insertion losses for each output port were 9dB. The coupler also achieved port coupling ratios between 12% and 13%. The insertion loss values obtained for the insertion and excess losses comply with the optical parameters specified in the GR-1209 CORE specification.

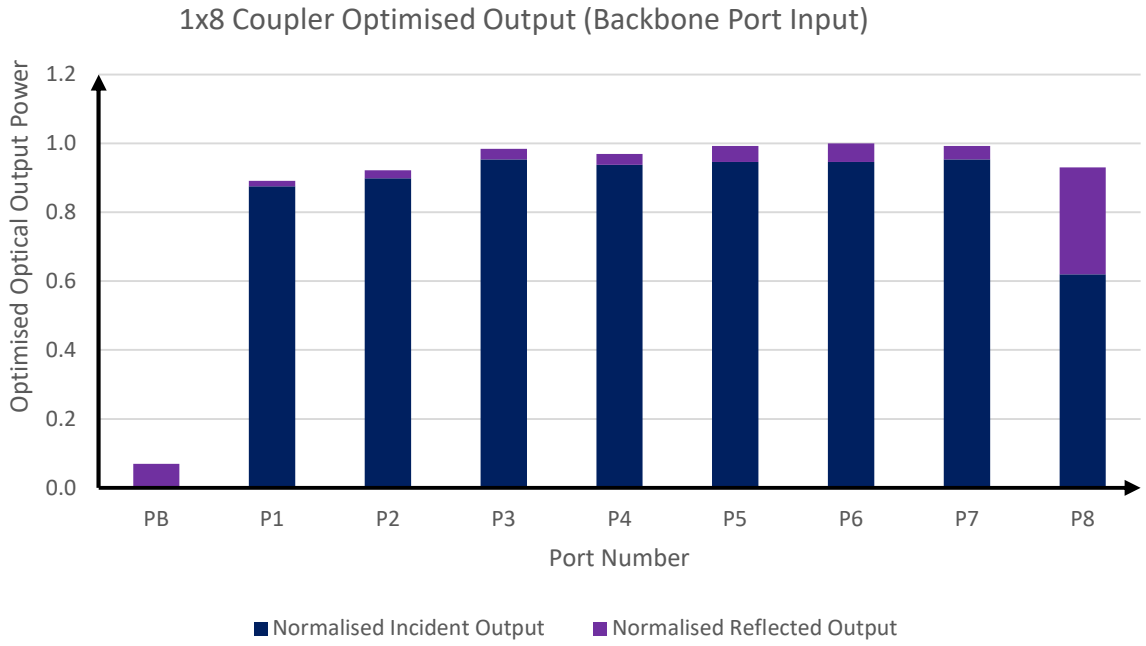

Figure 5-31: Complete optimisation of the received output optical power of the 1x4 array coupler with the backbone port used as the input port.

5.7.3 Transmitting 1x8 Array Coupler with Optimisation and Backbone POF End Reflector

As with the 1x4 array coupler, the design shown in Figure 5-30 will work well as a receiving coupler and not as a transmitting coupler. The immersion depths and the lengths of the optimisation reflectors used in this type of coupler would not give good coupler performance if ports 1 to 8 were the input ports. To make the coupler a transmitting coupler, the coupler configuration will need to be changed, specifically the immersion depths and the lengths of the optimisation reflectors. The reflector connected to the far end of the backbone POF remains the same. Ports 1 through 8 were used as input ports, as shown in Figure 5-32, and the results are shown in Figures 5-33 to 5-36. The calculated optical power received at each output port is tabulated in Table 5-14.

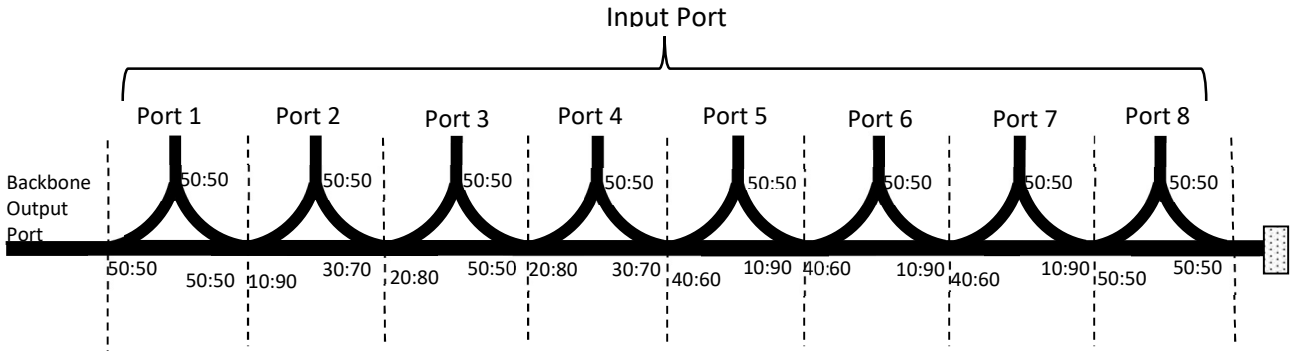

Figure 5-32: Transmitting 1x8 POF-based array coupler with ports 1 to 8 used as input ports.

Table 5-14: Transmitting 1x8 array coupler immersion depth and lengths of the optimisation reflectors.

Output Port	Immersion Depth	Reflector Length
P_B	----------	----------
P1	50:50 / 50:50	No Reflector
P2	10:90 /30:70	2.5mm / 1mm
P3	20:80 / 50:50	3.0mm / 1.5mm
P4	20:80 / 30:70	2.5mm / 1.5mm
P5	40:60 / 10:90	2.75mm/ 2mm
P6	40:60 / 10:90	2mm / No Reflector
P7	40:60 / 10:90	No Reflector
P8	50:50 / 50:50	No Reflector

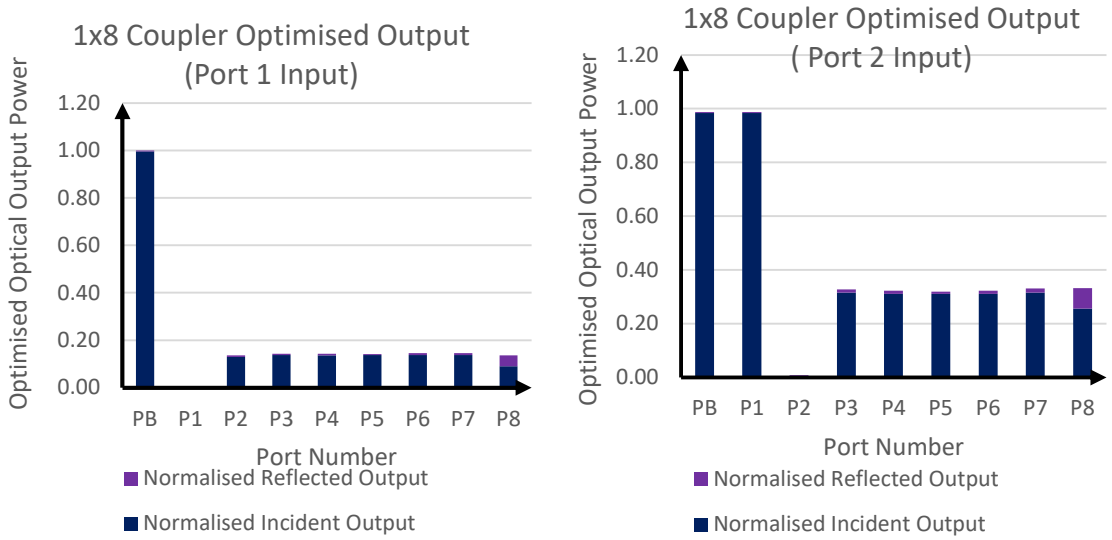

Figure 5-33: 1x8 coupler; port outputs with the input at ports 1 and 2, respectively

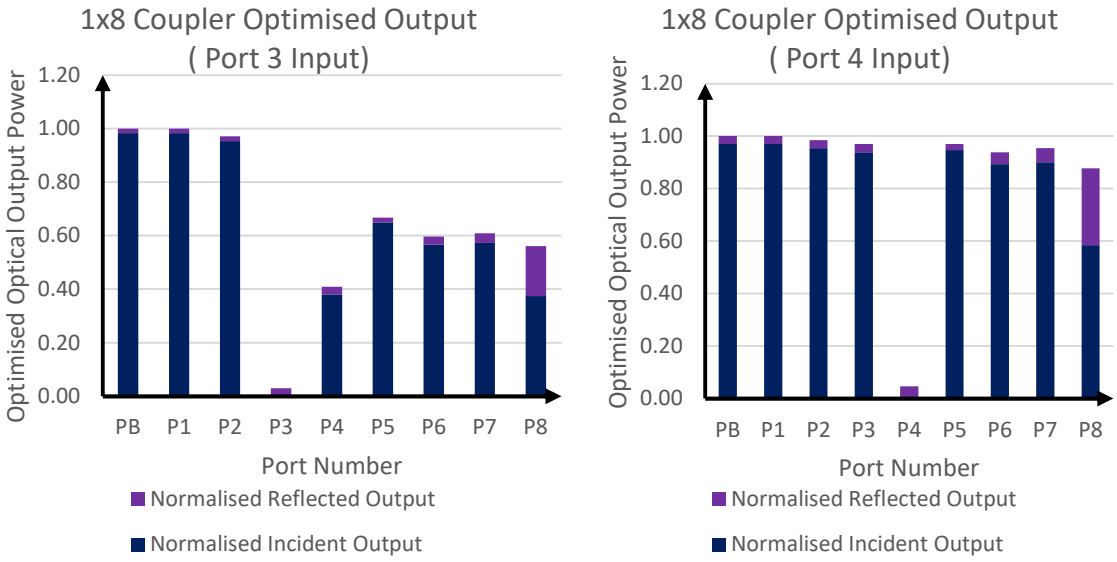

Figure 5-34: 1x8 coupler; port outputs with the input at ports 3 and 4, respectively.

Similar to the 1x4 array coupler, when port 1 was used as the input port, the backbone port received more than 50% of the optical power. The backbone receives this output power because the port 1 coupler splits the input power in half before it reaches the backbone POF. The other seven ports share the other half of the input power. Apart from the backbone port, the research achieved power optimisation for ports 2 to 8, but at a very low level.

It is important to note that when port 1 is the input port, the optical power travels the longest to reach port 8 and the end of the backbone POF. Therefore, port 1 input determines the dimensions and configuration (i.e. immersion depth and length of the optimisation reflectors) of this transmitting 1x8 array coupler. Port 2 input achieved power optimisation on ports 1 and backbone, and similarly on ports 3 to 8. However, the two power optimisations differ in levels; the coupler optimises ports 1 and backbone ports at a much higher level than ports 3 to 8.

Port 3 input yielded results similar to port 2 input; output ports 1 to 3 were optimised at a higher level than output ports 4 to 8. Port 4 input provided absolute optical power optimisation on all output ports except port 8, which received slightly less output power.

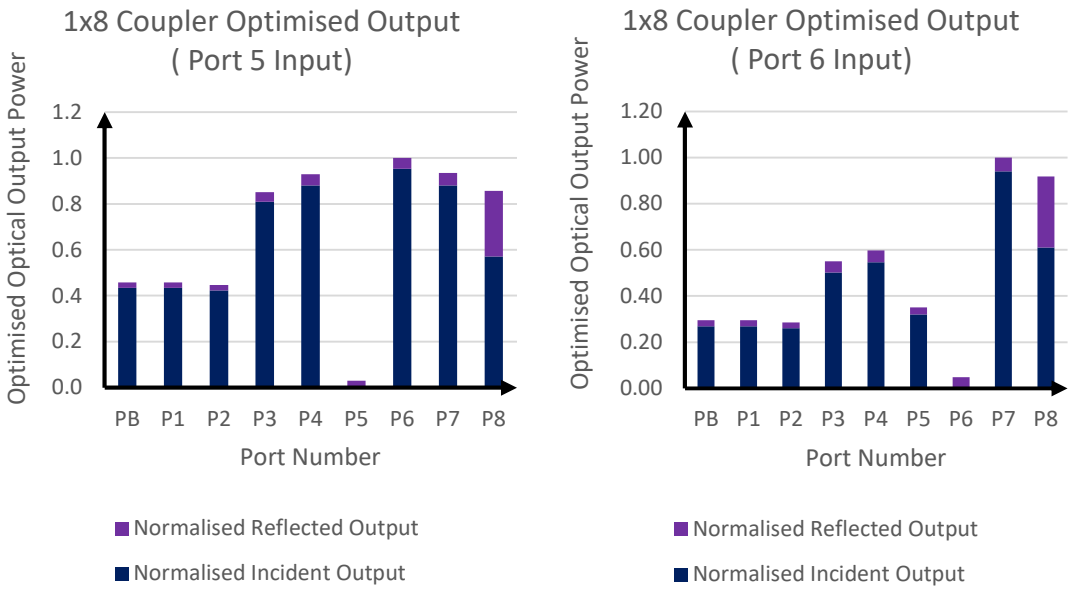

Figure 5-35: 1x8 coupler; port outputs with the input at ports 5 and 6, respectively.

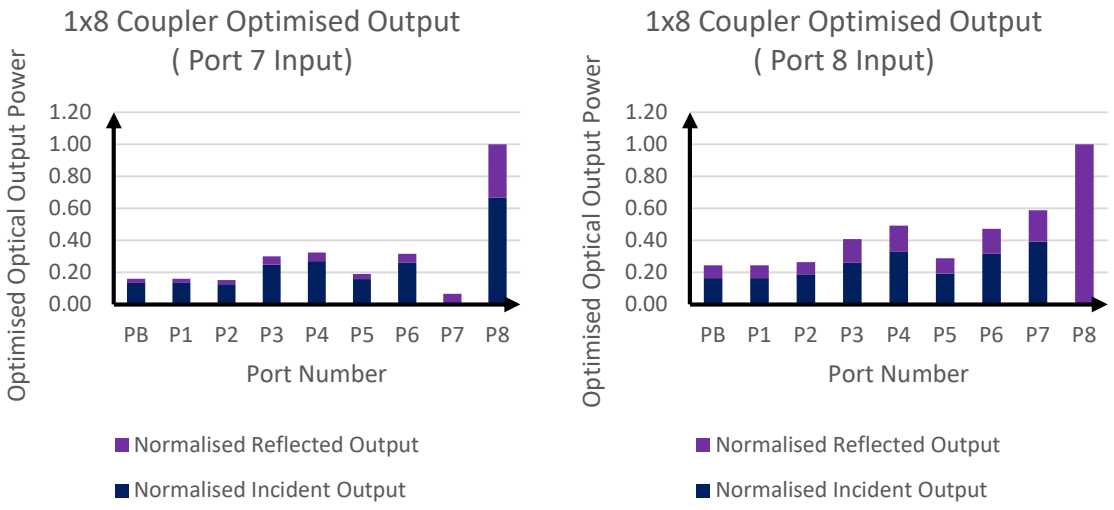

Figure 5-36: 1x8 coupler; port outputs with the input at ports 7 and 8, respectively.

In the coupler configuration in Figures 5-38 and 536, the inputs to ports 5 to 8 did not achieve the output port optimisation required by the research. With these port inputs, the coupler optimised only output ports 1 to 3. The coupler could be optimised with ports 5 to 8 if the coupler configuration changes, i.e., the immersion depths and lengths of the optimisation reflectors. However, changing the coupler configuration also disrupts the optimisation of the other input ports.

5.7.4 1x8 POF Coupler Performance Parameters

The performance parameters of the 1x8 POF-based array coupler were explored in this sub-section. The performance parameters of interest in this research are insertion loss, excess loss, uniformity, coupling (splitting) ratio, and coupler efficiency. The directivity and directionality are beyond the scope of this research.

5.7.4.1 Excess Loss, Coupler Loss uniformity and Coupler Efficiency

The coupler provides an excess loss of 0dB at almost all input ports, except port 8. The uniformity of all the input ports was less than 1 dB. Notably, the backbone port and input port 4 gave uniformity of 0dB. The coupler achieves a coupler efficiency above 99% on most input ports, except port 8, which has an efficiency of 75%. The poor coupler efficiency for port 8 resulted in 25% of the input power being reflected into the input port (Port 8) by the reflector at the far end of the backbone POF.

Table 5-15: 1x8Coupler Performance parameters: Excess Loss, Coupler Loss, Uniformity and Coupling Efficiency

Input Port	Excess Loss (dB)	Uniformity (dB)	Coupler Efficiency (%)
P_B	0.0	0	99.1
1	0.0	0.4	99.9
2	0.0	0.2	99.8
3	0.0	0.1	99.4
4	0.0	0	99.7
5	0.0	0.1	99.1
6	0.0	0.3	94.8
7	0.1	0.4	97.4
8	1.3	0.2	75

5.7.4.2 Insertion Loss

The insertion loss depends on the input port used. The insertion losses ranged from 3dB to 12 dB. When the backbone and port 4 were the input ports, the coupler exhibited a consistent insertion loss of 9dB at every input port. In terms of insertion loss, port 1 is the most inconsistent, with a minimum of 3dB and a maximum of 12dB, followed by port 7.

Table 5-16: 1x8 Coupler Performance parameters: Insertion loss

Output Port	Insertion Loss(dB)								
	P_B	P1	P2	P3	P4	P5	P6	P7	P8
P_B	0	3	6	8	9	11	12	12	10
1	9	0	6	8	9	11	12	12	11
2	9	12	0	8	9	11	12	12	10
3	9	11	11	0	9	8	9	10	10
4	9	11	11	12	0	8	9	9	9
5	9	11	11	9	9	0	11	11	10
6	9	11	11	10	9	8	0	9	8
7	9	11	11	10	9	8	6	0	7
8	9	12	11	10	9	8	7	4	0

5.7.4.3 Splitting (Coupling Ratio) Ratio

Like the insertion loss, the coupling ratio depends on the input port. The coupling ratio ranged from 6% to 50%. When port 1 was the input port, the coupler exhibited a consistent coupling ratio averaging 12%. There was some consistency on ports 1 and 2, as shown in Table 5-14.

Table 5-17: 1x4 Coupler Performance parameters: Coupling Ratio

Input Port	Coupling Ratio (%)								
	P_B	P1	P2	P3	P4	P5	P6	P7	P8
P_B	0	50	25	17	13	8	7	6	13
1	12	0	25	17	13	8	7	6	12
2	12	7	0	17	13	8	7	6	12
3	13	7	8	0	13	14	13	11	13
4	13	7	8	7	0	16	14	12	17
5	13	7	8	11	13	0	8	7	14
6	13	7	8	10	12	17	0	12	22
7	13	7	8	10	12	16	23	0	25
8	12	7	8	10	11	14	21	39	0

5.8 Data Rate Capability of the Port Array POF Couplers

In the array couplers discussed in sections 5-6, 5-7 and 5-8, when an incident pulse enters the backbone fibre, it propagates through the backbone POF until it reaches the end, where the optical reflector reflects it into the coupler. The principle of this optical transmission is depicted in Figure 5-37.

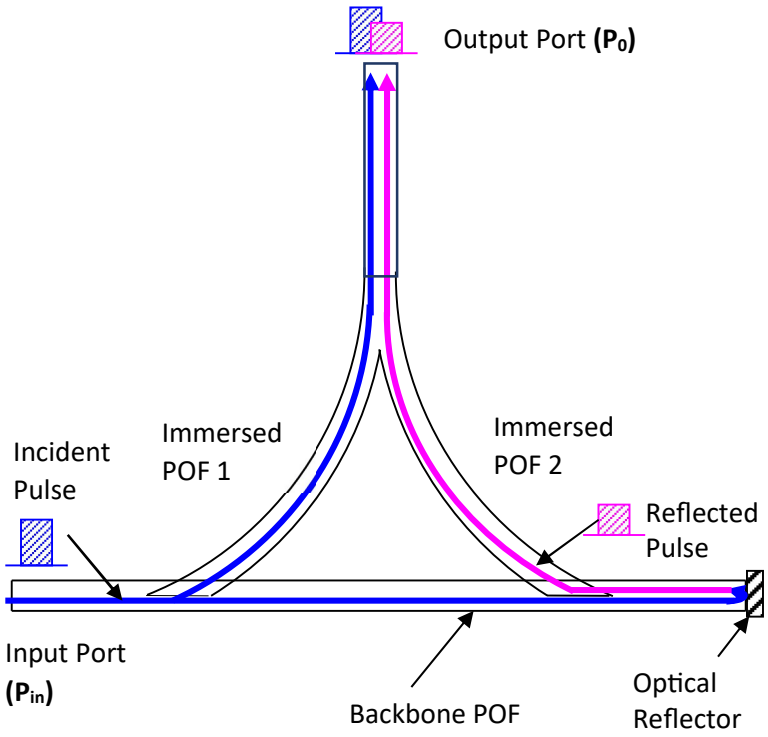

Figure 5-37: Coupler showing the interaction of the incident pulse and the reflected pulse.

As the incident pulse travels within the backbone fibre to the end of the backbone POF, part of its energy is coupled into the left-hand arm (Immersed POF 1) of the POF-based beam-splitting coupler, emerging at the output port as the received output power.

The reflected pulses at the far end of the backbone POF will also be coupled to the output port via the right-hand arm (immersed POF 2) beam-splitting coupler. The reflected pulses would then interact with the incident pulse. However, the reflected pulses possess a time delay because they would have travelled to the end of the backbone optical fibre and back. The resultant pulse at the output port would have a higher amplitude and substantially increased pulse width, as shown in the pulse waveforms in Figure 5-38.

The pulse width, a function of the refractive index, determines the transmission bit rate that the designed couplers can handle, making the couplers' dimensions critical. The pulse width is also a function of the optical path length travelled by the reflected pulse. The simulated specifications for the Plastic Optical Fibre are for the EskaTM CK-40, which has a refractive index (η) of 1.492.

The bit rate at the output port of the array couplers depends on the pulse spread (Pulse Width) caused by the incident transmitted pulse, plus the delayed reflected pulses received. The benefit of incorporating the reflected part of the pulse is overcoming the attenuation's effect on the data rate. Without the reflected part of the pulse, the data rate would not be limited by the path length but by the transmission characteristics of the plastic optical fibre used. The resultant pulse at the output port would be higher in amplitude and wider in width, as shown in the waveforms below (Agrawal, 2021).

$$\text{Bit Rate} = \frac{1}{\tau} \tag{5.20}$$

Where $\boldsymbol{\tau}$ is the pulse width.

The Index of Refraction (η) is the ratio of the speed of light in a vacuum (c) to the speed of light in that material (phase velocity, v).

$$\eta = \frac{c}{v} \tag{5.21}$$

Therefore, the speed of light in a material is given by:

$$v = \frac{c}{\eta} \tag{5.22}$$

Therefore, the Delay Time (τ) travelled by the reflected pulse can be found by:

$$\tau = \frac{d}{v} = d \Big/ \frac{c}{\eta}$$

$$\tau = \frac{\eta d}{c} \tag{5.23}$$

Substituting equation 23 into equation 20:

$$\text{Bit rate} = \frac{c}{\eta d} \qquad 5.24$$

Where: t is the delay time

d is the distance travelled by the reflected pulse

η is the refractive index

c is the speed of light in a vacuum

The product of the refractive index (η) and distance (d), ηd, is the Optical Path Length.

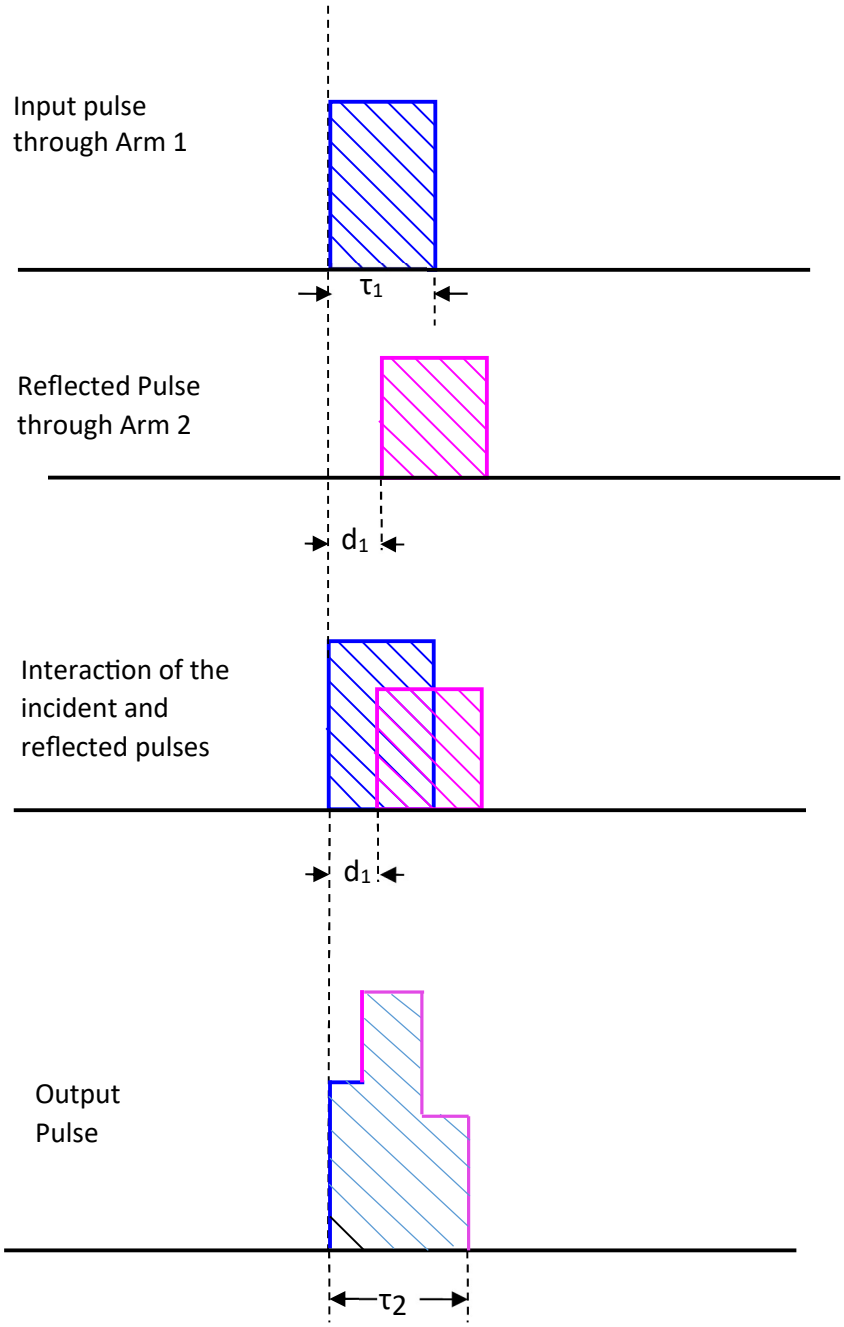

Figure 5-38: Pulse interaction diagram.

5.8.1 Calculation of the 1x2 Array Coupler Data Rate

The product of the refractive index (η) and distance (d), ηd, is called the Optical Path Length. When considering a 1x2 array coupler, the distance travelled by the reflected pulse to Port 1 = 0.17m. The delay time for the reflected pulse to Port 1 of the array coupler is therefore given by equation 5-23:

$$\tau = \frac{\eta d}{c}$$

$$\tau = \frac{1.49 \times 0.17}{3 \times 10^{8}}$$

$$\underline{\tau = 0.84 \text{ ns}}$$

Table 5-18 shows the delay times for each of the output ports of the POF coupler.

Table 5-18: Reflected pulse Delay times and distances to 1x2 POF coupler output ports.

Port Number	Port Designation	Distance (m)	Delay Time (ns)
1	P_1	0.17	0.844
2	P_2	0.07	0.347

The reflected pulse suffers the highest delay when travelling to port 1 (0.884 ns). The minimum pulse width of the incident pulse should be higher than the delay time of the reflected pulse for both the incident and reflected pulses to be received as one unit at the output port. The minimum pulse duration of the incident pulse should be approximately 1 ns for transmission and 2 ns for reception.

$$\text{Transmission Data Rate} = \frac{1}{\tau} = \frac{1}{1 \times 10^{-9}}$$

$$= \underline{1 \text{ Gbs}}$$

$$\text{Reception Data Rate} = \frac{1}{\tau} = \frac{1}{2 \times 10^{-9}}$$

$$= \underline{500 \text{ Mbs}}$$

As shown in the calculations, a transmission rate of 1Gb/s can be achieved with this pulse duration. The calculations show that the transmission date is twice the reception data rate.

5.8.2 Calculation of the 1x4 Array Coupler Data Rate

When considering the 1x4 array coupler, the distance travelled by the reflected pulse to Port 1 would equal 0.37m, as shown in Table 5-19. The delay time for the reflected pulse to Port 1 of the array coupler is therefore given by:

$$t_1 = \frac{1.49 \times 0.37}{3 \times 10^8}$$

$$t_1 = \underline{1.837\ ns}$$

Table 5-19: Delay times and distances to POF coupler ports.

Port Number	Port Designation	Distance (m)	Delay Time (ns)
1	P_1	0.37	1.837
2	P_2	0.27	1.34
3	P_3	0.17	0.844
4	P_4	0.07	0.347

The reflected pulse's highest delay time to port 1 is 1.837 ns, so the minimum pulse width of the incident pulse should be higher than that delay time for both the incident and reflected pulses to be received as one unit at all the output ports. The minimum pulse duration would be approximately 2 ns for transmission and 4 ns for reception. The calculation below shows that these pulse widths can achieve a transmission rate of 500/s and a reception data rate of 250 MB/s, respectively.

$$\text{Transmission Data Rate} = \frac{1}{\tau} = \frac{1}{2 \times 10^{-9}}$$

$$= \underline{500\ \text{Mb/s}}$$

$$\text{Reception Data Rate} = \frac{1}{\tau} = \frac{1}{4 \times 10^{-9}}$$

$$= \underline{250\ \text{Mb/s}}$$

5.8.3 Calculation of the 1x8 Array Coupler Data Rate

For the 1x8 coupler, the distance travelled by the reflected pulse to Port 1 is 0.77 m, as shown in the table below. The delay time for the reflected pulse to Port 1 of the array coupler is therefore given by:

$$t_1 = \frac{1.49 \times 0.77}{3x10^8}$$

$$\underline{t_1 = 3.824\ ns}$$

Table 5-20 illustrates the output delay times for a theoretical POF-based 1x8 array coupler.

Table 5-20: Delay times and distances to POF coupler ports.

Port Number	Port Designation	Distance (m)	Delay Time (ns)
1	P_1	0.77	3.824
2	P_2	0.67	3.327
3	P_3	0.57	2.831
4	P_4	0.47	2.334
5	P_5	0.37	1.837
6	P_6	0.27	1.34
7	P_7	0.17	0.844
8	P_8	0.07	0.347

The reflected pulse's time delay to port 1 is 3.824 ns, so the minimum pulse width of the incident pulse should be higher than that time delay (3.824 ns) for both incident and reflected pulses to receive one pulse at the output ports. The minimum pulse duration is approximately 4 ns for transmission and 8 ns for reception, as shown in the pulse diagram in Figure 5-39.

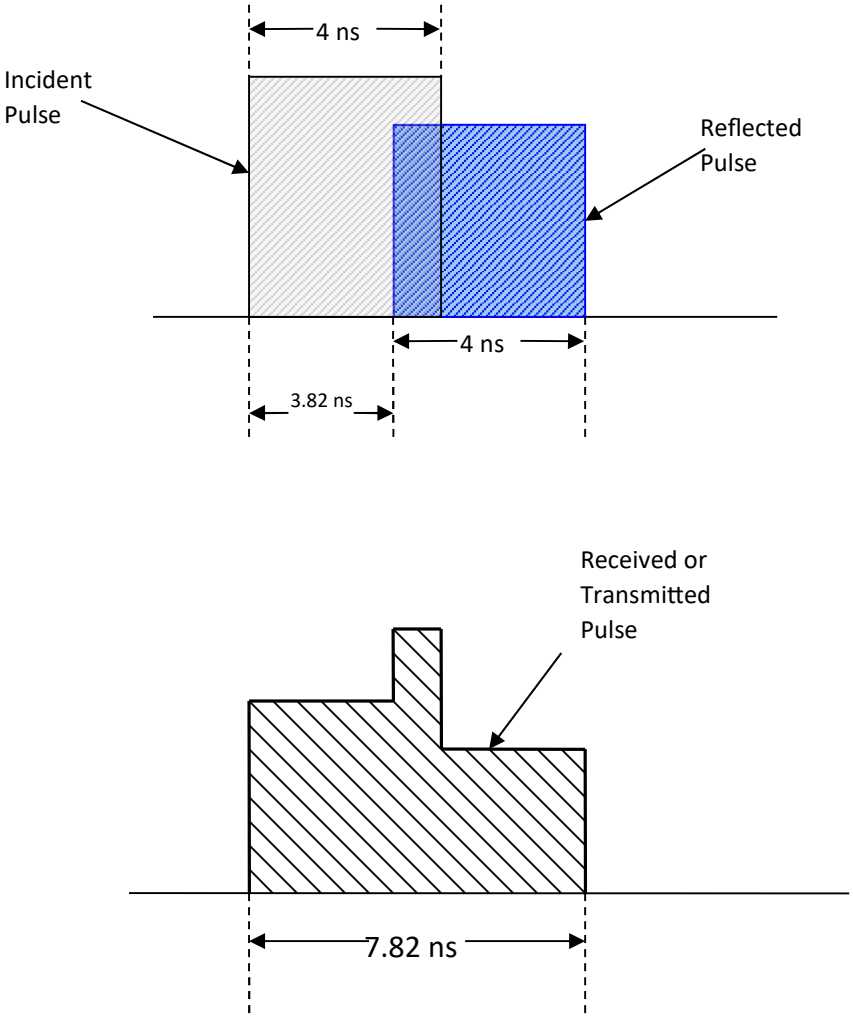

Figure 5-39: The pulse waveforms received at port 1.

The data rate calculation is as follows:

$$\text{Bit rate} = \frac{1}{\tau}$$

The Transmission Data Rate:

$$T_x \text{ Bit rate} = \frac{1}{4 \times 10^{-9}}$$

$$= 250 \times 10^{6}$$

$$= \underline{250 \text{ Mb/s}}$$

The Reception Data Rate:

$$R_x \text{ Bit Rate} = \frac{1}{8 \times 10^{-9}}$$

$$= \underline{125 \text{ Mb/s}}$$

In conclusion, theoretically, the proposed passive eight-port array POF coupler would be capable of transmitting at 200 Mb/s and receiving at a data rate of 125 Mb/s, which is sufficient to transmit Fast Ethernet transmissions at 100 Mb/s.

The reduction in the separation distance between the individual couplers massively increases the data rate capabilities of the array coupler. The bit rate at each port depends on the pulse spread or dispersion, which includes the received incident pulse and the reflected pulse. The pulse spread is a function of the optical path length travelled by the reflected pulse. Port 1 experiences the most significant pulse spread because the reflected pulse travels the longest optical path.

It is essential to incorporate the reflected part of the pulse to overcome attenuation affecting the data rate. Without the reflected part of the pulse, the data rate would not be limited by the path length but by the transmission characteristics of the plastic optical fibre used, i.e., bandwidth and the rise and fall times.

5.9 Summary

This chapter explores the theoretical analysis of the array of couplers that will be adapted to work in networking and other industrial applications. The chapter starts by presenting the basic calculations for the design and structure of hybrid (beam splitter combined with a bus coupler) POF-based array couplers. At the splitting joint of the beam splitter, a reflector will be inserted in the joint between the two arms of the beam splitter to prevent optical power from leaking from one arm to another.

All theoretical dimensions of the coupler and losses at each fibre joint were calculated based on the type of plastic optical fibre used. Two formulae were derived to calculate the port output power based on the precise optical power at each output port. The immersion depth influenced the first formula, while the optimisation reflector influenced the second formula. The validity of the derived formulae was expected to be verified through simulation analysis in the next chapter.

This chapter also investigated methods for optimising the optical power at the coupler's output ports. To achieve optimisation, the immersion depth connects a 100% reflector at the far end of the backbone POF (optimisation reflector) and inserts a reflector between the backbone POF and the immersed POF. The results were encouraging; immersion depth provided a coarse adjustment, while the optimisation reflector offered a fine adjustment of the port output power. The reflector at the far end of the backbone POF was assumed to reflect all the optical power into the backbone POF. Also, the performance results and parameters of the 1 x 2, 1 x 4, and 1 x 8 array couplers were calculated to provide a holistic insight into their performance.

During the research, it became apparent that using a single coupler for both transmission and reception was impractical, especially for 1x4 and 1x8 array couplers. As a result, the array couplers for transmission and reception had separate designs.

Section 5.9 calculated the transmission and reception data rates for POF-based 1 x 2, 1 x 4, and 1 x 8 array couplers, taking into account the time-delayed reflected pulse that interacts with the incident pulse at the output port. The reflected pulse augments the incident pulse. However, it will widen the incident pulse, reducing the data rate that the array coupler can handle. The calculation demonstrated that a POF-based 1x2 array could achieve a transmission data rate of 1 GB/s and a reception data rate of 500 Mb/s. The 1x4 coupler could achieve a transmission data rate of 500 Mb/s and a reception data rate of 250 Mb/s. Lastly, the 1 x 8 coupler can transmit at 250 Mb/s and receive at 125 Mb/s.

5.10 References

Korn, G. A. (2000). *Mathematical Handbook for Scientists and Engineers. .* New York: Dover Publications.

Agrawal, G. P. (2021). *Fiber-Optic Communication Systems.* (5th ed.). John Wiley & Sons.

Appajaiah, A. (2005). Climatic Stability of Polymer Optical Fibers (POF). *Potsdam University*. Berlin, German.

Chapter 6

Coupler Design Modelling and Ray Tracing Simulations

6.1 Introduction

This chapter focuses on simulating plastic optical fibre (POF) couplers and analysing the results to provide a detailed understanding of the proposed coupler's characteristics, performance, and parameters. The simulation results presented here confirm the findings from the theoretical analysis conducted in a previous chapter.

All simulations were carried out using the LightTools ray-tracing optical simulation software, with LEDs as the optical sources at four wavelengths: 470 nm (Blue), 520 nm (Green), 570 nm (Yellow), and 650 nm (Red). These wavelengths were chosen to evaluate how the properties of POF and POF couplers vary with wavelength. The parameters set in Light Tools were designed to model an ideal POF.

The chapter used theoretical analysis and optical simulations to investigate the characteristics and performance parameters of POF-based array couplers (1x1, 1x2, 1x4, and 1x8) and to determine key coupler parameters, including insertion loss, excess loss, coupling ratio, and coupling efficiency.

Finally, simulations aimed at optimising the optical performance of the couplers were conducted to ensure that each output port received nearly equal optical power. In theory, for a 1x2 coupler, each output port was expected to receive 50% of the input power; for a 1x4 coupler, 25%; and for a 1x8 coupler, 12%.

6.2 Model Plastic Optical Fibre for Simulation Analysis

As outlined in Chapter 4, the optical couplers simulated in this research utilise cylindrical plastic optical fibres (POF) with a 1 mm diameter, including the cladding. The POF used in the simulations is a step-index PMMA POF with a core diameter of 0.98 mm, a thin polymer cladding layer of 10 μm, and a numerical aperture of 0.5. The refractive indices of the core and cladding are 1.49 and 1.402, respectively.

A predefined optical field profile served as the input light source, emitting 100 mW of power at four wavelengths: 470nm (Blue), 520nm (Green), 570nm (Yellow), and 650nm (Red). In the simulations described in this chapter, the optical light source is an LED transmitter that generates multimodal light pulses. The LED emitted 100 mW of power and 100,000 light rays, while the optical receiver used in the simulations is a photodiode.

6.3 Simulation 1: Beam Splitter Simulations

6.3.1 Background

This simulation investigates a beam-splitting coupler composed of two POF arms connected to a single POF, as shown in Figure 6-1. It examines the beam splitter's performance characteristics. To maximise the output optical power, no reflector was placed between the two arms of the beam splitter. A bending radius of 25 mm was used for the POF to prevent optical power loss through the cladding.

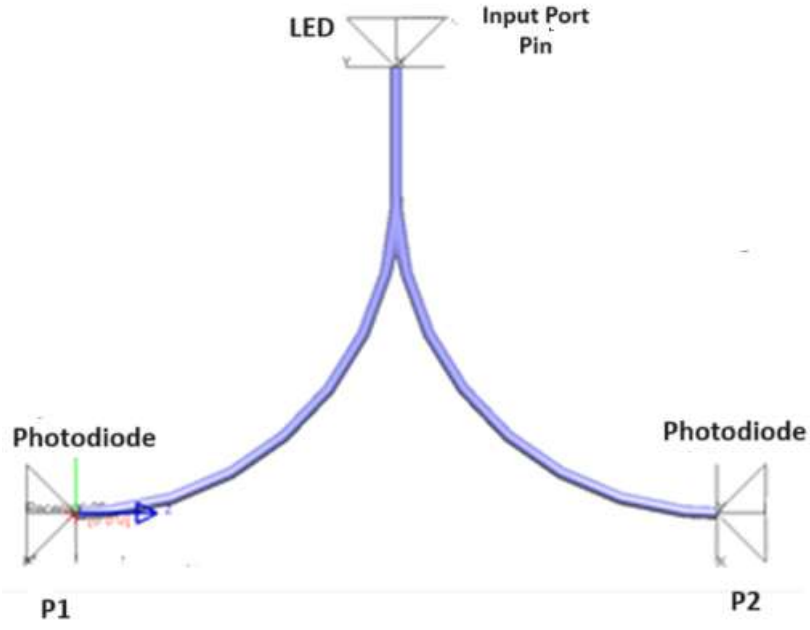

Figure 6-1: Beam splitter used in the simulation.

This simulation confirms the expected outcome that the beam splitter (Y-Coupler) divides the input optical power nearly equally, as shown in Figure 6-2. Both output ports

received approximately 50% of the input power. Additionally, a key observation was the high optical power concentration at the centre of the optical fibres. The beam splitter exhibited a minor excess loss of -17.9 dB.

When one of the splitter arms (P_1) was used as the input port, a significant portion of the input power was directed to the primary output port (P_{in}), while only a small amount reached the secondary output (P_2). Specifically, about 90% of the input optical power was transmitted to P_{in}, while P_2 received approximately 9%.

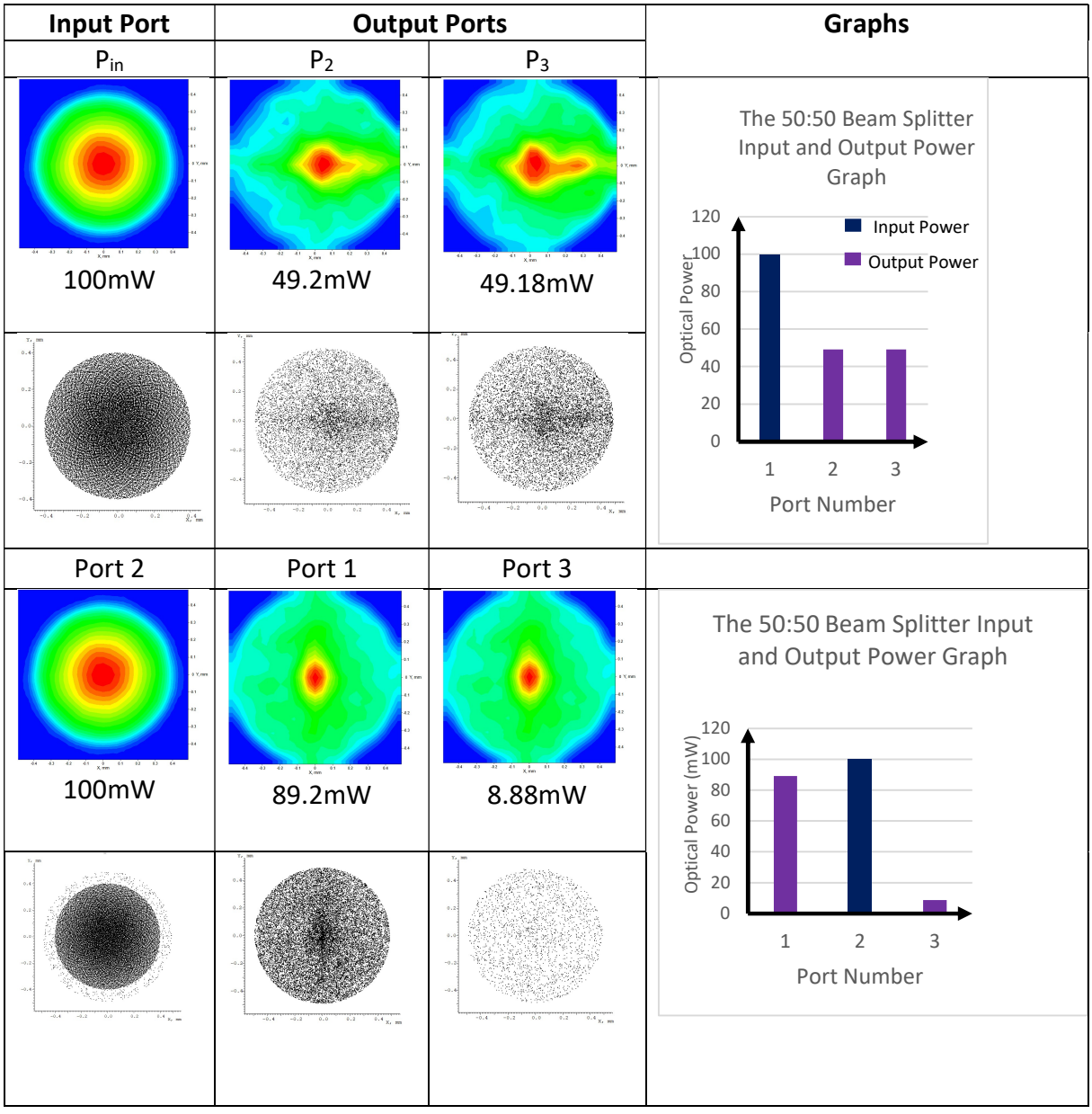

Figure 6-2: Beam splitter irradiance, scatter plots, and optical power output.

6.4 Simulation 2: 1x2 Coupler Simulations

6.4.1 Background

In this simulation, a backbone POF was introduced, and the previous beam-splitting coupler was adjusted to a 20:80 splitting ratio. The 1x1 coupler model used in the simulation is shown in Figure 6-3. The simulation was repeated as described in Section 6.3 to investigate and analyse the performance characteristics of the 1x2 optical coupler. The dimensions of the plastic optical fibre coupler were determined from calculations in the theoretical analysis chapter.

First, the simulation was conducted with Port 1 as the input, and the output was measured from the two backbone fibre ports (Ports 2 and 3). The exact process was then repeated, using one of the backbones POF ports (Port 2) as the input. The optical output measurements for each configuration were plotted as bar graphs and compared visually.

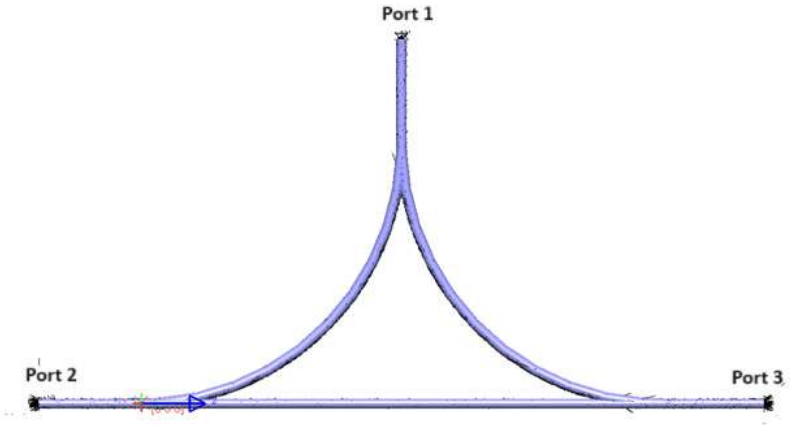

Figure 6-3: 1x1 coupler model used in the simulation.

6.4.2 The Simulation

When Port 1 was used as the input in the beam splitter, the simulation produced results consistent with those from the beam splitter simulation in Section 6.3. Both backbone POF output ports (Ports 2 and 3) received 50% of the input optical power. In the second simulation, one of the backbone ports was used as the input.

6.4.3 The Results and Discussion

The optical output measurements from both simulations were plotted as bar graphs and visually compared, as shown in Figure 6-4.

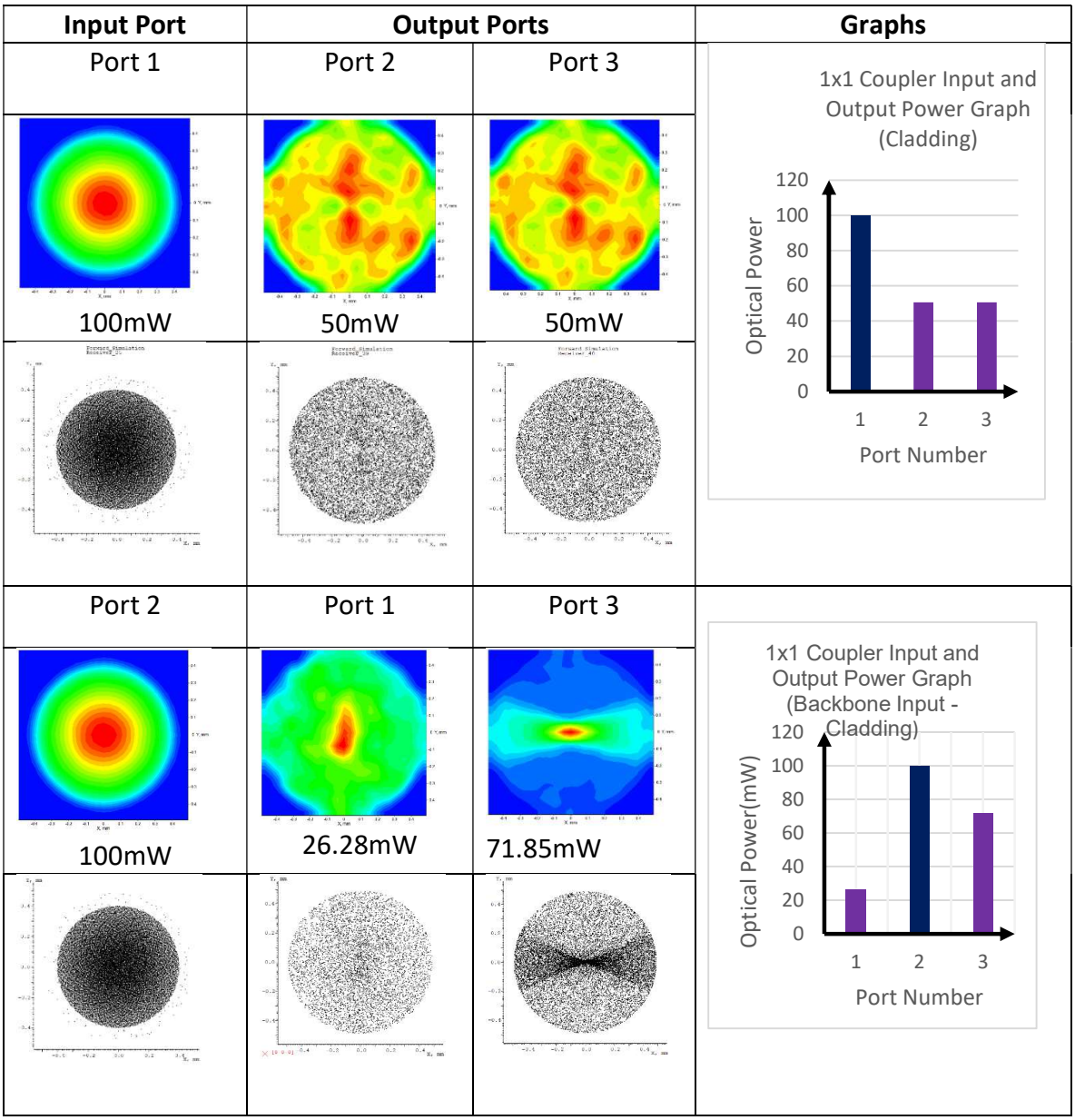

Figure 6-4: The irradiance and scatter plot for the 1x1 coupler

When Port 1 was used as the input for the beam splitter, both backbone output ports received 50% of the optical power. However, when compared to the beam splitter output shown in Figure 6-2, a key difference was observed in the distribution of optical power. In the

beam splitter, shown in Figure 6-4, the optical power was concentrated at the centre of the POF, while in the 1x2 coupler, the optical power was more dispersed around the circumference of the output POF. This scattering occurred due to the optical modes travelling across the junction between the backbone POF and the immersed POF.

In the second simulation, in which one of the backbone ports served as the input, the results followed the expected theoretical patterns. According to the theoretical analysis, specific optical modes at the backbone output port do not interact with the immersed POF, and only the interacting modes appear at the output port. The depth of immersion of the POF influences the amount of optical power at the output ports.

6.5 Simulation 3: 1x2 Array Coupler Characteristics Measurements

6.5.1 Background

This simulation aims to investigate and assess the performance characteristics of the 1x2 optical coupler. The dimensions of the plastic optical fibre coupler were based on calculations from the theoretical analysis chapter. Initially, the simulation was conducted without an optical reflector connected to the backbone fibre output. The same simulation was then repeated with an optical reflector attached to the backbone POF output. The optical output measurements from both simulations were plotted as bar graphs and compared visually. A third simulation was performed to optimise the output by inserting an optical reflector between the polished surfaces of the backbone POF and the immersed POF.

6.5.2 1x2 Array Coupler Simulation Without a Backbone Reflector

The first simulation was conducted using a 1x2 model coupler without a reflector attached to the end of the backbone POF. The immersion depth used in the simulation was based on the calculations from the theoretical analysis. Figure 6-5 shows the 1x2 coupler model used in this simulation.

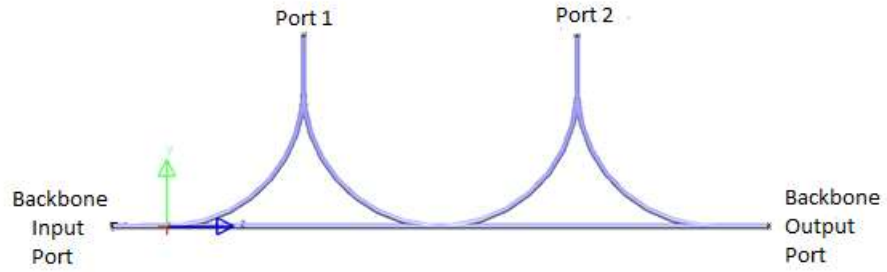

Figure 6-5: The 1x2 coupler model used in the simulation with no reflector at the backbone port.

The immersion depth used in the simulation was 30% (30:70), and the results aligned with the theoretical analysis, indicating that the output optical power decays exponentially from the first output port. Without a reflector at the end of the backbone POF, only 56% of the input optical power reached the output ports, resulting in a significant loss of 43% at the end of the backbone POF.

The simulation aimed for each output port to receive at least 40% of the input power; however, output Port 1 received only 35%, and output Port 2 received 21%. These measured output power values were consistent with the calculated values of 36% for Port 1 and 23% for Port 2. The calculated values were slightly higher because POF losses were not accounted for in the calculations.

6.5.3 1x2 Array Coupler Simulation with a Backbone Reflector

When the exact simulation was conducted with an optical reflector at the end of the backbone POF, as shown in Figure 6-6, the optical power received at the output ports increased significantly.

Output Port 1 received 43.5% of the optical power, while Output Port 2 received nearly 35%. As a result, the coupler's coupling efficiency increased from 54% to 78%. This improvement occurred because the optical power that would have been lost in the backbone POF was reflected into the coupler, thereby increasing the received output optical power, as explained in the theoretical analysis. The results are summarised in Table 6-1, and Figure 6-7 illustrates these findings.

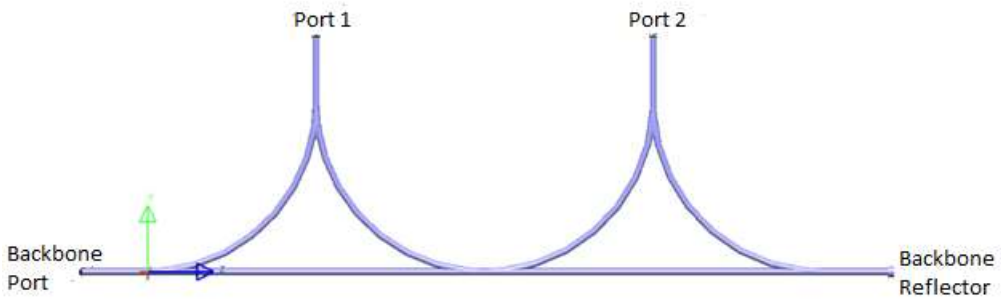

Figure 6-6: The 1x2 coupler model used in the simulation with a reflector at the backbone port.

Table 6-1: 1x2 Coupler Output Optical Power

Port Number	Output without a Reflector (mW)	Output with a Reflector (mW)
1	35.4	43.5
2	22.1	34.8
Total	57.5	78.3

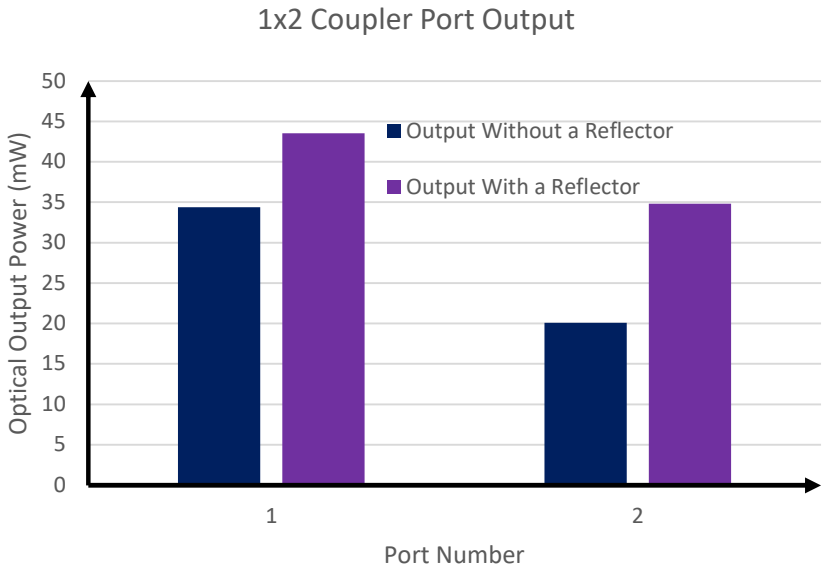

Figure 6-7: Graphs showing the 1x2 coupler output optical power.

6.5.4 Optimisation of the Output Optical Power

This simulation focuses on equalising the output power so that each port receives roughly the same amount of energy from the coupler. As observed in previous simulations, the optical power distribution varies significantly when the input is the backbone POF. To address this, the simulation tested different immersion depths and added an optical reflector at the end of the backbone fibre. However, this did not fully optimise the power received at each output port.

Various splitting ratios were also explored, including the 50:50 ratio used in the theoretical analysis, to balance the output power. Despite these efforts, complete optimisation was not achieved, and this approach made the array coupler more complex.

Fortunately, as discussed in Chapter 4, a technique was developed to adjust the port output power by inserting a reflector between the polished surfaces of the backbone POF and the splitting POF, as shown in Figure 6-8. This method was successfully used to optimise the output power distribution fully.

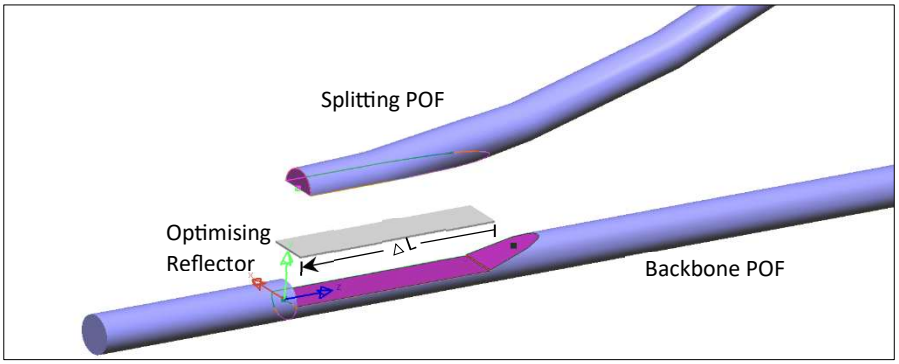

Figure 6-8: Components of the optimised splitting coupler.

The technique involves placing a reflector between the polished surfaces of the backbone POF and the polished splitting POF, which is immersed in the backbone fibre. The reflector reflects optical energy on all sides. The purpose of inserting the reflector is to divide the incoming optical power between the two independent POFs based on the immersion depth. One POF directs a portion of the optical energy to the output port, while the other POF carries the remaining portion of the optical power through the backbone POF.

6.5.5 Optimised 1x2 Array Coupler Simulation

This simulation combined three techniques—immersion depth, a backbone reflector, and an optimisation reflector—to balance and optimise the optical power at the output ports. The simulation investigated how to maximise the output power received at the ports and assessed the performance characteristics of the optimised 1x2 optical coupler.

The dimensions of the 1x2 POF coupler components were determined using calculations from the theoretical analysis chapter. In the simulation, 100 mW of input power was applied at the backbone port, with an optical reflector placed at the end of the same backbone POF, as shown in Figure 6-9. As in the theoretical analysis, there was no need to insert an optimisation reflector into the 1x2 array coupler simulated in Figure 6-9, because the immersion depths and the backbone reflector were sufficient to optimise the received optical power at ports 1 and 2. In this coupler, the immersion depths had to be adjusted to account for differences from the theoretically calculated values.

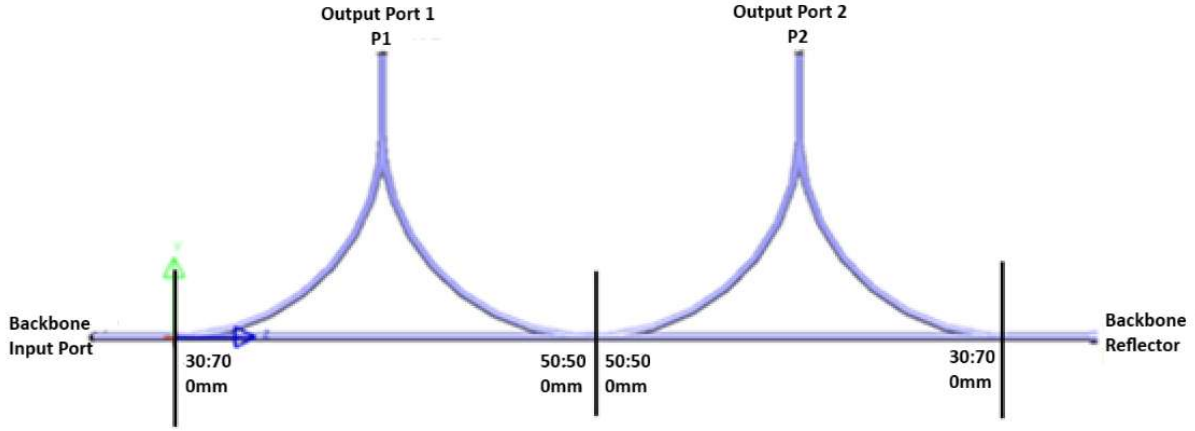

Figure 6-9: The simulated 1x2 array coupler showing the immersion depths and the length of the optimisation reflector at each junction with the backbone POF for optimisation.

These simulation results were used to calculate the coupler's performance parameters. Figure 6-9 and Table 6-2 also show the immersion depths used in this simulation.

Table 6-2: Optimised 1x2 Array Coupler Showing the Immersion Depth and Lengths of the Optimisation Reflector

Port No:	Immersion Depth	Reflector Length (mm)
1	30:70/50:50	No Reflector
2	50:50/30:70	No Reflector

The output optical power was obtained from the array of coupler output ports, as shown in Figures 6-10 and 6-11. The immersion depth and the backbone reflector influenced the output power at each port of the 1x2 array coupler.

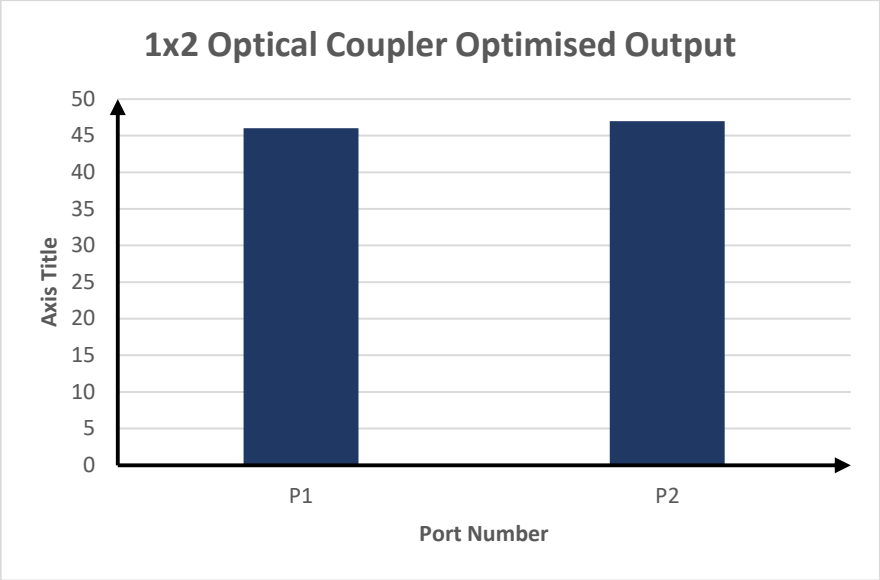

Figure 6-10: Optimised port output with the input port at the backbone port.

Using the backbone port as the input (Figure 6-10), the coupler balanced the outputs at P1 = 46 mW and P2 = 47 mW from a 100mW input—an overall coupling efficiency of 93%. The insertion loss was 3.3 dB per port, with uniformity of 0.1 dB and excess loss of 0.32 dB.

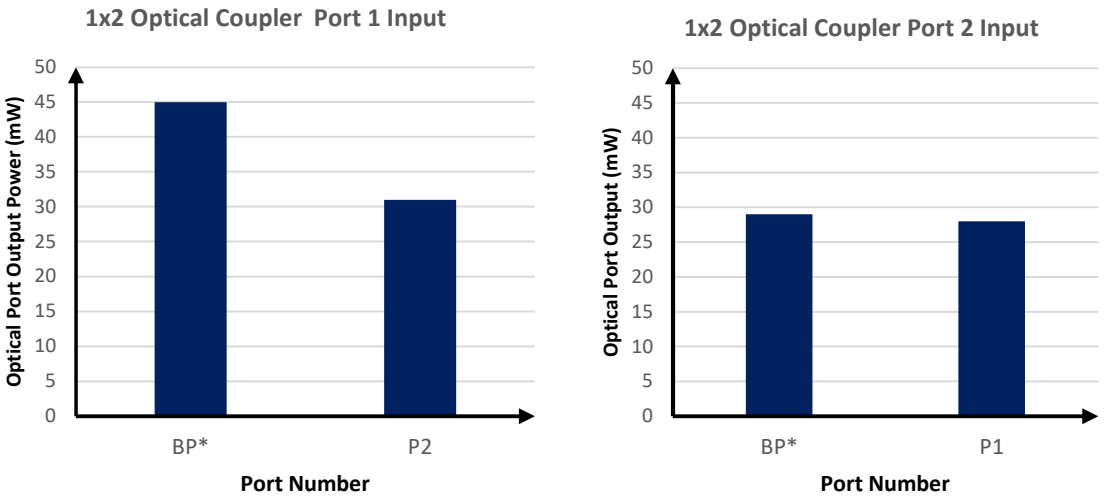

Figure 6-11: Optimised port output with the input port at port 1 and port 2, respectively.

In Figure 6-11, the simulation used ports 1 and 2 as the input ports, respectively. When port 2 was used as the input, the optical power received at port 1 and the backbone port was optimised. However, this optimisation negatively affected the coupler's efficiency and loss, reducing it to 57% with an insertion loss of 3.7 dB.

When port 1 was used as the input, the coupler did not achieve the desired optimisation because port 1 splits its power in half, with the backbone port directly receiving that split power without further optimisation. In this case, the input to port 1 resulted in a coupler efficiency of 76% and an insertion loss of 6.2 dB.

6.5.6 1x2 Array Coupler Performance Parameters

This sub-section presents the calculated performance parameters for the simulated 1x2 POF-based coupler. The parameters calculated include excess loss, insertion loss, coupling ratios, coupling efficiency, coupler loss, and uniformity. All of these performance metrics varied depending on the input port used. Sub-sections 6.5.6.1 to 6.5.6.2 display the coupler's performance parameters in tabular form. The simulation did not calculate directivity and directionality, as these are beyond the scope of this research.

6.5.6.1 Excess Loss, Coupler Loss, Uniformity and Coupler Efficiency

For the 1x2 array coupler shown in Figure 6-9, the coupling efficiency ranged from 57% to 84%, depending on the input port. The excess loss ranged from 0.76 dB to 2.44 dB, and the coupling loss ranged from 3.67 dB to 8.54 dB. The uniformity was approximately 0.0 dB.

Table 6-3: 1x2 simulated coupler performance parameters: Excess Loss, Coupler Loss, Uniformity and Coupler Efficiency

Input Port	Excess Loss (dB)	Coupler Loss (dB)	Uniformity (dB)	Coupler Efficiency (%)
P_B	0.0	1.1	0.1	93
1	1.2	6.2	0.07	76
2	2.4	3.7	0.01	57

6.5.6.2 Insertion Loss

Table 6-4: 1x2 Simulated Coupler Insertion Loss

Input Port	Insertion Loss (dB)		
	P_B	P1	P2
P_B	0	3.4	3.3
1	3.5	0	5.1
2	5.4	5.5	0

6.5.6.3 Splitting (Coupling) Loss

The splitting ratios ranged from 49% to 59%, and the insertion loss ranged from 3.47 dB to 5.53 dB, as shown in Table 6-5.

Table 6-5: 1x2 Simulated Coupler Splitting (Coupling) Ratios

Input Port	Splitting (Coupling) Ratio (%)		
	P_B	P1	P2
P_B	0	50.0	50.0
1	59.2	0	40.8
2	55.9	49.1	0

The simulation results indicated that the 1x2 coupler performed better when the backbone port was used as the input. Nevertheless, the 1x2 coupler shown in Figure 6-9 remains viable for either transmitting or receiving applications.

6.6 Simulation 5: 1x4 Array Coupler Characteristics and Measurements

6.6.1 Background

Like the 1x2 coupler simulation, this simulation aims to investigate and determine the performance characteristics of the 1x4 array coupler. The dimensions of the plastic optical fibre coupler were established based on calculations from the theoretical analysis chapter. Initially, the simulation was conducted without an optical reflector connected to the output of the backbone POF, as shown in Figure 6-12. The simulation was then repeated with an optical reflector attached to the backbone POF output. The optical output measurements from both simulations were plotted as bar graphs and compared visually. The third simulation for this coupler focused on optimising the optical power received at the output ports.

6.6.2 1x4 Array Coupler Simulation without a Backbone Reflector

The first simulation was conducted with a 1x4 coupler, without a reflector at the end of the backbone POF, as shown in Figure 6-12. The immersion depth used in this simulation, determined by calculations from the theoretical analysis, was 10% (10:90).

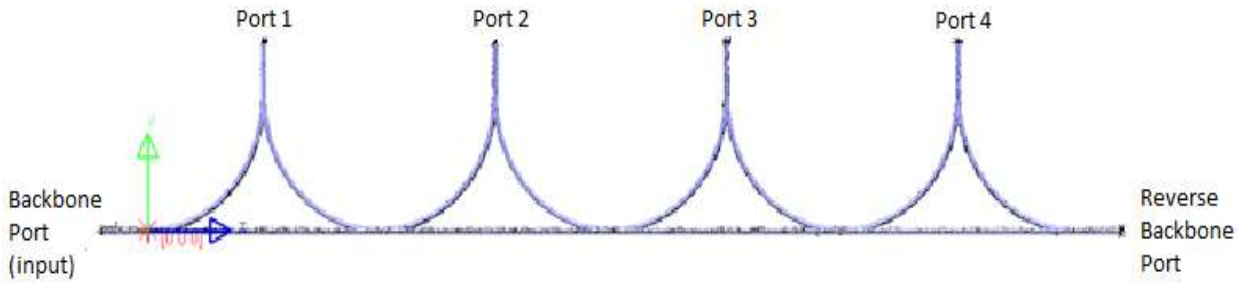

Figure 6-12: The 1x4 coupler model used in the simulation with no reflector at the backbone port.

The results aligned with the theoretical analysis, showing that the output optical power decays exponentially from the first output port. Without a reflector at the end of the

backbone fibre, only 62% of the input optical power reached the output ports, with a significant 38% lost at the end of the backbone optical fibre. Although the simulation aimed for each output port to receive at least 20% of the input power, the actual outputs ranged from 13% to 19%.

6.6.3 1x4 Array Coupler Simulation with a Backbone Reflector

When an optical reflector was connected to the end of the backbone POF, as shown in Figure 6-13, there was a marginal increase in the optical power received at the output ports.

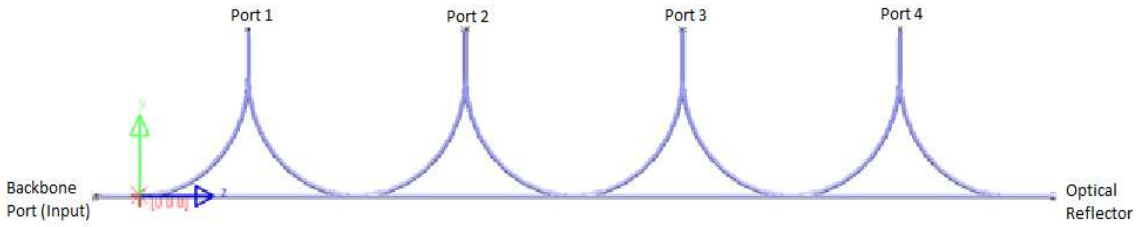

Figure 6-13: The 1x4 coupler model used in the simulation with a reflector at the backbone port.

Port 1 and Port 4 each received approximately 20% of the input optical power, while Port 2 received nearly 17% and Port 3 received about 19%. The coupler improved its coupling efficiency from 62% to 77%. Table 6-6 presents the results, and Figure 6-14 illustrates the received output power.

Table 6-6: 1x4 coupler output optical power

Port No	Output Without Reflector(mW)	Output with reflector (mW)
1	19.45	20.62
2	14.75	16.96
3	14.51	18.71
4	13.29	21.06
Total	62	77.35

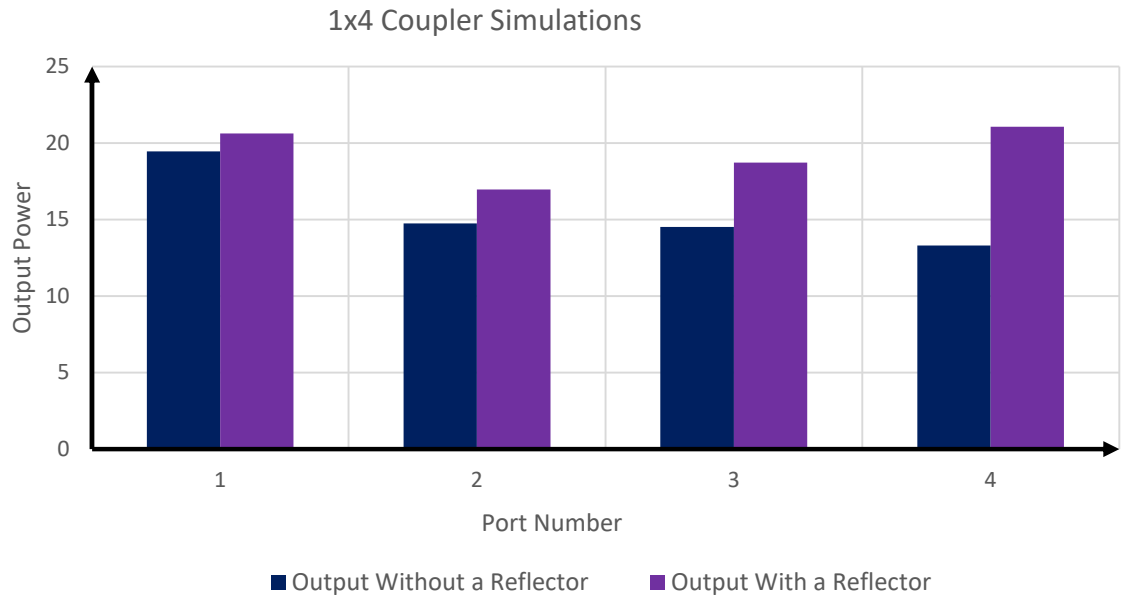

Figure 6-14: Graph showing the 1x4 coupler output optical power.

6.6.4 Optimised 1x4 Array Coupler Using Optimisation Reflectors

As with the 1x2 coupler, the optical power of the 1x4 coupler was optimised by adjusting various factors, including immersion depths, the length of the optimisation reflector, and the addition of a reflector at the end of the backbone POF. This simulation aims to optimise the output optical power received at the output ports and to evaluate the performance characteristics of the optimised 1x4 optical coupler.

The configuration of the optimised 1x4 array coupler is illustrated in Figure 6-15. Initially, the input power was applied to the backbone port, with an optical reflector connected at the end of the backbone POF. The immersion depth and the length of the backbone reflector at each splitting POF influenced the output optical power at each port of the 1x4 array coupler.

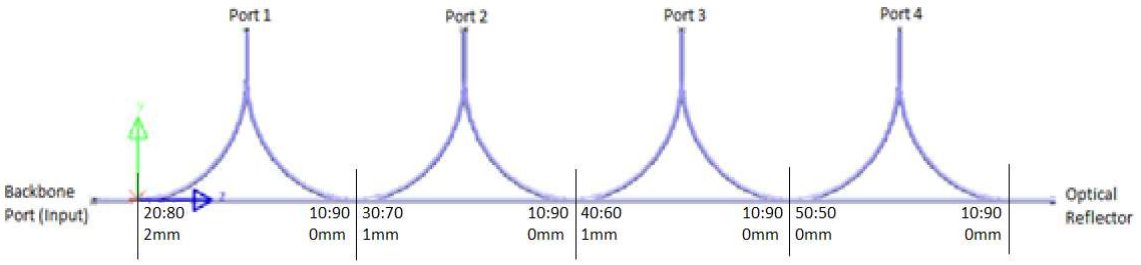

Figure 6-15: The simulated 1x4 array coupler showing the immersion depths and the length of the optimisation reflector at each junction with the backbone POF for optimisation.

Table 6-7 presents the port configuration iterations concerning the splitting ratios and the length of the optimisation reflector. The simulated measurements were used to calculate the coupler's performance parameters, which include excess loss, insertion loss, uniformity, coupler loss, coupling ratio, and coupling efficiency.

Table 6-7: Optimised 1x4 Array Coupler Showing the Immersion Depth and Lengths of the Optimisation Reflectors

Port No:	Immersion Depth	Reflector Length (mm)
1	20:80 / 10:90	2.0 / No Reflector
2	30:70 / 10:90	1.0 / No Reflector
3	40:60 / 10:90	1.0 / No Reflector
4	50:50 / 10:90	No reflector

When the backbone port was used as the input port, the author obtained the graphical output results shown in Figure 6-20. The optimised optical power was 21.5% of the input power at each output port, resulting in a coupling efficiency of 86% and an average coupling (splitting) ratio of 21.5%.

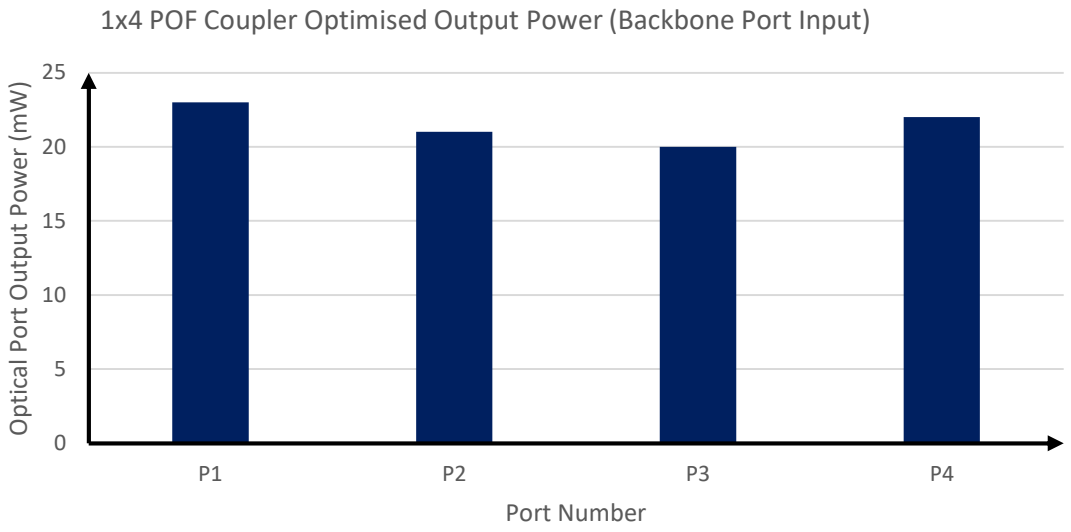

Figure 6-16: Simulated 1x4 coupler optimised port output with the input port at the backbone port.

The coupler achieved an excess loss of 0.66 dB, a coupling loss of 8.54 dB, and a uniformity of 0.03 dB, with an average insertion loss of 6.7 dB. The simulated 1x4 coupler

performed very well as a receiving coupler, meeting the GR-1209 CORE specification. However, performance significantly deteriorated when the coupler was used as a transmitting coupler. This decline in performance was due to the immersion depth and the optimising reflector being incompatible with the requirements for a transmitting coupler.

To address this issue, a different design model was needed to simulate a coupler that met the transmission specifications. Figure 6-21 and Table 6-8 illustrate the model design that fulfils the requirements for using the 1x4 coupler as a transmitting coupler.

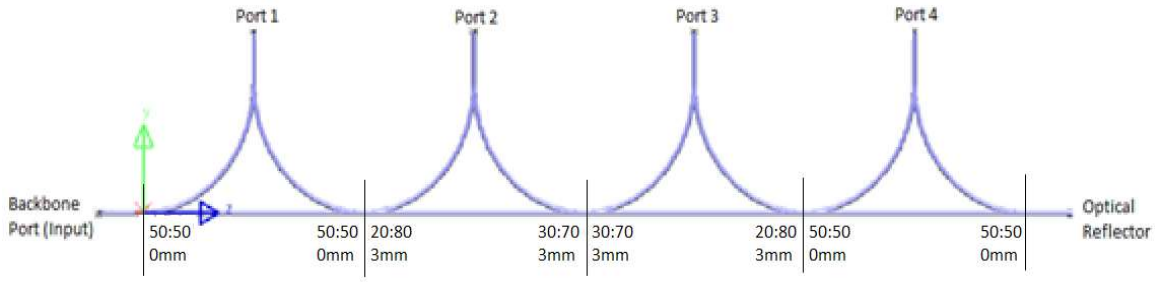

Figure 6-17: The simulated 1x4 array coupler showing the immersion depths and the length of the optimisation reflector at each junction with the backbone POF for optimisation. The simulation uses Ports 1 through 4 as input ports.

Table 6-8: Optimised 1x2 Array Coupler Showing the Immersion Depth and Lengths of the Optimisation Reflectors

Port Input No:	Immersion Depth	Reflector Length (mm)
1	50:50 / 50:50	No reflector
2	20:80 / 30:70	3mm/3mm
3	30:70 / 20:80	3mm/3mm
4	50:50 / 50:50	No reflector

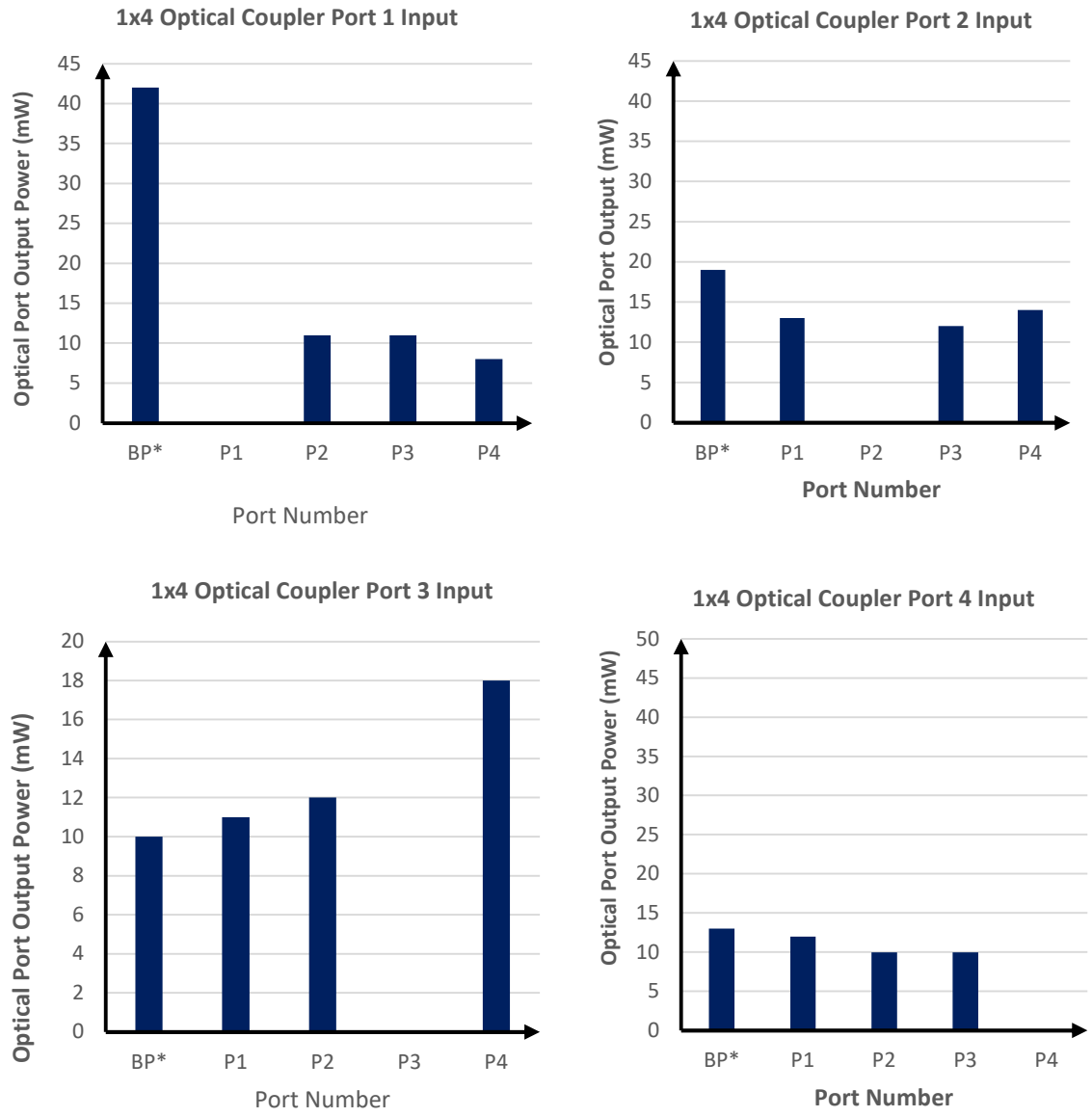

Figure 6-18: The simulated 1x4 array coupler bar graphs show each port's received optical power. The simulation uses ports 1 to 4 as input ports, respectively.

Figure 6-22 displays the graphical output results obtained from the simulation using ports 1 to 4 as input ports. The simulation did not achieve 100% optimisation, indicating that the model designs require further adjustments. Unfortunately, the license for the LightTools optical modelling software expired before the author could make these necessary redesigns to the coupler model.

6.6.5 1x4 Coupler Performance Parameters

The performance parameters of the coupler calculated include excess loss, insertion loss, coupling ratios, coupling efficiency, coupler loss, and uniformity. All these parameters depend on the input port used in the simulation. Sub-sections 6.6.5.1 to 6.6.5.3 present the coupler performance parameters in tabular form, specifically detailing excess loss, coupler loss, uniformity, and coupler efficiency. Table 6-9 provides the values for excess loss, coupler loss, uniformity, and coupler efficiency.

Table 6-9: 1x4 Coupler Performance Parameters: Excess Loss, Coupler Loss, Uniformity and Coupling Efficiency

Input Port	Excess Loss (dB)	Coupler Loss (dB)	Uniformity (dB)	Coupler Efficiency(%)
P_B	0.7	8.5	0.03	86
1	1.4	5.5	0.32	72
2	2.4	3.8	0.09	58
3	2.9	3.0	0.11	51
4	3.5	2.6	0.37	45

The simulation did not achieve 100% optimisation when using ports 1-4 as input ports. All performance parameters varied based on the input ports utilised. The excess loss ranged from 0.7 dB to 3.5 dB, the coupler loss ranged from 2.6 dB to 8.5 dB, and the uniformity ranged from 0.03 dB to 0.37 dB. Additionally, the coupler efficiency varied from 45% to 86%.

6.6.5.1 Insertion Loss

The insertion loss of the 1x4 optical coupler, as shown in Table 6-10, varied depending on the input ports used. The backbone port consistently produced an average insertion loss of approximately 6.5 dB. In contrast, the other input ports exhibited insertion loss values ranging from 3.2 dB to 10 dB.

Table 6-10: 1x4 Coupler Performance Parameter: Insertion Loss

Input Port	Insertion Loss (dB)				
	P_B	P1	P2	P3	P4
P_B	0	6.4	6.8	7.0	6.6
1	3.2	0	6.6	9.6	11.0
2	7.2	8.9	0	9.6	11.0
3	10.0	9.6	9.2	0	7.5
4	8.9	9.2	10.0	10.0	0

6.6.5.2 Splitting (Coupling) Loss

As with other performance parameters, the coupling ratio of the 1x4 optical coupler varied depending on the input ports used. However, the backbone port consistently yielded coupling ratio values averaging around 25%. In contrast, the other input ports yielded coupling ratios ranging from 11.1% to 58.3%.

Table 6-11: 1x4 Coupler Performance Parameter: Splitting (Coupling) loss

Input Port	Splitting (Coupling Ratio) (%)				
	P_B	P1	P2	P3	P4
P_B	0	26.8	24.4	23.3	25.6
1	23.3	0	15.3	15.3	11.1
2	21.8	22.4	0	20.7	24.1
3	20.6	21.6	23.5	0	35.3
4	22.9	26.7	22.2	22.2	0

6.7 Simulation 6: 1x8 Array Coupler Characteristics and Simulations

6.7.1 Background

This simulation aims to investigate and determine the performance characteristics of the 1x8 optical coupler. Following the same procedure as in the earlier simulations of the 1x2 and 1x4 array couplers, the initial simulation was conducted without an optical reflector connected to the backbone fibre output. This simulation was then repeated with an optical reflector attached to the backbone POF output. The optical output measurements for each output were

plotted as bar graphs for graphical comparison. Additionally, a third simulation was conducted to optimise or equalise the optical power received at the output ports. The 1x8 model array coupler used in this simulation is illustrated in Figure 6-15.

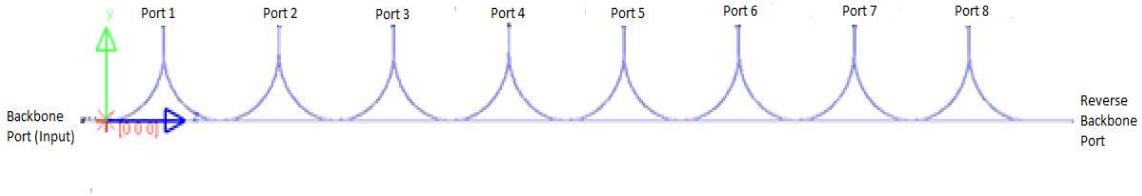

Figure 6-19: The 1x8 coupler model used in the simulation with no reflector at the backbone port.

6.7.2 1x8 Array Coupler Simulation Without a Reflector

The first simulation was conducted with a 1x8 coupler without a reflector attached to the end of the backbone POF. The immersion depth used in this simulation was determined by calculations performed in the theoretical analysis.

The immersion depth used was 10% (10:90), and the results were consistent with the theoretical analysis, which predicts that the output optical power decays exponentially from the first output port. Only 48% of the optical power reached the output ports without a reflector at the end of the backbone fibre. A significant amount (50%) of input optical power got lost at the end of the backbone optical fibre.

The simulation aimed for each output port to receive at least 10% of the input power, but the outputs ranged from 0.76% to 19%.

6.7.3 Simulation with a Reflector

When an optical reflector was attached to the end of the backbone POF, as shown in Figure 6-16, there was a slight increase in the optical power received at the output ports, as illustrated in Table 6-12 and Figure 6-17. The overall efficiency of the coupler increased marginally from 48% to 50%. However, 50% of the input optical power remained within the backbone.

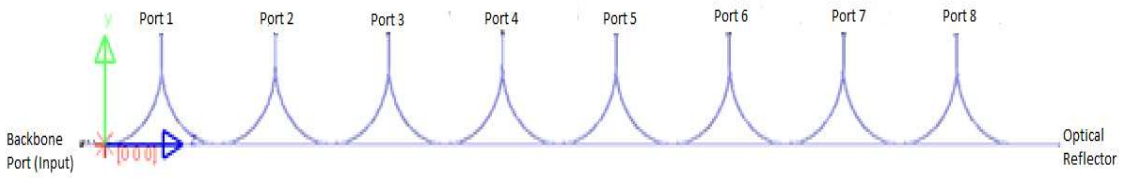

Figure 6-20: The 1x8 coupler model used in the simulation with a reflector at the backbone port.

Table 6-12: 1x8 Coupler Output Optical Power

Port Number	Output without a Reflector (mW)	Output with a Reflector (mW)
1	19.255	19.36
2	11.63	11.71
3	7.27	7.36
4	4.28	4.38
5	2.55	2.7
6	1.5	1.7
7	1.04	1.45
8	0.76	1.48
Total	48.285	50.14

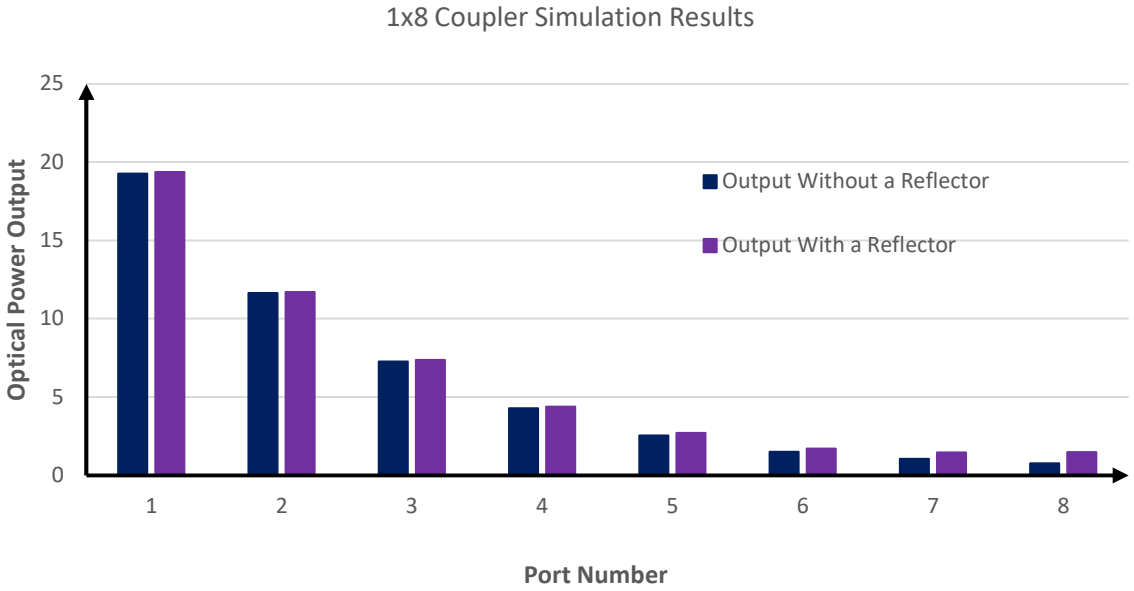

Figure 6-21: Graph showing the 1x8 coupler output optical power.

6.8 Simulation 7: 1x8 Coupler Performance at Different Immersion Depths

To improve the efficiency of the 1x8 array coupler, the simulation explored its performance at various immersion depths. Initially, the simulation was conducted without an optical reflector connected to the output of the backbone fibre. All eight splitting couplers were immersed in the backbone POF at the same depth, and the results were plotted, as shown in Figure 6-18. The simulation was repeated with immersion depths of up to 90% (90:10).

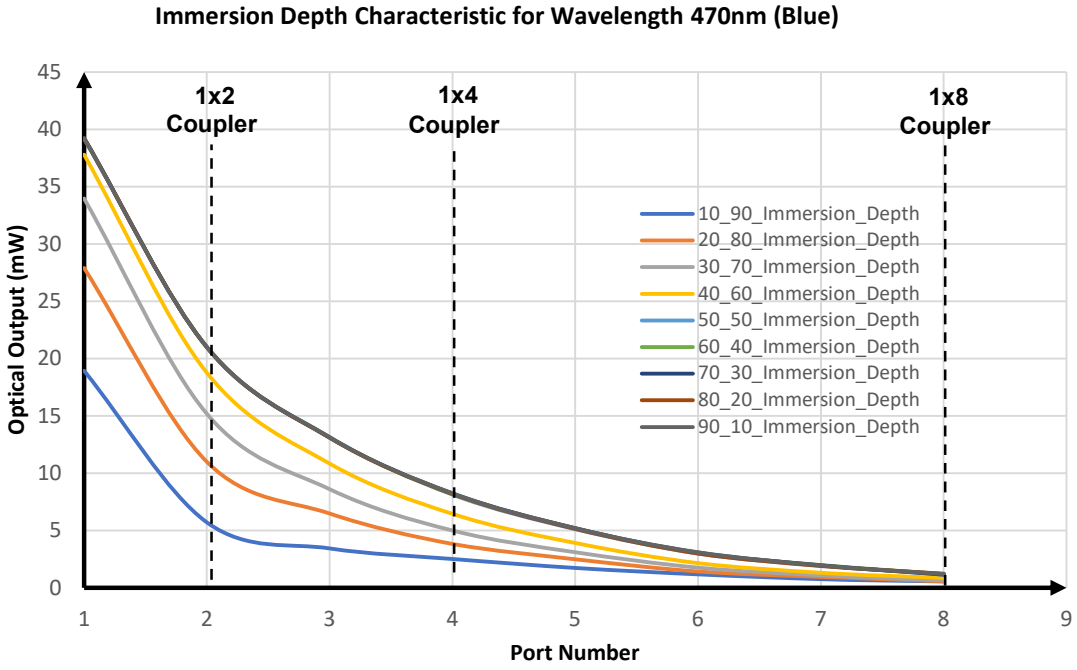

Figure 6-22: Graph showing the coupler performance at different immersion depths.

The graph above shows that each immersion depth has a distinct trendline until it reaches 50% (50:50). Beyond this point, the data indicates that all immersion depths align along the same trendline. This pattern suggests that the immersion-depth characteristics of both the 1x2 and 1x4 couplers can also be inferred from the figure above.

6.8.1 Optimisation of a 1x8 Array Coupler Characteristics and Measurements

The simulation utilised three techniques—immersion depth, optimisation reflector length, and backbone reflector—to enhance the optical power at the output ports. This investigation focuses on the performance characteristics of the optimised 1x8 optical array coupler.

The dimensions of the coupler components were determined from calculations in the theoretical analysis chapter. Initially, input power was applied to the backbone port, which was connected to an optical reflector at its end. The output optical power was then derived from the array of coupler output ports, as illustrated in Figure 6-23 below. The immersion depth and the length of the backbone reflector at each splitting POF determine the output optical power at each output port of the 1x8 array coupler.

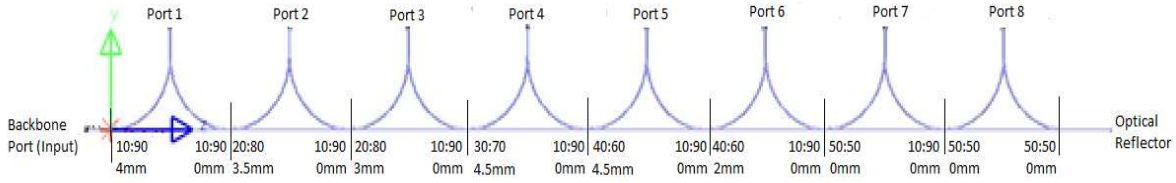

Figure 6-23: The simulated 1x8 array coupler showing the immersion depths and the length of the optimisation reflector at each junction with the backbone POF for optimisation. The simulation uses Ports 1 to 8 as input ports, respectively.

Table 6-13 displays the configuration of the simulated 1x8 array coupler, detailing the splitting ratio and the length of the optimisation reflector at each immersed POF. The splitting ratio of the incident optical power increases progressively from output port 1 to output port 8. Meanwhile, the immersion depth for the reflected optical energy remains consistent at 10:90 across all output ports.

Table 6-13: 1x8 Coupler Immersion Depths at Each Port and the Related Optimisation Reflector Length

Port No:	Immersion Depth	Reflector Length (mm)
1	10:90 / 10:90	4.0 / No Reflector
2	20:80 / 10:90	3.5 / No Reflector
3	20:80 / 10:90	3.0 / No Reflector
4	30:70 / 10:90	4.5 / No Reflector
5	40:60 / 10:90	4.5 / No Reflector
6	40:60 / 10:90	2.0 / No Reflector
7	50:50 / 10:90	No Reflector
8	50:50 / 10:90	No Reflector

When the simulation utilised the backbone port as the input port, the resulting graphical output is displayed in Figure 6-24. This configuration optimised the optical power received at each output port to an average of 8% of the input power, except for port 8, which received 6%. The coupler achieved a coupling efficiency of 64%, resulting in an average coupling (splitting) ratio of 8%.

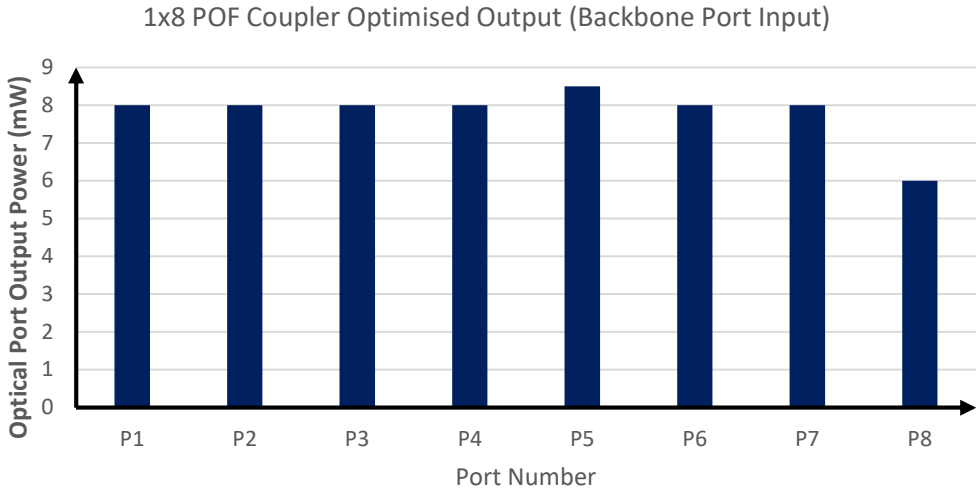

Figure 6-24: Simulated 1x8 coupler optimised port output with the input port at the backbone port.

When the simulation employed the coupler design shown in Figure 6-23 as a transmitting coupler, its performance significantly deteriorated. This decline in performance occurred because the immersion depth and optimisation reflector were not suitable for a transmitting coupler. Figure 6-25 illustrates the model design that satisfies the requirements for using the 1x8 coupler as a transmitting coupler.

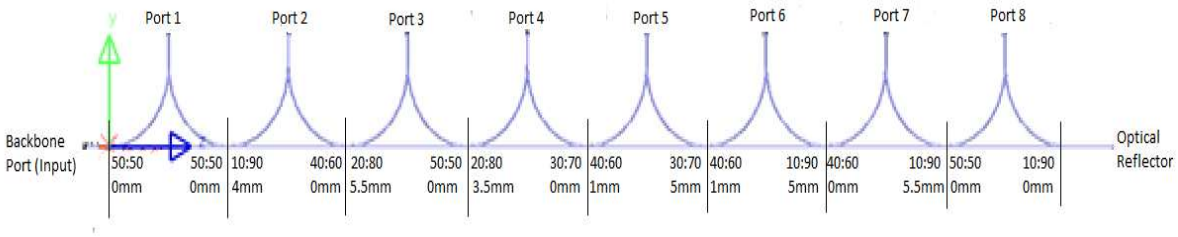

Figure 6-25: The simulated 1x8 array coupler showing the immersion depths at each junction with the backbone POF for optimisation. The simulation uses Ports 1 to 8 as input ports, respectively.

Table 6-14 presents the immersion depths for each output port of the simulated 1x8 optical coupler, along with their corresponding optimisation reflector lengths. The table indicates that various immersion depths and reflector lengths were employed in the simulation to optimise the optical energy received at each output port.

Table 6-14: 1x8 Coupler Immersion Depths and the Related Optimisation Reflector Lengths

Port No:	Immersion Depth	Reflector Length
1	50:50 / 50:50	No Reflector
2	10:90 / 40:60	4 mm / No Reflector
3	20:80 / 50:50	5.5 mm / No Reflector
4	20:80 / 30:70	3.5 mm / No Reflector
5	40:60 / 30:70	1 mm / 5 mm
6	40:60 / 10:90	1 mm / 5 mm
7	40:60 / 10:90	No Reflector / 5.5 mm
8	50:50 / 10:90	No Reflector

Figure 6-26 shows the simulation results when ports 1-8 are used as input ports. Although the simulation produced graphical output similar to the theoretical analysis, it did not achieve 100% optimisation, indicating that further adjustments to the model designs are necessary. Unfortunately, the author was unable to redesign the coupler model due to the expiration of the LightTools optical modelling software license.

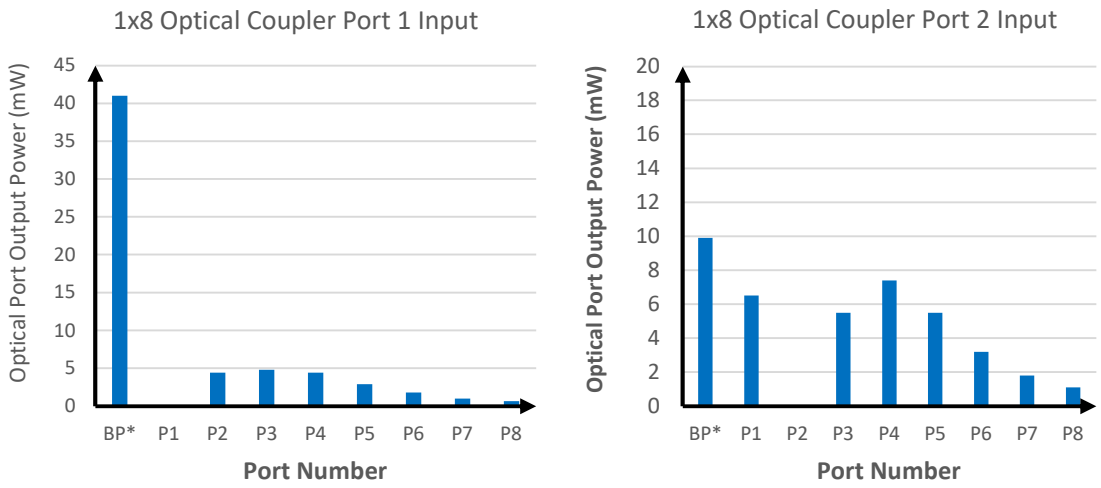

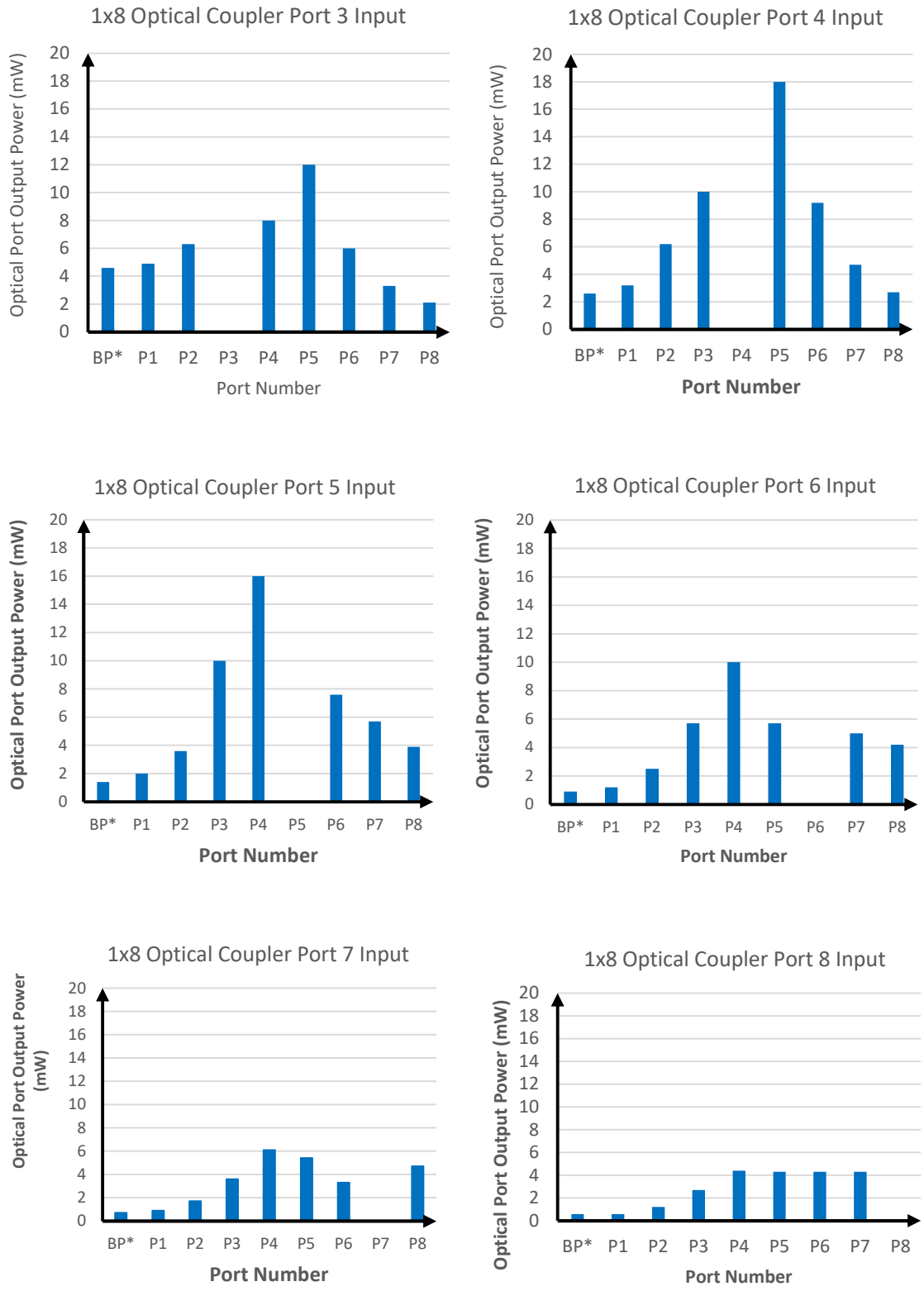

Figure 6-26: The simulated 1x8 array coupler bar graphs show each port's received optical power. The simulation uses Port 1 up to Port 8 as input ports.

6.8.2 1x8 Coupler Performance Parameters

This section presents the performance parameters of the simulated 1x8 POF-based coupler, derived from the simulation results. The calculated parameters include excess loss, insertion loss, coupling ratios, coupling efficiency, coupler loss, and uniformity. All these performance metrics are influenced by the input port used in the simulation. The tables in sub-sections 6.8.3.1 to 6.8.3.3 summarise the coupler performance parameters. However, the measurements obtained using LightTools optical modelling software were not sufficient to assess the directivity and directionality performance parameters.

6.8.2.1 Excess Loss, Coupler Loss, Uniformity and Coupler Efficiency

Table 6-15: 1x8 Coupler Performance Parameters: Excess Loss, Coupler Loss, Uniformity and Coupling Efficiency

Input Port	Excess loss (dB)	Coupler Loss (dB)	Uniformity (dB)	Coupler Efficiency (%)
P_B	2.0	4.3	-0.1	62.5
1	2.2	4.1	-0.3	61.0
2	3.9	2.3	-0.4	41.0
3	3.3	2.8	-0.3	47.2
4	2.5	3.6	-0.4	56.6
5	3.0	3.0	-0.5	50.2
6	4.5	1.1	-0.5	35.2
7	5.8	1.3	-0.4	26.4
8	6.5	1.1	-0.4	22.4

The simulation did not achieve 100% optimisation when using ports 1-8 as input ports. The performance parameters varied based on the input ports utilised. Specifically, the excess loss ranged from 2.0 dB to 6.5 dB, while the coupler loss varied from 1.1 dB to 4.3 dB. The uniformity was measured between -0.01 dB and -0.5 dB. Coupler efficiency ranged from 22.4% to 62.5%, with the backbone and port 1 inputs exceeding 60%. In contrast, ports 7 and 8 exhibited the lowest coupler efficiencies.

6.8.2.2 Insertion Loss

The insertion loss of the 1x8 optical coupler varied based on the input ports used. The backbone port consistently exhibited an average insertion loss of approximately 11 dB per port. In contrast, the other input ports had insertion losses ranging from 3.9 dB to 22.4 dB.

Table 6-16: 1x8 Coupler Performance Parameters: Insertion Loss

Input Port	Insertion Loss (dB)								
	P_B	P1	P2	P3	P4	P5	P6	P7	P8
P_B	0	11.0	11.0	11.0	11.0	11.0	11.0	11.0	12.2
1	3.9	0	13.6	13.2	13.6	15.4	17.4	20.0	21.8
2	10.0	11.9	0	12.6	11.3	12.6	15.0	17.5	19.6
3	13.4	13.1	12.0	0	11.0	9.2	12.2	14.8	16.8
4	15.9	15.0	12.1	10.0	0	7.5	10.4	13.3	15.7
5	18.5	17.0	14.4	10.0	8.0	0	11.2	12.4	14.1
6	20.5	19.2	16.0	12.4	10.0	12.4	0	13.0	13.8
7	21.2	20.5	17.7	14.4	12.2	12.7	14.8	0	13.3
8	22.4	22.3	19.2	15.7	13.6	13.7	13.7	13.7	0

6.8.2.3 Splitting (Coupling) Loss

As with other performance parameters, the coupling ratio of the 1x8 optical coupler varied depending on the input ports used. The backbone port consistently produced an average coupling ratio of approximately 12.8%. In contrast, the other input ports had coupling ratios ranging from 1.1% to 67.3%.

Table 6-17: 1x4 Coupler Performance Parameters: Splitting (Coupling) Loss

Input Port	Coupling Ratio (%)								
	P_B	P1	P2	P3	P4	P5	P6	P7	P8
P_B	0	12.8	12.8	12.8	12.8	13.6	12.8	12.8	9.6
1	8	0	7.2	7.9	7.2	4.8	2.95	1.64	1.1
2	8	15.8	0	13.5	18.1	13.5	7.82	4.40	2.7
3	8	10.4	13.4	0	17.0	25.4	12.71	6.99	4.5
4	8	5.7	11.0	17.7	0	31.8	16.25	8.30	4.8
5	8.5	4.0	7.2	19.9	31.9	0	15.14	11.35	7.8
6	8	3.4	7.1	16.2	28.4	16.2	0	14.20	11.9
7	8	3.4	6.4	13.6	23.1	20.5	12.50	0	17.8
8	6	2.6	5.4	12.1	19.7	19.2	19.23	19.23	0

6.9 Summary

This chapter examined the simulations of plastic optical fibre couplers and analysed the results to provide a comprehensive understanding of the proposed coupler characteristics, performance, and parameters. All simulations were conducted using LightTools, a ray-tracing software that enabled precise modelling and analysis of optical behaviour.

The initial simulations focused on determining the coupling characteristics of a 1×2 optical beam splitter. Following this, the research investigated the characteristics of various POF-based array couplers, including the 1x1, 1x2, 1x4, and 1x8 configurations. The results from these simulations were systematically tabulated and graphically presented to facilitate a more precise comparison of performance metrics.

Three distinct simulations were conducted for each array coupler. The first simulation was performed without an optical reflector at the output of the backbone fibre, providing a baseline measurement of the optical power distribution. The second simulation repeated this setup, but with an optical reflector connected to the backbone POF output. This modification aimed to assess the impact of the reflector on the optical output. For comparative analysis, two sets of optical output measurements from each output were plotted as bar graphs, illustrating the differences in performance between the two scenarios. The third simulation concentrated on optimising the optical power received at the output ports by inserting

optimisation reflectors of appropriate lengths between the polished surfaces of the backbone POF and the immersed POF. This adjustment was essential for enhancing the coupling efficiency.

Another critical factor influencing the optical energy received at the output port was the immersion depth of the splitting POF into the backbone POF. The simulations assessed immersion depths to determine their effects on the coupler's overall performance.

In the simulations of the 1x4 and 1x8 array couplers, it was found that 100% coupler optimisation was achieved when the backbone port served as the input port. In these scenarios, the optical power distribution was maximised, resulting in optimal performance. Although adjustments could be made to the optical energy received at the output ports when using other input ports, complete optimisation could not be achieved. Consequently, the coupler's performance parameters varied significantly across the chosen input ports, highlighting its sensitivity to configuration.

Additionally, the research determined that the same array coupler could not function effectively as both a transmitting and receiving coupler. The design requirements for each function were distinct, necessitating separate designs for the array couplers to serve these two different purposes effectively. This finding underscored the complexity involved in optimising optical couplers for specific applications, emphasising the need for careful design considerations in future implementations.

Chapter 7

Coupler Theoretical and Simulation Analysis Comparison

7.1 Introduction

This chapter examines the similarities and differences between the theoretically designed and simulated array couplers. It begins by analysing the simulated step-index Eska™ CK-40 POF and the feasible bending radii used in the coupler simulations, focusing on how these parameters influence overall performance.

The chapter then evaluates the effect of immersion depth on the output power received at the ports of a splitting coupler. In conjunction with immersion depth, the analysis also investigates the impact of inserting a reflector between the backbone POF and the immersed POF, as well as how varying the reflector lengths affects the results.

Finally, the chapter compares the theoretical and simulated results by plotting them on the same graph, allowing for a detailed comparison of their performance characteristics. The theoretical and simulated performance parameters of the 1x2, 1x4, and 1x8 array couplers are also compared, providing insight into their similarities and differences and overall feasibility.

7.2 Optical Array Couplers Comparison

In this section, the author compared the performance characteristics of the theoretical and simulated optimised 1x2, 1x4, and 1x8 optical array couplers. The comparison focused on key performance metrics, including the optical power received at the output ports, excess loss, insertion loss, coupler loss, splitting (coupling) ratio, and coupling efficiency.

7.2.1 1x2 Array Coupler

The theoretical and simulated received-power values were normalised to facilitate comparison with the port output optical power. The simulated energy values presented in the graphs included both the incident and reflected components of the optical power.

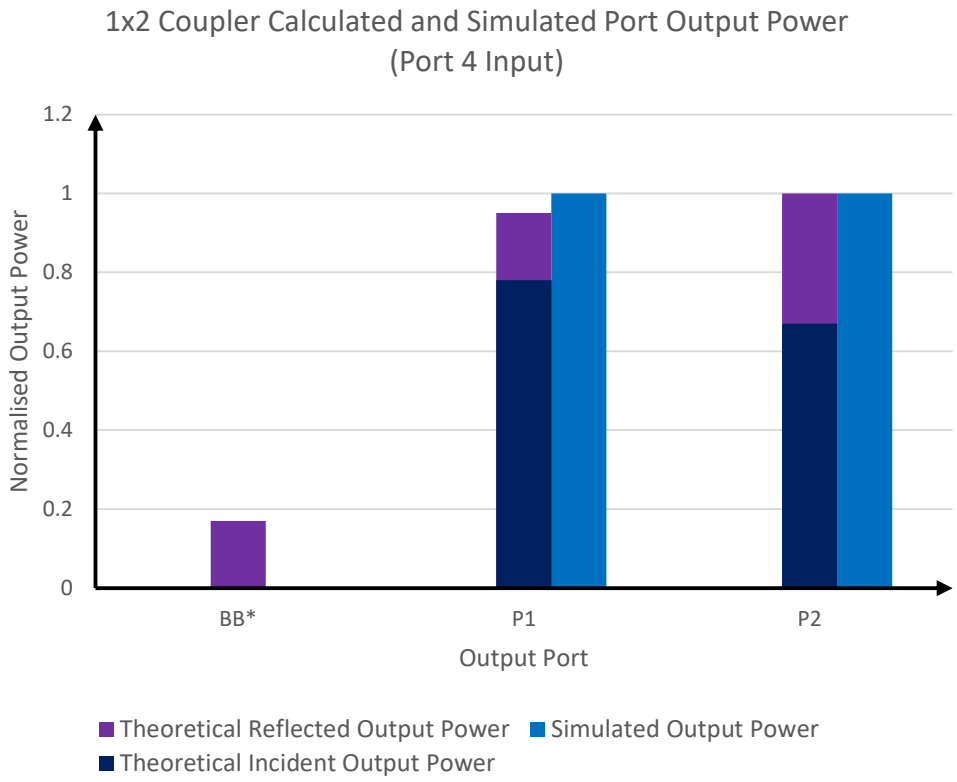

Figure 7-1: 1x2 Optical array coupler: comparison of the received output power with the backbone port used as the input port.

When the backbone port of the coupler was used as the input port, both the theoretical analysis and LightTools simulations achieved 100% optimisation. The graphs showed a similar trend, with ports 1 and 2 receiving equal power. The simulation did not require an optimisation reflector, as the simulated 1x2 coupler was optimised solely by adjusting the immersion depth.

When ports 1 and 2 were used as the input ports, both the theoretical and simulation analyses achieved 100% optimisation. The theoretical analysis relied solely on immersion depth to achieve this optimisation. However, the simulation failed to optimise using only the immersion depth.

In Figures 7-2 and 7-3, the theoretical values were slightly lower than the simulated ones. This discrepancy was expected, as the theoretical analysis did not account for optical optimisation, while the simulations did.

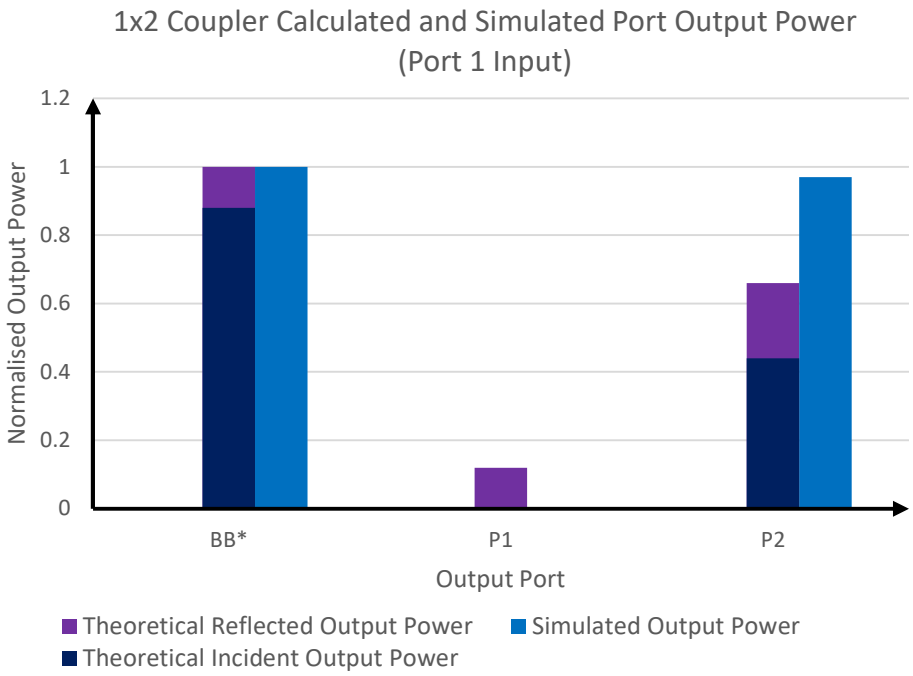

Figure 7-2: 1x2 Optical Array Coupler: Comparison of the received output power with port 1 used as the input port.

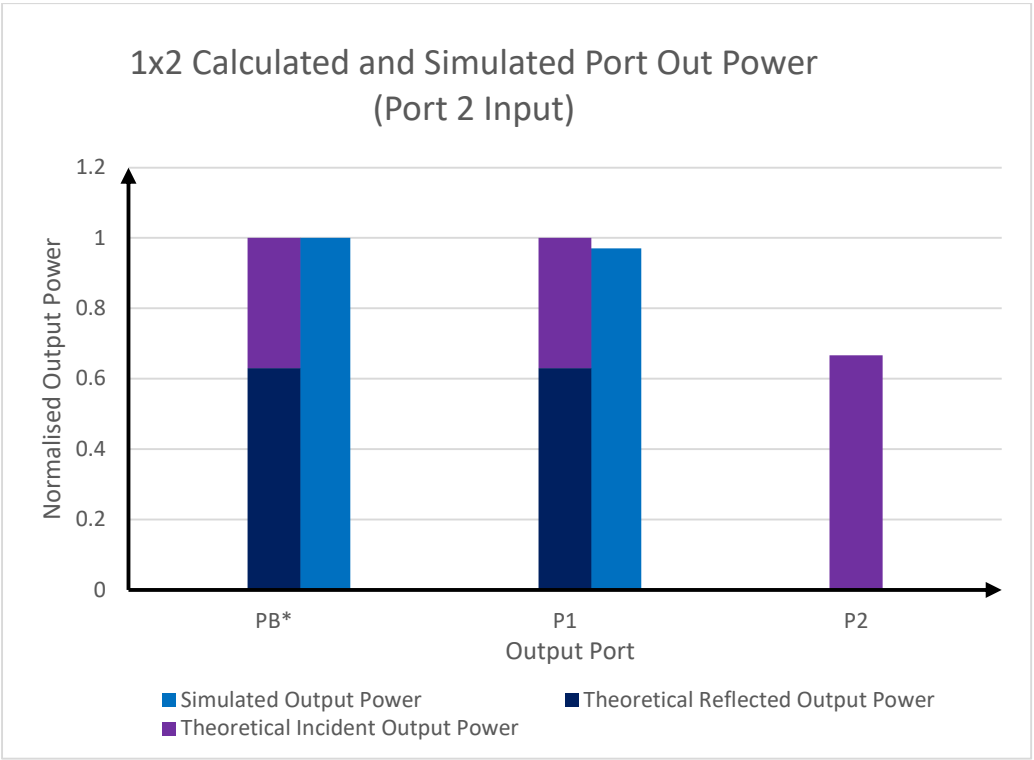

Figure 7-3: 1x2 Optical Array Coupler: Comparison of the received output power with port 2 used as the input port.

7.2.2 1x2 Array Coupler Performance Parameters

This section compares the performance parameters of the theoretical and simulated couplers, focusing on the 1x2, 1x4, and 1x8 optical couplers. The key performance parameters examined in this comparison include excess loss, insertion loss, coupler loss, uniformity, and coupling efficiency. The results for the 1x2 array coupler performance parameters are shown in Table 7-1; the insertion loss in Table 7-2; and the coupling (splitting) ratio in Table 7-3.

Table 7-1: 1x2 Coupler Performance parameters comparison: Excess loss, Coupler Loss, Uniformity and Coupling Efficiency

Input Port	Excess Loss (dB)		Coupler Loss (dB)		Uniformity (dB)		Coupler Efficiency (%)	
	Cal	Sim	Cal	Sim	Cal	Sim	Cal	Sim
P_B	0.8	0.8	7.5	8.0	0.0	0.00	82.4	84
1	0.4	1.2	10.8	6.2	-0.2	-0.07	91.6	76
2	1.0	2.4	7.0	3.3	-0.2	-0.01	80.0	57

Table 7-2: 1x2 Coupler Performance parameters comparison: Insertion Loss

Input Port	Insertion Loss (dB)					
	P_B		P1		P2	
	Cal	Sim	Cal	Sim	Cal	Sim
P_B	0	0	2.0	3.8	3.2	3.8
1	3.0	3.4	0	0	5.0	5.1
2	3.0	3.3	5.4	5.5	0	0

Table 7-3: 1x2 Coupler Performance parameters comparison: Insertion Loss

Input Port	Coupling Ratio (%)					
	P_B		P1		P2	
	Cal	Sim	Cal	Sim	Cal	Sim
P_B	0	0	68.3	50.0	40	50.0
1	50.7	59.2	0.0	0	60	40.8
2	49.3	5.4	31.7	5.5	0	0

7.3 1x4 Array Coupler

As with the 1x2 coupler, the author normalised the theoretical and simulated received power values to compare the port output optical power. A comparison bar graph was then plotted, with the simulated energy bars accounting for both the incident and reflected components.

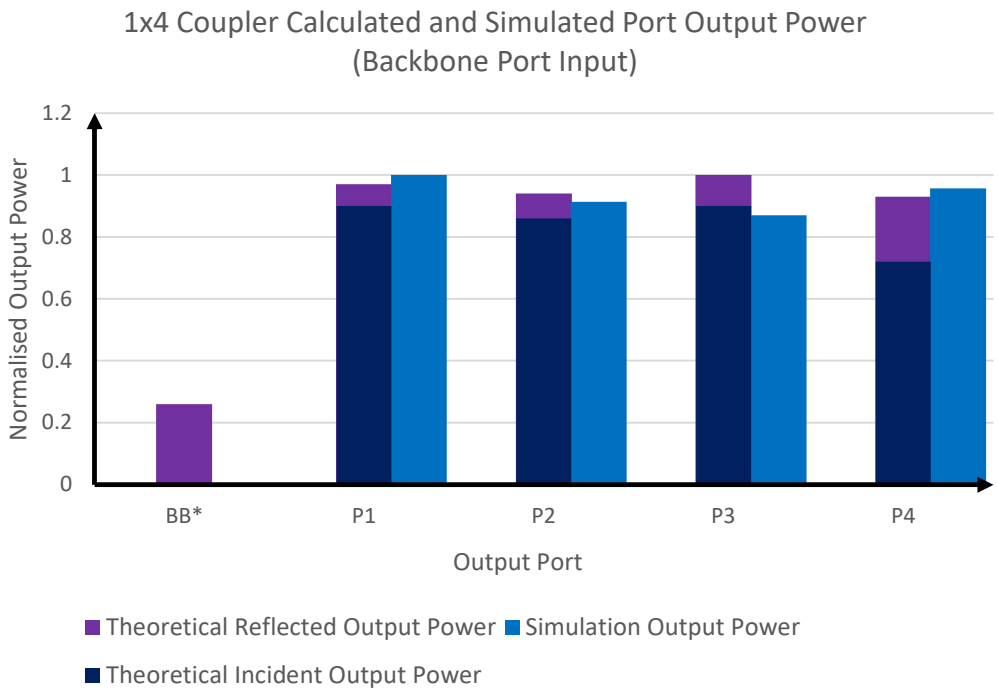

Figure 7-4: 1x4 Optical Array Coupler: Comparison of the received output power with the backbone port used as the input port.

When the backbone port of the coupler was used as the input port, both the theoretical analysis and the LightTools simulation achieved optimisation. The graphs show that ports 1 to 4 received nearly equal amounts of optical power.

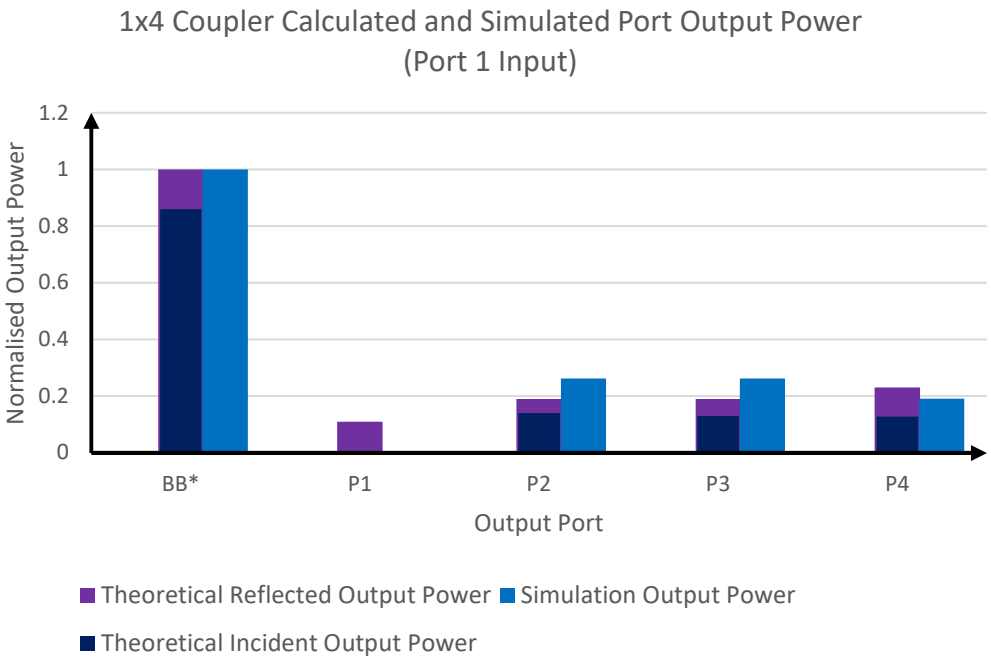

Figure 7-5: 1x4 Optical Array Coupler: Comparison of the received output power with port 1 used as the input port.

When port 1 was used as the input port, both the theoretical and simulated couplers exhibited similar performance characteristics. As expected, the backbone port received more than half of the total optical power because port 1 split the input power equally between the backbone port and the other output ports. In other words, the backbone port received half of the optical power, while the remaining output ports shared the other half. In Figure 7-5, the thesis optimised ports 2, 3, and 4 using both theoretical and simulated values.

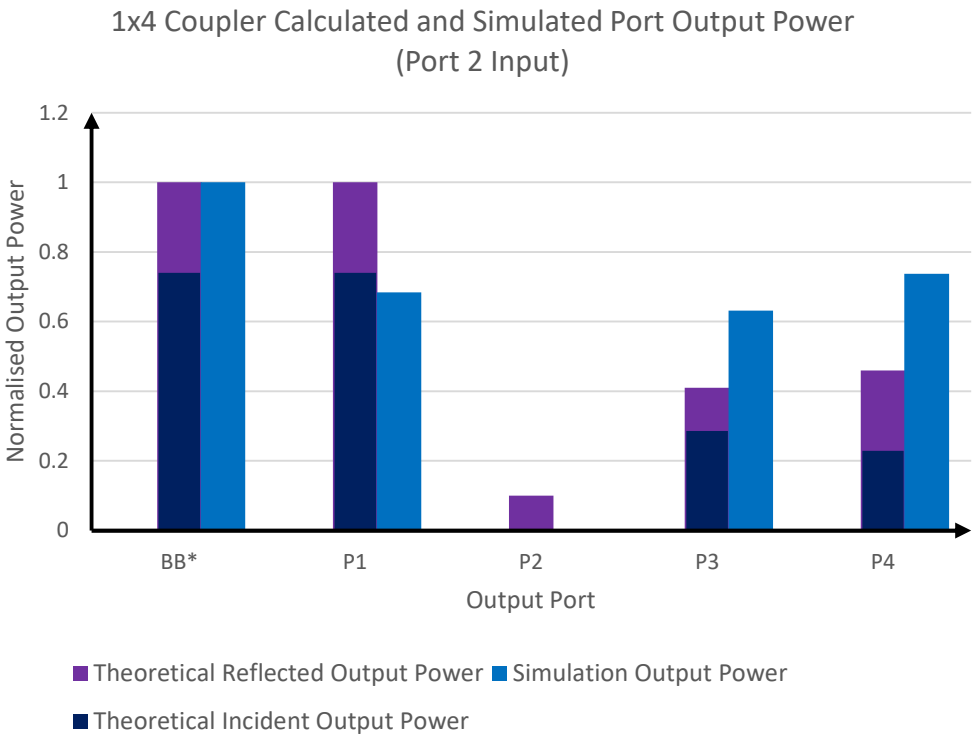

Figure 7-6: 1x4 Optical Array Coupler: Comparison of the received output power with port 2 used as the input port.

When port 2 was used as the input port, the theoretical and simulated couplers exhibited similar performance. As expected, the backbone port received more optical power than the other ports. However, the remaining ports nearly achieved optimisation. In Figure 7-6, the thesis demonstrates the optimisation of ports 2, 3, and 4 using both theoretical and simulated values.

When port 3 was used as the input port, the theoretical and simulated couplers exhibited different performance characteristics. The theoretical coupler could not achieve optimisation, resulting in its backbone port receiving more power than the other ports. In contrast, the simulated coupler optimised ports 1 and 2 and the backbone port. Figure 7-7 illustrates that the simulated coupler performed better than the theoretical coupler in achieving optimisation.

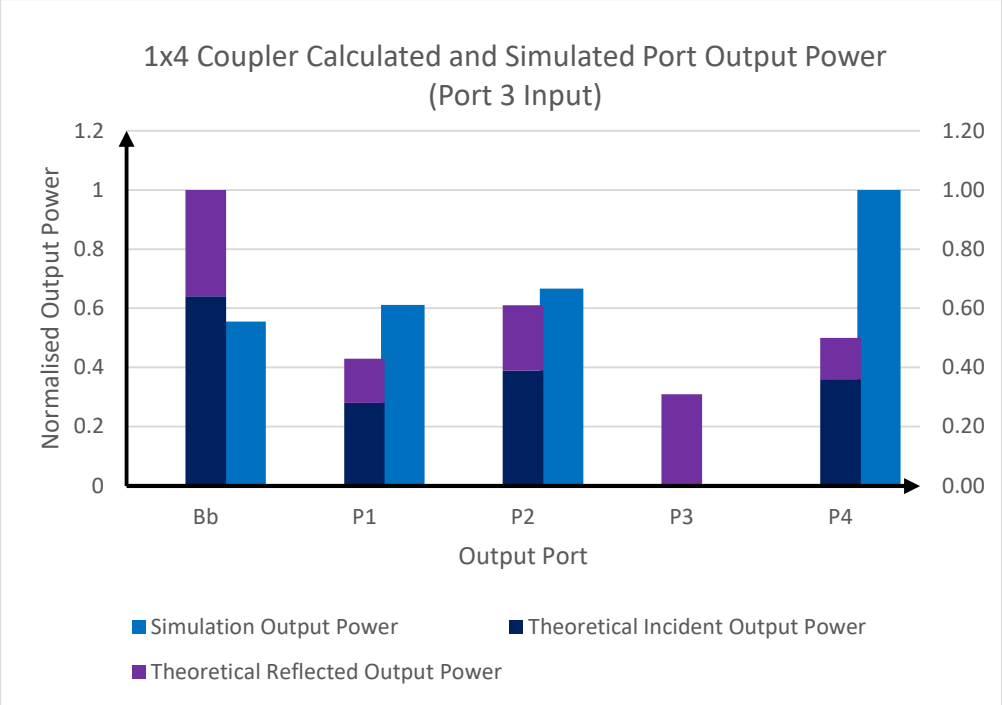

Figure 7-7: 1x4 Optical Array Coupler: Comparison of the received output power with port 3 used as the input port.

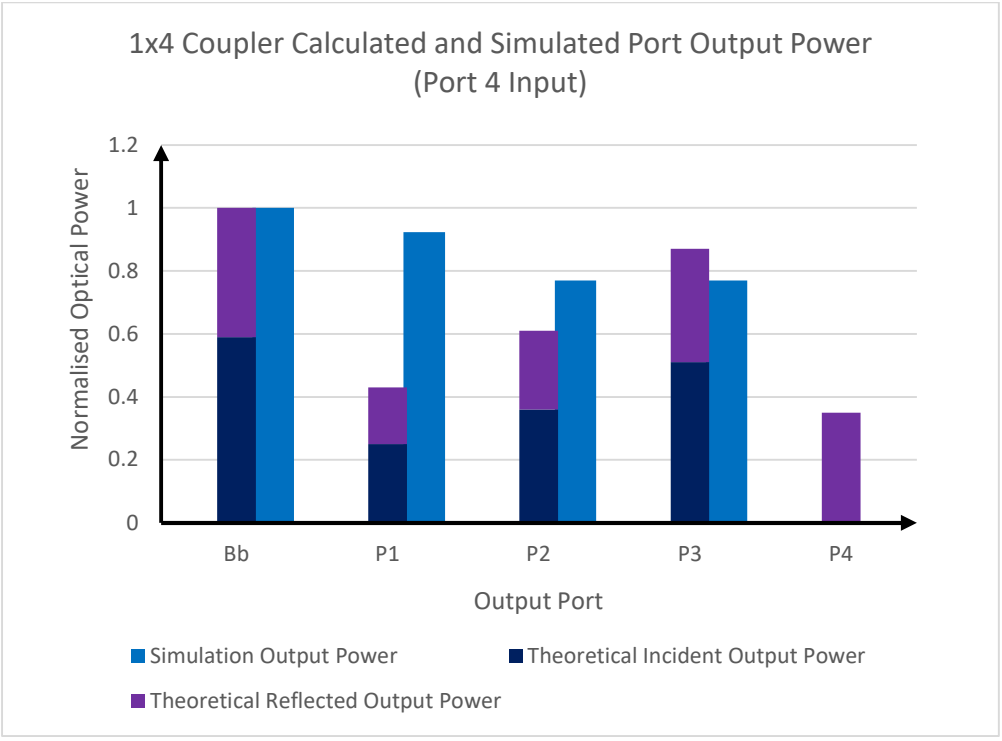

Figure 7-8: 1x4 Optical Array Coupler: Comparison of the received output power with port 4 used as the input port.

Port 4 exhibits performance characteristics similar to those of Port 3. When port 4 serves as the input port, the theoretical and simulated couplers show different

performance characteristics. The theoretical coupler failed to optimise, resulting in its backbone port receiving more power than the other ports. In contrast, the simulated coupler demonstrated some level of optimisation for ports 1, 2, 3, and the backbone port. Figure 7-8 illustrates that the simulated coupler outperforms the theoretical coupler in achieving optimisation.

7.3.1 1x4 Array Coupler Performance Parameters

This section compares the performance parameters of the theoretical and simulated 1x4 coupler. The key performance parameters analysed include excess loss, insertion loss, coupler loss, uniformity, and coupling efficiency. The 1x4 Array Coupler Performance Parameters are shown in Table 7-4, the insertion loss in Table 7-5, and the coupling ratio in Table 7-6.

Table 7-4: 1x4 Coupler Performance Parameters Comparison: Excess Loss, Coupler Loss, Uniformity and Coupling Efficiency

Input Port	Excess Loss			Coupler Loss			Uniformity			Coupler Efficiency(%)		
	Cal	Sim	Diff	Cal	Sim	Diff	Cal	Sim	Diff	Cal	Sim	Diff
Bb	0.5	0.7	0.2	10.1	8.5	1.6	-0.02	-0.03	0.01	90	86	-4
1	0.1	1.4	1.3	15.8	5.5	10.3	-0.28	-0.32	0.04	97	72	-25
2	0.2	2.4	2.2	13.3	3.8	9.5	-0.18	-0.09	0.09	95	58	-37
3	0.4	2.9	2.5	10.8	3.0	7.8	-0.11	-0.11	0	92	51	-41
4	0.7	3.5	2.8	8.2	2.6	6.4	-0.16	0.37	0.21	85	45	-40

*Table 7-5: 1x2 Coupler Performance Parameters Comparison: I*nsertion *Loss*

Input Port	Insertion Loss(dB)									
	P_B		P1		P2		P3		P4	
	Cal	Sim	Cal	Sim	Cal	Sim	Cal	Sim	Cal	Sim
P_B	0	0	2.51	6.38	3.70	6.78	4.67	6.99	5.35	6.58
1	6.2	3.2	0	0	3.38	6.59	8.35	9.59	9.03	10.97
2	6.6	7.2	8.61	8.86	0	0	6.80	9.59	7.48	10.97
3	6.7	10.0	8.74	9.59	7.77	9.21	0	0	5.93	7.45
4	6.5	8.9	8.51	9.21	7.54	10.00	6.58	10.00	0	0

Table 7-6: 1x2 Coupler Performance Parameters Comparison: Coupling Ratio

Input Port	Coupling Ratio (%)									
	P_B		P1		P2		P3		P4	
	Cal	Sim	Cal	Sim	Cal	Sim	Cal	Sim	Cal	Sim
P_B	0	0	57.67	26.74	44.79	24.42	37.23	23.26	34.30	25.58
1	26.90	58.33	0	0	19.20	15.28	15.96	15.28	14.70	11.11
2	24.40	32.76	14.14	22.41	0	0	22.79	20.69	21.00	24.14
3	23.80	2.38	13.74	26.19	17.55	28.57	0	0	30.00	42.86
4	25.00	28.89	14.46	26.67	18.47	22.22	24.02	22.22	0	0

7.4 1x8 Array Coupler

As in the previous couplers, this chapter normalised the theoretical and simulated received power values to facilitate comparison of the port output optical power. The results were presented in a bar graph, with the simulated energy bars combining the incident and reflected components.

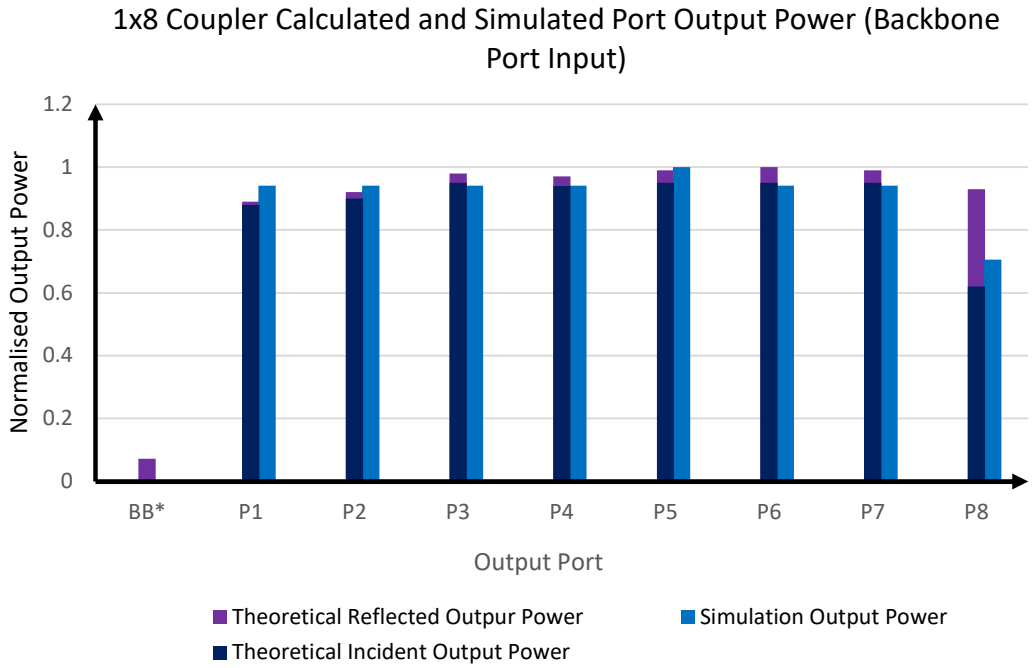

Figure 7-9: 1x8 Optical array coupler: comparison of the received output power with the backbone port used as the input port.

When the backbone port of the coupler serves as the input port, the author achieves optimisation in both the theoretical and simulated measurements. The graphs illustrate that ports 1 to 8 received nearly equal power. In Figure 7-9, the theoretical values are slightly higher than the simulated values, as anticipated, because the theoretical measurements do not account for losses associated with the plastic optical fibre (POF).

In the 1x8 array coupler, the performance characteristics of both the theoretical and simulated couplers depend on the input port used. In each case, the performance characteristics differ considerably, as shown in Figures 7-10 to 7-17.

In the theoretical coupler, the backbone port receives most of the optical power. Apart from the backbone port, the coupler optimises when ports 1, 2 and 3 are the input ports. Besides that, the simulated coupler never optimised the optical energy at the output port for any other input port. Ports 4 and 5 received most of the available optical power. The author believes the reason for non-optimisation is that the thesis used the wrong length of optimisation reflector in the coupler. More work still needs to be done to optimise all output ports of the 1x8 coupler. Unfortunately, the LightTools optical modelling software licence expired before the author could do more modelling iterations.

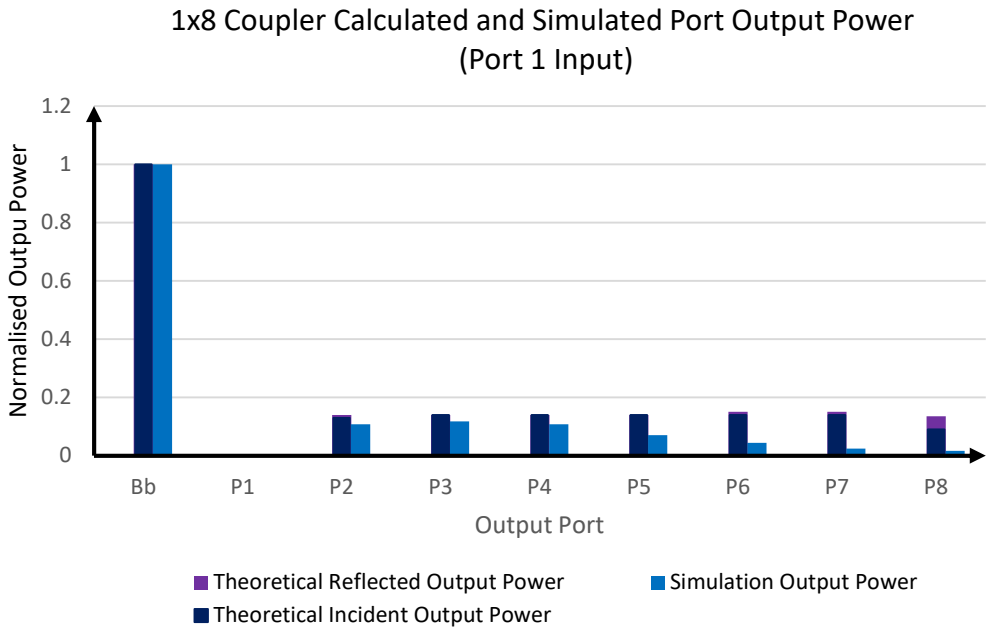

Figure 7-10: 1x8 Optical Array Coupler: Comparison of the received output power with port 1 used as the input port.

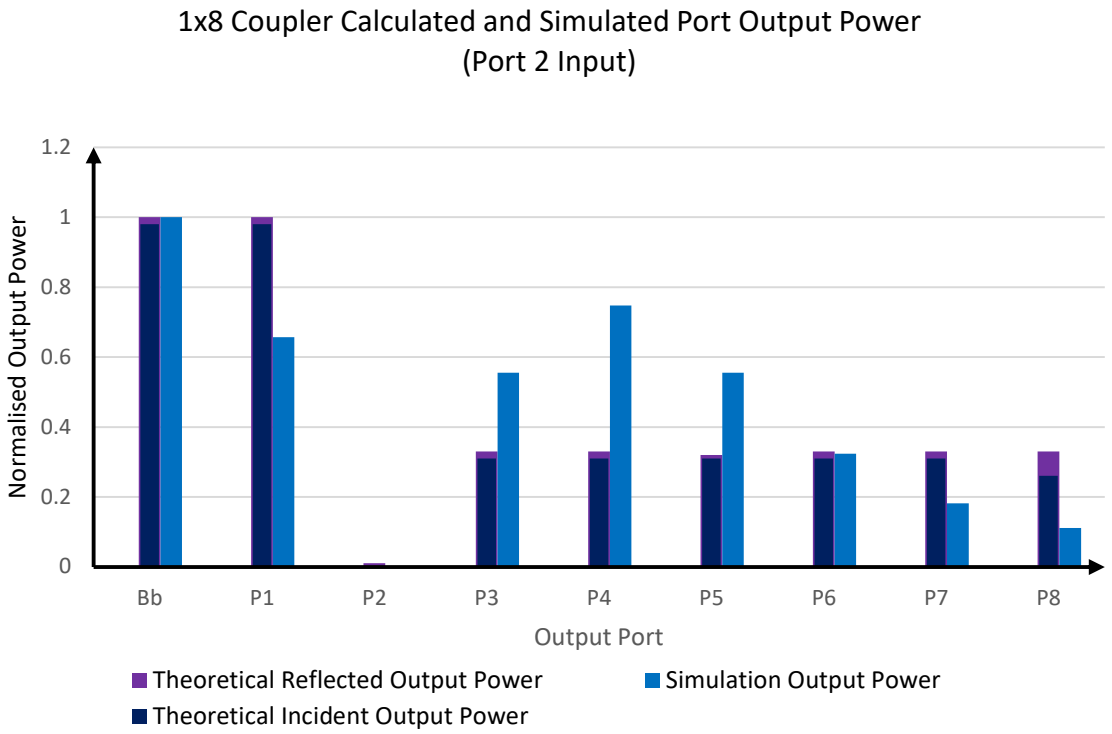

Figure 7-11: 1x8 Optical array coupler: comparison of the received output power with port 2 used as the input port.

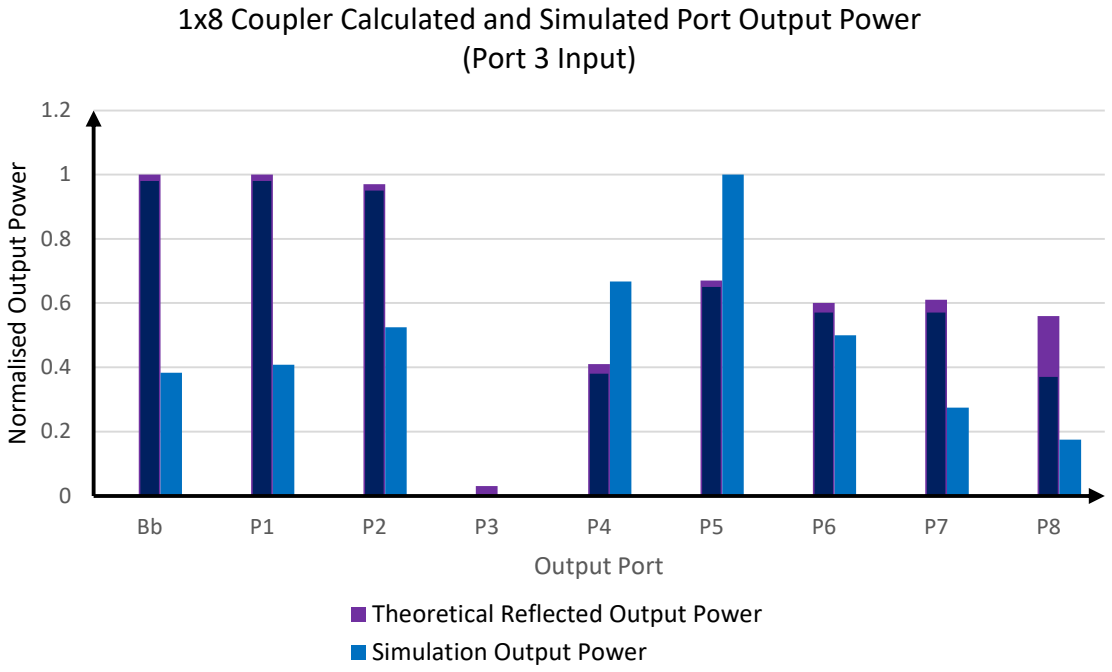

Figure 7-12: 1x8 Optical array coupler: comparison of the received output power with port 3 used as the input port.

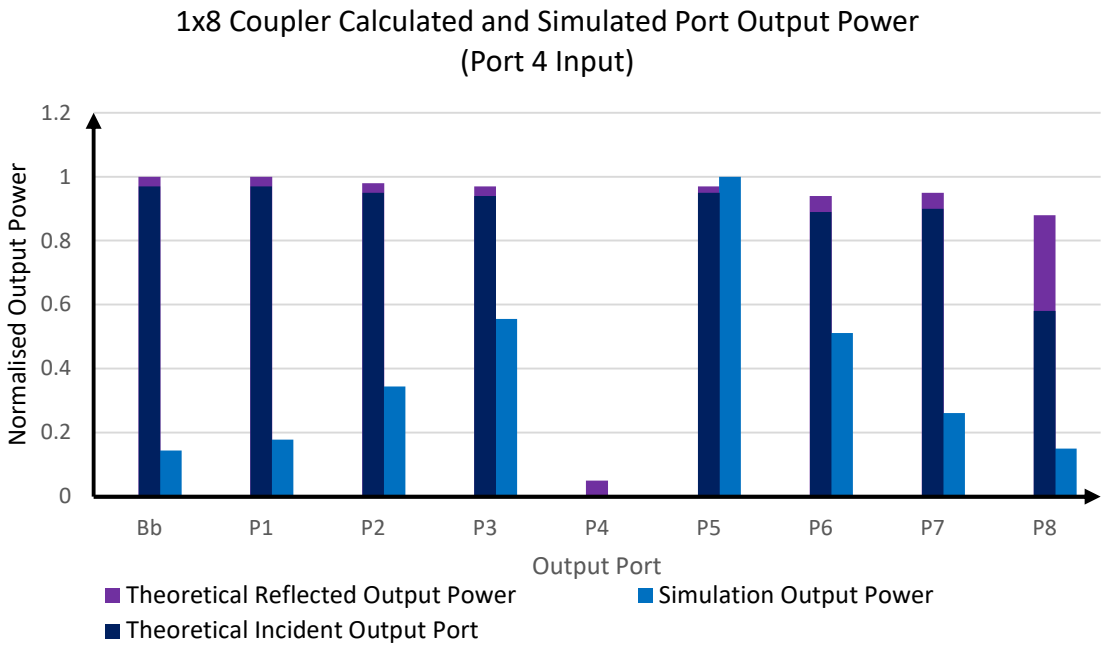

Figure 7-13: 1x8 Optical array coupler: comparison of the received output power with port 4 used as the input port.

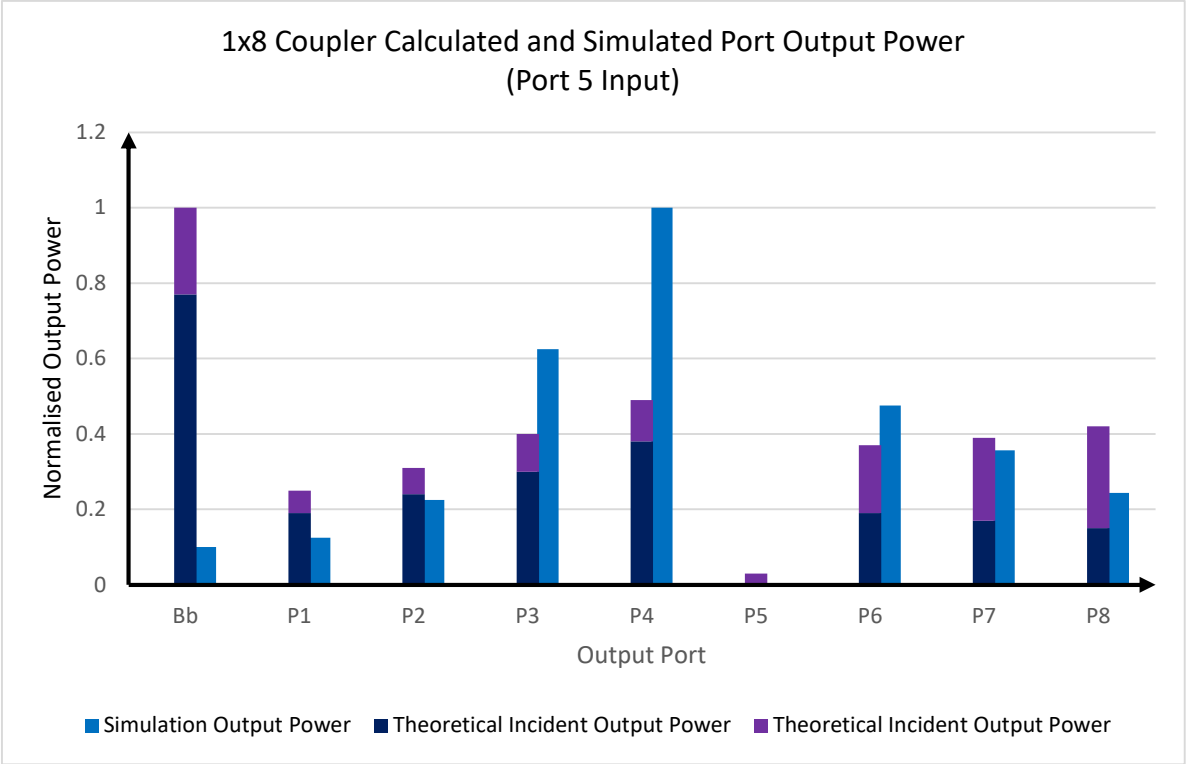

Figure 7-14: 1x8 Optical array coupler: comparison of the received output power with port 5 used as the input port.

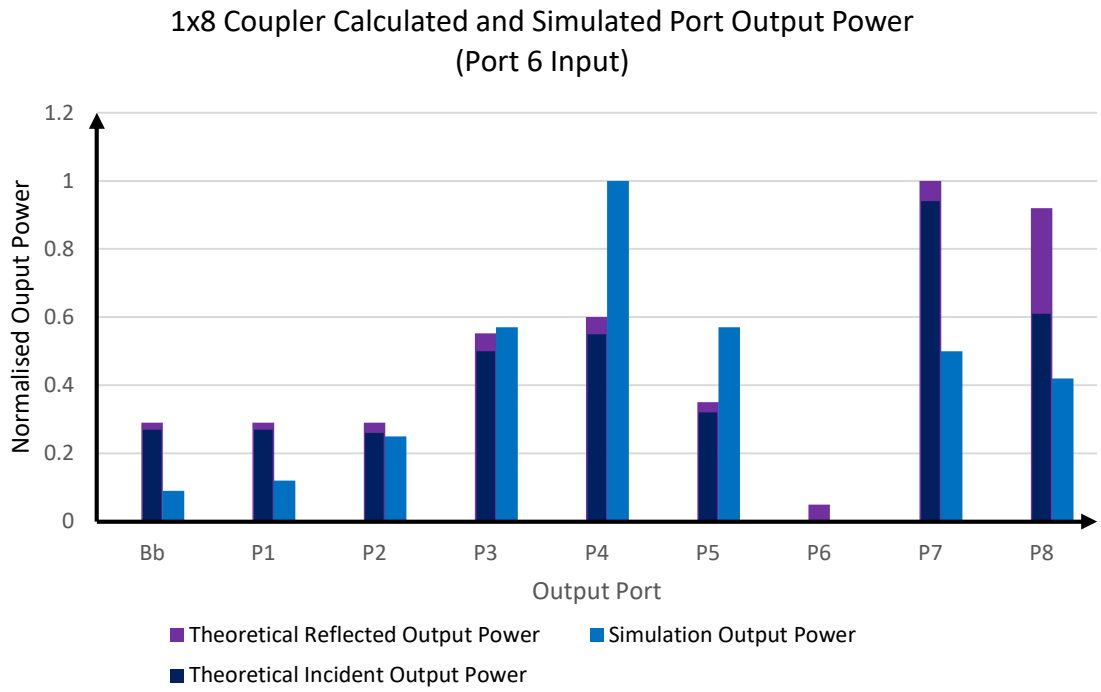

Figure 7-15: 1x8 Optical array coupler: comparison of the received output power with port 6 used as the input port.

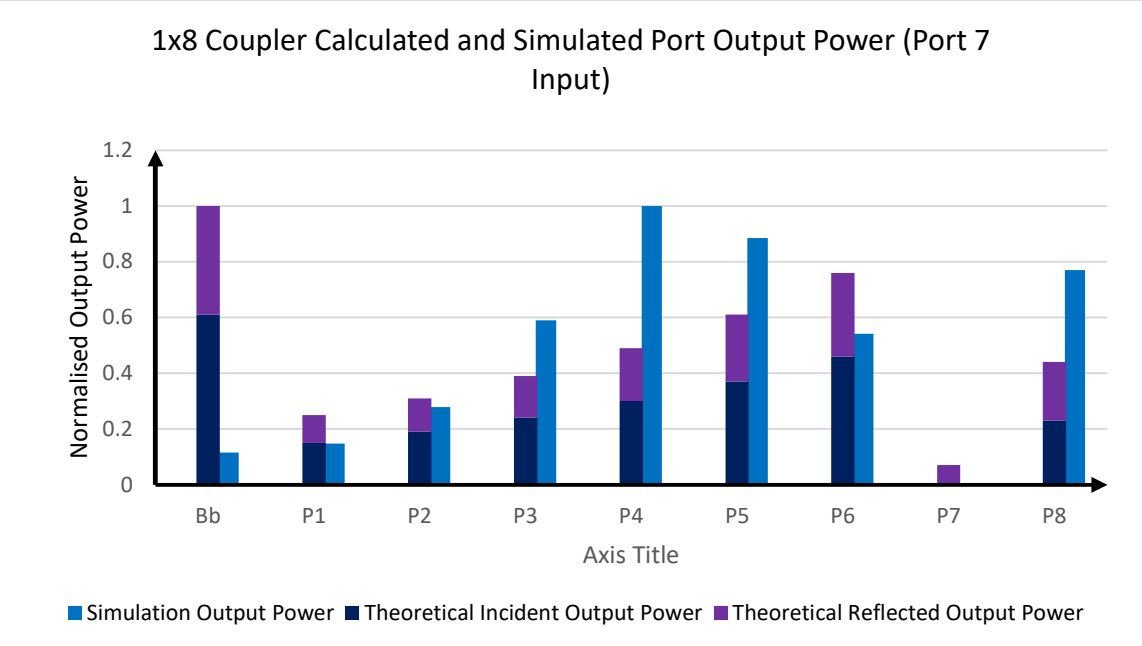

Figure 7-16: 1x8 Optical array coupler: comparison of the received output power with port 7 used as the input port.

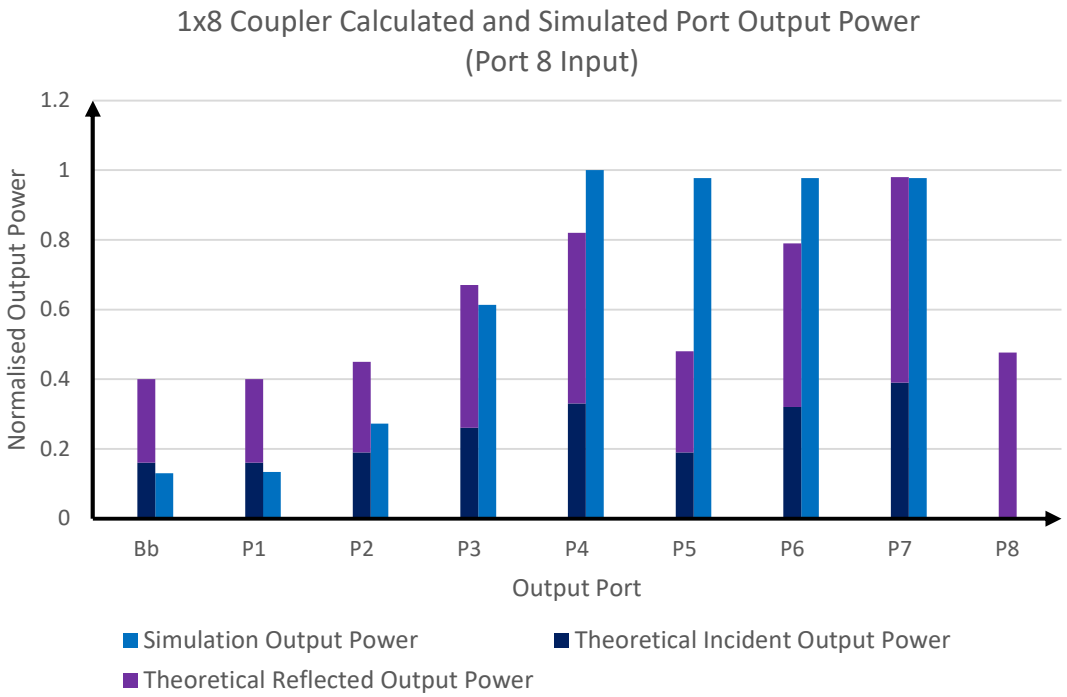

Figure 7-17: 1x8 Optical array coupler: comparison of the received output power with port 3 used as the input port.

7.5 Comparison of 1x8 Array Coupler Performance Parameters

This section compares the performance parameters of the theoretical and simulated 1x4 coupler. The performance parameters of interest are excess loss, insertion loss, coupler loss, uniformity and coupling efficiency. Table 7-7 shows the 1x8 array coupler performance parameters.

Table 7-7: 1x8 Coupler Performance parameters comparison: Excess loss, Coupler Loss, Uniformity and Coupling Efficiency

Input Port	Excess Loss		Coupler Loss		Uniformity		Coupler Efficiency (%)	
	Cal	Sim	Cal	Sim	Cal	Sim	Cal	Sim
Bb	0.37	2.04	10.86	4.26	-0.04	-0.07	91.8	62.5
1	0.04	2.15	19.00	4.08	-0.44	-0.29	99.0	61.0
2	0.06	3.88	18.54	2.28	-0.37	-0.44	98.6	41.0
3	0.08	3.26	17.13	2.77	-0.31	-0.34	98.1	47.2
4	0.12	2.47	15.71	3.63	-0.23	-0.38	97.3	56.6

5	0.17	2.99	14.28	3.03	-0.27	-0.49	96.3	50.2
6	0.23	4.53	12.85	1.88	-0.27	-0.48	94.8	35.2
7	0.37	5.78	10.92	1.33	-0.27	-0.43	92.0	26.4
8	0.22	6.51	13.01	1.10	-0.27	-0.40	95.0	22.4

Note: Appendix 1 shows the comprehensive comparison tables of insertion losses and coupling ratios for the 1x8 coupler.

7.6 The GR1209 CORE Specifications

Measuring insertion loss is essential for verifying that the manufactured splitter meets the GR-1209-CORE optical performance requirements (Teleweaver, 2025). Insertion loss—expressed in decibels (dB)—quantifies signal power attenuation. Table 7-8 lists the typical insertion-loss limits specified by GR-1209-CORE and compares them with this work's theoretical predictions and simulation results. As shown, the designed and simulated coupler complies with the GR-1209-CORE specification.

Table 7-8: The table showing the typical coupler insertion losses under the typical GR1209 CORE specification

Coupler Splitting Ratio	Ideal Insertion Loss per port (dB)	Maximum Excess Loss (dB)	Typical Insertion Loss (dB)	Insertion Loss of the Designed Couplers (dB)
1 x 2	3	1	4	3.3
1 x 4	6	1	7	6.7
1 x 8	9	2	11	11

According to the GR1209 Specification**,** the maximum allowable insertion loss is given by the formula (Teleweaver, 2025):

$$L_{insertion} = 0.8 + 3.4\text{Log}_2 N \qquad 7.1$$

Where: $L_{insertion}$ is the coupler insertion loss per port

N is the number of ports

From Equation 7.1, the maximum allowable insertion loss per port is 4.2 dB (1×2), 7.6 dB (1×4), and 11 dB (1×8). Assuming ideal losses of 3, 6, and 9 dB for 1×2, 1×4, and 1×8

couplers, the corresponding practical targets with tolerance are approximately 3.6 ± 0.6 dB (~16%), 6.8 ± 0.8 dB (~12%), and 10 ± 1 dB (~10%). The couplers designed in this work achieved average insertion losses of 3.3 dB (1×2), 6.7 dB (1×4), and 11 dB (1×8)—all within the GR-1209-CORE limits.

A key advantage of the proposed design is that port power can be symmetrised at the design stage, unlike other multi-port couplers—e.g., fused biconical taper (FBT) couplers (Bazakutsa et al.) and mixing-rod couplers (J. M. Senior, 2009)—which typically exhibit uneven per-port insertion loss, even though their absolute loss levels are of a similar order.

7.7 Summary

The first part of this chapter examines the characteristics of plastic optical fibre (POF) and analyses how immersion depth affects the received optical energy output. Additionally, the chapter compares the performance parameters of both theoretical and simulated array couplers.

The performance parameters of the 1x2, 1x4, and 1x8 array couplers were evaluated, focusing on key metrics such as excess loss, insertion loss, coupling (splitting) ratio, coupling loss, uniformity, and coupler efficiency.

In the case of the 1x2 array coupler, optimisation of received power was achievable across all input ports. For the 1x4 and 1x8 array couplers, the theoretical and simulated performance parameter values were consistent when the backbone port served as the input port. However, when ports other than the backbone were used as input ports, the analysis showed that performance parameters varied significantly depending on the selected input port. This variability indicated that the couplers' performance characteristics would differ considerably depending on the chosen input configuration.

7.8 References

Teleweaver. (2025, October 23). Fiber Optic Splitter Insertion Loss Table Reference for FBT and PLC types. Retrieved from https://fibrefibre.com/: https://fibrefibre.com/tutorial/fiber-optic-splitter-insertion-loss-reference/

Chapter 8

Practical Manufacturing Considerations for Plastic Optical Fibre-based Backbone Array Couplers

8.1 Introduction

Plastic-optical-fibre (POF) backbone array couplers offer a promising solution for short-reach, high-reliability networks in automotive, industrial, and in-home applications. Turning this concept into a manufacturable product, however, demands careful attention to material selection, fabrication processes, mechanical tolerances, and scalability for volume production. This chapter presents the key manufacturing considerations required to transition the proposed coupler from prototype to production.

8.2 Material Selection

Materials selection is pivotal to both performance and manufacturability. For POF-based couplers, fibres with low attenuation and tight mode-field (core) tolerances are preferred to maximise coupling efficiency and repeatability. In this design, polymer materials were chosen to achieve the required refractive-index contrast and to remain compatible with standard fabrication and polishing processes.

Protective coatings should be specified to improve environmental durability and mechanical robustness (e.g., against moisture, abrasion, and handling). Overall, the chosen materials must balance optical performance, thermal stability, mechanical strength, and cost, particularly when targeting high-volume production.

8.2.1 Optical Fibre

The preferred plastic optical fibre (POF) in this work is a cylindrical, 1 mm (core + cladding) step-index PMMA fibre, Eska™ CK-40 (Mitsubishi Rayon Co. Ltd.), selected for its availability and its suitability for low-cost LED sources and detectors. Eska™ CK-40 has a 0.98 mm core, a ~10 µm fluorinated-polymer cladding, NA = 0.5, n_core = 1.49, and n_clad = 1.402. The

system operates at 470 nm (blue), 520 nm (green), 570 nm (yellow), and 650 nm (red), where PMMA POF exhibits low attenuation in the visible band.

This fibre is well suited to prototype and production considerations: its large core and low cost simplify alignment and polishing relative to silica fibres, while maintaining adequate transmission for visible-light WDM with LED devices. Because polished-fibre couplers depend on precise fibre–fibre interaction, the chosen fibre type aligns with the target wavelength range and coupling efficiency requirements. Surrounding coatings and supports are specified to provide mechanical protection and thermal stability during polishing and alignment. Finally, material compatibility—especially with index-matching adhesives and housing components—is ensured to support long-term reliability.

8.2.2 Coupler Housing Block Design

The coupler's structural parts will be made from durable thermoplastics—such as ABS or polycarbonate—to ensure mechanical stability and compatibility with standard manufacturing methods (e.g., CNC machining and injection moulding). The coupler housing blocks were designed in AutoCAD, as shown in Figures 8-1 to 8-6.

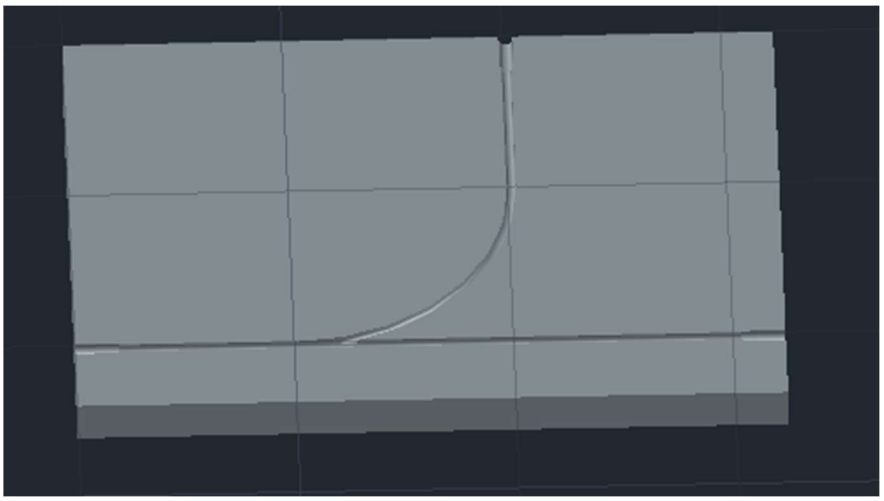

Figure 8-1: The housing block for a 1x2 splitting coupler to test the effect of immersion depth on the output received optical power.

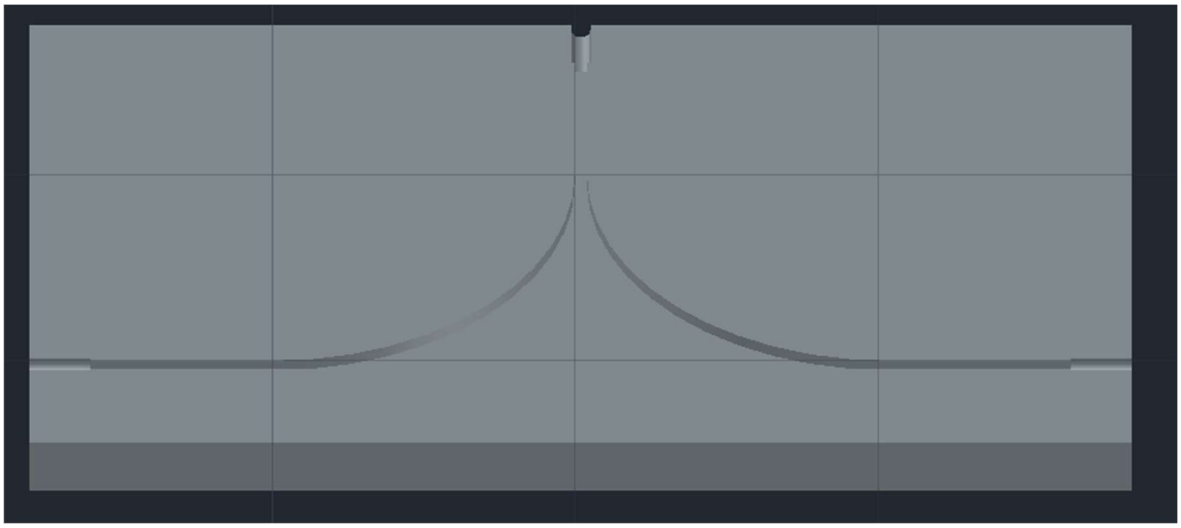

Figure 8-2: The housing block for a 1x2 splitting coupler to test the performance of the 1x2 non-backbone.

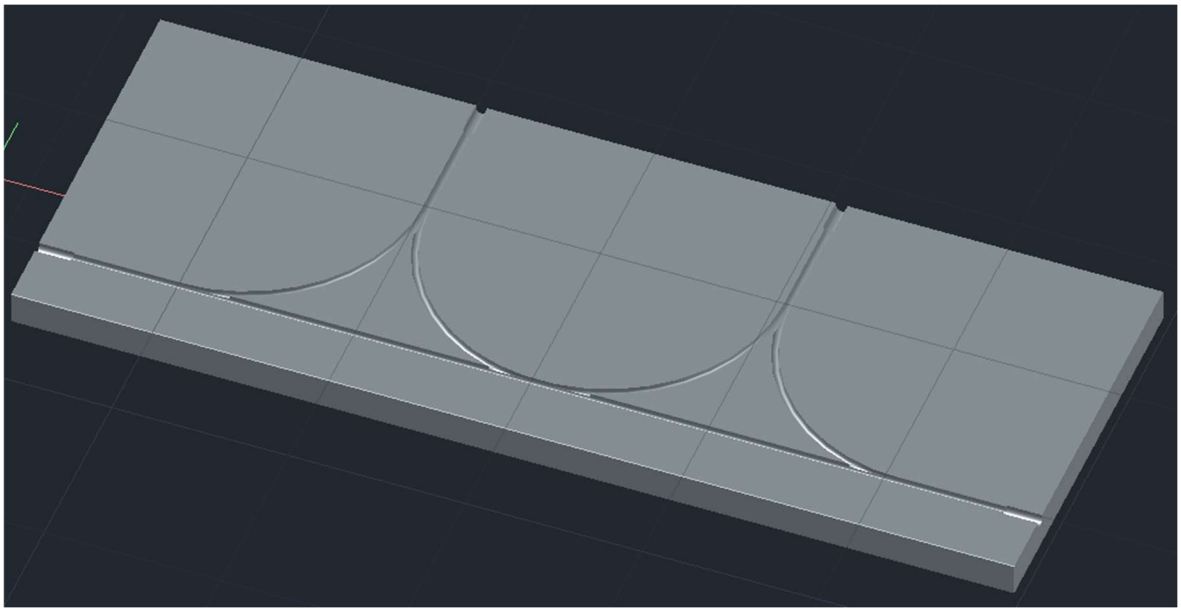

Figure 8-3: The housing block for the POF-based 1x2 array coupler.

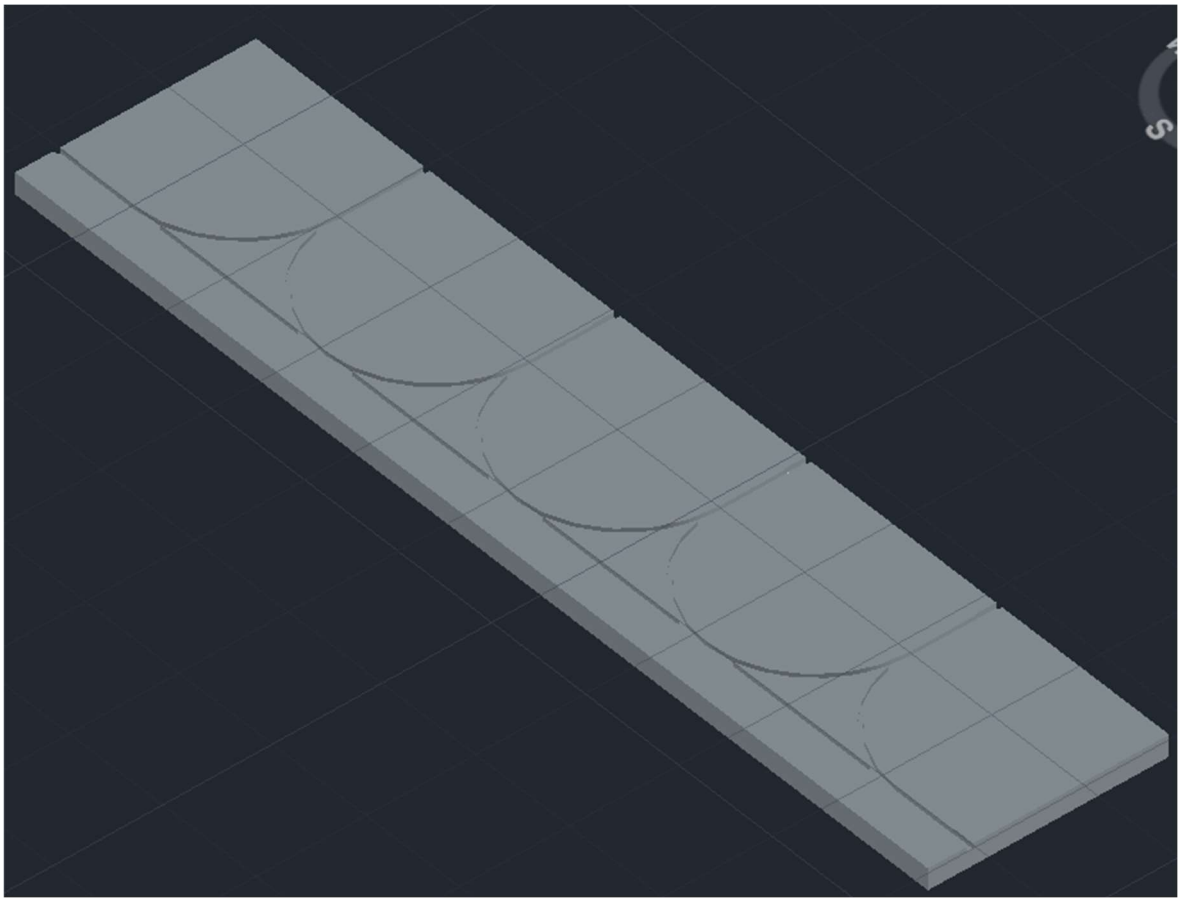

Figure 8-4: The housing block for the POF-based 1x4 array coupler.

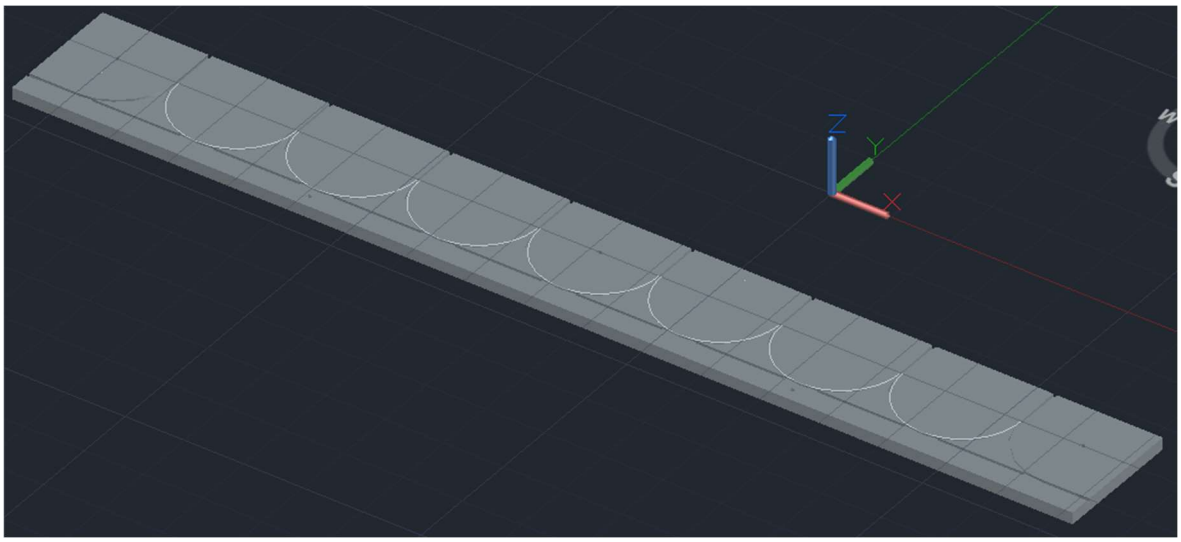

Figure 8-5: The housing block for the POF-based 1x2 array coupler.

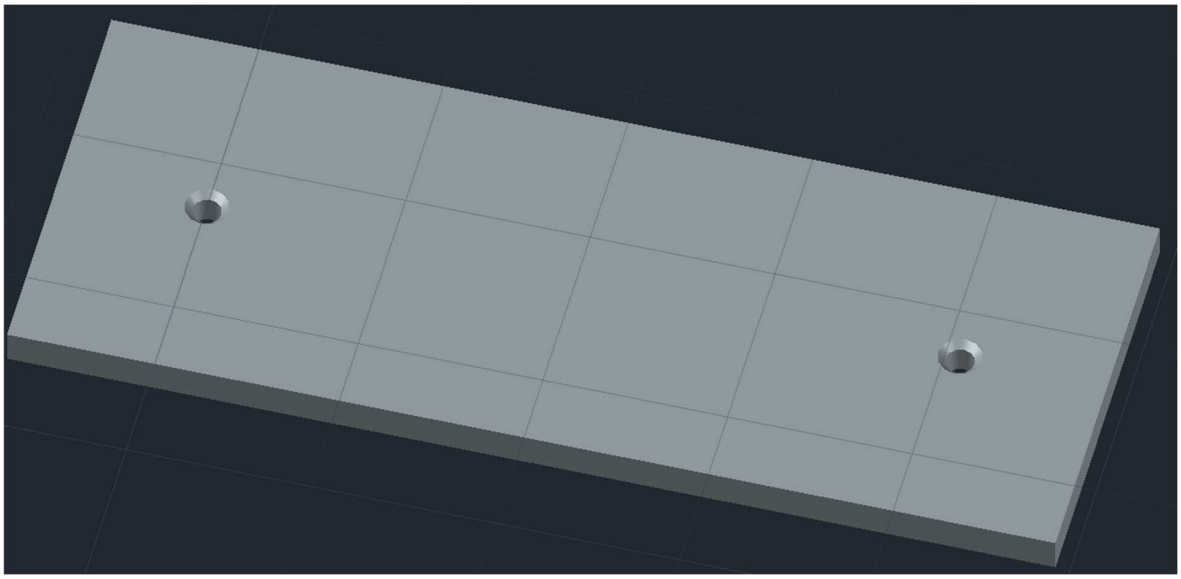

Figure 8-6: The housing block cover for the POF-based array couplers to prevent lateral and angular movement of the plastic optical fibres.

8.2.3 Adhesives and Fixatives

After fibre alignment, the fibres are secured using UV-curable index-matching adhesives or low-refractive-index epoxy resins. The selected adhesive must provide high optical clarity, thermal stability, and low shrinkage to ensure long-term alignment and stable optical performance.

8.2.4 Optimisation reflector

After side-polishing the input backbone fibre to the specified depth and fixing it in the housing block, the precision-cut optimisation reflector (tolerance < 0.01 mm) is placed on the polished surface under a microscope in a dust-free environment. The reflector is then tacked with index-matching adhesive until the polished coupling POF is inserted and aligned.

8.3 Fabrication Techniques

8.3.1 Fibre Preparation

Achieving accurate, low-loss fibre-to-fibre coupling hinges on high-quality side-polished faces. Progressive polishing with finer abrasive films (down to ≤1 µm) produces an optically smooth surface, reducing insertion loss and back-reflection. For this POF coupler, side-

polishing is essential to minimise scattering and maximise efficiency, and must deliver sub-micron flatness with low surface roughness and high repeatability.

The core process exposes the fibre's evanescent field by removing cladding and a controlled portion of the core—without damaging the remaining core. Polishing depth and surface quality directly determine coupling efficiency and insertion loss. After polishing, fibres are aligned with sub-micron accuracy using passive alignment while monitoring optical power. The polished section is then stabilised—e.g., in an AutoCAD-designed U-groove housing—and secured with index-matching adhesive and encapsulation to preserve alignment and protect against environmental stress.

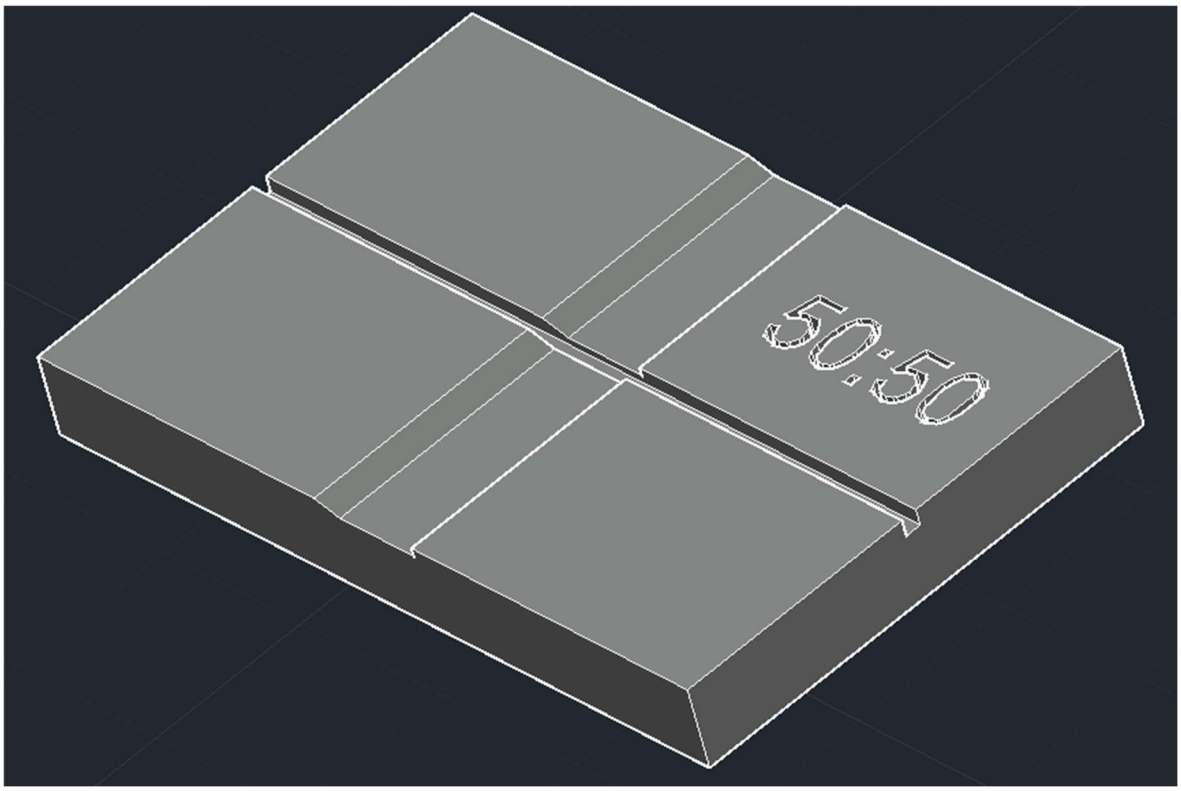

Figure 8-7: Polishing jig for the end splitters of the array couplers. There is a jig made for each immersion depth.

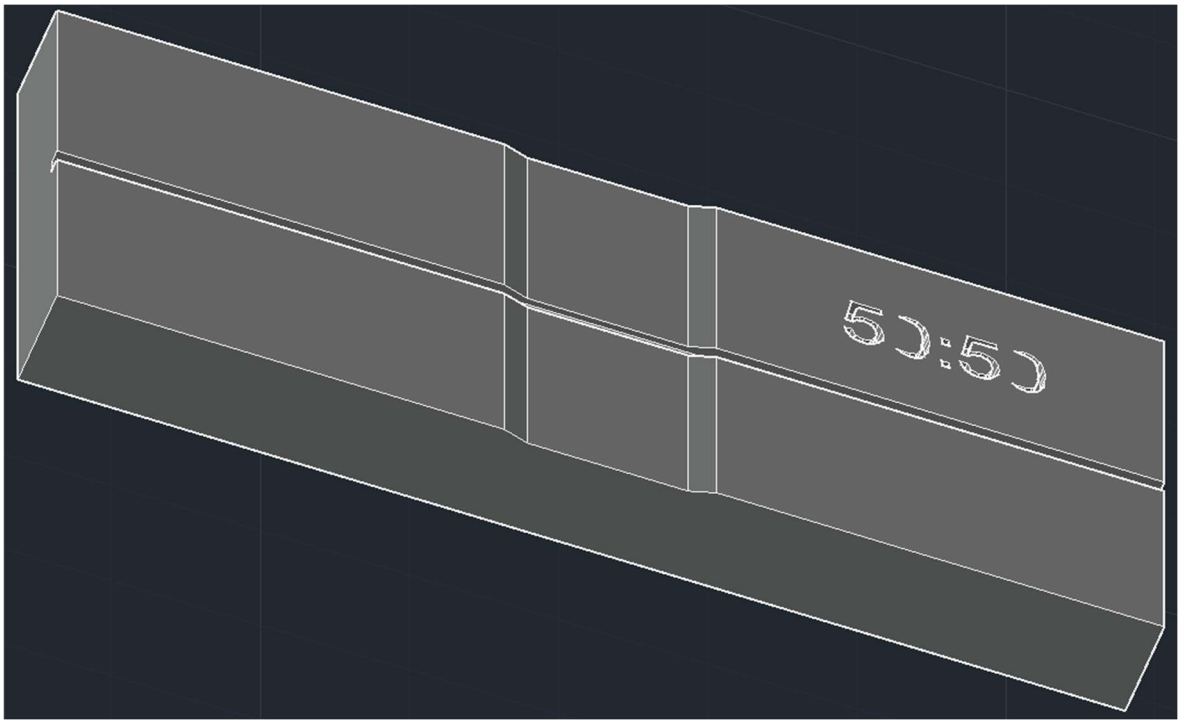

Figure 8-8: Polishing jig for the intermediate splitters of the array couplers. There are jigs made for each immersion depth.

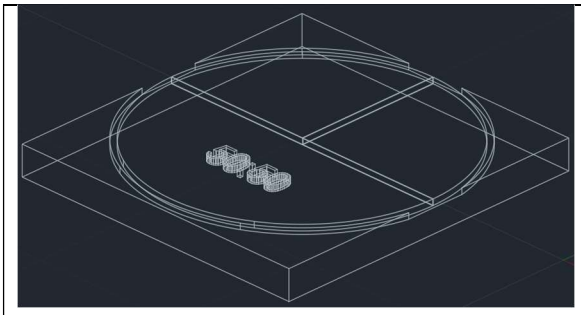

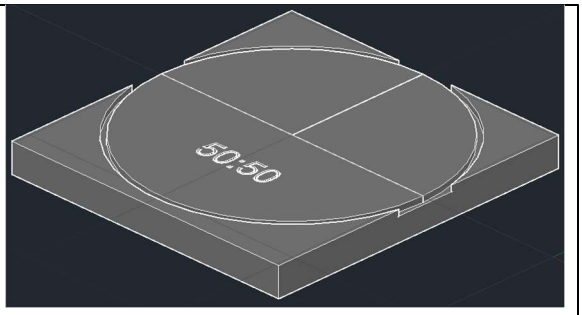

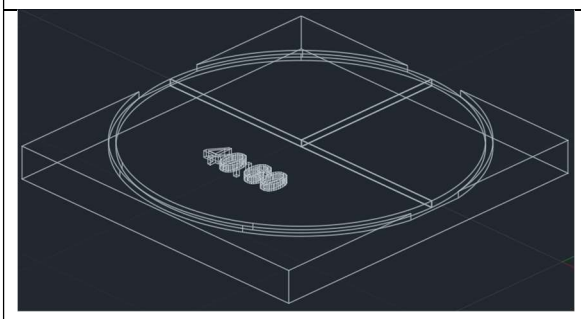

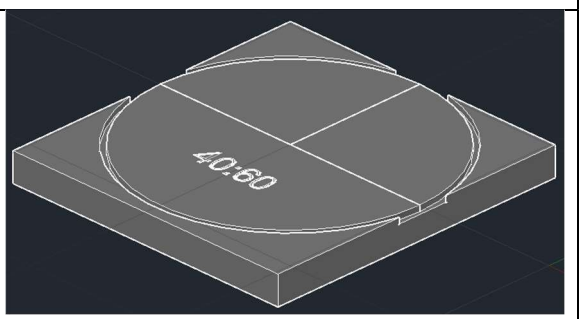

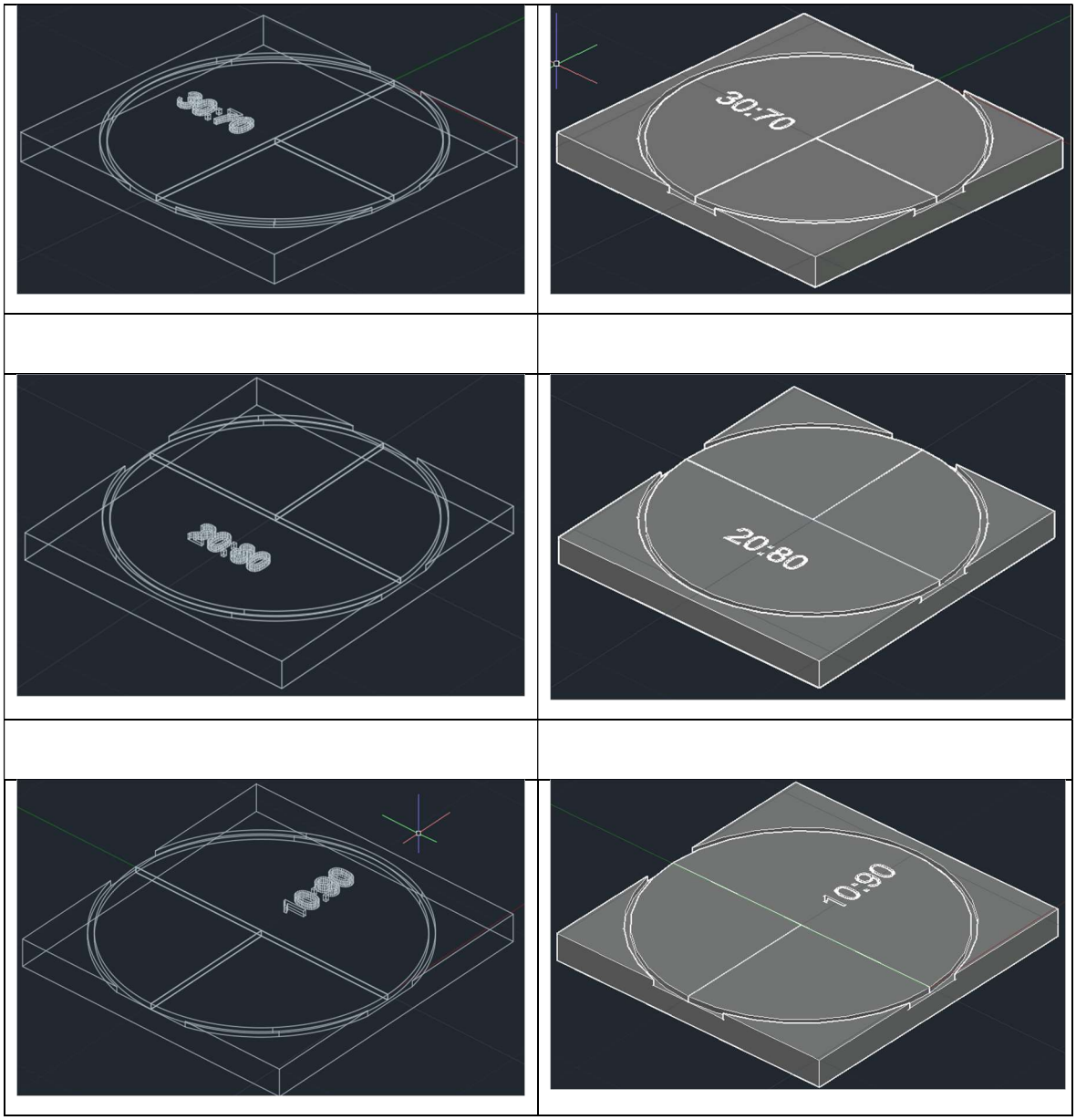

Figure 8-9: Polishing jig for various immersion depths used in the array couplers. There are jigs made for each immersion depth.

While polishing is the preferred technique for fabricating high-quality coupler prototypes, it is also time-consuming. For the proposed POF-based couplers, alternative methods such as sharp razor cutting, hot-blade cutting, or chemical etching can also produce clean, precise fibre surfaces. To determine the most effective fabrication approach, prototypes will be manufactured using each of these methods for comparison.

8.3.2 Coupling Plastic Optical Fibre Alignment and Coupler Assembly

The 1×2, 1×4, and 1×8 array couplers require precise registration of the input fibre to the output (coupling) fibres. In this design, alignment within the splitting region is passive, achieved with pre-designed CAD U-groove housing blocks and fibre holders that hold ±50 µm positional tolerances. No active alignment is performed inside the splitting region. Instead, coupling efficiency, balance, and output power are set at design time via immersion-depth control and reflector-length optimisation (see Chapter 4, §§4.4.3 and 4.4.5).

Elsewhere in the assembly, active alignment may be used—leveraging real-time optical feedback—to fine-tune fibre placement before final fixation. Components are then secured using UV-curable adhesives or thermal bonding. The package is designed to protect the optical path and maintain alignment under thermal and mechanical stress.

8.4 Mechanical Tolerances

8.4.1 Positional Accuracy

Thanks to its large ~1 mm core, POF is far easier to handle and align than single-mode silica fibre. Nevertheless, to achieve uniform power distribution, the backbone (input) and coupling (output) fibres should be positioned within ±20–50 µm in the general assembly; larger offsets cause power imbalance and higher insertion loss. Small shifts can also increase port-to-port variability over time, especially under vibration or temperature cycling.

Robust mechanical tolerancing is therefore essential. Even modest lateral or angular misalignments reduce coupling efficiency and must be minimised through: precision U-groove/vee-groove fixtures, controlled adhesive gaps, and rigid housings. Connectors and mounts should be designed for repeatable datum features, easy assembly, and error-proofing (e.g., keyed parts). A formal tolerance analysis (analytical and/or Monte-Carlo) should identify the dominant contributors to loss (polish depth, lateral offset, angular tilt, glue shrinkage) and set allowable variation windows.

Within the polished-region interface, requirements are more stringent:

- Polish depth control: ±0.5 µm to maintain consistent evanescent coupling length.

- Local alignment (polished region): ±1 μm lateral and ±0.1° angular to avoid mode truncation and excess scattering.
- Surface roughness: < 50 nm RMS to suppress Rayleigh–like scatter and back-reflection.
- Housing/fixture: must hold fibres without residual stress; tolerances should accommodate CTE mismatch so thermal excursions don't de-align the interface.

Process controls and metrology

- Use in-situ optical monitoring (live power on a reference photodiode) during alignment to peak coupling before cure.
- Verify polish depth with contact/non-contact profilometry; verify flatness/roughness by white-light interferometry or AFM on witness samples.
- Inspect alignment under a metrology microscope with calibrated reticle; record offsets for SPC.
- Select low-shrinkage, index-matched adhesives; characterise cure shrinkage and modulus—both influence post-cure drift.
- Bake or UV-pre-gel to reduce flow, then final-cure while constrained in the fixture.

Design-for-reliability considerations

- Specify mechanical stops and hard datums to limit over-travel during assembly.
- Include thermal and vibration testing (e.g., −20–70 °C, random vibration) and re-measure IL/Uniformity to confirm stability.
- Where feasible, introduce compliance features (flexures) or athermalisation (matched CTE materials) to maintain alignment across temperature.
- Use witness coupons per batch to validate polish/adhesive performance before building product.

By combining tight but achievable tolerances in the polished region with pragmatic assembly tolerances elsewhere—validated by metrology and SPC—the coupler can reliably meet insertion-loss and uniformity targets at scale.

8.4.2 Angular Alignment

Angular misalignments greater than ±2° can cause significant miscoupling and reduce power transfer efficiency. The polishing Jigs and housing blocks must therefore constrain angular displacement during assembly.

8.4.3 Surface Quality

Polished surfaces should exhibit minimal surface roughness (preferably <1 μm) to prevent scattering losses and signal degradation. The metallic polishing jigs were designed for these optical couplers to ensure repeatability in mass production.

8.5 Considerations for Mass Production

While manual methods are sufficient for prototyping, scaling to mass production introduces additional challenges. Material costs—especially for high-purity substrates or specialty POF—can rise sharply at volume. Alignment errors, contamination, and fabrication defects can reduce yield, so robust quality control is essential. Automation of polishing, alignment, and bonding improves throughput and consistency but requires upfront investment in equipment and process development. To ensure long-term reliability, packaging must account for thermal and mechanical stresses during handling and shipping. Accordingly, Design for Manufacturability (DFM) principles should be applied early to reduce risk and enable efficient, scalable production.

8.5.1 Assembly Automation

Manual fibre alignment is slow and prone to variability. In high-volume production, automated alignment systems equipped with machine vision can significantly increase both speed and precision. Robotic positioning systems can place and bond fibres with accuracies better than ±50 μm, ensuring consistent, repeatable performance across large production batches.

8.5.2 Housing Fabrication

In this research, 3D printing or Injection moulding offers a cost-effective solution for fabricating the coupler housing and alignment structures at scale. Tooling costs are significant initially but amortised over large production volumes.

8.5.3 Quality Control

Consistent optical performance requires rigorous quality assurance. Production will include inline optical test stations to verify compliance in real time.

Core tests and metrics

- Insertion loss, splitting uniformity, return loss, polarisation-dependent loss, bandwidth, and coupling-ratio accuracy.
- Typical targets: insertion loss per splitting POF < 1 dB, return loss > 40 dB (adjust to your spec as needed).

Inspection and metrology

- Optical microscopy to detect surface defects, contamination, or misalignment.
- Interferometry/profilometry to assess surface flatness and geometry of polished regions.

Environmental and reliability testing

- Temperature, humidity, and vibration stress testing; thermal cycling as required.
- Testing across operating ranges on automated benches to reduce human error and ensure repeatability.

Standards and process control

- Validate against Telcordia GR-1209 and GR-1221 for optical performance and environmental reliability.
- Maintain a closed feedback loop between test data and manufacturing to identify recurring issues and drive continuous improvement.

8.6 Environmental Durability

Plastic fibres and adhesives can degrade under UV exposure, high temperatures, or humidity. These POF-based array couplers are not intended for outdoor or industrial

applications; otherwise, they will require protective enclosures or coatings to extend their operational lifetime.

8.7 Sustainability and Lifecycle Considerations

PMMA, being an organic material, is recyclable; however, the adhesives and epoxy resins used in assembly typically are not. Therefore, end-of-life management should be addressed early in the design and fabrication stages. Designs should prioritise ease of disassembly, allowing recovery or reuse of connectors and fibre segments, and minimising environmental impact from non-recyclable components.

8.8 Conclusion

The proposed POF backbone array couplers (1×2, 1×4, and 1×8) are well-suited for prototyping. The optical architecture has been validated through theory and LightTools ray-tracing, with predicted insertion loss, efficiency, and uniformity that meet GR-1209-CORE requirements. Materials, geometries, and tolerances are clearly defined: step-index PMMA POF (Eska™ CK-40), submicron side-polish flatness, controlled immersion depth, and reflector-length adjustment provide a practical and buildable foundation. The mechanical design uses CAD U-groove housings compatible with standard fabrication methods such as CNC machining or injection moulding, while assembly steps such as passive alignment within ±20–50 µm, index-matching adhesives, and encapsulation follow established POF practices.

From a manufacturability perspective, the design incorporates Design for Manufacturability (DFM) principles, including hard datums, repeatable fixturing, low-shrinkage adhesives, and a defined quality assurance plan. This plan includes inline insertion-loss and uniformity testing, visual and interferometric inspection, and environmental stress testing to Telcordia GR-1209 and GR-1221 standards. These considerations minimise process variation and support consistent optical performance. Overall, the coupler designs present a complete and practical pathway from concept to prototype fabrication, providing a strong foundation for further optimisation and real-world application.

Chapter 9

Conclusion and Further Work

9.1 Conclusion

This thesis conducts a comprehensive investigation of plastic optical fibre (POF) array couplers through theory and optical simulations to assess their suitability as connectivity devices for industrial and domestic networks. The work focuses on 1×2, 1×4, and 1×8 POF-based array couplers. Although no physical devices were built, realistic models were implemented and analysed using LightTools.

POF was selected as the transmission medium for short-reach applications due to its favourable handling, cost, and visible-band performance. The theoretical framework is based on ray optics, covering the critical angle, total internal reflection, Snell's law, numerical aperture (NA), and V-parameter considerations needed for coupler design. The study also evaluates loss mechanisms and other propagation effects in POF to determine its viability for constructing practical POF-based couplers.

The performance parameters of the POF-based optical couplers were calculated, including insertion loss, excess loss, coupling (splitting) ratio, coupler uniformity and coupler efficiency. The theoretical and modelling simulation phases yielded significant results, summarised in the following conclusions:

1. The first simulation focused on determining the optimal bending radius for the optical coupler arms using Mitsubishi Eska™ CK-40 POF, characterised by a core refractive index of 1.492 and a cladding refractive index of 1.405. The results demonstrated two key phenomena: first, a bending radius of 10 mm or greater does not negatively affect the optical output power of the POF, as all optical modes maintain angles greater than the critical angle due to TIR. Second, the simulation results indicated that POF attenuation varies with wavelength, with 470 nm (blue) experiencing the least attenuation, followed by 520 nm (green), 570 nm (yellow), and 650 nm (red). The manufacturer's data sheet specifies a minimum bending radius of 20 mm, which is

double that determined from the simulation. Consequently, a bending radius of 25 mm was adopted for all subsequent coupler simulations.

2. The thesis also explored the effect of immersion depth on the optical energy received by a bent and side-polished POF immersed in a straight backbone POF. The findings showed a consistent correlation between the immersion depth (ranging from 10% to 50%) and the theoretical analysis. According to the theoretical framework, only optical modes that interact with the immersed POF contribute to the output power; those that do not interact with it do not. The immersion depth significantly influenced the optical power at the output ports, as it determined the interaction arc between the immersed polished POF and the transmitted propagation modes. A deeper immersion depth led to a wider interaction angle, thereby coupling more optical modes into the immersed POF. Notably, the coupled optical power was found to be proportional to the immersion depth, although the relationship was not linear—an immersion depth of 10% yielded approximately 20% of the optical power coupled to the output port.
3. Adjusting immersion depth provided only coarse tuning of the received output power. To achieve finer control, a method involving the insertion of a 100% reflector between the side-polished immersed POF and the backbone POF was implemented. Simulation results revealed that the optical energy received at the output port was inversely proportional to the length of the optimisation reflector; specifically, increasing the reflector's length reduced the optical energy at the output ports. While the immersion depth enhanced the received output power, the length of the optimisation reflector had the opposite effect.
4. The foundational component of the optical array couplers was the 50:50 splitting coupler, immersed in a backbone POF. Initial simulations focused on the beam splitter's performance characteristics, with a reflector inserted between its arms to maximise the output optical power. The results confirmed that the beam splitter (Y-Coupler) equally divides the input optical power, with a notable concentration observed at the centre of the optical fibres.
5. When the beam splitter was polished at the output ports and immersed in the backbone POF at a depth of 20%, both output ports received 50% of the optical power. Unlike the beam splitter, the optical power distribution in the 1x1 coupler was

scattered within the circumference of the output POF core due to optical modes travelling across the junction between the backbone and the immersed POF.

6. Multiple beam splitters immersed in the backbone POF were employed to simulate POF-based 1x2, 1x4, and 1x8 optical array couplers, with dimensions calculated in the theoretical analysis chapter. These simulations evaluated the performance characteristics of the couplers, with input power applied to one end of the backbone POF. Results indicated that most of the optical power remained in the backbone POF, with exponential decay at the output ports. The first port consistently received the highest power, while the last port received the least, particularly evident in the 1x8 coupler. The coupling efficiency was determined to be 54% for the 1x2 coupler, 62% for the 1x4 coupler, and 48% for the 1x8 coupler.
7. Repeating the simulations with a 100% optical reflector attached to the opposite end of the backbone POF resulted in increased output power and improved coupling efficiency. The 1x2 coupler's efficiency increased from 54% to 77%, the 1x4 coupler from 62% to 77%, while the 1x8 coupler showed a modest increase from 48% to 50%, attributed to the shallow immersion depth (10:90 and 20:80). The theoretical analysis indicated that in digital communication, reflected optical energy could delay pulses, potentially enhancing the incident pulses received at the output ports. However, the reception of reflected pulses could broaden the received signals, impacting the optical couplers' data rate capabilities. The calculated data rates were 1 Gb/s for the 1x2 coupler, 500 Mb/s for the 1x4 coupler, and 250 Mb/s for the 1x8 coupler, all sufficient to support fast Ethernet signals at 100 Mb/s.
8. The findings revealed that achieving optimisation —defined as equal optical power at each output port —was complex, particularly when input ports other than the backbone were used. Optimisation was achieved by inserting an optimisation reflector of appropriate length between the immersed end of the splitting coupler and the backbone POF. When the backbone port was the input port, 100% optimisation was attained across all couplers (1x2, 1x4, and 1x8). However, introducing the optimisation reflector resulted in additional coupler losses: the 1x2 coupler optimised at 42% of the input power at each output port, the 1x4 coupler at around 22%, and the 1x8 coupler at 8%. Coupling efficiencies improved significantly, with the 1x2 achieving 84%, the 1x4

86%, and the 1x8 62%. Although the 1x2 coupler was effective for receiving communication signals, it was less suitable for transmitting due to the losses introduced by the optimised reflector configuration.

9. For the optical couplers to function as transmitting devices using ports other than the backbone as input ports, the optimisation reflectors required reconfiguration. The 1x2 coupler achieved optimisation with port 2 as the input, while the 1x4 and 1x8 couplers could not achieve optimisation when using non-backbone input ports. Additionally, the performance parameter values of the simulated couplers were found to depend on the chosen input port, mirroring the trends observed in the theoretical analysis.
10. Overall, the performance parameters of both theoretical and simulated couplers were consistent when the backbone port served as the input. Key parameters compared included excess loss, insertion loss, coupling (splitting) ratio, coupling loss, uniformity, and coupler efficiency.

9.2 Further Work

The findings from this thesis on Plastic Optical Fibre (POF)-based array optical couplers open up several promising avenues for future research. Here are some potential directions for further exploration:

1. Physical Prototyping and Experimental Validation

- Create physical prototypes of the optimised 1x2, 1x4, and 1x8 POF-based optical couplers to validate the theoretical and simulated results.
- Conduct experiments to assess coupler performance across various real-world environments and applications, including industrial and domestic settings.

2. Enhanced Simulation Models

- Develop more sophisticated simulation models that account for nonlinear optical effects and their impact on signal quality in high-power applications.
- Utilise 3D modelling software to create more intricate designs that mimic actual physical constraints and geometries in real-world applications.

3. Investigation of Alternative POF Types

- Investigate different types of POF with varying refractive indices, core diameters, and optical properties to assess their performance in array-coupler applications.

- Consider integrating POF with other optical fibres or technologies (such as glass fibres) to create hybrid couplers that combine the advantages of both media.

4. Optimisation Techniques

- Develop dynamic optimisation techniques that adapt the coupling efficiency in real-time based on varying input conditions or operational requirements.
- Explore alternative designs for optimisation reflectors that could provide enhanced performance or adaptability.

5. Integration with Advanced Communication Technologies

- Evaluate the performance of the POF-based couplers when used with advanced communication protocols, including 5G networks and future optical communication standards.
- Investigate the role of these couplers in larger optical network architectures, including their compatibility with existing infrastructure.

6. Data Rate and Performance Enhancement

- Conduct studies to increase the data transmission rates and overall performance of optical couplers, potentially through improved design or by exploring advanced modulation techniques.
- Explore the possibility of multi-wavelength coupling to enhance bandwidth and performance in optical communication systems.

9.3 Publications drafted

1. *The Characterisation of the POF-Based 1x2 Splitting Optical Coupler With Different Immersion Depths and Backbone Reflector.*
2. *Output Power Optimisation of Plastic Optical Fibre (POF) based 1x2 and 1x4 Array Couplers Using Optical Reflectors.*

References

A. Bunge, M. B. (2017). *Polymer Optical Fibres.* Aachen, German: Woodhead Publishing.

Agrawal, G. P. (2021). *Fiber-Optic Communication Systems.* (5th ed.). John Wiley & Sons.

Albakay, N. A., & Nguyen, L. (2017). Achieving 1 Gbps Over Step-Index Plastic Optical Fiber Using Spatial Mode Air-Gap Filter. *IEEE Photonics Technology Letters (Volume: 29, Issue: 8, 15 April 2017)*, 655 - 658. doi:10.1109/LPT.2017.2677083

Alicia López, M. Á. (2018). Characterization of a Y-Coupler and Its Impact on the Performance of Optical Fiber Links. *MDPI*, 1-8. Retrieved from https://www.mdpi.com/2079-6439/6/4/96/htm

Appajaiah, A. (2005). Climatic Stability of Polymer Optical Fibers (POF). *Potsdam University*. Berlin, German.

Azusa Inque, Y. K. (2019, April). Unconventional plastic optical fiber design for very short multimode fiber link. *Optics Express, Vol 27*(9), 1-9. doi:https://doi.org/10.1364/OE.27.012061

Bazakutsa, P. V., Boev, M. A., & Nikitin, A. I. (2022). Fused optical couplers: power transfer between optical fibers. *2012 IEEE 4th International Conference on Adaptive Science & Technology (ICAST)* (pp. 1-5). Moscow: IEEE. doi:10.1109/REEPE53907.2022.9731448

Carmen Vázquez, F. M.-Z. (2021). SI-POF Supporting Power-Over-Fiber in Multi-Gbit/s Transmission for In-Home Networks. *Journal of Lightwave Technology (Volume: 39, Issue: 1, 01 January 2021)*, 112 - 121. doi:10.1109/JLT.2020.3025444

Cisco. (2018 - 2023). *Annual Internet Report .* Cisco Syatems.

Cong Zhang, L. S. (2021). Design of an all-fiber mode power splitter for mode division multiplexing. *Applied Optics*, 8480-8484. doi:https://doi.org/10.1364/AO.435477

D. Zaremba, R. E. (2017). Materials, chemical properties and analysis. In T. G. Christian-Alexander Bunge, *Polymer Optical Fibres, Fibre Types, Materials, Fabrication, Characterisation and Applications* (pp. 153-186). ScienceDirect. doi:https://doi.org/10.1016/C2014-0-00562-X

David R. Gozzard, R. C. (2022). Optical couplers and step-index fibers fabricated using FDM 3D printers. *Optics Letters, Vol 47*(19/1), 5124-5127. doi:https://doi.org/10.1364/OL.470523

Fund, F. (2017, February 13). Retrieved from Run my testbed experiment: https://witestlab.poly.edu/blog/nyquist-formula-relating-data-rate-and-bandwidth/?utm_source=chatgpt.com

Ghosh, K. (2024, August 22). Novel Breakthroughs in Plastic Optical Fiber Technology Are Restructuring the Industry: An Overview. *Allied Market Research*, p. 1. Retrieved

from https://blog.alliedmarketresearch.com/innovations-in-plastic-optic-fiber-technology-2221

Guo, Z., Lu, L., Zhou, L., Shen, L., & Chen, J. (2018). 16 × 16 Silicon Optical Switch Based on Dual-Ring-Assisted Mach–Zehnder Interferometers. *Journal of Lightwave Technology (Volume: 36, Issue: 2,)*, 225 - 232. doi:10.1109/JLT.2017.2751562

Hadi Guna, Mohammad Syuhaimi Ab-Rhaman, Norhana Arsad, Roslan Shukor, Sabudin Shaari. (2020). In IntechOpen, *Innovation in Global Green Technologies 2020* (pp. 37-54). IntechOpen. Retrieved from https://books.google.co.uk/books?hl=en&lr=&id=FGH9DwAAQBAJ&oi=fnd&pg=PA37&dq=%22POF+Coupler%22&ots=CjNmEaKCnw&sig=PvZcGON1Z5slem_a5M0b_QrldXk&redir_esc=y#v=onepage&q=%22POF%20Coupler%22&f=false

Heidarialamdarloo, J. (2018). Advanced Communications with Plastic Optical Fibers. *Proquest*. Proquest. Retrieved May 15, 2023, from https://www.proquest.com/docview/2406664946?pq-origsite=gscholar&fromopenview=true

Inoue, A., & Koike, Y. (2018). Low-Noise Graded-Index Plastic Optical Fiber for Significantly Stable and Robust Data Transmission. *Journal of Lightwave Technology (Volume: 36, Issue: 24, 15 December 2018)*, 5887 - 5892. doi:10.1109/JLT.2018.2877386

Isaac N. Osahon, M. S. (2018). 10-Gb/s Transmission Over 10-m SI-POF With M-PAM and Multilayer Perceptron Equalizer. *2018 IEEE Photonics Conference (IPC).* Reston, VA, USA: 2018 IEEE Photonics Conference (IPC). doi:10.1109/IPCon.2018.8527269

J.M. Senior. (2009). Optical Fibre Communications, Principles and Practise, 3rd ed, Harlow, UK, l, 2009, p269. In J. Senior, *Optical Fibre Communications, Principles and Practise, 3rd Edition* (pp. p256 - p275). Harlow, UK: Prentice Hall.

Jamshid Heidarialamdarloo. (2018). Advanced communications with plastic optical fibers. Miami: ProQuest. Retrieved from https://ria.ua.pt/handle/10773/25881

Jing Yang, 1. Y. (2021, October). Variable-fiber optical power splitter design based on triangular prisms. *Applied Optics, Vol. 60*(No. 30), Vol. 60, No. 30. doi:https://doi.org/10.1364/AO.437983

Jing Yang, Y. L. (2021). Variable-fiber optical power splitter design based on a triangular prism. *Applied Optics*, 1-6. Retrieved from https://opg.optica.org/view_article.cfm?pdfKey=84da9f1f-cd95-45b8-924ea63a16b5b7ae_460558

K. Sunil Kumar1, D. (2016). Fabrication and characterization of Low cost Plastic optical fiber couplers. *International Research Journal of Engineering and Technology (IRJET)*(Volume: 03 Issue: 06 | June-2016), 1972 - 1975. Retrieved from www.irjet.net

Kazovsky, L. G. (2012). *Broadband Optical Access Networks.* John Wiley & Sons.

Keiser, G. (2011). *Optical Fiber Communications* (4th ed.). New York: McGraw-Hill.

KOIKE, A. I. (2019, April 29). Unconventional plastic optical fiber design for very short multimode fiber link. *OPTICS EXPRESS*, 1-9. doi:https://doi.org/10.1364/OE.27.012061

Korn, G. A. (2000). *Mathematical Handbook for Scientists and Engineers. .* New York: Dover Publications.

L.S. Supian, M. A.-R. (2021). Chapter 3, Polymer optical fiber spllitter using tapered techniques for green technologies. In IntechOpen, *Green Computing Technologies and and Computing Industry 2021* (pp. 57-75). London: IntechOpen. Retrieved from https://books.google.co.uk/books?hl=en&lr=&id=FGH9DwAAQBAJ&oi=fnd&pg=PA37&dq=%22POF+Coupler%22&ots=CjNmEaKCnw&sig=PvZcGON1Z5slem_a5M0b_QrldXk&redir_esc=y#v=onepage&q=%22POF%20Coupler%22&f=false

Lange, V., & Hönl, R. (2018). LED as transmitter and receiver in POF - based bidirectional communication systems. *2018 International IEEE Conference and Workshop in Óbuda on Electrical and Power Engineering (CANDO-EPE)* (pp. 1-6). Budapest, Hungary: IEEE. doi:10.1109/CANDO-EPE.2018.8601162

Langer, H. K. (2020). Plastic Optical Fibers in the New Age of Photonics: Developments and Applications. . *IEEE Photonics Journal, 12(4).*

Lee, B. (2021, November). *PASSIVE OPTICAL.* Retrieved from Senko Advanced Components: https://www.senko.com/wp-content/uploads/2021/08/Optical-Splitter-Whitepaper.pdf?utm_source=chatgpt.com

Liao, S., Bao, H., Zhang, T., & Liu, J. (2020). Integrated Optical Power Splitter With Continuously Adjustable Power Splitting Ratio. *IEEE Photonics Journal (Volume: 12, Issue: 6)*. doi:10.1109/JPHOT.2020.3038379

Lina Sanchez-Botero, D. S.-B. (2022). Are Liquid Metals Bulk Conductors? *Advanced Materials*, 1-12. doi:DOI: 10.1002/adma.202109427

López, A., Villar, N., Losada, A., Laporta, E., & Mateo, J. (2020). Experimental Characterization of the Transmission Properties of Large-Core Graded-Index PMMA Fibers. *2020 22nd International Conference on Transparent Optical Networks (ICTON)* (pp. 1-5). Bari, Italy: IEEE. doi:10.1109/ICTON51198.2020.9203441

M. Beckers, B. W.-A. (2017). *Polymer Optical Fibres.* Aachen, German: Woodhead Publishing.

M.S.M. Ghazali, F. R. (2021). Manufacturing of Polymer-based 1×2 Y-branch Symmetric and Asymmetric Waveguide Coupler through Moulding Technique. *INTERNATIONAL JOURNAL OF AUTOMOTIVE AND MECHANICAL ENGINEERING (IJAME)*, 8998 – 9005. doi:https://doi.org/10.15282/ijame.18.3.2021.12.0689

Matoumona, A. A. (2012). Comparative analysis of plastic optical fiber and glass optical fiber for home networks. *2012 IEEE 4th International Conference on Adaptive Science &*

Technology (ICAST) (pp. 1-4). Kumasi, Ghana: IEEE Explore. doi:10.1109/ICASTech.2012.6381084

Mohamed-Kassim, N. S. (2017). Analysis of POF Splitters and Couplers with Fixed Branching Ratios. . *Optoelectronics Letters, 13(3)*.

N S Mohamed-Kassim, M. K.-R. (2019). Plastic optical fibre power splitter for surface profiling of 3-D. *1st International Symposium on Engineering and Technology (ISETech) 2019* (p. 767). Selangor, Malaysia : IOP Publishing. doi:doi:10.1088/1757-899X/767/1/012055

N. S Mohamed-Kassim, e. a. (2017). High resolution tunable POF multimode power splitter. *Optics Communications*, 136-143. doi:https://doi.org/10.1016/j.optcom.2017.05.014

Naji Ali, A. L. (2017). Achieving 1 Gbps Over Step-Index Plastic Optical Fiber Using Spatial Mode Air-Gap Filter. *IEEE PHOTONICS TECHNOLOGY LETTERS, VOL. 29, NO. 8, APRIL 15, 2017, VOL. 29*(NO. 8).

Panchuk, M., Panchuk, A., Szkodo, M., Stanisławska, A., & Prunco, I. (2022). Polymer Optic Fibers: Potential of Development and Application in Networks. Sakheer, Bahrain: IEEE. doi:10.1109/3ICT56508.2022.9990760

Paschotta, D. R. (2024, January 04). *https://www.rp-photonics.com/beam_splitters.html*. doi:https://doi.org/10.61835/mjw

Polishuk, P. (2006, September). Plastic optical fibers branch out. *IEEE Communications Magazine (Volume: 44, Issue: 9, September 2006)*, pp. 140 - 148. doi:10.1109/MCOM.2006.1705991

Sariki, R. K., Kambavalasa, S. K., Bandari, N. K., & Moningi, R. K. (September 2021). Design and fabrication of POF Couplers/Splitters for Networking and Displacement Sensing. *2021 International Symposium of Asian Control Association on Intelligent Robotics and Industrial Automation (IRIA)* (pp. 183 -186). Goa, India: IEEE. doi:10.1109/IRIA53009.2021.9588705

Sasho, S., Takahashi, S., & Sugihara, O. (2017). Optical Coupler With Multicore Plastic Optical Fiber. *IEEE Photonics Technology Letters (Volume: 29, Issue: 8, 15 April 2017)* (pp. 659 - 662). IEEE. doi:10.1109/LPT.2017.2677478

Seiji Sasho, S. T. (2017). Optical Coupler With Multicore Plastic. *IEEE PHOTONICS TECHNOLOGY LETTERS*, 659-662. Retrieved July 10, 2021

Silvio Abrate, R. G. (2013). Step Index PMMA Fiber and their Applications. In IntechOpen, *Current Developments Optical Fiber Technology.* Rijeka, Croatia: IntechOpen.

Soref, R. (2018). Silicon Photonics: A Review of Recent Advances. . *IEEE Journal of Selected Topics in Quantum Electronics, 23(2)*.

Sugihara, O. (2019). Gigabit and Multi-Gigabit Data Transmissionfor Next-Generation Automotive Optical Network. (pp. 1-3). Fukuoka, Japan: IEEE. doi:10.23919/PS.2019.8818083

Sun, C. (2019). Integrated Photonics for Dense and Complex Networks. (pp. 165–173). Nature Photonics, 13.

Syed Azer Reza, T. S. (2019). A dual-mode variable optical power splitter using a Digital Spatial Light Modulator and a variable focus lens. *Optical Fiber Technology*, 118-125. doi:https://doi.org/10.1016/j.yofte.2018.11.03

Teleweaver. (2025, October 23). *Fiber Optic Splitter Insertion Loss Table Reference for FBT and PLC types*. Retrieved from https://fibrefibre.com/: https://fibrefibre.com/tutorial/fiber-optic-splitter-insertion-loss-reference/

Thiago R. Raddo, S. R. (2019). The Optical Fiber and mmWave Wireless Convergence for 5G Fronthaul Networks. *2019 IEEE 2nd 5G World Forum (5GWF)* (pp. 1-6). Dresden, Germany: IEEE. doi:10.1109/5GWF.2019.8911613

Thomas, G. B. (2018). *Thomas' Calculus* (14th Ed ed.). London: Pearson Education.

Uematsu, T. (2017, December). Design of a Temporary Optical Coupler Using Fiber Bending for Traffic Monitoring. *IEEE Photonic Journal*, 1-14. doi:DOI: 10.1109/JPHOT.2017.2762662

Ulrich H. P. Fischer, M. J. (2022). High-speed Wavelength Division Multiplexing Transmission over SI-Polymer Fibers. *Sensors & Transducers, Vol. 258, Issue 4, July 2022,*, 18-24. Retrieved from https://www.sensorsportal.com/HTML/DIGEST/july_2022/Vol_258/P_3270.pdf

Ulrich H.P. Fischer-Hirchert, M. H. (2017). High-Speed Optical In-House Networks Using Polymeric Fibers. In IntechOpen, *Broadband Communications Networks - Recent Advances and Lessons from Practice* (pp. 181-198). Rijeka,Croatia: IntechOpen. doi:DOI:10.5772/intechopen.72204

Usama Adnan, Z. A. (2022, December). Radio over plastic optical fibers – a tutorial and review. *Journal of Optical Communications*, 1-12. doi:https://doi.org/10.1515/joc-2022-0064

Václav Prajzler, J. Z. (2019). Polymer large core optical splitter 1 × 2 Y for high-temperature operation. *Optical and Quantum Electronics*, Article 216. Retrieved from https://link.springer.com/article/10.1007/s11082-019-1933-6

Václav Prajzler, P. K. (2017). Large core plastic planar optical splitter fabricated by 3D printing technology. *Optics Communications Volume 400*, 38-42. Retrieved from https://www.sciencedirect.com/science/article/pii/S0030401817303589?via%3Dihub

Waseem, M., López, A., Carro, P. L., & Losada, M. A. (2022). Radio Over Plastic Optical Fiber Transmissionfor Short-Range Future. *2022 Global Conference on Wireless and Optical Technologies (GCWOT)* (pp. 1-4). Malaga, Spain: IEEE. doi:10.1109/GCWOT53057.2022.9772881

Xiaopeng YANG, Y. F. (2017). Core Technology for Achieving Plastic Optical Fibersin an All-optical Network. *2017 16th International Symposium on Distributed Computing and Applications to Business, Engineering and Science* (pp. 127-130). Anyang, China: IEEE. doi:10.1109/DCABES.2017.35

Yau I., S. S. (2021). Mitigating the Effect of Modal Dispersion of Plastic Optical Fibre. *JOURNAL OF SCIENCE TECHNOLOGY AND EDUCATION*, 1-7. Retrieved from http://www.atbuftejoste.net/index.php/joste/article/view/1371

Yau, I., Sani, S. M., Usman, A. D., & Tekanyi, A. M. (2022). Enhancing the Transmission Performance of Step Index Plastic Optical Fiber. *2022 5th Information Technology for Education and Development (ITED).* Abuja, Nigeria: IEEE. doi:10.1109/ITED56637.2022.10051295

Yulianti, M. S. (2018). Back scattering method based-plastic optical fiber coupler viscocity sensors. *Journal of Physics*, 1-8. doi:10.1088/1742-6596/1918/2/022014

Ziemann, O. K. (2014). *POF Handbook: Optical Short Range Transmission Systems. .* Springer Science & Business Media.

Appendix 1

1x2, 1x4 and 1x8 Coupler Performance Parameters: Excess Loss, Coupler Loss, Uniformity and Coupler Efficiency

1x2 Coupler

Input Port	Excess Loss(dB)		Coupler Loss(dB)		Uniformity(dB)		Coupler Efficiency(%)	
	Calculation	Simulation	Calculation	Simulation	Calculation	Simulation		
$P_{B(in)}$	0.84	0.76	7.54	7.96	0.00	0.00	82.4	84
1	0.38	1.19	10.76	6.20	-0.24	-0.07	91.6	76
2	0.97	2.44	6.99	3.67	-0.22	-0.01	80	57

1x4 Coupler

Input Port	Excess Loss		Coupler Loss		Uniformity		Coupler Efficiency(%)	
	Calculation	Simulation	Calculation	Simulation	Calculation	Simulation		
$P_{B(in)}$	0.45	0.66	10.07	8.54	-0.02	-0.03	90	86
1	0.12	1.43	15.79	5.53	-0.28	-0.32	97	72
2	0.21	2.37	13.28	3.77	-0.18	-0.09	95	58
3	0.38	2.92	10.76	3.0	-0.11	-0.11	92	51
4	0.71	3.47	8.24	2.60	-0.16	0.37	85	45

Note: $P_{B(in)}$is the backbone plastic optical fibre input.

1x8 Coupler

Input Port	Excess Loss		Coupler Loss		Uniformity		Coupler Efficiency(%)	
	Calculation	Simulation	Calculation	Simulation	Calculation	Simulation	Calculation	Simulation
$P_{B(in)}$	0.37	2.04	10.86	4.26	-0.04	-0.07	91.8	62.5
1	0.04	2.15	19.00	4.08	-0.44	-0.29	99.0	61.0
2	0.06	3.88	18.54	2.28	-0.37	-0.44	98.6	41.0
3	0.08	3.26	17.13	2.77	-0.31	-0.34	98.1	47.2
4	0.12	2.47	15.71	3.63	-0.23	-0.38	97.3	56.6
5	0.17	2.99	14.28	3.03	-0.27	-0.49	96.3	50.2
6	0.23	4.53	12.85	1.88	-0.27	-0.48	94.8	35.2
7	0.37	5.78	10.92	1.33	-0.27	-0.43	92.0	26.4
8	0.22	6.51	13.01	1.10	-0.27	-0.40	95.0	22.4

1x2, 1x4 and 1x8 Coupler Performance Parameters: Insertion Loss

1x2 Coupler

Input Port	Insertion Loss(dB)					
	$P_{B(in)}$		P1		P2	
	Cal	Sim	Cal	Sim	Cal	Sim
$P_{B(in)}$	0	0	2.0	3.8	3.2	3.8
1	3.0	3.5	0	0	5.0	5.1
2	3.0	5.4	5.4	5.5	0	0

1x4 Coupler

Input Port	Insertion Loss(dB)									
	$P_{B(in)}$		P1		P2		P3		P4	
	Cal	Sim	Cal	Sim	Cal	Sim	Cal	Sim	Cal	Sim
$P_{B(in)}$	0	0	2.51	6.38	3.70	6.78	4.67	6.99	5.35	6.58
1	6.2	3.2	0	0	3.38	6.59	8.35	9.59	9.03	10.97
2	6.6	7.2	8.61	8.86	0	0	6.80	9.59	7.48	10.97
3	6.7	10.0	8.74	9.59	7.77	9.21	0	0	5.93	7.45
4	6.5	8.9	8.51	9.21	7.54	10.00	6.58	10.00	0	0

1x8 Coupler

Input Port	Insertion Loss(dB)																	
	$P_{B(in)}$		P1		P2		P3		P4		P5		P6		P7		P8	
	Cal	Sim	Cal	Sim	Cal	Sim	Cal	Sim	Cal	Sim	Cal	Sim	Cal	Sim	Cal	Sim	Cal	Sim
$P_{B(in)}$	0	0	2.68	10.97	3.52	10.97	4.32	10.97	5.07	10.97	5.75	10.71	6.35	10.97	6.66	10.97	7.01	12.22
1	9.28	3.87	0	0	9.54	13.57	10.34	13.19	11.09	13.57	11.77	15.38	12.37	17.45	12.68	20.00	13.03	21.80
2	9.48	10.04	12.04	11.87	0	0	9.37	12.60	10.12	11.31	10.80	12.60	11.40	14.95	11.71	17.45	12.06	19.59
3	9.62	13.37	12.17	13.10	11.71	12.01	0	0	9.15	10.97	9.83	9.21	10.43	12.22	10.74	14.81	11.09	16.78
4	9.66	15.85	12.21	14.95	11.75	12.08	11.30	10.00	0	0	8.87	7.45	9.46	10.36	9.77	13.28	10.12	15.69
5	9.60	18.54	12.15	16.99	11.69	14.44	11.24	10.00	10.78	7.96	0	0	8.49	11.19	8.80	12.44	9.15	14.09
6	9.42	20.46	11.98	19.21	11.52	16.02	11.06	12.44	10.61	10.00	10.15	12.44	0	0	7.83	13.01	8.18	13.77
7	9.51	21.20	11.98	20.46	11.23	17.70	10.77	14.44	10.32	12.15	9.86	12.68	9.40	14.81	0	0	7.21	13.28
8	8.73	22.44	11.28	22.29	10.83	19.21	10.37	15.69	9.91	13.57	9.45	13.67	9.00	13.67	10.22	13.67	0	0

1x2, 1x4 and 1x8 Coupler Performance Parameters: Coupling Ratio

1x2 Coupler

Input Port	Coupling Ratio (%)					
	$P_{B(in)}$		P1		P2	
	Cal	Sim	Cal	Sim	Cal	Sim
$P_{B(in)}$	0	0	68.34	50	40	50
1	50.7	59.21	0	0	60	40.79
2	49.3	5.38	31.66	5.53	0	0

1x4 Coupler

Input Port	Coupling Ratio (%)									
	$P_{B(in)}$		P1		P2		P3		P4	
	Cal	Sim	Cal	Sim	Cal	Sim	Cal	Sim	Cal	Sim
$P_{B(in)}$	0	0	57.67	26.74	44.79	24.42	37.23	23.26	34.30	25.58
1	26.90	58.33	0	0	19.20	15.28	15.96	15.28	14.70	11.11
2	24.40	32.76	14.14	22.41	0	0	22.79	20.69	21.00	24.14
3	23.80	2.38	13.74	26.19	17.55	28.57	0	0	30.00	42.86
4	25.00	28.89	14.46	26.67	18.47	22.22	24.02	22.22	0	0

1x8 Coupler Ratio

Input Port	Coupling Ratio (%)																	
	$P_{B(in)}$		P1		P2		P3		P4		P5		P6		P7		P8	
	Cal	Sim	Cal	Sim	Cal	Sim	Cal	Sim	Cal	Sim	Cal	Sim	Cal	Sim	Cal	Sim	Cal	Sim
$P_{B(in)}$	0	0	54.56	12.80	45.09	12.80	36.95	12.80	5.07	12.80	5.75	13.60	24.45	12.80	23.50	12.80	20.97	9.60
1	12.87	67.26	0	0	11.27	7.22	9.24	7.87	7.99	7.22	11.77	4.76	6.11	2.95	5.88	1.64	5.24	1.08
2	12.27	24.21	12.27	15.89	0	0	11.55	13.45	9.99	18.09	10.80	13.45	7.64	7.82	7.35	4.40	6.55	2.69
3	11.90	9.75	11.90	10.38	6.84	13.35	0	0	12.49	16.95	9.83	25.42	9.55	12.71	9.18	6.99	8.19	4.45
4	11.79	4.59	11.79	5.65	6.77	10.95	7.57	17.67	0	0	8.87	31.80	11.94	16.25	11.48	8.30	10.24	4.77
5	11.95	2.79	11.95	3.98	6.87	7.17	7.67	19.92	8.59	31.87	0	0	14.92	15.14	14.35	11.35	12.80	7.77
6	12.44	2.56	12.44	3.41	7.15	7.10	7.98	16.19	8.94	28.41	10.15	16.19	0	0	17.93	14.20	8.18	11.93
7	12.20	2.65	12.20	3.41	7.64	6.44	8.53	13.64	9.56	23.11	9.86	20.45	12.11	12.50	0	0	7.21	17.80
8	14.59	2.55	14.59	2.64	8.38	5.37	9.37	12.08	10.49	19.68	9.45	19.23	13.39	19.23	10.34	19.23	0	0